FACULDADE DE ENGENHARIA DA UNIVERSIDADE DO PORTO

Optimal and Robust Quantum Control Strategies for Stability, Fidelity, and Entanglement Enhancement

Nahid Binandeh Dehaghani



Doctoral Program in Electrical and Computer Engineering (PDEEC)

Supervisor: António Pedro Aguiar

06 February 2025

Optimal and Robust Quantum Control Strategies for Stability, Fidelity, and Entanglement Enhancement

Nahid Binandeh Dehaghani

Doctoral Program in Electrical and Computer Engineering
(PDEEC)

06 February 2025

Resumo

O controlo quântico é fundamental para o desenvolvimento das tecnologias quânticas emergentes, incluindo a computação quântica, a deteção quântica e a comunicação quântica. A fragilidade inerente dos sistemas quânticos, caracterizada pela suscetibilidade ao ruído, decoerência e perturbações externas, apresenta desafios significativos para o seu funcionamento fiável. Esta tese aborda esses desafios ao desenvolver estratégias de controlo robusto avançadas, com foco nos avanços teóricos mas também nas implementações práticas.

A tese começa por identificar os principais obstáculos no controlo quântico, particularmente na necessidade de manipulação precisa dos estados quânticos. Uma revisão aprofundada dos modelos e metodologias de controlo quântico, incluindo as propriedades de controlo do sistema e vários métodos de controlo em malha aberta e controlo por realimentação, estabelece a base. Em seguida, baseando-se nisto, o Princípio do Máximo (Mínimo) de Pontryagin (PMP) é aplicado para formular estratégias de controlo ótimo para sistemas quânticos em operações-chave, como transformações de estado quântico, otimização de recursos e maximização da fidelidade.

Outra contribuição da tese é a introdução das Redes Neurais Informadas pela Física (PINNs) como uma ferramenta poderosa para resolver problemas de controlo ótimo quântico. Em particular, demonstra-se como estas redes neurais facilitam o processo de obtenção de estratégias de controlo ótimo para sistemas quânticos fechados e abertos, com aplicações na preservação da pureza quântica em ambientes dissipativos. Ao utilizar o método revisitado de Gamkrelidze, em conjunto com a função de saturação e a abordagem de extensão do sistema, a tese estuda a conservação da pureza quântica em ambientes dissipativos através de um problema de controlo ótimo com restrições de estado e controlo.

Além disso, a tese explora métodos de controlo estocástico, com foco em estratégias baseadas em Lyapunov e Filtro de Kalman Estendido (EKF) para estabilizar sistemas quânticos sob dinâmicas incertas e ruído de medição, particularmente em sistemas governados por deteção homódina. Esta combinação de filtragem estocástica e controlo assegura estabilidade e maior robustez em ambientes quânticos ruidosos.

Uma outra contribuição é o controlo quântico usado para otimizar a síntese de emaranhamento, um recurso fundamental para o avanço das tecnologias quânticas. A tese demonstra a eficácia do Princípio do Mínimo de Pontryagin na conceção de estratégias ótimas de controlo para a geração de estados maximamente emaranhados em sistemas quânticos bipartidos. O algoritmo Chopped Random Basis (CRAB) é também utilizado para ilustrar o controlo do estado quântico em sistemas de dois qubits, melhorando a síntese de estados maximamente emaranhados.

Finalmente, propomos uma abordagem integrada quântica-clássica que combina a dinâmica computacional quântica com metodologias de computação clássica, adaptadas

para resolver problemas de controlo baseados no PMP no âmbito do PINN. Ao aproveitar um circuito quântico dinâmico que combina portas Gaussianas e não Gaussianas, o estudo apresenta uma abordagem inovadora para otimizar as manipulações de estados quânticos.

Palavras-chave: Controlo quântico, Controlo baseado em Lyapunov, Princípio do máximo de Pontryagin, Redes neurais informadas pela física, Estruturas híbridas quântico-clássicas.

Abstract

Quantum control is a cornerstone of emerging quantum technologies, including quantum computing, quantum sensing, and quantum communication. The inherent fragility of quantum systems, characterized by susceptibility to noise, decoherence, and environmental disturbances, poses significant challenges to their reliable operation. This thesis addresses these challenges by developing advanced novel robust control strategies, with a focus on both theoretical advancements and practical implementations.

The research begins by identifying the primary obstacles in quantum control, particularly the need for precise manipulation of quantum states. A thorough review of quantum control models and methodologies, including system control properties and various control methods in open-loop, and feedback control, sets the foundation. Next, building on this, Pontryagin's Maximum (Minimum) Principle (PMP) is applied to formulate optimal control strategies for quantum systems in key operations such as quantum state transformations, resource optimization and maximizing fidelity.

Another key contribution of the thesis is the introduction of Physics-Informed Neural Networks (PINNs) as a powerful tool for solving boundary value problems in quantum optimal control. We demonstrate how these neural networks streamline the process of achieving optimal control strategies for both closed and open quantum systems, with applications in conserving quantum purity in dissipative environments. By leveraging Gamkrelidze's revisited method together with saturation function and system extension approach, the thesis studies quantum purity conservation in dissipative environments through a state and control constrained optimal control problem.

Additionally, the thesis explores stochastic control methods, focusing on Lyapunov-based strategies and Extended Kalman Filtering (EKF) to stabilize quantum systems under uncertain dynamics and measurement noise, particularly in systems governed by homodyne detection. This combination of stochastic filtering and control ensures practical stability and improved robustness in noisy quantum environments.

The research further advances quantum control by optimizing the synthesis of entanglement, a key resource for enhancing quantum technologies. We demonstrate the efficacy of Pontryagin's Minimum Principle in designing optimal control strategies for generating maximally entangled states in bipartite quantum systems. The Chopped Random Basis (CRAB) algorithm is also employed to illustrate quantum state control in two-qubit systems, improving the synthesis of maximally entangled states.

Finally, we propose an integrated quantum-classical approach that merges quantum computational dynamics with classical computing methodologies tailored to address control problems based on PMP within PINN framework. By leveraging a dynamic quantum circuit that combines Gaussian and non-Gaussian gates, the study presents a novel approach to optimizing quantum state manipulations.

Keywords: Quantum control, Lyapunov-based control, Pontryagin's Maximum Principle, Physics-informed neural networks, Quantum-classical hybrid frameworks.

Acknowledgement

I would like to wholeheartedly express my deepest gratitude to my exceptional supervisor, Professor António Pedro Aguiar, for his unwavering support, insightful guidance, and constant encouragement throughout my research journey. His commitment to academic excellence and his invaluable feedback have played a pivotal role in shaping the direction and quality of this work.

I would also like to extend my heartfelt thanks to Professor Rafał Wisniewski for his invaluable support and the opportunity to collaborate with Aalborg University during my Short PhD Mobility Program. His expertise, constructive feedback, and openness to new ideas significantly contributed to the depth and breadth of my research.

This work is done in honor and memory of Professor Fernando Lobo Pereira, whose mentorship and pioneering contributions continue to inspire my academic path. His influence remains a guiding force, and his legacy lives on through this research.

Financial Support

I am grateful to the Portuguese Foundation for Science and Technology (FCT) for their financial support through the grant 2021.07608.BD. I also extend my appreciation to the Research Center for Systems and Technologies (SYSTEC) for their support during my PhD studies.

Nahid Binandeh Dehaghani

dedicate

To my father Gholamali,
for his steadfast guidance, wisdom, and the countless efforts he made to help me reach this point.

To my mother Masoumeh,
for her boundless love, unwavering strength, and her endless belief in my dreams.

To my sister Azita,
for her constant encouragement and unwavering support.

To my sister Parinaz,
who was always there for me, even on the tough days.

To my brother-in-law Masoud,
for his kindness and support.

To my nephews, Ashkan and Hooman,
for filling my life with joy and laughter.

And to my furry son, Pico,
for his unconditional companionship and the happiness he brings to my days.

Nahid Binandeh Dehaghani

"Quantum physics thus reveals a basic oneness of the universe."

Erwin Schrödinger

Contents

1 Introduction **1**
- 1.1 Motivation . . . 1
  - 1.1.1 Challenges in Quantum Control . . . 2
  - 1.1.2 Role of Stochastic Control and Filtering . . . 3
  - 1.1.3 Hybrid Approaches: Quantum-Classical Control Frameworks . . . 4
  - 1.1.4 Motivation for Optimal Control Strategies . . . 5
  - 1.1.5 Extending Quantum Control to Quantum Sensing and Communication . . . 6
- 1.2 Main Contributions . . . 6
- 1.3 Thesis Organization . . . 7
- 1.4 List of Publications . . . 9
  - 1.4.1 Journal Publications & Chapters . . . 9
  - 1.4.2 Conferences . . . 10
  - 1.4.3 Preprints (Submitted for Publication) . . . 11

2 Quantum Control Modelling, Methods, and Applications **12**
- 2.1 An Overview of Quantum Control Theory . . . 12
- 2.2 Quantum Control Models . . . 17
  - 2.2.1 Bilinear Models . . . 18
  - 2.2.2 Master Equations . . . 20
- 2.3 Concluding Remarks and Discussions . . . 24

3 Optimal Control of Quantum Systems **25**
- 3.1 The Minimum Principle of Pontryagin . . . 26
- 3.2 Schrödinger Dynamics and Control via Pontryagin's Principle . . . 27
  - 3.2.1 Pontryagin's Principle in the Control of Spin Systems . . . 28
  - 3.2.2 Existence of the Optimal Control . . . 32
- 3.3 From Schrödinger to Liouville-von Neumann equation . . . 33
- 3.4 Quantum Optimal Control with Bounded Input Constraints . . . 33
  - 3.4.1 Necessary Conditions of Optimality for the Matrix-Valued Dynamics 35
  - 3.4.2 Bounded-Control Iterative Adjoint-State Shooting Algorithm . . . 35
  - 3.4.3 Numerical Implementation . . . 38
- 3.5 State-Constrained Optimal Control for Coherence Preservation in Multi-Level Open Quantum Systems . . . 38
  - 3.5.1 Density Matrix Dynamics and Coherence in Multi-Level Systems . 39
  - 3.5.2 Optimal Control Problem Statement . . . 41
  - 3.5.3 Pontryagin's Minimum Principle in Gamkrelidze Form . . . 43
  - 3.5.4 Application of the Algorithm to a Qutrit System . . . 48

3.6 Concluding Remarks and Discussions 55

4 Quantum Pontryagin Neural Networks **57**
4.1 The Lindbladian Dynamics Equation 57
4.2 Optimal Control Formulation 59
4.2.1 Quantum purity 59
4.2.2 Problem Formulation 60
4.3 Pontryagin's Minimum Principle in Gamkrelidze Form with Saturation Functions 61
4.4 Physics-Informed Neural Networks Based on the Theory of Functional Connections 63
4.5 Simulation Results 65
4.6 Concluding Remarks and Discussions 67

5 State Estimation and Control for Stochastic Quantum Dynamics with Homodyne Measurement: Stabilizing Qubits under Uncertainty **69**
5.1 Stochastic Quantum Control and Estimation 69
5.1.1 Quantum Stochastic Evolution 70
5.1.2 Problem Statement 71
5.2 Estimation Techniques in Stochastic Quantum Dynamics 72
5.2.1 Quantum Filter Estimator 73
5.2.2 Quantum Kalman Filter estimator 73
5.2.3 Multiple-model adaptive estimator 76
5.3 Lyapunov-based state feedback control 77
5.4 Application to Qubits in Leaky Cavities 80
5.5 Concluding Remarks and Discussions 86

6 Quantum Entanglement Synthesis and Optimization **88**
6.1 Entanglement Monotones and Measures 88
6.1.1 Analysis of Quantum Entanglement Using Concurrence 89
6.2 Optimal Control Based on Quantum Entanglement Measures 90
6.2.1 Optimal Control Problem Statement 90
6.2.2 Necessary Optimality Conditions in the Form of Pontryagin's Minimum Principle 91
6.3 Numerical Validation of Optimal Entanglement Control 95
6.4 Application of CRAB Algorithm for Enhanced Entanglement Synthesis . . 97
6.4.1 CRAB Algorithm in Quantum Optimal Control 99
6.4.2 Application of CRAB Algorithm in Entanglement Synthesis 100
6.5 Concluding Remarks and Discussions 104

7 A Hybrid Quantum-Classical Physics-Informed Neural Network Architecture for Solving Quantum Optimal Control Problems **106**
7.1 Hybrid Quantum-Classical Optimization 106
7.1.1 Quantum Circuit implementation 107
7.1.2 Implementation of a Hybrid Approach Based on the Theory of Functional Connections 110
7.2 Quantum Optimal Control 113
7.2.1 System Description 113
7.2.2 Optimal Control Problems (Indirect Method) 114

7.2.3 Application of the integrated quantum-classical approach 116
7.3 Simulations and Results 117
7.4 Concluding Remarks and Discussions 119

8 Conclusions **121**
8.1 Summary of Contributions 121
8.2 Impact on the Field of Quantum Control 122
8.3 Limitations of the Work 123
8.4 Future Directions 123
8.5 Final Remarks 124

A Exploring Strange Entanglement: Experimental and Theoretical Perspectives on Neutral Kaon Systems **126**
A.1 Introduction 127
A.1.1 Notation 128
A.2 Properties of the Neutral Kaons 129
A.2.1 Strangness and Charge Parity Violation 129
A.2.2 Strangeness oscillation 130
A.2.3 Regeneration of K_S 131
A.3 Bases in quasi–spin space 132
A.4 Entangled states of kaon pairs 134
A.4.1 Maximally entangled neutral kaons 134
A.4.2 Non–maximally entangled states 135
A.5 Decoherence effects on entangled kaons 136
A.5.1 Density matrix description of entangled kaon system 137
A.5.2 Decoherence parameter associated to entangled kaon system . . . 139
A.6 Loss of entanglement 142
A.6.1 Von Neumann entanglement entropy 142
A.6.2 Entanglement of formation 143
A.6.3 Concurrence 144
A.7 Concluding Remarks and Discussions 145

References **147**

List of Figures

1.1 Quantum computers and accelerated discovery 2
1.2 Representation of decoherence and noise affecting a quantum state 3
1.3 Diagram of the generic stack of elements needed for quantum computing 4
1.4 Visualization of a hybrid quantum-classical architecture 5

3.1 Spin-$\frac{1}{2}$ controlled by an electromagnetic field in NMR experiments. 29
3.2 Convergence behavior, state trajectory evolution, and transition probabilities of the algorithm. 37
3.3 Coherence Dynamics and Off-Diagonal Density Matrix Evolution Without Control 53
3.4 Coherence and Density Matrix Evolution Under Constant Control with Dephasing 53
3.5 Optimized Control Effects on Density Matrix Evolution, Coherence, Adjoint Variables, and Control Amplitudes 54
3.6 Convergence Plot Depicting Iterative Progress Towards Optimal Solution 54

4.1 Population evolution under quantum dynamics. 67
4.2 State transition probability quantified by purity. 68

5.1 A qubit coupled to a leaky cavity monitored via homodyne detection. . . 70
5.2 Comparative evolution of quantum state populations. 79
5.3 Comparative analysis of true state, quantum filter, and quantum extended Kalman filter. 81
5.4 Comparison of true density matrix elements with quantum and quantum extended Kalman filter estimates. 81
5.5 Fidelity comparison over time between true and estimated density matrices. 82
5.6 Evolution of the trace of the error covariance matrix over time. 83
5.7 Time evolution of quantum state populations with multiple models. . . . 84
5.8 Dynamic evolution of model weights in the MMAE framework. 85
5.9 Control signal, controlled state evolution, and fidelity over 100 stochastic realizations. 85

6.1 Control field amplitudes u_1, u_2, and u_3 as a function of time. 97
6.2 Evolution of concurrence as a function of time using optimal switching control fields 98
6.3 Two qubits positioned in separated cavities linked by a closed-loop optical fiber. 101
6.4 Initial and optimized control fields for quantum state transfer. 104

6.5 Comparison of quantum state infidelity in controlled vs. uncontrolled evolutions 104

7.1 An integrated quantum-classical approach to solve differential equations. 107
7.2 Schematic depiction of a quantum neural network unit utilizing continuous variable quantum gates. 110
7.3 Input encoding by means of a displacement gate on the vacuum. 111
7.4 Time evolution of population dynamics in a two-level quantum system . . 118
7.5 Time evolution of population dynamics in a three-level quantum system . 118

A.1 Probability of finding a K^0 or $\bar{K}^0$ state in an initially produced K^0 beam over time 132
A.2 Division of the overall system into the system of interest and the environment. 136
A.3 Detection of $\bar{K}^0$ and K^0 at different positions with strangeness measurement 140
A.4 Time dependence of von neumann entropy and loss of entanglement of formation 145

Abbreviations and Symbols

BVP	Boundary Value Problem
BS	Beam-Splitter
CPTP	Completely Positive Trace-Preserving
CRAB	Chopped Random Basis
CV	Continuous Variable
DE	Differential Evolution
EKF	Extended Kalman Filter
ELM	Extreme Learning Machine
HL	Heisenberg Limit
KF	Kalman Filter
LOCC	Local Operations and Classical Communication
MES	Maximally Entangled State
MMAE	Multiple Model Adaptive Estimator
NISQ	Noisy Intermediate-Scale Quantum
NSpS	Noise-to-State Practically Stable
NSS	Noise-to-State Stable
OCP	Optimal Control Problem
ODE	Ordinary Differential Equation
PINN	Physics-Informed Neural Network
PMP	Pontryagin Maximum/Minimum Principle
PoNN	Pontryagin Neural Network
QF	Quantum Filter
QNN	Quantum Neural Network
QOC	Quantum Optimal Control
QPINN	Quantum Physics-Informed Neural Network
SDE	Stochastic Differential Equation
SME	Stochastic Master Equation
SQL	Standard Quantum Limit
TFC	Theory of Functional Connections

Chapter 1

Introduction

This chapter provides a comprehensive introduction to the key themes and objectives of the thesis. It begins by outlining the motivation for investigating advanced quantum control strategies, focusing on the challenges posed by the stochastic nature of quantum systems and the need for robust control solutions. Following this, the chapter summarizes the main contributions of the research. The structure of the thesis is then presented, offering a roadmap for the reader to understand how the research progresses from foundational theories to applications in quantum control. This chapter ends with providing a list of publications.

1.1 Motivation

The field of quantum control sits at the crossroads of quantum mechanics and control theory, promising significant advancements in technology, particularly in areas such as quantum computing, quantum sensing, and quantum communication. Quantum systems, which exploit the principles of superposition and entanglement, offer unprecedented capabilities for processing and transmitting information. However, the practical realization of quantum technologies is hindered by several critical challenges. Quantum systems are inherently fragile and highly susceptible to noise, decoherence, and environmental disturbances, which degrade their performance and limit their scalability. Figure 1.1 shows a state-of-the-art quantum computer, which represents the forefront of computational technology. The physical hardware itself is complex and sophisticated, highlighting the challenges in managing and controlling qubits to perform accurate quantum computations.

As quantum technologies evolve, the need for precise and robust control becomes paramount. Quantum systems, especially those intended for computing or sensing, must be carefully manipulated to maintain coherence and fidelity. Without effective control, the promise of quantum technologies remains largely theoretical. This thesis is motivated by the urgent need to develop robust, efficient, and scalable control strategies that can

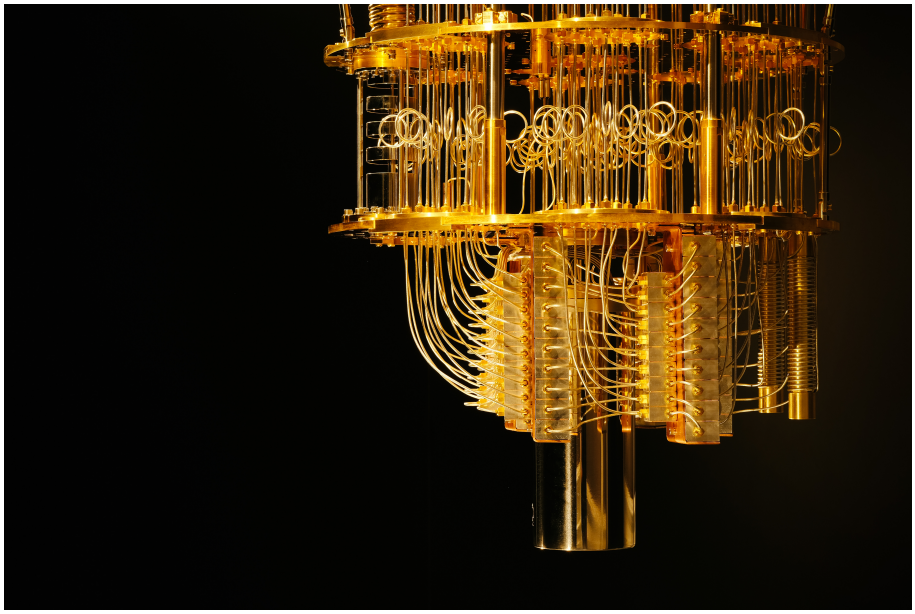


Figure 1.1: Quantum computers and accelerated discovery (Source: IBM[1]).

mitigate the stochastic and unpredictable behavior of quantum systems, ensuring their stability in practical applications.

1.1.1 Challenges in Quantum Control

At the heart of quantum control is the task of guiding a quantum system from an initial state to a desired target state, while ensuring that the system remains stable despite external disturbances. Traditional control methods, which have been highly effective in classical systems, often fail when applied to quantum systems. Quantum dynamics are governed by the Schrödinger equation or, in more complex systems, by stochastic master equations that incorporate both deterministic and random components. These stochastic effects, which include noise and decoherence, can drastically alter the system's evolution, making robust control a complex challenge.

One of the major hurdles in quantum control is managing *decoherence*, the process by which a quantum system loses its coherence and begins to behave more classically. This is particularly problematic in systems that need to maintain delicate quantum properties, such as superposition and entanglement, over long periods of time. *Quantum decoherence*, caused by interactions with the environment, is one of the main obstacles to the development of reliable quantum computers and sensors. Effective control strategies must mitigate these environmental disturbances, ensuring that quantum states are preserved and that computations or measurements are performed with high fidelity. Figure 1.2 illustrates how environmental disruptions can cause a quantum state to lose coherence

[1]More details at https://newsroom.ibm.com/media-center?l=100&keywords=quantum+computer.

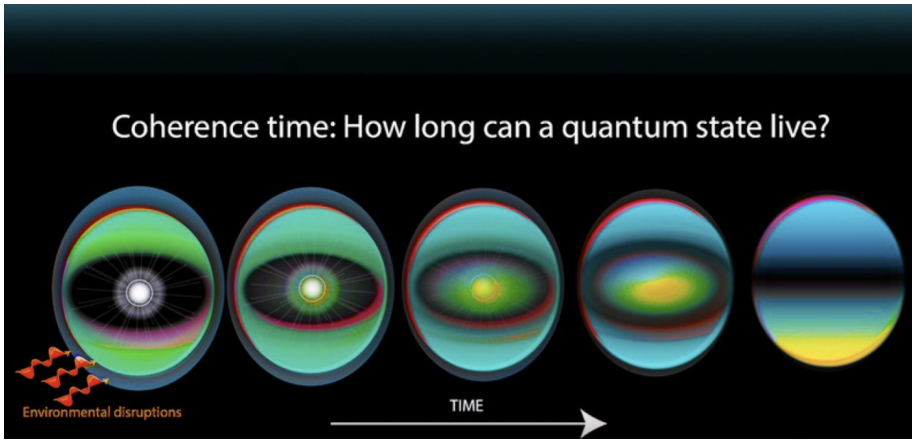


Figure 1.2: Representation of decoherence and noise affecting a quantum state (Source: Scott Amyx[2]).

over time. The image visualizes the process of decoherence, showing the gradual degradation of the quantum state due to noise and external disturbances. This underscores the necessity for advanced control techniques to maintain the coherence of quantum systems.

Moreover, real-world quantum systems are subject to *hardware limitations* that constrain the types of control signals that can be applied. In quantum computing, for example, the control pulses used to manipulate qubits must be designed within the bandwidth and amplitude constraints of available technology. Developing control protocols that can suppress noise while remaining within these physical limits is essential for the advancement of quantum technologies. Figure 1.3 illustrates the generic architecture of a quantum computer, showcasing the interactions between qubit control systems, classical computing resources, and the quantum plane. The control and readout layers play a critical role in stabilizing qubits and ensuring that quantum operations are executed with high fidelity.

1.1.2 Role of Stochastic Control and Filtering

Quantum systems are particularly challenging to control because they exhibit inherently stochastic behavior. The presence of random noise and uncertainty in system parameters complicates the task of state estimation and control. This has led to the adoption of stochastic control techniques, which account for these uncertainties and provide robust strategies for guiding quantum systems.

In this context, *Lyapunov-based control strategies* combined with *filtering methods*, such as the *Extended Kalman Filter (EKF)*, offer powerful tools for stabilizing quantum systems. These techniques allow for real-time estimation of the system's state, even in the presence of noise, and enable adaptive control policies that can dynamically adjust to fluctuations in the system's environment. In this thesis, we develop a Lyapunov-based approach to

[2]More details at https://scottamyx.com/2017/08/24/quantum-computing-part-8-decoherence/.

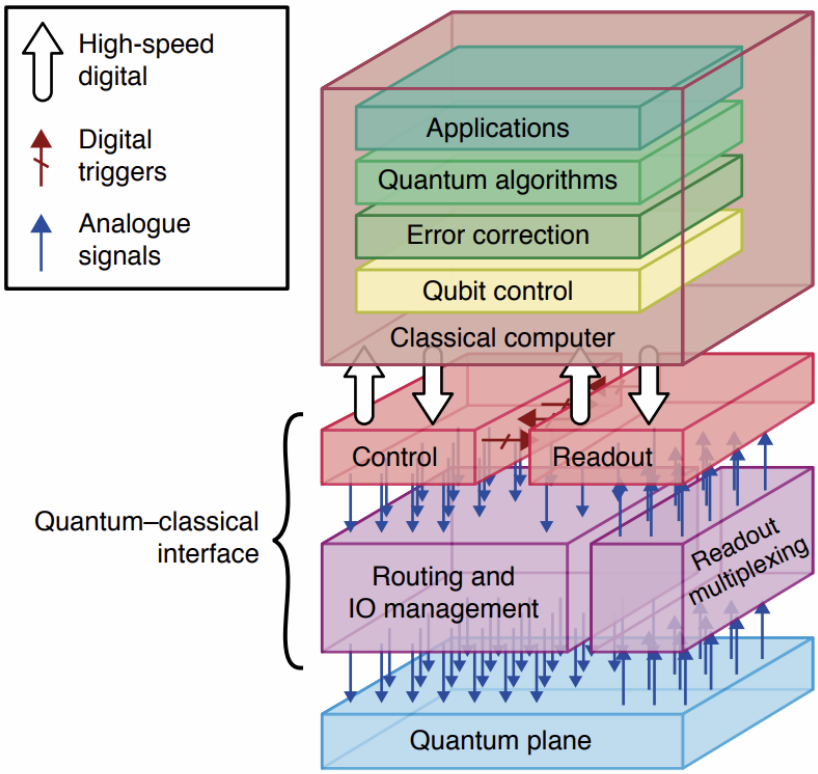


Figure 1.3: Diagram of the generic stack of elements needed for quantum computing, showcasing qubit interactions and control systems (Source: (Pauka et al., 2021)).

control the evolution of quantum systems, particularly in the presence of measurement noise. By incorporating stochastic filtering, we are able to reduce the estimation errors and improve the robustness of quantum control, ensuring that systems remain stable despite uncertainties.

Additionally, this work addresses the challenge of *unknown system parameters*, which can degrade the performance of control strategies. By using multiple model estimation schemes alongside traditional filters, we demonstrate how control strategies can be adapted to handle systems with unknown dynamics. This flexibility is critical for practical applications where system parameters may change over time or be difficult to measure accurately.

1.1.3 Hybrid Approaches: Quantum-Classical Control Frameworks

As quantum systems become increasingly complex, there is growing interest in hybrid control frameworks that combine classical and quantum methodologies. One promising approach is the integration of *Physics-Informed Neural Networks (PINNs)* into quantum control. PINNs are designed to solve differential equations by embedding the physical

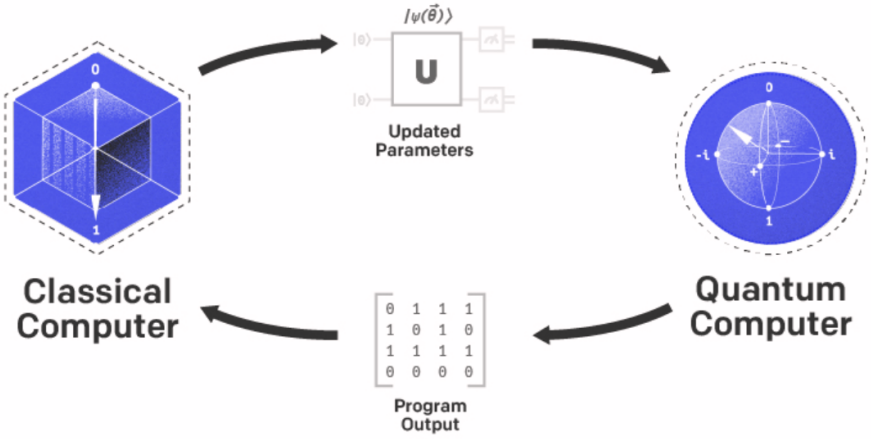


Figure 1.4: Visualization of a hybrid quantum-classical architecture, illustrating feedback between classical and quantum systems (Source: IonQ[3]).

laws governing the system directly into the architecture of a neural network. In this thesis, we leverage PINNs to solve complex optimal control problems in quantum systems, where traditional numerical techniques struggle with the nonlinearity and high dimensionality of quantum dynamics.

The hybrid quantum-classical framework provides a flexible approach to control, allowing for the optimization of quantum systems with fewer computational resources. By combining the strengths of quantum and classical computation, this approach can be used to tackle complex problems such as *state estimation* and *optimal control* under noise. PINNs, in particular, enable the efficient computation of control strategies that minimize both time and energy, which are critical resources in quantum systems. Figure 1.4 provides a visualization of a hybrid quantum-classical architecture. It illustrates how feedback between classical and quantum systems is used to update parameters and optimize performance. This interaction between the two computational paradigms highlights the potential of hybrid methods in achieving robust control over quantum systems.

1.1.4 Motivation for Optimal Control Strategies

One of the primary motivations for developing optimal control strategies in quantum systems is the need to combat the detrimental effects of noise and decoherence. Quantum systems are inherently sensitive to their environments, and maintaining coherence is essential for their functionality. Optimal control provides a framework for devising control pulses that not only mitigate these adverse effects but also enhance the overall performance of quantum operations. By minimizing the impact of noise through carefully designed control sequences, we can improve the reliability of quantum computations, thus making practical quantum technologies feasible.

[3]More details at https://ionq.com/resources/what-is-hybrid-quantum-computing.

Furthermore, as quantum systems grow increasingly complex, the demand for efficient resource utilization becomes more pressing. Optimal control strategies enable the efficient allocation of resources—both in terms of energy and time—by identifying control protocols that achieve desired outcomes with minimal overhead. This is particularly important in applications such as quantum computing and quantum communication, where the trade-off between control fidelity and resource consumption is critical for scalability.

Additionally, the exploration of optimal control strategies extends to the integration of machine learning techniques, which can further enhance the adaptability and efficiency of control systems. By employing algorithms that can learn from data and adjust control inputs in real-time, we can create adaptive control frameworks that respond to changing conditions and uncertainties in quantum systems. This not only improves the robustness of quantum control but also opens up new avenues for research into self-optimizing quantum technologies.

1.1.5 Extending Quantum Control to Quantum Sensing and Communication

The need for robust quantum control extends beyond quantum computing and into other domains, such as *quantum sensing* and *quantum communication*. Quantum sensors, which exploit the unique properties of quantum systems to measure physical quantities with extreme precision, rely on effective control to maintain their sensitivity. Similarly, quantum communication networks, which aim to transmit quantum information securely over long distances, depend on control strategies that preserve the coherence of quantum states over time.

This thesis also investigates the application of optimal control strategies for optimizing entanglement, with potential applications to sensing and communication. For instance, in quantum sensor networks, these control techniques can enhance the performance of quantum sensors, improving both their accuracy and resilience to noise. The work presented here offers insights into how quantum systems might be effectively controlled and stabilized in practical applications.

1.2 Main Contributions

The main contributions of this thesis are rooted in the systematic exploration and enhancement of quantum control strategies across multiple dimensions. We establish the motivation for the research, emphasizing the necessity for robust and optimal control methods to address the complexities inherent in quantum systems. The main contributions of this thesis are as follows:

- Provision of a foundational overview of core concepts in quantum control theory, reviewing various control methods and their applications in advancing quantum technologies (Dehaghani et al., 2022a).
- Formulation of constrained optimal control problems for quantum systems, leveraging Pontryagin's Maximum (Minimum) Principle (PMP) to develop computational techniques that address state transformations, fidelity maximization, and energy minimization in two- and three-level quantum systems (Dehaghani and Pereira, 2022b,a; Dehaghani et al., 2022b; Dehaghani and Aguiar, 2023b; Dehaghani et al., 2024d).
- Application of Physics-Informed Neural Networks (PINNs) to solve quantum optimal control problems (Dehaghani and Aguiar, 2023a; Dehaghani et al., 2023b).
- Development of state estimation and control methods for stochastic quantum dynamics, proposing Lyapunov-based control strategies and extended Kalman filtering to stabilize qubits in leaky cavities under homodyne detection (Dehaghani et al., 2024e).
- Exploration of control strategies for quantum entanglement synthesis and optimization, including entanglement-driven optimal control methods and the Chopped Random Basis (CRAB) algorithm with application to quantum communication and metrology (Dehaghani et al., 2024b,a).
- Proposal of a novel hybrid PINN architecture for solving quantum optimal control problems, integrating quantum and classical computing for effective state control (Dehaghani et al., 2024c).
- Contribution to high-energy physics through a comprehensive analysis of the quantum properties of neutral K-mesons, offering experimental and theoretical insights into entanglement dynamics and decoherence (Dehaghani et al., 2023a).

Overall, the contributions outlined in this thesis not only advance the theoretical foundations of quantum control but also pave the way for practical applications in various quantum technologies, offering insights that will inform future research directions.

1.3 Thesis Organization

This thesis is structured to provide a comprehensive exploration of quantum control strategies, modeling, and applications, while also presenting the novel contributions made throughout the research. Each chapter builds on fundamental concepts, leading to advanced methods and their application to real-world quantum systems.

- **Chapter 1: Introduction**
  The introduction provides the motivation behind this research and outlines the main contributions. It also briefly summarizes the key challenges in quantum control and the importance of developing robust and optimal control strategies for quantum systems.

- **Chapter 2: Quantum Control Modeling, Methods, and Applications**
  This chapter aims to offer an overview of various quantum control theories, their applications, and the modeling approaches used in quantum control. This chapter introduces various control methods such as open-loop, closed-loop, including robust control, from the lens of quantum control.

- **Chapter 3: Optimal Control of Quantum Systems**
  This chapter delves into the formulation of optimal control problems for quantum systems. It covers the application of Pontryagin's Maximum (or Minimum) Principle (PMP) to quantum systems and provides computational techniques for solving these control problems, with examples such as state transformations, fidelity maximization, and energy minimization in two- and three-level quantum systems.

- **Chapter 4: Quantum Pontryagin Neural Networks**
  This chapter demonstrates how Physics-Informed Neural Networks (PINNs) can streamline the solution of boundary value problems in quantum optimal control problems, providing energy- and time-optimal strategies across various system types. This approach is studied for closed systems and extended to open quantum systems for studying quantum purity conservation in dissipative environments by leveraging Gamkrelidze's revisited method for state constraints and also saturation functions for control limits.

- **Chapter 5: State Estimation and Control for Stochastic Quantum Dynamics with Homodyne Measurement**
  This chapter focuses on the development of estimation and control techniques for quantum systems under stochastic dynamics. It introduces Lyapunov-based control strategies and extended Kalman filtering methods for stabilizing qubits in leaky cavities under homodyne detection.

- **Chapter 6: Quantum Entanglement Synthesis and Optimization**
  This chapter studies an optimal control strategy to generate maximally entangled states in bipartite quantum systems. By leveraging the Pontryagin Principle, the results showcase the effectiveness of switching control fields in optimizing entanglement. This chapter also offers a thorough exploration of quantum control strategies, including the Chopped Random Basis (CRAB) algorithm and entanglement-driven

optimal control methods. These techniques focus on maximizing quantum entanglement, which is critical for high-precision applications in quantum computing, communication, and metrology.

- **Chapter 7: A Hybrid Quantum-Classical Physics-Informed Neural Network Architecture for Solving Quantum Optimal Control Problems**
  This chapter proposes an integrated quantum-classical approach that merges quantum computational dynamics with classical computing methodologies tailored to address control problems based on PMP within PINN framework. By leveraging a dynamic quantum circuit that combines Gaussian and non-Gaussian gates, the study showcases an innovative approach to optimizing quantum state manipulations.

- **Chapter 8: Conclusions**
  The concluding chapter summarizes the key findings of the thesis, highlighting the contributions to the field of quantum control. It also discusses future research directions and potential advancements in quantum technologies based on the insights gained from this work.

- **Appendix: Exploring Strange Entanglement - Experimental and Theoretical Perspectives on Neutral Kaon Systems**
  The Appendix presents a comprehensive analysis of the quantum properties of neutral K-mesons, focusing on their entanglement dynamics and the effects of decoherence. This appendix expands upon the core principles explored in the thesis, offering both experimental and theoretical perspectives to guide future research directions.

1.4 List of Publications

1.4.1 Journal Publications & Chapters

1. Nahid Binandeh Dehaghani, A. Pedro Aguiar, and Rafal Wisniewski. "State Estimation and Control for Stochastic Quantum Dynamics with Homodyne Measurement: Stabilizing Qubits under Uncertainty." IEEE Access (2024), DOI: 10.1109/ACCESS.2024.3455170.

2. Nahid Binandeh Dehaghani, A. Pedro Aguiar, and Rafal Wisniewski. "Exploring Strange Entanglement: Experimental and Theoretical Perspectives on Neutral Kaon Systems." Quantum Entanglement in High Energy Physics, IntechOpen (2023), DOI: 10.5772/intechopen.1002527.

3. Nahid Binandeh Dehaghani, A. Pedro Aguiar, and Rafal Wisniewski. "Quantum Pontryagin Neural Networks in Gamkrelidze Form Subjected to the Purity of Quantum Channels." IEEE Control Systems Letters LCSS-CDC (2023), DOI: 10.1109/LCSYS.2023.3286303.

4. Nahid Binandeh Dehaghani, Fernando Lobo Pereira and A. Pedro Aguiar. "Quantum control modelling, methods, and applications." Journal of Extensive Reviews (2022), DOI: 10.21467/exr.2.1.5037.

5. Nahid Binandeh Dehaghani, and Fernando Lobo Pereira. "Optimal Control of Quantum Systems by Pontryagin Maximum Principle." U.Porto Journal of Engineering (2022), DOI: 10.24840/2183-6493_008.002_0015.

1.4.2 Conferences

6. Nahid Binandeh Dehaghani, A. Pedro Aguiar, Rafal Wisniewski, and David Q. Liu. "A Hybrid Quantum-Classical Approach to Complex Optimization Using a Variational Quantum Classifier." European Quantum Technologies Conference EQTC (2024).

7. Nahid Binandeh Dehaghani, A. Pedro Aguiar, and Rafal Wisniewski. "A Hybrid Quantum-Classical Physics-Informed Neural Network Architecture for Solving Quantum Optimal Control Problems." IEEE International Conference on Quantum Computing and Engineering QCE (2024).

8. Nahid Binandeh Dehaghani, A. Pedro Aguiar, and Rafal Wisniewski. "Application of CRAB Algorithm for Enhanced Entanglement Synthesis." 16th APCA International Conference on Automatic Control and Soft Computing CONTROLO (2024).

9. Nahid Binandeh Dehaghani, and A. Pedro Aguiar. "Quantum State Transfer Optimization: Balancing Fidelity and Energy Consumption using Pontryagin Maximum Principle." 11th IEEE International Conference in Systems and Control ICSC (2023), DOI: 10.1109/ICSC58660.2023.10449792.

10. Nahid Binandeh Dehaghani, and A. Pedro Aguiar. "An Application of Pontryagin Neural Networks to Solve Optimal Quantum Control Problems." 9th IEEE International Conference on Control, Decision and Information Technologies CoDIT (2023), DOI: 10.1109/CoDIT58514.2023.10284049.

11. Nahid Binandeh Dehaghani, Fernando Lobo Pereira, and A. Pedro Aguiar. "A Quantum Optimal Control Problem with State Constrained Preserving Coherence." 61st IEEE Conference on Decision and Control CDC (2022), DOI: 10.1109/CDC51059.2022.9993086.

12. Nahid Binandeh Dehaghani, and Fernando Lobo Pereira. "High fidelity quantum state transfer by Pontryagin maximum principle." IFAC-PapersOnLine (2022), DOI: 10.1016/j.ifacol.2022.09.026.

1.4.3 Preprints (Submitted for Publication)

13. Nahid Binandeh Dehaghani, A. Pedro Aguiar, and Rafal Wisniewski. "State-Constrained Optimal Control for Coherence Preservation in Multi-Level Open Quantum Systems." DOI: arXiv:2411.10840.

14. Nahid Binandeh Dehaghani, A. Pedro Aguiar, and Rafal Wisniewski. "Optimizing Maximally Entangled State Generation via Pontryagin's Principle"

Chapter 2

Quantum Control Modelling, Methods, and Applications

This chapter concerns quantum control results and methods that, over the years, have been used in the various operations involving quantum systems. Most of these methods have been originally developed outside the context of quantum physics, and, then, adapted to take into account the specificities of the various quantum physical platforms. Quantum control consists in designing adequate control signals required to efficiently manipulate systems conforming the laws of quantum mechanics in order to ensure the associated desired behaviours and performances. This chapter attempts to provide an introduction to various quantum control theories and their applications, as well as quantum control modelling. A detailed version of this study has been published in (Dehaghani et al., 2022a).

2.1 An Overview of Quantum Control Theory

Quantum control is about actively manipulating chemical and physical processes on atomic and molecular scales. With recent advancements in quantum technologies, quantum control has found practical applications in various fields such as quantum optics (Madronero et al., 2006), cavity quantum electrodynamics (QED) (Miguel-Sánchez et al., 2013), atomic spin ensembles (Bauch et al., 2018), ion trapping (Alonso et al., 2013), Bose–Einstein condensates (Amri et al., 2019), and nitrogen vacancy centers (Liu et al., 2019), among others. These developments highlight the growing importance of understanding and controlling quantum systems.

At the heart of quantum mechanics are phenomena like entanglement and coherence, which are both rooted in the principle of superposition. Entanglement is the curious phenomenon where the state of one quantum system is tied to another, such that they cannot be described independently (Gamble, 2019). Coherence, on the other hand, refers to a quantum system's ability to exist in a superposition of states, such as a qubit being

both "0" and "1" at the same time. This property is key to the computational power of quantum systems. However, this delicate quantum behavior is often disrupted by decoherence, which is caused by interactions with the environment and leads to the loss of quantum properties (Zyga, 2015).

The goal of quantum control is to guide the evolution of quantum systems, steering them along specific trajectories or towards particular states, using external control inputs. Achieving this requires a careful balance between leveraging the natural properties of the system and counteracting the effects of environmental disturbances, such as noise and decoherence. Some of the core ideas and methods that form the foundation of quantum control are pointed out in the following:

Controllability: A fundamental concept in quantum control is Controllability, which addresses whether a quantum system can be guided from an initial state to a desired target state using appropriate control signals. This property is central to many quantum technologies, as it directly links to the feasibility of performing arbitrary transformations, which are essential for the universality of quantum computing (Ramakrishna and Rabitz, 1996; Albertini and D'Alessandro, 2001).

In practice, achieving controllability is not always straightforward. It requires the development of sophisticated actuation strategies capable of precisely manipulating quantum systems. This challenge becomes even greater when dealing with multi-qubit systems, where interactions between qubits and with the environment introduce noise and decoherence. These unwanted effects can disrupt the delicate quantum properties that are crucial for control tasks (Rabitz et al., 2000).

For quantum systems that are controllable, the objective is to design control signals that steer the system efficiently and robustly, even in the presence of environmental disturbances. Achieving this often involves a combination of theoretical insights and practical techniques to address the complexities of real-world quantum systems.

Open-Loop Control: Open-loop control is one of the foundational approaches in quantum control, where control laws are designed prior to the experiment and remain fixed during system evolution. This method is particularly effective for systems with well-characterized dynamics and minimal external disturbances. Since the control inputs are predetermined, open-loop control relies heavily on accurate modeling of the quantum system and its environment.

One of the earliest and most widely used strategies in open-loop control is coherent control. By applying time-dependent potentials, coherent control ensures the maintenance of quantum coherence, which is critical for achieving specific quantum tasks. This approach has been successfully applied to various problems, such as controlling chemical reactions (Warren et al., 1993; Gordon et al., 1999).

A significant advancement within open-loop control is the application of optimal control theory. Optimal control provides a systematic framework for designing control laws by formulating the quantum control problem as the minimization of a cost functional

subject to the system's dynamics. The choice of the cost functional depends on the specific objectives, which could include minimizing time (Tibbetts et al., 2012), reducing energy consumption (Dehaghani and Pereira, 2022a), or achieving an optimal unitary transformation (Palao and Kosloff, 2003). These methods have been widely applied in quantum technologies to improve performance, such as enhancing the sensitivity of magnetic resonance experiments (Untidt et al., 1998).

Optimal control methods often rely on mathematical tools, such as Pontryagin's Maximum Principle and convergent iterative algorithms, to design control laws that satisfy the desired criteria (Dehaghani and Pereira, 2022b). However, the computational complexity of solving two-point boundary value problems can pose challenges, especially for systems that require rapid responses or operate in high-dimensional spaces (Cong, 2014).

In addition to optimal control, other strategies like bang-bang control and geometric control have been employed in open-loop settings. Bang-bang control involves discrete switching between control inputs and is particularly effective for bounded control problems, such as population transfer and decoherence suppression (Wu et al., 2007). Geometric control, which utilizes the Bloch sphere representation, has proven valuable for low-dimensional quantum systems and tasks involving state transformations (Boscain and Piccoli, 2003). While open-loop control provides a powerful framework for systems with predictable dynamics, its reliance on pre-designed control laws highlights the need for more adaptive and feedback-based strategies to address the challenges posed by dynamic and noisy environments.

Closed-loop Control: Closed-loop control is a dynamic approach in quantum control where the system's evolution is continuously monitored and control inputs are iteratively refined based on feedback. This paradigm contrasts with open-loop control by incorporating real-time measurements, enabling adaptive responses to disturbances and uncertainties.

One key method in closed-loop control is learning-based control, which employs iterative procedures to optimize performance. In this approach, each iteration uses updated feedback from the system to refine the control strategy (Rabitz et al., 2000). Several learning algorithms have been successfully applied in quantum control, including gradient-based methods like the D-MORPH search algorithm (Zhdanov, 2017), and stochastic optimization techniques such as Genetic Algorithms (GA) (Tsubouchi and Momose, 2008), Differential Evolution (DE) (Storn and Price, 1997), Particle Swarm Optimization (PSO) (Yang et al., 2004), and Reinforcement Learning (RL) (Sutton and Barto, 2018; Dong et al., 2008). These methods provide robust frameworks for exploring complex control landscapes, often combining global search capabilities with gradient-like rewards.

Adaptive feedback control, another closed-loop strategy, iteratively refines control inputs based on measurements taken during the process (Judson and Rabitz, 1992). By closing the loop, the system evaluates the success of applied controls and continuously adjusts them to converge toward the desired target state (Brif et al., 2010). Such meth-

ods have been effectively used in experiments, and comparative studies of optimization algorithms like GA, DE, and gradient descent highlight their respective advantages in quantum control (Sun et al., 2014).

Feedback control methods can be further categorized into measurement-based feedback and coherent feedback.

Measurement-Based Feedback: In this approach, observables of the quantum system are measured, and the resulting classical signals are processed to generate control inputs. Techniques such as projective (von Neumann) measurements (Johansen, 2007) and continuous weak measurements (Korotkov and Averin, 2001) are commonly employed. Markovian feedback control (Wiseman, 1994), which assumes no time delays and employs memoryless controllers, has been applied to various physical systems. Bayesian feedback methods extend this paradigm by incorporating non-Markovian dynamics, enabling continuous estimation of dynamical variables and adaptive feedback for state preparation and error correction (Ruskov and Korotkov, 2002; Ahn et al., 2002). Weak measurements can also be used in stochastic master equations to gradually influence system dynamics, with applications in entanglement generation (Hill and Ralph, 2008) and single-qubit control (Brańczyk et al., 2007). However, the stochastic nature of measurements and their potential to disturb the quantum system remain significant challenges.

Coherent Feedback: Unlike measurement-based feedback, coherent feedback retains quantum coherence by employing quantum systems as controllers within the feedback loop. This method is particularly useful for tasks such as entanglement generation, transformation, and transfer, which require preserving quantum coherence (James et al., 2008; Nurdin et al., 2009). Noise-reducing controllers, such as H^∞ controllers (James et al., 2008) and linear quadratic Gaussian (LQG) controllers (Shaiju et al., 2007), have been adapted for coherent feedback systems. These controllers optimize quadratic cost functionals, making them well-suited for managing noise in stochastic systems.

Additionally, Lyapunov-based control provides a framework for designing feedback laws aimed at achieving stability and asymptotic convergence to target states. This method is effective in driving systems into decoherence-free subspaces and generating entanglement (Wang and Schirmer, 2010; Cong and Meng, 2013). Variable structure control, which adjusts the controller's structure based on the state trajectory, offers another closed-loop approach for qubit state preparation (Dong and Petersen, 2009b, 2011).

From quantum control perspective, closed-loop and feedback control strategies represent powerful tools for addressing the challenges posed by quantum systems, particularly in dynamic and noisy environments. These methods enable adaptive and robust control, making them indispensable for advancing quantum technologies.

Robust Control: Robust control is a crucial aspect of quantum technologies, addressing the inevitable disturbances, uncertainties, and noise inherent in quantum systems. The goal is to design control strategies that ensure reliable performance despite these

challenges, which are particularly significant in practical implementations of quantum computing, communication, and sensing.

One of the frameworks for robust control is the synthesis of H^∞ controllers. These controllers are specifically designed to handle uncertainties in quantum systems, particularly non-commutative linear stochastic systems, which encompass a wide range of quantum processes (James et al., 2008). By optimizing a worst-case performance criterion, H^∞ controllers ensure that the system remains stable and functional even under adverse conditions.

Sliding mode control, another effective robust control technique, is a variable structure method traditionally used in classical systems. It has been adapted to quantum systems to address uncertainties in dynamics and environmental interactions. Sliding mode control has proven effective for quantum systems with nonlinear equations (Chen et al., 2013), bounded uncertainties in the Hamiltonian (Dong and Petersen, 2009a), two-level quantum systems (Dong and Petersen, 2012), and robust control of single qubits (Dong et al., 2013). Its strength lies in its ability to switch between different control structures to maintain stability, making it particularly useful in feedback-based quantum control.

Risk-sensitive optimal control provides another robust approach, particularly in the context of linear quadratic Gaussian (LQG) design. In this framework, two types of cost functions are considered: additive costs in risk-neutral optimal control and multiplicative costs in risk-sensitive optimal control. The latter is closely connected to robustness, as it explicitly accounts for uncertainty and disturbances in its formulation (Yamamoto and Bouten, 2009).

Quantum filtering and estimation have also been extended to include robustness properties, such as guaranteed-cost filters (Shaiju et al., 2007) and risk-sensitive filtering methods. These approaches enhance the reliability of quantum state estimation, which is critical for feedback control and error correction.

Quantum ensemble control is another powerful robust control strategy. It involves managing a continuum of dynamical systems characterized by varying parameters using a single control signal (Li and Khaneja, 2009). This method is particularly valuable for systems with inherent parameter uncertainties, where traditional control approaches may fail.

Sequential convex programming provides a local optimization method that can be used to ensure error suppression in quantum control tasks (Kosut et al., 2013). By iteratively refining the control inputs, this technique achieves robustness against noise and imperfections in experimental setups.

Dynamical decoupling represents a widely used strategy for robust control, especially in preserving quantum coherence. By applying a sequence of pulses, this method mitigates the effects of environmental noise, enabling the system to maintain its desired quantum properties (Yang et al., 2011). Dynamical decoupling has been successfully integrated with quantum gates to enhance their fidelity and robustness (West et al., 2010).

Robust control encompasses a variety of strategies aimed at ensuring the stability and performance of quantum systems under realistic conditions. These methods are indispensable for advancing quantum technologies, providing the tools needed to overcome the challenges posed by uncertainties and disturbances.

2.2 Quantum Control Models

The mathematical formulation of quantum mechanics provides a framework for describing and analyzing the dynamics of quantum systems. For closed quantum systems, the state is represented by a unit vector $|\psi\rangle$ in a complex Hilbert space $\mathcal{H}$, often expressed using the Dirac notation (Dirac, 1981). A pure quantum state can be written as a wavefunction:

$$|\psi\rangle = \cos\frac{\theta}{2}|0\rangle + e^{i\varphi}\sin\frac{\theta}{2}|1\rangle,$$

where $\theta \in [0,\pi]$ and $\varphi \in [0,2\pi]$ are parameters defining the state on the Bloch sphere. The states $|0\rangle$ and $|1\rangle$ correspond to the classical bit values 0 and 1, respectively (Nielsen and Chuang, 2002).

For open quantum systems, or quantum ensembles, the description via a unit vector is insufficient due to interactions with the environment. Instead, these systems are represented by a density operator $\rho : \mathcal{H} \to \mathcal{H}$, which is a Hermitian, positive-semidefinite operator with unit trace. For example, an ensemble of pure states $|\psi_j\rangle$ with respective probabilities p_j is described by

$$\rho = \sum_j p_j |\psi_j\rangle\langle\psi_j|,$$

where $\sum_j p_j = 1$, and $\langle\psi_j| = |\psi_j\rangle^\dagger$ represents the adjoint. The density operator allows for a unified description of both pure and mixed quantum states, accommodating the statistical nature of quantum ensembles.

The modeling of quantum control systems depends on whether the system is open or closed. For closed systems, bilinear models such as the Schrödinger equation and quantum Liouville equation are commonly used. These models describe the unitary evolution of the system governed by the Hamiltonian. Open systems, which interact with their environment, are modeled using Markovian master equations or stochastic master equations, which incorporate dissipative and stochastic effects.

An alternative approach to quantum system modeling is the Heisenberg picture, where observables evolve over time rather than the states. This is often formulated using linear quantum stochastic differential equations, which are particularly useful for describing quantum systems interacting with dynamic environments or measurement devices.

In the subsections that follow, we provide a detailed review of the most relevant quantum control models, including their mathematical foundations and practical applications.

2.2.1 Bilinear Models

Bilinear models are fundamental to describing the dynamics of quantum systems in the mathematical framework of quantum mechanics. These models characterize the evolution of quantum states under the influence of Hamiltonian dynamics and external controls. For pure states, the Schrödinger equation provides a detailed description of the unitary evolution of the state vector. For mixed states or statistical ensembles, the Liouville-von Neumann equation governs the evolution of the density operator, capturing the probabilistic nature of quantum ensembles. Bilinear models also facilitate the inclusion of control inputs through interaction Hamiltonians, enabling external influences such as electromagnetic fields to guide the quantum system.

In the following subsections, we delve into two primary formulations of bilinear models: the Schrödinger equation for pure states and the Liouville-von Neumann equation for mixed states. These formulations provide the mathematical foundation for understanding and designing control strategies in quantum systems.

2.2.1.1 Schrödinger Equation

In quantum mechanics, the evolution of a state vector $|\psi(t)\rangle$ is governed by the Schrödinger equation

$$i\hbar\frac{\partial}{\partial t}|\psi(t)\rangle = H(t)|\psi(t)\rangle, \quad |\psi(0)\rangle = |\psi_0\rangle, \tag{2.1}$$

where i is the imaginary unit, $H(t)$ is the time-dependent Hamiltonian operator (Hermitian), and $\hbar$ is the reduced Planck constant. The Hamiltonian in this context represents the total energy operator of the system, distinct from the Pontryagin Hamiltonian used in optimization.

Control inputs are incorporated through a set of control functions $\{u_k(t)\}$ associated with interaction Hamiltonians $\{H_k\}$, leading to a total Hamiltonian

$$H(t) = H_0 + \sum_k u_k(t)H_k,$$

where H_0 is the free (uncontrolled) Hamiltonian, and H_k represents interaction terms. This allows external control fields to influence the quantum state trajectory.

The evolution of the system can be expressed using the unitary time evolution operator $U(t,t_0)$, which satisfies

$$i\hbar\frac{\partial}{\partial t}U(t,t_0) = H(t)U(t,t_0), \quad U(t_0,t_0) = I, \tag{2.2}$$

where I is the identity operator. The time evolution operator transforms the state from $|\psi(t_0)\rangle$ to $|\psi(t)\rangle$ as $|\psi(t)\rangle = U(t,t_0)|\psi(t_0)\rangle$.

For systems with time-independent Hamiltonians, the solution simplifies to

$$U(t,t_0) = e^{-iH(t-t_0)/\hbar}.$$

However, for time-dependent Hamiltonians, the solution requires the time-ordered exponential

$$U(t,t_0) = \mathcal{T}_{\leftarrow} \exp\left(-\frac{i}{\hbar}\int_{t_0}^{t} H(s)\,ds\right),$$

where $\mathcal{T}_{\leftarrow}$ is the time-ordering operator[1].

For an N-dimensional quantum system, the state can be expressed as a superposition of eigenstates $\{|\phi_j\rangle\}$, forming an orthonormal basis of the Hilbert space $\mathcal{H}$:

$$|\psi(t)\rangle = \sum_{j=1}^{N} c_j(t)\,|\phi_j\rangle,$$

where $c_j(t)$ are the time-dependent coefficients. This expansion leads to the matrix form:

$$i\hbar\frac{d}{dt}C(t) = H(t)C(t), \quad C(t_0) = C_0, \tag{2.3}$$

where $C(t)$ is the vector of coefficients. The Schrödinger equation, the unitary evolution equation, and this matrix representation are equivalent provided the system's state can be fully described in terms of the chosen basis and the Hamiltonian dynamics are appropriately represented (Dirac, 1981).

2.2.1.2 Liouville-von Neumann Equation

For mixed states or quantum statistical ensembles, the density operator $\rho(t)$ provides a complete description:

$$\rho(t) = U(t,t_0)\rho(t_0)U^{\dagger}(t,t_0),$$

where $\rho(t_0)$ is the initial density operator:

$$\rho(t_0) = \sum_{\alpha} w_\alpha\,|\psi_\alpha\rangle\langle\psi_\alpha|,$$

with probabilities $w_\alpha \geq 0$ and $\sum_\alpha w_\alpha = 1$.

Differentiating $\rho(t)$ yields the Liouville-von Neumann equation

$$i\hbar\frac{d}{dt}\rho(t) = [H(t),\rho(t)], \tag{2.4}$$

[1]The time-ordering operator $\mathcal{T}$ arranges operators so that those with larger time arguments appear to the left. For example, $\mathcal{T}[A(t_1)A(t_2)] = A(t_2)A(t_1)$ if $t_1 < t_2$. It is crucial for defining the time-ordered exponential $\mathcal{T}e^{\int_{t_0}^{t} A(\tau)d\tau}$, where each term in the expansion is ordered such that earlier times are to the right.

where $[A, B] = AB - BA$ is the commutator. This equation describes the unitary evolution of the density matrix.

The Liouville-von Neumann equation can also be written using the Liouville superoperator $\mathcal{L}$:

$$\frac{d}{dt}\rho(t) = \mathcal{L}(t)\rho(t),$$

where $\mathcal{L}$ acts on ρ as a linear operator. The solution is given by

$$\rho(t) = \mathcal{T}_{\leftarrow} \exp\left(\int_{t_0}^{t} \mathcal{L}(s)\, ds\right) \rho(t_0),$$

for time-dependent $\mathcal{L}$, or

$$\rho(t) = e^{\mathcal{L}(t-t_0)}\rho(t_0),$$

for time-independent $\mathcal{L}$ (Breuer and Petruccione, 2002). The Liouville-von Neumann formalism extends the Schrödinger equation to mixed states, making it indispensable for studying open quantum systems and ensembles.

2.2.2 Master Equations

Open quantum systems interact with their environment, leading to non-unitary evolution characterized by the exchange of energy and information between the system and its surroundings. Master equations play a fundamental role in understanding and controlling quantum systems under realistic conditions. These equations are particularly vital for systems subjected to decoherence and dissipation, which are prevalent in quantum technologies. In this section, we focus on the formalism of master equations, starting with the Markovian model, which assumes a memoryless environment, and extending to more general formulations such as the adjoint and stochastic master equations.

2.2.2.1 Markovian Model

An open quantum system $\mathcal{S}$ is typically coupled to an external environment $\mathcal{B}$, such that the Hilbert space of the total system is represented as $\mathcal{H} = \mathcal{H}_{\mathcal{S}} \otimes \mathcal{H}_{\mathcal{B}}$, where $\otimes$ denotes the tensor product. The total Hamiltonian of the combined system can be expressed as

$$H(t) = H_{\mathcal{S}} \otimes I_{\mathcal{B}} + I_{\mathcal{S}} \otimes H_{\mathcal{B}} + \hat{H}_I(t),$$

where $H_{\mathcal{S}}$ and $H_{\mathcal{B}}$ are the system and environment Hamiltonians, respectively, $\hat{H}_I(t)$ describes the interaction between $\mathcal{S}$ and $\mathcal{B}$, and $I_{\mathcal{S}}$ and $I_{\mathcal{B}}$ are the identity operators on the respective Hilbert spaces. Observables[2] associated with $\mathcal{S}$ take the form $A \otimes I_{\mathcal{B}}$, where A is an operator acting on $\mathcal{H}_{\mathcal{S}}$.

[2] In quantum mechanics, an observable is a physical quantity that can be measured, such as position, momentum, energy, or spin. Mathematically, observables are represented by Hermitian operators (self-adjoint operators) acting on a Hilbert space.

The expectation value of an observable A is given by

$$\langle A \rangle = \mathrm{tr}_{\mathcal{S}}\{A\rho_{\mathcal{S}}\},$$

where $\rho_{\mathcal{S}}(t) = \mathrm{tr}_{\mathcal{B}}\rho(t)$ is the reduced density operator of the open system, obtained by tracing out the environmental degrees of freedom, and $\mathrm{tr}_{\mathcal{X}}$ represents the partial trace over the space $\mathcal{X}$. The evolution of $\rho_{\mathcal{S}}$ is described by

$$\frac{d}{dt}\rho_{\mathcal{S}}(t) = -i\mathrm{tr}_{\mathcal{B}}\left[H(t),\rho(t)\right].$$

By assuming negligible memory effects in the environment, the dynamics of $\rho_{\mathcal{S}}$ can be formulated as a quantum dynamical semigroup. This approach is based on the dynamical map $V(t) : \mathcal{S}(\mathcal{H}_{\mathcal{S}}) \to \mathcal{S}(\mathcal{H}_{\mathcal{S}})$, a convex linear completely positive trace-preserving (CPTP) quantum operation describing the state evolution. The map can be represented as

$$V(t)\rho_{\mathcal{S}} = \sum_{\alpha,\beta} W_{\alpha\beta}(t)\rho_{\mathcal{S}}W^{\dagger}_{\alpha\beta}(t),$$

where $W_{\alpha\beta}$ are operators in $\mathcal{H}_{\mathcal{S}}$ satisfying $\sum_{\alpha,\beta} W^{\dagger}_{\alpha\beta}(t)W_{\alpha\beta}(t) = I_{\mathcal{S}}$.

The generator $\mathcal{L}$ of the semigroup generalizes the Liouville superoperator. The semigroup is expressed in exponential form as $V(t) = \exp(\mathcal{L}t)$, leading to the Markovian quantum master equation

$$\frac{d}{dt}\rho_{\mathcal{S}}(t) = \mathcal{L}\rho_{\mathcal{S}}(t),$$

commonly referred to as the Lindblad equation. The standard form of $\mathcal{L}$ for an N-dimensional Hilbert space $\mathcal{H}_{\mathcal{S}}$ is

$$\mathcal{L}\rho_{\mathcal{S}} = -i[H,\rho_{\mathcal{S}}] + \sum_{j,k=1}^{N^2-1} a_{jk}\left(F_j\rho_{\mathcal{S}}F_k^{\dagger} - \frac{1}{2}\{F_k^{\dagger}F_j,\rho_{\mathcal{S}}\}\right),$$

where H is the effective Hamiltonian, F_j are orthonormal operators in the Liouville space, and a_{jk} is a positive semidefinite matrix describing dissipation. The dissipative part is commonly written as

$$\mathcal{D}(\rho_{\mathcal{S}}) = \sum_{l=1}^{N^2-1} \gamma_l\left(A_l\rho_{\mathcal{S}}A_l^{\dagger} - \frac{1}{2}\{A_l^{\dagger}A_l,\rho_{\mathcal{S}}\}\right),$$

where γ_l are relaxation rates, and A_l are Lindblad operators. The master equation is then given by

$$\frac{d}{dt}\rho_{\mathcal{S}}(t) = -i[H,\rho_{\mathcal{S}}(t)] + \mathcal{D}(\rho_{\mathcal{S}}(t)) \tag{2.5}$$

This framework is essential for describing Markovian dynamics, where memory effects are absent. For systems driven by time-dependent fields, the generator $\mathcal{L}(t)$ becomes

explicitly time-dependent, generalizing the Lindblad equation for non-autonomous systems.

2.2.2.2 Adjoint Model

In the theory of quantum dynamical semigroups, the Heisenberg picture is often preferred over the Schrödinger picture for describing operator evolution. For a system operator A in the Hilbert space $\mathcal{H}_S$, its corresponding operator in the Heisenberg picture, $A_H(t)$, can be defined through the relation

$$\mathrm{tr}_S\{AV(t,0)\rho_S\} = \mathrm{tr}_S\left\{\left(V^\dagger(t,0)A\right)\rho_S\right\} = \mathrm{tr}_S\{A_H(t)\rho_S\},$$

where $V(t,0)$ is the dynamical map in the Schrödinger picture, and $V^\dagger(t,0)$ is the adjoint propagator in the Heisenberg picture.

The adjoint propagator $V^\dagger(t,t_0)$ can be expressed as

$$V^\dagger(t,t_0) = T_\rightarrow \exp\left(\int_{t_0}^{t} \mathcal{L}^\dagger(s)\,ds\right),$$

where $T_\rightarrow$ denotes the chronological time-ordering operator, and $\mathcal{L}^\dagger$ is the adjoint generator of the semigroup. The adjoint generator satisfies

$$\mathrm{tr}_S\{A\mathcal{L}(t)\rho_S\} = \mathrm{tr}_S\left\{\left(\mathcal{L}^\dagger(t)A\right)\rho_S\right\}.$$

The time evolution of an operator $A_H(t)$ in the Heisenberg picture is then governed by the adjoint master equation

$$\frac{d}{dt}A_H(t) = V^\dagger(t,0)\left\{\mathcal{L}^\dagger(t)A\right\}.$$

In the special case where the Lindblad generator is time-independent, the adjoint master equation simplifies to

$$\frac{d}{dt}A_H(t) = \mathcal{L}^\dagger A_H(t) \tag{2.6}$$

indicating that the right-hand side of the equation depends only on $A_H(t)$ at the given time. This simplification makes it particularly useful for studying systems with stationary dynamics.

The Heisenberg picture provides a powerful framework for analyzing operator evolution in open quantum systems, particularly in scenarios where the focus is on observables rather than state vectors or density matrices. This approach complements the Schrödinger picture and is widely used in fields such as quantum optics and quantum information theory (Breuer and Petruccione, 2002).

2.2.2.3 Stochastic Master Equation

In feedback control, a quantum system is continuously monitored to extract real-time information, which is then used to dynamically adjust the system Hamiltonian to achieve desired behaviors. The evolution of the quantum state over an infinitesimal time increment dt can be described by the stochastic Schrödinger equation

$$d|\psi\rangle = \left[-\kappa(X - \langle X\rangle)^2 dt + \sqrt{2\kappa}(X - \langle X\rangle) dW\right]|\psi(t)\rangle, \tag{2.7}$$

where X is an observable with expectation value $\langle X\rangle = \mathrm{tr}(X\rho)$, κ is the measurement strength parameter, and dW is a Wiener increment representing stochastic noise.

The measurement record is given by

$$dy(t) = \langle X\rangle dt + \frac{dW}{\sqrt{8\kappa}},$$

and captures the information gained from continuous measurement.

Equation (2.7) can also be reformulated in terms of the density operator, yielding the stochastic master equation

$$d\rho = -\kappa[X,[X,\rho]]dt + \sqrt{2\kappa}(X\rho + \rho X - 2\langle X\rangle\rho)dW. \tag{2.8}$$

This equation describes the conditional evolution of the density matrix ρ, which incorporates information obtained from measurements. Here, all terms must be consistent with the stochastic calculus rule $dW^2 = dt$, and the density matrix evolves as $\rho(t+dt) = \rho(t) + d\rho$.

The stochastic master equation depends on the specific measurement process, and variations of this equation exist for different measurement strategies (Van Handel et al., 2005; Zhang et al., 2012). Notably, the primary distinction between Markovian and non-Markovian systems lies in the presence or absence of memory effects in the environment, which influence the system dynamics.

2.2.2.4 Linear Quantum Stochastic Differential Equation

In the Heisenberg picture, time-dependent operators are often employed to describe quantum dynamics. A class of non-commutative linear stochastic systems can be modeled using the following equations:

$$\begin{aligned} dx(t) &= Ax(t)dt + Bdw(t), \quad x(0) = x_0, \\ dy(t) &= Cx(t)dt + Ddw(t), \end{aligned} \tag{2.9}$$

where A, B, C, and D are real matrices of dimensions $\mathbb{R}^{n\times n}$, $\mathbb{R}^{n\times n_w}$, $\mathbb{R}^{n_y\times n}$, and $\mathbb{R}^{n_y\times n_w}$, respectively. Here: $x(t) = [x_1(t),\ldots,x_n(t)]^T$ represents the state variables, x_0 is the initial

state vector, $w(t)$ represents the input signals and admits the decomposition $dw(t) = \beta_w(t)dt + d\tilde{w}(t)$, $\beta_w(t)$ is a self-adjoint adapted process, and $\tilde{w}(t)$ is a vector of self-adjoint quantum noises. The noise components $\tilde{w}(t)$ satisfy

$$d\tilde{w}(t)d\tilde{w}^T(t) = F_{\tilde{w}}dt,$$

where $F_{\tilde{w}}$ is a non-negative Hermitian matrix (Attal, 2006).

To ensure physical realizability, additional constraints must be imposed on the matrices A, B, C, and D. These constraints depend on the system under consideration and the specific structure of the quantum noise processes. Linear quantum stochastic differential equations are particularly useful in quantum optics and quantum information, where they describe the evolution of open quantum systems interacting with classical and quantum noise sources.

2.3 Concluding Remarks and Discussions

Quantum control focuses on designing efficient methods to manipulate quantum systems and achieve desired behaviors in accordance with the principles of quantum mechanics. In this chapter, we have reviewed key aspects of quantum control theory, including quantum system modeling, open- and closed-loop control strategies, and robust control approaches.

Open-loop control, often straightforward to implement, has demonstrated success in numerous applications. However, when open-loop methods are insufficient, closed-loop quantum control (that can provide adaptive solutions by incorporating real-time feedback. The effectiveness of closed-loop control has been validated in several experimental studies. Feedback control, a cornerstone of classical control systems, faces unique challenges in quantum systems, such as measurement-induced disturbances and time delays. Despite these hurdles, feedback control has shown promise for enhancing quantum control strategies. Robust control methods, essential for addressing uncertainties and environmental disturbances in quantum systems, is also important in practical quantum technologies.

While progress in quantum control has enabled the manipulation of some quantum systems, there remains significant room for development. Continued advancements in this field are essential to extend control capabilities to a broader range of quantum systems. This progress will require interdisciplinary collaboration among experts in control engineering, quantum physics, artificial intelligence, computer science, physical chemistry, and atomic physics, among others.

Chapter 3

Optimal Control of Quantum Systems

In this chapter, we explore various approaches to quantum optimal control, focusing on methods to improve the performance and efficiency of quantum state transformations. The research begins by reviewing the Pontryagin Minimum (or Maximum) Principle (PMP), a key tool for deriving necessary conditions for optimality in quantum systems. By applying PMP to a two-level quantum system, we demonstrate how optimal control strategies can be formulated and implemented to achieve desired outcomes.

We then extend this framework to address a quantum optimal control problem, where the goal is to steer a quantum system from an initial state to a target state using Liouville-Von Neumann dynamics. In this context, we introduce a cost functional that balances the dual objectives of maximizing fidelity and minimizing energy consumption. A computational scheme based on PMP is developed to solve this problem, with an application to the control of a spin particle in a magnetic field, illustrating the efficacy of this approach.

Finally, we consider a more complex scenario involving a multi-level quantum system under the influence of decoherence. In this case, the objective is to minimize energy while maintaining quantum coherence within pre-defined bounds. The problem is formulated as an optimal control problem with state constraints, and the necessary optimality conditions are derived using PMP in Gamkrelidze's form. These conditions provide a comprehensive framework for calculating the optimal control strategy in systems affected by decoherence.

This combined study highlights the versatility of PMP-based methods in addressing a wide range of quantum control challenges, from simple two-level systems to more complex, constrained environments, contributing to advancements in quantum state manipulation and optimization. The main contents of this chapter were published in (Dehaghani and Pereira, 2022b,a; Dehaghani et al., 2022b; Dehaghani and Aguiar, 2023b; Dehaghani et al., 2024d).

3.1 The Minimum Principle of Pontryagin

Optimal control theory extends the classical calculus of variations to problems subject to dynamical constraints, often involving closed velocity sets (Liberzon, 2011). A cornerstone of this theory is the PMP (Pontryagin et al., 1964), which provides necessary conditions for optimality. An optimal control problem in its general form can be stated as follows: Consider a control system (or dynamical constraint) given by

$$\dot{x} = f(x(t), u(t), t), \quad x(0) = x_0, \quad t \in [0, T] \tag{3.1}$$

where $x(t) = (x_1, x_2, \ldots, x_n) \in \mathbb{R}^n$ is the state vector and $u(t) \in U \subseteq \mathbb{R}^m$ is the control signal, with U being the set of admissible controls, determine a state-control pair trajectory $(x(t), u(t))$, such that the dynamical constraint (3.1) is satisfied, while minimizing a given cost functional $\mathcal{J} : \mathbb{R}^n \times U \to \mathbb{R}$ (d'Alessandro, 2021). For a system with state vector $x(t)$ influenced by control function $u(t)$ over the time interval $t \in [0, T]$, the cost functional $\mathcal{J}$ in the Bolza form is expressed as

$$\mathcal{J} = \phi(x(T), T) + \int_0^T L(x(t), u(t), t)\, dt, \tag{3.2}$$

where ϕ and L are smooth functions. Specifically, $\phi : \mathbb{R}^n \times \mathbb{R} \to \mathbb{R}$ represents the terminal cost, depending only on the final state $x(T)$ and terminal time T, and $L : \mathbb{R}^n \times \mathbb{R}^m \times \mathbb{R} \to \mathbb{R}$ denotes the running cost, which depends on the entire trajectory $x(t)$, control $u(t)$, and time t.

Assuming that the problem is well-posed (all the regularity conditions for the dynamical constraint and the cost functional holds), let $(x^\star(t), u^\star(t))$ be an optimal state-control pair. Hence, the Pontryagin-Hamilton function, involving the time-varying Lagrange multiplier vector $\lambda(t)$, also denoted by adjoint vector or co-state, is written as

$$\mathcal{H}(x(t), u(t), \lambda(t), t) = \lambda^T(t) f(x(t), u(t), t) + L(x(t), u(t), t).$$

The necessary conditions of optimality in the form of a PMP entail that the minimum condition

$$\mathcal{H}(x^*, u^*, \lambda^*, t) \leq \mathcal{H}(x, u, \lambda, t), \quad \forall u \in U$$

holds and the costate differential equation with its transversality condition, which in this case involves only the terminal condition, satisfies

$$\dot{\lambda}^T(t) = -\mathcal{H}_x(x^*(t), u^*(t), \lambda(t), t),$$

$$\lambda^T(T) = \phi_x^T(x(T)),$$

where $\mathcal{H}_x$ denotes the partial derivative of $\mathcal{H}$ with respect to x. In the case of free final

state problems, that is, the final state $x(T)$ is not fixed, there is an additional transversality condition:

$$\left.\frac{\partial \phi(x,T)}{\partial T}\right|_{x=x(T)} + \mathcal{H}(x(T),u^*(T),\lambda(T),T) = 0.$$

3.2 Schrödinger Dynamics and Control via Pontryagin's Principle

The state of quantum systems can be described using a pure state vector, a density operator, or the evolution operator. For simplicity, we consider the pure quantum state ψ, whose dynamics are governed by the Schrödinger equation

$$\hbar \frac{d}{dt}\psi = -iH(u)\psi, \tag{3.3}$$

where $\psi = \psi_R + i\psi_I$ is a column vector corresponding to $|\psi\rangle$ in a given basis, as described in the Dirac representation (Dirac, 1981). Here, ψ_R and ψ_I represent real vectors, and the Hamiltonian is decomposed as

$$-iH(u) = R(u) + iI(u),$$

where $R(u)$ and $I(u)$ are real-valued $n \times n$ matrices. Specifically, $R(u)$ is skew-symmetric, and $I(u)$ is symmetric. For simplicity, we consider the reduced Planck constant, $\hbar$, to be unitary.

It is important to note that the quantum mechanical Hamiltonian in the Schrödinger equation is distinct from the Pontryagin-Hamilton function. Using this formulation, the dynamics can be rewritten as the following real-valued differential equations:

$$\frac{d}{dt}\psi_R = R(u)\psi_R - I(u)\psi_I,$$

$$\frac{d}{dt}\psi_I = I(u)\psi_R + R(u)\psi_I,$$

which can be expressed in matrix form as

$$\dot{x} = \tilde{H}(u)x, \tag{3.4}$$

where

$$x := \left[\psi_R^T, \psi_I^T\right]^T, \tag{3.5}$$

and

$$\tilde{H}(u) = \begin{bmatrix} R(u) & -I(u) \\ I(u) & R(u) \end{bmatrix}.$$

The general cost functional described in (3.2) is reformulated using appropriately defined functions $\tilde{\Phi}$ and $\tilde{L}$ as

$$J := \tilde{\Phi}(x(T), T) + \int_0^T \tilde{L}(x(t), u(t), t)\, dt. \tag{3.6}$$

Using Pontryagin's Minimum Principle, the Pontryagin-Hamilton function is written as

$$\mathcal{H}(\lambda, x, u) = \lambda^T \tilde{H}(u)x + \tilde{L}(x, u), \tag{3.7}$$

and must satisfy the minimum condition

$$\mathcal{H}(\lambda, x^*, u^*) \leq \mathcal{H}(\lambda, x, u), \quad \forall u \in U, \tag{3.8}$$

for all admissible λ, x, and u.

The adjoint equation is derived as

$$\dot{\lambda}^T = -\lambda^T \tilde{H}(u) + \tilde{L}_x,$$

and, since $\tilde{H}(u)$ is skew-symmetric, this can be rewritten in its transposed form as:

$$\dot{\lambda} = \tilde{H}(u)\lambda + \tilde{L}_x^T. \tag{3.9}$$

The boundary condition for the adjoint variable is:

$$\lambda(T) = \frac{\partial \tilde{\Phi}^T(x(T))}{\partial x} \tag{3.10}$$

3.2.1 Pontryagin's Principle in the Control of Spin Systems

By means of the PMP, we can transform an infinite dimensional optimization problem into a finite dimensional one, which means that the search over a set of functions is replaced by the search for a set of parameters in a finite dimensional space. The optimal control problem for two-level quantum systems has been studied in (D'alessandro and Dahleh, 2001) and generalized to n-level quantum systems in (Boscain and Charlot, 2004). Here, we review the problem, and consider a single spin particle

$$\vec{S} := \frac{1}{2}\{\sigma_x, \sigma_y, \sigma_z\},$$

with σ_x, σ_y, and σ_z being the so-called Pauli matrices. Spin is an intrinsic property of fundamental particles in quantum mechanics, and a spin-$\frac{1}{2}$ shows that the particle has to be rotated by two full turns before getting to the initial configuration. In nuclear magnetic resonance (NMR) analysis, a spin-$\frac{1}{2}$ is typically controlled through interacting with an

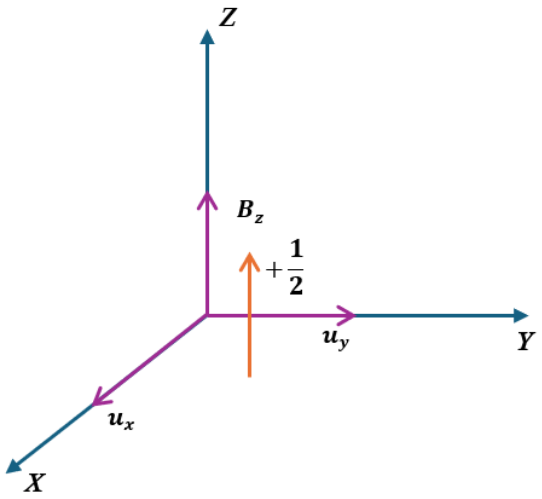


Figure 3.1: Spin-$\frac{1}{2}$ controlled by an electromagnetic field in NMR experiments.

electromagnetic field

$$\vec{B} := \{B_x, B_y, B_z\},$$

which is supposed to vary in time while being constant in space. Two components of the field, usually B_x and B_y, are considered to vary in time so that they can change the spin's direction, and the B_z component is considered time invariant, (See Figure 3.1). The quantum mechanical Hamiltonian is a Hermitian matrix function that is time dependent through controls $u_k(t) \in R$, and thus it can be expressed as

$$H(u) = H_0 + \sum_k H_k u_k(t) \tag{3.11}$$

in which H_0 and H_k are called drift and control Hamiltonians, respectively. By setting the components of the magnetic field as controls, and also by scaling the magnetic field and time, the dynamics of the system indicated in (3.3) is expressed as

$$\frac{d}{dt}|\psi\rangle = \frac{1}{2}\left(\bar{\sigma}_z u_z + \bar{\sigma}_x u_x(t) + \bar{\sigma}_y u_y(t)\right)|\psi\rangle \tag{3.12}$$

in which the matrices $\bar{\sigma}_{x,y,z}$ are the multiples of Pauli matrices spanning the Lie algebra $su(2)$, defined as

$$\bar{\sigma}_x = \begin{pmatrix} 0 & i \\ i & 0 \end{pmatrix}, \quad \bar{\sigma}_y = \begin{pmatrix} 0 & -1 \\ 1 & 0 \end{pmatrix}, \quad \bar{\sigma}_z = \begin{pmatrix} i & 0 \\ 0 & -i \end{pmatrix}$$

with the commutator bracket satisfying

$$[\bar{\sigma}_z, \bar{\sigma}_x] = 2\bar{\sigma}_y, \quad [\bar{\sigma}_x, \bar{\sigma}_y] = 2\bar{\sigma}_z, \quad [\bar{\sigma}_y, \bar{\sigma}_z] = 2\bar{\sigma}_x.$$

Following the same procedure explained in the Section 3.2, we can obtain a Lie algebra isomorphism mapping $\bar{\sigma}_x \leftrightarrow \tilde{H}_x(u)$, $\bar{\sigma}_y \leftrightarrow \tilde{H}_y(u)$, $\bar{\sigma}_z \leftrightarrow \tilde{H}_z(u)$ as follows:

$$\bar{\sigma}_x = \begin{pmatrix} 0 & i \\ i & 0 \end{pmatrix} = \begin{pmatrix} 0 & 0 \\ 0 & 0 \end{pmatrix} + i \begin{pmatrix} 0 & 1 \\ 1 & 0 \end{pmatrix} \rightarrow \tilde{H}_x = \begin{pmatrix} 0 & 0 & 0 & -1 \\ 0 & 0 & -1 & 0 \\ 0 & 1 & 0 & 0 \\ 1 & 0 & 0 & 0 \end{pmatrix}$$

$$\bar{\sigma}_y = \begin{pmatrix} 0 & -1 \\ 1 & 0 \end{pmatrix} = \begin{pmatrix} 0 & -1 \\ 1 & 0 \end{pmatrix} + i \begin{pmatrix} 0 & 0 \\ 0 & 0 \end{pmatrix} \rightarrow \tilde{H}_y = \begin{pmatrix} 0 & -1 & 0 & 0 \\ 1 & 0 & 0 & 0 \\ 0 & 0 & 0 & -1 \\ 0 & 0 & 1 & 0 \end{pmatrix}$$

$$\bar{\sigma}_z = \begin{pmatrix} i & 0 \\ 0 & -i \end{pmatrix} = \begin{pmatrix} 0 & 0 \\ 0 & 0 \end{pmatrix} + i \begin{pmatrix} 1 & 0 \\ 0 & -1 \end{pmatrix} \rightarrow \tilde{H}_z = \begin{pmatrix} 0 & 0 & -1 & 0 \\ 0 & 0 & 0 & 1 \\ 1 & 0 & 0 & 0 \\ 0 & -1 & 0 & 0 \end{pmatrix}$$

satisfying the commutation relations

$$[\tilde{H}_x, \tilde{H}_y] = 2\tilde{H}_z, \quad [\tilde{H}_y, \tilde{H}_z] = 2\tilde{H}_x, \quad [\tilde{H}_z, \tilde{H}_x] = 2\tilde{H}_y.$$

Hence, the problem transformation to a real one, and also considering (3.5) and dynamics (3.4) results in the following dynamics

$$\dot{x} = \frac{1}{2}\left(\tilde{H}_z u_z + \tilde{H}_x u_x(t) + \tilde{H}_y u_y(t)\right) x. \tag{3.13}$$

Depending on the problem, we may choose different performance functionals. For instance, we may intend to minimize the energy of the laser electric field in the interval $[0, T]$ used in controlling the quantum system, i.e., $k\int_0^T u^2(t)\,dt$ for some constant $k > 0$. In some cases, it is very important that the control function drives the state of the system towards a desired target state at time T. In this case, it is of interest to maximize the overlap of the desired state $|\psi_f\rangle$ with the final state $|\psi(T)\rangle$, i.e., $(\psi^\dagger(T)\psi_f)$, which is called fidelity for pure quantum states. Moreover, the cost functional may also be a composition of these if it is of interest to choose a trade-off between two distinct goals which, may, for example, transfer the state of the system to some desired target state, while also minimizing the energy of the applied control field. In this case, the cost functional will have the form

$$\mathcal{J}(u_x, u_y) = -\mathrm{Re}(\psi^\dagger(T)\psi_f) + k\int_0^T \left(u_x^2(t) + u_y^2(t)\right) dt. \tag{3.14}$$

By considering (3.5), we can reformulate the cost (3.14) as

$$\mathcal{J}(u_x, u_y) = -x^T(T)x_f + k\int_0^T \left(u_x^2(t) + u_y^2(t)\right) dt. \tag{3.15}$$

From (3.15), the Pontryagin Hamilton function (3.7) is then expressed as

$$\mathcal{H} = \frac{1}{2}\lambda^T \left(\tilde{H}_z u_z + \tilde{H}_x u_x(t) + \tilde{H}_y u_y(t)\right) x + k(u_x^2(t) + u_y^2(t)). \tag{3.16}$$

Now, we can apply the necessary conditions for optimality in the form of the PMP. For this problem, since the running cost functional is not dependent on x, the adjoint equation turns out to have the same form as the state equation,

$$\dot{\lambda} = \frac{1}{2}\left(\tilde{H}_z u_z + \tilde{H}_x u_x(t) + \tilde{H}_y u_y(t)\right)\lambda. \tag{3.17}$$

To obtain the form of the optimal controls, PMP implies that $u^* = \arg\min \mathcal{H}(t, x^*, u, \lambda)$, so

$$\frac{\partial \mathcal{H}}{\partial u_x} = 0 \implies \frac{1}{2}\lambda^T \tilde{H}_x x - 2k u_x(t) = 0 \implies u_x = \frac{1}{4k}\lambda^T \tilde{H}_x x, \tag{3.18}$$

$$\frac{\partial \mathcal{H}}{\partial u_y} = 0 \implies \frac{1}{2}\lambda^T \tilde{H}_y x - 2k u_y(t) = 0 \implies u_y = \frac{1}{4k}\lambda^T \tilde{H}_y x. \tag{3.19}$$

We can replace u_x and u_y obtained from (3.18) and (3.19) in both state and costate equations, and then, solve the obtained two-point boundary value problem. However, when the controls are differentiable functions, we can also take the derivatives of the controls, and then, by means of state and costate equations and also the commutation relations, try to obtain the form of optimal controls. By differentiating the controls, we have

$$\dot{u}_x = \frac{1}{4k}\left(\lambda^T \tilde{H}_z x u_y - u_z u_y\right), \tag{3.20}$$

$$\dot{u}_y = \frac{1}{4k}\left(-\lambda^T \tilde{H}_z x u_x + u_z u_x\right). \tag{3.21}$$

Obviously, from (3.20) and (3.21), we can write

$$\dot{u}_x = \alpha u_y, \quad \dot{u}_y = -\alpha u_x \tag{3.22}$$

where $\alpha = \frac{1}{4k}\left(\lambda^T \tilde{H}_z x - u_z\right)$, so we can conclude the form of controls are sinusoidal functions

$$u_x(t) = M\cos(\omega t + \gamma), \quad u_y(t) = M\sin(\omega t + \gamma) \tag{3.23}$$

for which we can obtain the optimal values of M, ω, and γ by substituting the controls and solving the differential equations. These two controls form the controlling components of the electromagnetic field used in NMR experiments.

3.2.2 Existence of the Optimal Control

Since we rely on the necessary optimality conditions, it is essential also to address the problem of existence of the optimal control. There are already some standard results, well explained in (Fleming and Rishel, 2012, Chapter III), that are applicable to the case considered in our work. According to (Fleming and Rishel, 2012), the existence theorem guarantee the existence of an optimal control in the Lebesgue Integrable (LI) set if a control steering a given initial state to a desired target state exists. The control functions $u_k(t)$ in (3.4) are supposed to be LI as well. We also will suppose in this chapter that the optimal controls are in the set LI, according to the above-mentioned theorem. In order to guarantee the existence of a control, one needs to address the question of controllability. The controllability concerns the possibility of steering the system from one state to another for every pair of states.

The complex sphere $\mathbb{S}^{2N-1} \subset \mathbb{H}$, representing the pure quantum states, is a homogeneous space of the Lie group $\mathbb{U}(N) = \left\{U \in GL(N,\mathbb{C}) \,\middle|\, UU^\dagger = U^\dagger U = I\right\}$, and its proper subgroup $\mathbb{SU}(N) = U(N)/U(1)$. The Lie algebras of $\mathbb{U}(N)$ and $\mathbb{SU}(N)$ are

$$\mathfrak{u}(N) = \left\{A \in \mathbb{C}^{N\times N} \,\middle|\, A^\dagger = -A\right\}$$

and

$$\mathfrak{su}(N) = \{A \in u(N) \,|\, \mathrm{Tr}(A) = 0\},$$

respectively. The Schrödinger equation stated in (3.3) can be lifted to the Lie group $\mathbb{SU}(N)$ to obtain the Schrödinger equation for the unitary propagator as

$$i\frac{d}{dt}U(t) = \left(H_0 + \sum_{k=1}^{m} u_k(t) H_k\right) U(t), \quad U(0) = I \tag{3.24}$$

where $U \in \mathbb{SU}(N)$, and $|\psi(t)\rangle = U(t)|\psi_0\rangle$. Equation (3.24) is a right invariant control system on the compact Lie group $\mathfrak{su}(n)$, so

$$Lie\{iH_0, \ldots, iH_m\} = \mathfrak{su}(n) \tag{3.25}$$

where $Lie\{\cdot\}$ denotes the Lie algebra generated by the set of matrices inside the curly braces. Note that the condition (3.25) represents a necessary and sufficient condition for the controllability of the system indicated in (3.24) (Boothby and Wilson, 1979). The controllability of a right invariant system results in the controllability of bilinear systems (Sachkov, 1997). Therefore, if the evolution operator of the system satisfies a controllable equation, then the bilinear system described by the certain quantum-mechanical Hamiltonian $H(u(t))$ is controllable as well, so it is possible to design controls to steer the bilinear system from one state to another state in the state-space. Consequently, the system indicated in (3.3) is controllable provided that (3.25) holds, which is the case for

the indicated two-level quantum systems. For more details, see (D'Alessandro, 2000).

3.3 From Schrödinger to Liouville-von Neumann equation

In non-relativistic quantum mechanics, the time evolution of a quantum system can be described either by the Schrödinger equation or the Liouville-von Neumann equation, and both formulations provide equivalent predictions for physical observables (Dehaghani et al., 2022a). Every state vector $|\psi_j(t)\rangle$ at time t can be obtained by $|\psi_j(t)\rangle = U(t)|\psi_j(0)\rangle$ in which $U(t)$ is the solution of (3.24) expressed as $U(t) = \exp\left(-i\int_0^t H(s)\,ds\right)$ called Dyson's series in the physics context and is similar to a Volterra series in control theory (Altafini and Ticozzi, 2012). Hence, the outer product $|\psi_j(t)\rangle\langle\psi_j(t)|$ results in

$$|\psi_j(t)\rangle\langle\psi_j(t)| = U(t)|\psi_j(0)\rangle\langle\psi_j(0)|U^\dagger(t)$$

and the same for any convex sum of $|\psi_j(t)\rangle\langle\psi_j(t)|$. More precisely, let p_j be the fraction of population of an ensemble $\{p_j, |\psi_j(t)\rangle\}$, so the corresponding quantum density operator is expressed as

$$\rho = \sum_j p_j |\psi_j\rangle\langle\psi_j|, \quad p_j \geq 0, \quad \sum_j p_j = 1 \tag{3.26}$$

which belongs to the set of Hermitian, semi definite, and positive matrices with trace equal to one on the system's Hilbert space $\mathbb{H}$. Hence, we can rewrite (3.26) as

$$\rho(t) = U(t)\rho(0)U^\dagger(t) \tag{3.27}$$

The infinitesimal version of (3.27) is the quantum Liouville-von Neumann equation, (Berman and Kosloff, 1991), expressed by

$$\dot{\rho}(t) = -i[H(u(t)), \rho(t)], \quad \rho(0) = \rho_0 \tag{3.28}$$

3.4 Quantum Optimal Control with Bounded Input Constraints

In this section, we address a bounded-input optimal control problem pertaining to the transformation of quantum states. Our objective is to steer a quantum system from an initial state to a desired target state while adhering to the principles of the Liouville-von Neumann equation. To achieve this, we introduce a cost functional that balances

the dual goals of fidelity[1] maximization and energy consumption minimization. We derive optimality conditions in the form of Pontryagin's Minimum Principle (PMP) for the matrix-valued dynamics associated with this problem. Subsequently, we present a time-discretized computational scheme designed to solve the optimal control problem. This computational scheme is rooted in an indirect method grounded in the PMP. To illustrate the practicality and applicability of our methodology, we consider the case of a spin-$\frac{1}{2}$ particle subjected to interaction with a magnetic field.

In optimal control of quantum state transfer problems, a possible cost to be minimized involves a trade-off between maximizing fidelity to signify a security level for quantum state transformation and minimizing the energy of the control field. Motivated by this consideration, we propose the following bounded-control optimal control problem (P_1):

$$(P_1)\begin{cases} \min\limits_{u}\left\{J=-\mathcal{F}(\rho(T),\sigma)+\eta\int\limits_0^T u^T(t)u(t)dt\right\}, \quad t\in[0,T], \quad \eta\in[0,1], \\ \text{subject to:} \\ \textit{Dynamics: } \dot{\rho}(t)=-i\left[H\left(u\left(t\right)\right),\rho\left(t\right)\right], \quad \text{a.e. } t\in[0,T], \quad \rho(t)\in\mathbb{C}^{n\times n}, \\ \textit{Initial Condition: } \rho(0)=\rho_0, \\ \textit{Control Constraint: } u(t)\in\mathcal{U}:=\left\{u(t)\in\Omega\subset\mathbb{R}^2\right\}, \end{cases}$$

where the coefficient $\eta\geq 0$ signifies the importance of energy minimization. The density operator $\rho(t)\in\mathbb{C}^{n\times n}$ represents the quantum state variable, evolving according to the Liouville-von Neumann equation (3.28), and ρ_0 denotes the initial quantum state. The set of admissible controls Ω is defined as

$$\Omega=\left\{u=\begin{bmatrix}u_x(t) & u_y(t)\end{bmatrix}:|u_x(t)|\leq u_{\max},|u_y(t)|\leq u_{\max}\right\},$$

where $u_{\max}$ is a given positive parameter.

In (P_1), the fidelity functional is defined using the well-established Uhlmann-Jozsa criterion, which captures the maximal transition probability between the purification of a pair of density matrices. For the final quantum state $\rho(T)$ and the target state σ, fidelity is given by

$$\mathcal{F}\left(\rho(T),\sigma\right):=\left(\operatorname{Tr}\sqrt{\sqrt{\rho(T)}\sigma\sqrt{\rho(T)}}\right)^2. \tag{3.29}$$

Given the formulation of the optimal control problem, we will now proceed in the next section to derive the necessary conditions for optimality.

[1] In quantum mechanics, fidelity is a measure of the closeness or similarity between two quantum states. Fidelity values range from 0 to 1, where 0 indicates that the states are orthogonal (completely different), and 1 indicates that the states are identical.

3.4.1 Necessary Conditions of Optimality for the Matrix-Valued Dynamics

The Pontryagin-Hamilton function $\mathcal{H}$ is defined for almost all $t \in [0,T]$ by introducing the matrix-valued time-varying multiplier Λ, designated as the costate or adjoint variable of the system (Dehaghani and Pereira, 2022a). Thus, the Pontryagin-Hamiltonian is expressed as

$$\mathcal{H}(\rho,u,\Lambda) = \mathrm{Tr}\left(\Lambda^{\dagger} F(\rho,u)\right) + L(u(t)),$$

where $L(u(t))$ represents the running cost.

According to Pontryagin's Minimum Principle, for the optimal state trajectory $\rho^*(t)$ and the corresponding adjoint variable $\Lambda(t)$, the optimal control $u^*(t)$ minimizes the Pontryagin-Hamiltonian function $\mathcal{H}$ for almost all $t \in [0,T]$ and all admissible control values $\mathbf{u} \in \Omega$, that is,

$$\mathcal{H}(\rho^*(t),u^*(t),\Lambda(t)) \leq \mathcal{H}(\rho(t),u(t),\Lambda(t)).$$

The adjoint equation is derived as

$$-\dot{\Lambda}^{\dagger}(t) = \frac{\partial \mathcal{H}(\rho^*(t),u^*(t),\Lambda(t))}{\partial \rho} = i\left[H(u^*(t)),\Lambda^{\dagger}(t)\right], \tag{3.30}$$

where $H^*(t)$ denotes the quantum mechanical Hamiltonian evaluated at each time along the optimal control u^*. Equation (3.30) has the formal solution

$$\Lambda^{\dagger}(t) = e^{i\int_t^T H^*(s)ds}\Lambda^{\dagger}(T)e^{-i\int_t^T H^*(s)ds}.$$

The boundary condition at the final time for the adjoint variable is determined by

$$\Lambda^{\dagger}(T) = \frac{-\partial \mathcal{F}(\rho(T),\sigma)}{\partial \rho(T)}, \tag{3.31}$$

3.4.2 Bounded-Control Iterative Adjoint-State Shooting Algorithm

In this section, we solve the bounded-control optimal control problem defined in (P_1) using an indirect method based on Pontryagin's Minimum Principle (PMP). The proposed algorithm discretizes the time interval $[0,T]$ into N subintervals, such that $t_k = \frac{kT}{N}$ for $k = 0,\ldots,N-1$. The iteration counter is denoted by $j = 0,1,\ldots$. Hence, the j^{th} iteration of a function f at time t_k is represented as f_k^j.

To solve the optimal control problem, both the system dynamics and the adjoint equation are approximated using a first-order Euler method. The algorithm iteratively refines the control and state trajectories to satisfy the optimality conditions derived from PMP. The steps of the proposed algorithm are described in Algorithm 3.1.

Algorithm 3.1 Iterative Adjoint-State Shooting Algorithm with Bounded Control.

Step 1 - Initialization:
Initialize the values of $\mathrm{u}_{x_k^j}$ and $\mathrm{u}_{y_k^j}$ for $k = 0, \ldots, N-1$, and set $j = 1$.
Step 2 - Computation of the State Trajectory:
for $k = 0$ to $N-1$ **do**
    Compute $U_k^j = e^{\sum_{l=0}^{k-1} \frac{T}{N} \tilde{H}_l^j}$
    Obtain $\rho_k^j = U_k^j \rho_0^j U_k^{j\dagger}$
end for
Step 3 - Computation of the Adjoint Trajectory:
Compute Λ_N^j using ρ_N^j computed in Step 2.
for $k = 0$ to $N-1$ **do**
    Compute $V_k^j = e^{\sum_{k}^{N-1} \frac{T}{N} \tilde{H}_k^j}$
    Obtain $\Lambda_k^{j\dagger} = V_k^{j\dagger} \Lambda_N^{j\dagger} V_k^j$
end for
Step 4 - Computation of the Pontryagin Hamilton Function:
for $k = 0$ to $N-1$ **do**
    Let $\mathcal{H}_k^j(u_k^j) = \mathrm{Tr}\left({\Lambda_k^j}^{\dagger} F_k^j(\rho_k^j, u_k^j) \right) + L_k^j$
end for
Step 5 - Computation of the Control Function:
for $k = 0$ to $N-1$ **do**
    Compute temporary control values $\mathrm{u}_{\mathrm{temp},x_k^j}$ and $\mathrm{u}_{\mathrm{temp},y_k^j}$ that mainimize the map
    $(u_x, u_y) \to \mathcal{H}_k^j(u_x, u_y)$
end for
Step 6 - Apply the Control Constraints:
for $k = 0$ to $N-1$ **do**
    $\mathrm{u}_{x_k^j} = \min(|\mathrm{u}_{\mathrm{temp},x_k^j}|, u_{\max}) \cdot \mathrm{sign}(\mathrm{u}_{\mathrm{temp},x_k^j})$
    $\mathrm{u}_{y_k^j} = \min(|\mathrm{u}_{\mathrm{temp},y_k^j}|, u_{\max}) \cdot \mathrm{sign}(\mathrm{u}_{\mathrm{temp},y_k^j})$
end for
Step 7 - Stopping Test:
For a determined tolerance error $\varepsilon > 0$, check if:
$\max_{k=0,\ldots,N-1}\{|\mathrm{u}_{x_k^j} - \mathrm{u}_{x_k^{j-1}}|\} < \varepsilon$
$\max_{k=0,\ldots,N-1}\{|\mathrm{u}_{y_k^j} - \mathrm{u}_{y_k^{j-1}}|\} < \varepsilon$
if convergence criteria met **then**
    Let $\mathrm{u}_{x^*(t_k)} = \mathrm{u}_{x_k^j}$ and $\mathrm{u}_{y^*(t_k)} = \mathrm{u}_{y_k^j}$ for $k = 0, \ldots, N-1$, and exit the algorithm.
else
    Update temporary control values:
    $\mathrm{u}_{\mathrm{temp},x_k^j} = \mathrm{u}_{x_k^{j-1}} + \delta(\mathrm{u}_{x_k^j} - \mathrm{u}_{x_k^{j-1}})$
    $\mathrm{u}_{\mathrm{temp},y_k^j} = \mathrm{u}_{y_k^{j-1}} + \delta(\mathrm{u}_{y_k^j} - \mathrm{u}_{y_k^{j-1}})$
    Check the control constraints according to **Step 6**.
    Increment j: $j = j + 1$, and go to **Step 2**.
end if

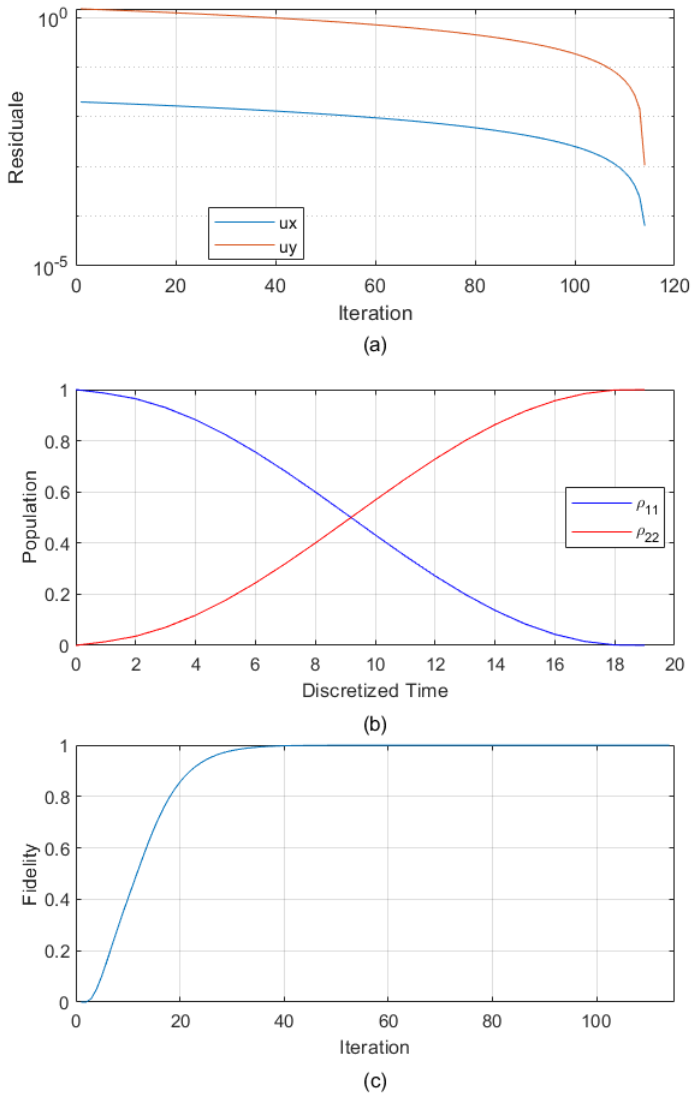


Figure 3.2: (a) Convergence plot of residuals shows the algorithm converges after 114 iterations. (b) Evolution of diagonal elements of the State trajectory at final iteration over the discretized time. (c) State transition probability.

3.4.3 Numerical Implementation

Consider the quantum state transfer problem given the initial state $\rho_0 = \left(\begin{smallmatrix} 1 & 0 \\ 0 & 0 \end{smallmatrix}\right)$ and the desired target state $\sigma = \left(\begin{smallmatrix} 0 & 0 \\ 0 & 1 \end{smallmatrix}\right)$. By means of implementing the algorithm explained in the previous section, we solve the quantum state transfer problem P_1 to drive the given initial quantum state to a desired set while simultaneously minimizing the required control energy with the factor $\eta = 0.01$. In this simulation, the control is constrained to $u_x, u_y \in [-1,1]$, and the algorithm has been considered to evolve in $t \in [0,1]$ to accomplish the desired fidelity. The control signal in z direction is considered constant as $u_z = 0.001$, and in x and y directions is initialized by $u_{x_k}^j = 0$ and $u_{y_k}^j = 0$ for $k = 0, \ldots, N-1$. By setting the time-slicing $N = 20$, the learning coefficient $\delta = 0.1$, and the stopping threshold $\varepsilon = 10^{-3}$, the algorithm converges after 114 iterations. The residual graph showing the convergence of the algorithm is displayed in Fig. 3.2(a). In Fig. 3.2(b), the evolution of the diagonal elements of the density matrix during the time in the last iteration is presented. As seen, a smooth evolution targeting the desired state is obtained at the final iteration. The density matrix has unit trace and is Hermitian during its evolution over the time. The resulted final state is $\rho(T) = \left(\begin{smallmatrix} 0.0005 & 0.0157 + 0.0145\mathrm{i} \\ 0.0157 - 0.0145\mathrm{i} & 0.9995 \end{smallmatrix}\right)$.

The fidelity evolution, as depicted in Fig. 3.2(c), reveals a rapid ascent, surpassing 99.8 percent within a mere 44 iterations. Impressively, the optimization persists, consistently pushing the fidelity beyond the 99.9 percent mark. This sustained upward trend serves as compelling evidence for the algorithm's proficiency in efficiently optimizing the combined fidelity and control power aspects of the system dynamics. The achieved high fidelity values underscore the algorithm's efficacy in striking a harmonious balance between precision and resource optimization in steering the quantum system toward the specified target state

3.5 State-Constrained Optimal Control for Coherence Preservation in Multi-Level Open Quantum Systems

In this section, we focus on the problem of preserving the coherence of a multi-level quantum system subjected to Markovian decoherence in a minimum energy optimal control problem. We explore the dynamics of the system's density matrix, which governs both the population of states and the off-diagonal coherence elements. Using the Lindblad formalism, we model the non-unitary evolution of a multi-level quantum system and investigate how control fields can be applied to counteract decoherence.

The main contributions of this part are twofold: (1) we develop a minimum energy optimal control strategy while preserving coherence, and (2) we implement state constraints to ensure the system's coherence remains within specified bounds throughout the evolution. By applying Pontryagin's Minimum Principle in Gamkrelidze form, we derive the necessary conditions for the optimal control, taking into account both the

Hamiltonian evolution and the dissipative effects of the environment. Numerical simulations, given for a qutrit system with three energy levels, demonstrate the feasibility of this approach in maintaining coherence, providing insight into the control mechanisms necessary to mitigate decoherence in realistic quantum systems.

3.5.1 Density Matrix Dynamics and Coherence in Multi-Level Systems

The state of an N-level quantum system is represented by a density matrix ρ of size $N \times N$, where N is the number of quantum levels. The general form of the density matrix ρ is

$$\rho = \begin{pmatrix} \rho_{11} & \rho_{12} & \cdots & \rho_{1N} \\ \rho_{21} & \rho_{22} & \cdots & \rho_{2N} \\ \vdots & \vdots & \ddots & \vdots \\ \rho_{N1} & \rho_{N2} & \cdots & \rho_{NN} \end{pmatrix}.$$

The set of density operators for an N-level quantum system, denoted by $\mathcal{D} \subset \mathbb{C}^{N\times N}$, is the set of all matrices ρ that satisfy

$$\mathcal{D} = \left\{ \rho \in \mathbb{C}^{N\times N} : \rho = \rho^\dagger, \rho \geq 0, \mathrm{Tr}(\rho) = 1 \right\}.$$

These properties ensure that ρ represents a valid quantum state, whether pure or mixed, and allow for the evolution of the system while maintaining the correct physical constraints.

The diagonal elements ρ_{jj} represent the populations of the system in the corresponding states, while the off-diagonal elements ρ_{jk} for $j \neq k$ represent the coherence between states j and k. These off-diagonal elements are crucial for describing quantum coherence, as they reflect the superpositions between different quantum states. When these elements are non-zero, the system exhibits quantum coherence. If they vanish, the system becomes a classical mixture of states. Therefore, preserving or manipulating these coherences is essential in quantum control.

The time evolution of the density matrix ρ for an open quantum system is governed by the Lindblad master equation, which takes into account both the coherent dynamics of the system (described by the Hamiltonian H) and the dissipative processes (described by the Lindblad operators $\mathcal{L}$), which represent the interaction of the system with its environment.

In this case, the total Hamiltonian H consists of the *free Hamiltonian* H_0 that describes the intrinsic energy levels and interactions within the system, and a term that depends explicitly on the input signal $u(t)$, such that

$$H(t) = H_0 + H_C(t) \tag{3.32}$$

where $H_C = H_c(t)u(t)$ represents the time-dependent control Hamiltonian.

The general form of the Lindblad master equation is given by

$$\dot{\rho} = -\frac{i}{\hbar}[H(t),\rho] + \mathcal{L}(\rho). \tag{3.33}$$

Here, $\hbar$ represents the reduced Planck constant, which governs the relation between energy and frequency in quantum mechanics. The first term describes the unitary evolution due to the total Hamiltonian $H(t)$, where $[H(t),\rho]$ is the commutator of $H(t)$ and ρ. The second term, $\mathcal{L}(\rho)$, accounts for the non-unitary evolution resulting from the interaction of the system with its environment, leading to decoherence and dissipation. The Lindblad operator $\mathcal{L}(\rho)$ for a multi-level system can be written as

$$\mathcal{L}(\rho) = \sum_k \gamma_k \left(L_k \rho L_k^\dagger - \frac{1}{2}\left\{ L_k^\dagger L_k, \rho \right\} \right), \tag{3.34}$$

where γ_k are the decay rates associated with different decoherence channels, and L_k are the Lindblad operators that describe the specific interactions between the system and the environment. These dissipative effects typically degrade the coherence in the system by causing the off-diagonal elements of the density matrix to decay over time. Lindblad superoperators can be categorized as either unital or non-unital. A superoperator $\mathcal{L}$ is considered unital if it satisfies $\mathcal{L}(I) = 0$, implying that the identity operator (representing a completely mixed state) remains unchanged under its action. This condition holds true if and only if all Lindblad operators L_k are Hermitian, as demonstrated by the relation $\mathcal{L}(I) = \sum_k [L_k, L_k^\dagger]$ (Rooney, 2012).

3.5.1.1 Quantum Coherence in Multi-Level Systems

Quantum coherence in multi-level systems is a generalization of the superposition concept from two-level systems (qubits) to systems with N energy levels. In these systems, coherence is distributed across multiple off-diagonal elements of the density matrix, representing superpositions between different quantum states.

To further analyze the coherence between specific pairs of states, we define operators that capture the real and imaginary parts of the coherence. For two states $|j\rangle$ and $|k\rangle$, these operators are described as

$$\begin{aligned} \delta_{jk}^{\mathrm{Re}} &= |j\rangle\langle k| + |k\rangle\langle j|, \\ \delta_{jk}^{\mathrm{Im}} &= -i|j\rangle\langle k| + i|k\rangle\langle j|. \end{aligned}$$

The operator $\delta_{jk}^{\mathrm{Re}}$ describes the real part of the coherence, which captures the population coherence between the two states, while $\delta_{jk}^{\mathrm{Im}}$ captures the imaginary part, which encodes the phase coherence. Both components are essential for understanding quantum interference and superposition phenomena in multi-level systems.

The expectation values of these operators with respect to the density matrix ρ provide the real and imaginary contributions to the coherence:

$$\langle \delta_{jk}^{\mathrm{Re}} \rangle_\rho = \mathrm{Tr}(\rho \delta_{jk}^{\mathrm{Re}}),$$
$$\langle \delta_{jk}^{\mathrm{Im}} \rangle_\rho = \mathrm{Tr}\left(\rho \delta_{jk}^{\mathrm{Im}}\right).$$

A global measure of coherence for an N-level system can be constructed by summing the contributions from the real and imaginary parts of the coherence between all pairs of states. The coherence function $C(\rho)$ is defined as (Cong, 2014)

$$C(\rho) = \sqrt{\sum_{j<k} \left(\langle \delta_{jk}^{\mathrm{Re}} \rangle_\rho\right)^2 + \left(\langle \delta_{jk}^{\mathrm{Im}} \rangle_\rho\right)^2}. \tag{3.35}$$

This function provides a comprehensive measure of the system's coherence by considering both the real and imaginary parts of the coherence for every pair of states (j,k). It captures the overall coherence present in the system and serves as an indicator of how well quantum superpositions are maintained as the system evolves according to the Lindblad equation.

3.5.2 Optimal Control Problem Statement

This section outlines the formulation of the quantum optimal control problem. The methodology proposed here for designing an optimal quantum controller hinges on several key factors: the selection of the cost functional, the formulation of the Pontryagin-Hamiltonian, and the computational approach used to solve the optimality conditions defined by Pontryagin's Minimum Principle (PMP). In quantum control, achieving minimal energy expenditure while preserving system coherence presents a significant challenge. To address this, we focus on an energy minimization approach that incorporates state constraints specifically aimed at maintaining quantum coherence within the control problem. Specifically, we consider the following cost function:

$$J = \int_{t_0}^{t_f} u^2(t)\, dt,$$

which represents the total energy of the control field over the (fixed) time interval $[t_0, t_f]$. This cost functional is a standard choice in quantum and molecular control problems. Here, the control signal $u(t) : [t_0, t_f] \to \mathcal{U} := \{u \in L_\infty : u(t) \in \Omega \subset \mathbb{R}\}$ is assumed to be bounded and measurable. The optimal control problem with state constraints denoted

as (P), is formulated as follows:

$$(P)\begin{cases} \min\limits_{u(\cdot)} \int_{t_0}^{t_f} u^2(t)\,dt, \\ \text{subject to} \\ \dot{\rho} = -\dfrac{i}{\hbar}[H,\rho] + \mathcal{L}(\rho), \quad \text{for almost every } t \in [t_0,t_f] \\ \rho(t_0) = \rho_0 \in \mathbb{C}^{N\times N} \\ u(t) \in \mathcal{U} \quad \text{for almost every } t \in [t_0,t_f] \\ \alpha \leq C^2(\rho) \leq \beta, \quad \text{for all } t \in [t_0,t_f] \end{cases}$$

The inequality constraint $\alpha \leq C^2(\rho(t)) \leq \beta$ introduces state constraints that enforce the preservation of quantum coherence during the evolution of the system, where $C^2(\rho)$ represents a coherence-related measure of the quantum state ρ defined in (3.35).

In this setting, all sets are assumed to be Lebesgue measurable, and all functions are assumed to be Lebesgue measurable and integrable. The objective is to determine an optimal pair $(\rho^\star, u^\star)$ that minimizes the cost functional J while satisfying the dynamic equations, and state constraints.

Before presenting the optimality conditions we first analyze the feasibility of the optimal control problem (P), that is, if there is a solution $u^\star(t)$ that solves (P). The following result holds.

Proposition 3.1 *Let the initial condition ρ_0 be such that $C^2(\rho_0) \in [\alpha,\beta]$. Consider also that the time-evolution of*

$$\Phi = -2i\sum_{j<k}\left(\langle \delta_{jk}^{Re}\rangle_\rho \langle [\delta_{jk}^{Re}, H_c]\rangle_\rho + \langle \delta_{jk}^{Im}\rangle_\rho \langle [\delta_{jk}^{Im}, H_c]\rangle_\rho\right) \tag{3.36}$$

is bounded away from zero for every $t \in [t_0,t_f]$ and Ω is sufficiently large. Then, there exists a nonempty set of admissible input signals $\bar{\mathcal{U}}([t_0,t_f])$ such that

$$\bar{\mathcal{U}}([t_0,t_f]) = \left\{u : [t_0,t_f] \to \mathcal{U} : C^2(\rho(t)) \in [\alpha,\beta], \forall t \in [t_0,t_f]\right\}$$

and in particular an optimal $u^\star[t_0,t_f]) \in \bar{\mathcal{U}}([t_0,t_f])$.

Proof: The proof follows by showing that it is always possible to pick an input signal $u(t)$ that makes $C^2(\rho)$ increase/decrease in time when the coherence is at the lower/upper

bound. To show this, we start to compute the evolution of $C^2(\rho)$, which gives

$$\begin{aligned}
\mathrm{Tr}(\frac{\partial C^2(\rho)}{\partial t}) &= \mathrm{Tr}\Big(\frac{\partial C^2(\rho)}{\partial \rho}\dot{\rho}\Big) \\
&= 2\,\mathrm{Tr}\Big((\sum_{j<k}\delta_{jk}^{\mathrm{Re}}\langle\delta_{jk}^{\mathrm{Re}}\rangle_\rho + \delta_{jk}^{\mathrm{Im}}\langle\delta_{jk}^{\mathrm{Im}}\rangle_\rho)(-i[H,\rho]+\mathcal{L}(\rho))\Big) \\
&= 2\sum_{j<k}\langle\delta_{jk}^{\mathrm{Re}}\rangle_\rho\Big(\mathrm{Tr}\Big(-i[\delta_{jk}^{\mathrm{Re}},H]\rho\Big)+\mathrm{Tr}\Big(\delta_{jk}^{\mathrm{Re}}\mathcal{L}(\rho)\Big)\Big) \\
&\quad + \langle\delta_{jk}^{\mathrm{Im}}\rangle_\rho(\mathrm{Tr}\Big(-i[\delta_{jk}^{\mathrm{Im}},H]\rho\Big)+\mathrm{Tr}\Big(\delta_{jk}^{\mathrm{Im}}\mathcal{L}(\rho)\Big) \\
&= 2\sum_{j<k}\langle\delta_{jk}^{\mathrm{Re}}\rangle_\rho\Big(\mathrm{Tr}\Big(-i[\delta_{jk}^{\mathrm{Re}},H_0]\rho\Big)+\mathrm{Tr}\Big(-iu(t)[\delta_{jk}^{\mathrm{Re}},H_c]\rho\Big) \\
&\quad + \mathrm{Tr}\Big(\delta_{jk}^{\mathrm{Re}}\mathcal{L}(\rho)\Big)\Big) + \langle\delta_{jk}^{\mathrm{Im}}\rangle_\rho\Big(\mathrm{Tr}\Big(-i[\delta_{jk}^{\mathrm{Im}},H_0]\rho\Big) \\
&\quad + \mathrm{Tr}\Big(-iu(t)[\delta_{jk}^{\mathrm{Im}},H_c]\rho\Big)+\mathrm{Tr}\Big(\delta_{jk}^{\mathrm{Im}}\mathcal{L}(\rho)\Big)\Big)
\end{aligned}$$

From which one concludes that $\mathrm{Tr}\Big(\frac{\partial C^2(\rho)}{\partial t}\Big) = \Phi u + \Delta$, where

$$\begin{aligned}
\Delta = 2\sum_{j<k}\langle\delta_{jk}^{\mathrm{Re}}\rangle_\rho\,\mathrm{Tr}\Big(-i[\delta_{jk}^{\mathrm{Re}},H_0]\rho+\delta_{jk}^{\mathrm{Re}}\mathcal{L}(\rho)\Big) \\
+\langle\delta_{jk}^{\mathrm{Im}}\rangle_\rho\,\mathrm{Tr}\Big(-i[\delta_{jk}^{\mathrm{Im}},H_0]\rho+\delta_{jk}^{\mathrm{Im}}\mathcal{L}(\rho)\Big)
\end{aligned}$$

Thus, the result follows since Φ and Δ are bounded and Φ is bounded away from zero by assumption. □

Remark 3.1 *The assumption of $|\Phi|$ being bounded away from zero depends on control Hamiltonian H_C. In particular, from (3.36) one can immediately conclude that at least one of the coherence operators must not commute with H_c.*

3.5.3 Pontryagin's Minimum Principle in Gamkrelidze Form

Let the pair (ρ,u) be a feasible process, that is, $u(t)$ and $\rho(t)$ satisfy for a.e. $t\in[t_0,t_f]$ the Lindblad dynamics with the stated initial condition, the state and the input constraints. The pair $\Big(\rho^\star,u^\star\Big)$ is termed as optimal and therefore solves (P) if the value of the cost function J is the minimum possible over the set of all feasible processes. In order to deal with the indicated problem, we indicate two Lagrangian multipliers: π and μ, where $\pi:\big[t_0,t_f\big]\to\mathbb{C}^{N\times N}$ is the time-varying Lagrange multiplier matrix, whose elements are called the costates of the system, and μ is a time varying scalar Lagrange multiplier enforcing the coherence constraint. To satisfy the coherence state constraints on $C(\rho)$, we define $\tilde{C}(\rho)$ as the following

$$\tilde{C}(\rho) = \begin{pmatrix} C^2(\rho)-\beta \\ \alpha - C^2(\rho)\end{pmatrix} \tag{3.37}$$

such that $\{\tilde{C}(\rho) \leq 0, \forall t \in [t_0, t_f]\}$. We will now derive the necessary optimality conditions.

Proposition 3.2 *Consider the optimal control problem (P). Let $u^\star(t)$ be an optimal control and $\rho^\star(t)$ be the corresponding state trajectory. Then, there exists a multiplier π that, together with μ, satisfies the necessary conditions according to Gamkrelidze form of PMP. Based on the given setup, we express the extended Pontryagin Hamiltonian function as follows:*

$$\begin{aligned}\mathcal{H}(\rho,\pi,u,\mu) = \mathrm{Tr}\Bigg(\Bigg(\pi + \mu\sum_{j<k}\Big(\langle\delta_{jk}^{Re}\rangle_\rho \delta_{jk}^{Re} + \langle\delta_{jk}^{Im}\rangle_\rho \delta_{jk}^{Im}\Big)\Bigg)^\dagger \\ \Big(-\frac{i}{\hbar}[H(t),\rho] + \mathcal{L}(\rho)\Big)\Bigg) + u^2(t)\end{aligned} \tag{3.38}$$

Specifically, we have the condition

$$\mathcal{H}(\rho^\star,\pi^\star,u^\star,\mu^\star,t) \leq \mathcal{H}(\rho,\pi,u,\mu,t),$$

for all $t \in [t_0,t_f]$, and for all feasible controls $u \in \Omega$. Moreover, the control $u(t)$ must satisfy

$$\frac{\partial\mathcal{H}}{\partial u} = \frac{-i}{\hbar}\mathrm{Tr}\left(\left(\pi^\star + \mu\sum_{j<k}\Big(\langle\delta_{jk}^{Re}\rangle_{\rho^\star}\delta_{jk}^{Re} + \langle\delta_{jk}^{Im}\rangle_{\rho^\star}\delta_{jk}^{Im}\Big)\right)^\dagger [H_C,\rho^\star]\right) + 2u(t) = 0 \tag{3.39}$$

The adjoint equation is derived as follows:

$$\begin{aligned}\dot{\pi} = -\frac{\partial\mathcal{H}}{\partial\rho} = \chi\Big(\pi^\dagger\Big) + \mu\sum_{j<k}\Big(\delta_{jk}^{Re}\langle\chi(\delta_{jk}^{Re^\dagger})\rangle_{\rho^\star} \\ + \delta_{jk}^{Im}\langle\chi(\delta_{jk}^{Im^\dagger})\rangle_{\rho^\star} + \langle\delta_{jk}^{Re}\rangle_{\rho^\star}\chi(\delta_{jk}^{Re^\dagger}) + \langle\delta_{jk}^{Im}\rangle_{\rho^\star}\chi(\delta_{jk}^{Im^\dagger})\Big),\end{aligned} \tag{3.40}$$

and its final condition implies that $\pi(t_f) = 0_{N\times N}$. The function χ for a generic variable ϕ is defined as

$$\chi(\phi) = \frac{-i}{\hbar}[\phi,H(t)] + \mathcal{L}(\phi) + \mathcal{L}_0(\phi), \tag{3.41}$$

with $\mathcal{L}_0(\phi) = \sum_k \gamma_k(L_k^\dagger\phi L_k - L_k\phi L_k^\dagger)$.

Proof: We follow the necessary optimality conditions of the PMP in the form of Gamkrelidze for state-constrained optimal control problems, as studied in (Arutyunov et al., 2011). We extend these arguments to the quantum context for matrix-valued dynamics. To this end, the extended Pontryagin Hamiltonian is defined as:

$$\mathcal{H}(\rho,\pi,u,\mu,t) = \mathrm{Tr}\left(\pi^\dagger\dot{\rho} + (\boldsymbol{\mu}^T\frac{\partial\tilde{C}(\rho)}{\partial\rho})^\dagger\dot{\rho}\right) + u^2(t),$$

where $\boldsymbol{\mu}^T \frac{\partial \tilde{C}(\rho)}{\partial \rho} = (\mu_1 \quad \mu_2) \begin{pmatrix} \frac{\partial C^2(\rho)}{\partial \rho} \\ -\frac{\partial C^2(\rho)}{\partial \rho} \end{pmatrix}$, simplifying to

$$(\mu_1 - \mu_2)\frac{\partial C^2(\rho)}{\partial \rho} = 2(\mu_1 - \mu_2)\sum_{j<k}\Big(\langle \delta_{jk}^{\mathrm{Re}}\rangle_\rho \delta_{jk}^{\mathrm{Re}} + \langle \delta_{jk}^{\mathrm{Im}}\rangle_\rho \delta_{jk}^{\mathrm{Im}}\Big)$$

From this, we define $\mu = 2(\mu_1 - \mu_2)$. Thus, the Pontryagin Hamiltonian is formulated as shown in equation (3.38), from which the necessary conditions according to the PMP are derived. In the following, we show the derivation of the adjoint equation (3.40). Due to the complexity of computation, we break $\mathcal{H}$ into four main terms, such that $\mathcal{H} = \mathcal{H}_1 + \mathcal{H}_2 + \mathcal{H}_3 + \mathcal{H}_4$, where

$$\begin{aligned}
\mathcal{H}_1 &= -\frac{i}{\hbar}\mathrm{Tr}\Big(\pi^\dagger([H,\rho])\Big) = -\frac{i}{\hbar}\Big(\mathrm{Tr}\Big(\pi^\dagger H\rho\Big) - \mathrm{Tr}\Big(\pi^\dagger \rho H\Big)\Big) \\
\mathcal{H}_2 &= \mathrm{Tr}\Big(\pi^\dagger \mathcal{L}(\rho)\Big) = \sum_k \gamma_k\Big(\mathrm{Tr}\Big(\pi^\dagger L_k \rho L_k^\dagger\Big) - \frac{1}{2}\mathrm{Tr}\Big(\pi^\dagger L_k^\dagger L_k \rho\Big) - \frac{1}{2}\mathrm{Tr}\Big(\pi^\dagger \rho L_k^\dagger L_k\Big)\Big) \\
\mathcal{H}_3 &= \mu\,\mathrm{Tr}\Big((\sum_{j<k}\langle \delta_{jk}^{\mathrm{Re}}\rangle_\rho \delta_{jk}^{\mathrm{Re}^\dagger} + \langle \delta_{jk}^{\mathrm{Im}}\rangle_\rho \delta_{jk}^{\mathrm{Im}^\dagger})(-\frac{i}{\hbar}[H,\rho])\Big) \\
&= \frac{-i\mu}{\hbar}\sum_{j<k}\langle \delta_{jk}^{\mathrm{Re}}\rangle_\rho(\mathrm{Tr}\Big(\delta_{jk}^{\mathrm{Re}^\dagger} H\rho\Big) - \mathrm{Tr}\Big(\delta_{jk}^{\mathrm{Re}^\dagger}\rho H\Big)) + \langle \delta_{jk}^{\mathrm{Im}}\rangle_\rho(\mathrm{Tr}\Big(\delta_{jk}^{\mathrm{Im}^\dagger} H\rho\Big) - \mathrm{Tr}\Big(\delta_{jk}^{\mathrm{Im}^\dagger}\rho H\Big)) \\
\mathcal{H}_4 &= \mu\,\mathrm{Tr}\Big(\sum_{j<k}\Big(\langle \delta_{jk}^{\mathrm{Re}}\rangle_\rho \delta_{jk}^{\mathrm{Re}^\dagger} + \langle \delta_{jk}^{\mathrm{Im}}\rangle_\rho \delta_{jk}^{\mathrm{Im}^\dagger}\Big)\mathcal{L}(\rho)\Big) \\
&= \mu\sum_{j<k}\langle \delta_{jk}^{\mathrm{Re}}\rangle_\rho \sum_k \gamma_k\Big(\mathrm{Tr}\Big(\delta_{jk}^{\mathrm{Re}^\dagger} L_k\rho L_k^\dagger\Big) - \frac{1}{2}\mathrm{Tr}\Big(\delta_{jk}^{\mathrm{Re}^\dagger} L_k^\dagger L_k\rho\Big) \\
&\quad -\frac{1}{2}\mathrm{Tr}\Big(\delta_{jk}^{\mathrm{Re}^\dagger}\rho L_k^\dagger L_k\Big)\Big) + \mu\sum_{j<k}\langle \delta_{jk}^{\mathrm{Im}}\rangle_\rho \sum_k \gamma_k\Big(\mathrm{Tr}\Big(\delta_{jk}^{\mathrm{Im}^\dagger} L_k\rho L_k^\dagger\Big) \\
&\quad -\frac{1}{2}\mathrm{Tr}\Big(\delta_{jk}^{\mathrm{Im}^\dagger} L_k^\dagger L_k\rho\Big) - \frac{1}{2}\mathrm{Tr}\Big(\delta_{jk}^{\mathrm{Im}^\dagger}\rho L_k^\dagger L_k\Big)\Big)
\end{aligned}$$

Now, we compute $\frac{\partial \mathcal{H}}{\partial \rho}$ by computing the derivative of all the above four terms.

$$\frac{\partial \mathcal{H}_1}{\partial \rho} = -\frac{i}{\hbar}(\pi^\dagger H - H\pi^\dagger) = -\frac{i}{\hbar}[\pi^\dagger, H]$$

$$\frac{\partial \mathcal{H}_2}{\partial \rho} = \sum_k \gamma_k(L_k^\dagger \pi^\dagger L_k - \frac{1}{2}\pi^\dagger L_k^\dagger L_k - \frac{1}{2}L_k^\dagger L_k \pi^\dagger + L_k \pi^\dagger L_k^\dagger - L_k \pi^\dagger L_k^\dagger) = \mathcal{L}(\pi^\dagger) + \mathcal{L}_0(\pi^\dagger)$$

$$\begin{aligned}
\frac{\partial \mathcal{H}_3}{\partial \rho} &= \frac{-i\mu}{\hbar}\sum_{j<k}\delta_{jk}^{\mathrm{Re}}(\mathrm{Tr}\Big(\delta_{jk}^{\mathrm{Re}^\dagger}H\rho\Big) - \mathrm{Tr}\Big(\delta_{jk}^{\mathrm{Re}^\dagger}\rho H\Big)) \\
&+ \delta_{jk}^{\mathrm{Im}}(\mathrm{Tr}\Big(\delta_{jk}^{\mathrm{Im}^\dagger}H\rho\Big) - \mathrm{Tr}\Big(\delta_{jk}^{\mathrm{Im}^\dagger}\rho H\Big)) + \langle\delta_{jk}^{\mathrm{Re}}\rangle_\rho(\delta_{jk}^{\mathrm{Re}^\dagger}H - H\delta_{jk}^{\mathrm{Re}^\dagger}) \\
&+ \langle\delta_{jk}^{\mathrm{Im}}\rangle_\rho(\delta_{jk}^{\mathrm{Im}^\dagger}H - H\delta_{jk}^{\mathrm{Im}^\dagger}) = \frac{-i\mu}{\hbar}\sum_{j<k}\delta_{jk}^{\mathrm{Re}}\,\mathrm{Tr}\Big([\delta_{jk}^{\mathrm{Re}^\dagger},H]\rho\Big) \\
&+ \delta_{jk}^{\mathrm{Im}}\,\mathrm{Tr}\Big([\delta_{jk}^{\mathrm{Im}^\dagger},H]\rho\Big) + \langle\delta_{jk}^{\mathrm{Re}}\rangle_\rho[\delta_{jk}^{\mathrm{Re}^\dagger},H] + \langle\delta_{jk}^{\mathrm{Im}}\rangle_\rho[\delta_{jk}^{\mathrm{Im}^\dagger},H]
\end{aligned}$$

$$\begin{aligned}
\frac{\partial \mathcal{H}_4}{\partial \rho} &= \mu\sum_{j<k}\delta_{jk}^{\mathrm{Re}}\sum_k\gamma_k\Big(\mathrm{Tr}\Big(\delta_{jk}^{\mathrm{Re}^\dagger}L_k\rho L_k^\dagger\Big) - \frac{1}{2}\mathrm{Tr}\Big(\delta_{jk}^{\mathrm{Re}^\dagger}L_k^\dagger L_k\rho\Big) \\
&- \frac{1}{2}\mathrm{Tr}\Big(\delta_{jk}^{\mathrm{Re}^\dagger}\rho L_k^\dagger L_k\Big)\Big) + \mu\sum_{j<k}\delta_{jk}^{\mathrm{Im}}\sum_k\gamma_k\Big(\mathrm{Tr}\Big(\delta_{jk}^{\mathrm{Im}^\dagger}L_k\rho L_k^\dagger\Big) \\
&- \frac{1}{2}\mathrm{Tr}\Big(\delta_{jk}^{\mathrm{Im}^\dagger}L_k^\dagger L_k\rho\Big) - \frac{1}{2}\mathrm{Tr}\Big(\delta_{jk}^{\mathrm{Im}^\dagger}\rho L_k^\dagger L_k\Big)\Big) + \mu\sum_{j<k}\langle\delta_{jk}^{\mathrm{Re}}\rangle_\rho \\
&\sum_k\gamma_k\Big(\mathrm{Tr}\Big(L_k^\dagger\delta_{jk}^{\mathrm{Re}^\dagger}L_k\Big) - \frac{1}{2}\mathrm{Tr}\Big(\delta_{jk}^{\mathrm{Re}^\dagger}L_k^\dagger L_k\Big) - \frac{1}{2}\mathrm{Tr}\Big(L_k^\dagger L_k\delta_{jk}^{\mathrm{Re}^\dagger}\Big)\Big) \\
&+ \mu\sum_{j<k}\langle\delta_{jk}^{\mathrm{Im}}\rangle_\rho\sum_k\gamma_k\Big(\mathrm{Tr}\Big(L_k^\dagger\delta_{jk}^{\mathrm{Im}^\dagger}L_k\Big) - \frac{1}{2}\mathrm{Tr}\Big(\delta_{jk}^{\mathrm{Im}^\dagger}L_k^\dagger L_k\Big) \\
&- \frac{1}{2}\mathrm{Tr}\Big(L_k^\dagger L_k\delta_{jk}^{\mathrm{Im}^\dagger}\rho\Big)\Big) \\
&= \mu\Big(\sum_{j<k}\delta_{jk}^{\mathrm{Re}}\Big(\mathrm{Tr}\Big(\mathcal{L}(\delta_{jk}^{\mathrm{Re}^\dagger})\rho\Big) + \Big(\mathrm{Tr}\Big(\mathcal{L}_0(\delta_{jk}^{\mathrm{Re}^\dagger})\rho\Big)\Big) \\
&+ \sum_{j<k}\delta_{jk}^{\mathrm{Im}}\Big(\mathrm{Tr}\Big(\mathcal{L}(\delta_{jk}^{\mathrm{Im}^\dagger})\rho\Big) + \mathrm{Tr}\Big(\mathcal{L}_0(\delta_{jk}^{\mathrm{Im}^\dagger})\rho\Big)\Big) \\
&+ \sum_{j<k}\langle\delta_{jk}^{\mathrm{Re}}\rangle_\rho\Big(\mathcal{L}(\delta_{jk}^{\mathrm{Re}^\dagger}) + \mathcal{L}_0(\delta_{jk}^{\mathrm{Re}^\dagger})\Big) \\
&+ \sum_{j<k}\langle\delta_{jk}^{\mathrm{Im}}\rangle_\rho\Big(\mathcal{L}(\delta_{jk}^{\mathrm{Im}^\dagger}) + \mathcal{L}_0(\delta_{jk}^{\mathrm{Im}^\dagger})\Big)\Big)
\end{aligned}$$

By summing the four derivatives, we compute the adjoint equation

$$-\dot{\pi} = \frac{\partial \mathcal{H}}{\partial \rho} = \frac{\partial \mathcal{H}_1}{\partial \rho} + \frac{\partial \mathcal{H}_2}{\partial \rho} + \frac{\partial \mathcal{H}_3}{\partial \rho} + \frac{\partial \mathcal{H}_4}{\partial \rho}$$

$$
\begin{aligned}
-\dot{\pi} = &-\frac{i}{\hbar}[\pi^\dagger, H] + \mathcal{L}(\pi^\dagger) + \mathcal{L}_0(\pi^\dagger) \\
&- \frac{i\mu}{\hbar}\sum_{j<k}\delta_{jk}^{\mathrm{Re}}\,\mathrm{Tr}\Big([\delta_{jk}^{\mathrm{Re}^\dagger}, H]\rho\Big) \\
&+ \mu\sum_{j<k}\delta_{jk}^{\mathrm{Re}}\left(\mathrm{Tr}\Big(\mathcal{L}(\delta_{jk}^{\mathrm{Re}^\dagger})\rho\Big) + \mu\sum_{j<k}\delta_{jk}^{\mathrm{Re}}\,\mathrm{Tr}\Big(\mathcal{L}_0(\delta_{jk}^{\mathrm{Re}^\dagger})\rho\Big)\right. \\
&- \frac{i\mu}{\hbar}\sum_{j<k}\langle\delta_{jk}^{\mathrm{Re}}\rangle_\rho[\delta_{jk}^{\mathrm{Re}^\dagger}, H] + \mu\sum_{j<k}\langle\delta_{jk}^{\mathrm{Re}}\rangle_\rho\left(\mathcal{L}(\delta_{jk}^{\mathrm{Re}^\dagger}) + \mathcal{L}_0(\delta_{jk}^{\mathrm{Re}^\dagger})\right) \\
&- \frac{i\mu}{\hbar}\sum_{j<k}\delta_{jk}^{\mathrm{Im}}\,\mathrm{Tr}\Big([\delta_{jk}^{\mathrm{Im}^\dagger}, H]\rho\Big) + \mu\sum_{j<k}\delta_{jk}^{\mathrm{Re}}\left(\mathrm{Tr}\Big(\mathcal{L}(\delta_{jk}^{\mathrm{Im}^\dagger})\rho\Big)\right. \\
&+ \mu\sum_{j<k}\delta_{jk}^{\mathrm{Im}}\,\mathrm{Tr}\Big(\mathcal{L}_0(\delta_{jk}^{\mathrm{Re}^\dagger})\rho\Big) - \frac{i\mu}{\hbar}\sum_{j<k}\langle\delta_{jk}^{\mathrm{Im}}\rangle_\rho[\delta_{jk}^{\mathrm{Im}^\dagger}, H] \\
&+ \mu\sum_{j<k}\langle\delta_{jk}^{\mathrm{Im}}\rangle_\rho\left(\mathcal{L}(\delta_{jk}^{\mathrm{Re}^\dagger}) + \mathcal{L}_0(\delta_{jk}^{\mathrm{Re}^\dagger})\right)
\end{aligned}
$$

which simplifies to

$$
\begin{aligned}
-\dot{\pi} = &-\frac{i}{\hbar}[\pi^\dagger, H] + \mathcal{L}(\pi^\dagger) + \mathcal{L}_0(\pi^\dagger) \\
&+ \mu\sum_{j<k}\left(\delta_{jk}^{\mathrm{Re}}\langle -\frac{i}{\hbar}[\delta_{jk}^{\mathrm{Re}^\dagger}, H] + \mathcal{L}(\delta_{jk}^{\mathrm{Re}^\dagger}) + \mathcal{L}_0(\delta_{jk}^{\mathrm{Re}^\dagger})\rangle_\rho\right. \\
&+ \delta_{jk}^{\mathrm{Im}}\langle -\frac{i}{\hbar}[\delta_{jk}^{\mathrm{Im}^\dagger}, H] + \mathcal{L}(\delta_{jk}^{\mathrm{Im}^\dagger}) + \mathcal{L}_0(\delta_{jk}^{\mathrm{Im}^\dagger})\rangle_\rho \\
&+ \langle\delta_{jk}^{\mathrm{Re}}\rangle_\rho\left(-\frac{i}{\hbar}[\delta_{jk}^{\mathrm{Re}^\dagger}, H] + \mathcal{L}(\delta_{jk}^{\mathrm{Re}^\dagger}) + \mathcal{L}_0(\delta_{jk}^{\mathrm{Re}^\dagger})\right) \\
&+ \left.\langle\delta_{jk}^{\mathrm{Im}}\rangle_\rho\left(-\frac{i}{\hbar}[\delta_{jk}^{\mathrm{Im}^\dagger}, H] + \mathcal{L}(\delta_{jk}^{\mathrm{Im}^\dagger}) + \mathcal{L}_0(\delta_{jk}^{\mathrm{Im}^\dagger})\right)\right)
\end{aligned}
$$

By defining the function (3.41), the adjoint equation (3.40) is proved. In addition, the transversality condition, which applies at the final time t_f, imposes that

$$
\pi(t_f) = -\frac{\partial J}{\partial \rho_f} = 0_{N\times N}.
$$

□

Proposition 3.3 *Let the quadruple $(\rho^\star, \pi^\star, u^\star, \mu^\star)$ be an optimal trajectory of problem (P) for the case where the state constraints are not active. Then, this quadruple is a local minimizer of the extended Pontryagin Hamiltonian (3.38).*

Proof: This follows from the fact that the second derivative of the extended Pontryagin Hamiltonian with respect to the control u is $\frac{\partial^2\mathcal{H}}{\partial u^2} = 2 > 0$. □

Proposition 3.4 *Consider problem (P) where the state constraints are active for some period of time $\tau \in [t_0, t_f]$ and let $\bar{\rho}(t)$, $t \in \tau$ be the corresponding density matrix for each $C^2(\bar{\rho}) = \alpha$ (or*

$C^2(\bar{\rho}) = \beta$ *for the upper bound case). Then, as long as the control Hamiltonian* H_c *does not commute with* $\bar{\rho}$*, there exists a feasible boundary control* $u(t)$ *for* $t \in \tau$ *given by*

$$u(t) = \frac{\left(-\frac{i}{\hbar}[H_0, \rho] + \mathcal{L}(\rho) \right)}{\frac{i}{\hbar}[H_c, \rho]}. \tag{3.42}$$

Proof: By imposing $\Gamma = \mathrm{Tr}\left(\boldsymbol{\mu}^T \frac{\partial \tilde{C}(\rho)}{\partial \rho} \dot{\rho}\right)$ equal to zero, we compute the control u that keeps the lower bound of state constraint, which is

$$\Gamma = 2\mu \sum_{j<k} \left(\langle \delta_{jk}^{\mathrm{Re}} \rangle_\rho \delta_{jk}^{\mathrm{Re}} + \langle \delta_{jk}^{\mathrm{Im}} \rangle_\rho \delta_{jk}^{\mathrm{Im}} \right) \left(-\frac{i}{\hbar}[H(t), \rho] + \mathcal{L}(\rho) \right)$$

From this it follows (3.42). □

Algorithm 3.2 provides a step-by-step method for solving the state-constrained quantum optimal control problem with coherence preservation. It initializes control variables and multipliers, computes state and adjoint trajectories through numerical methods, updates Lagrange multipliers to enforce state constraints, calculates the Pontryagin Hamiltonian, and iteratively updates control functions. The algorithm concludes with a convergence check to ensure optimal control, state trajectory, and multiplier conditions are met before termination.

Remark 3.2 (Control Constraints) *In addition to the state constraints handled by the presented algorithm, control constraints can also be efficiently addressed by applying the method of saturation functions, as described in (Graichen et al., 2010). This method transforms the control constraints into smooth functions that approximate the behavior of the original constraints, ensuring that the control variables remain within their prescribed limits without imposing hard bounds. The approach involves dynamically extending the system by incorporating these saturation functions into the Pontryagin Hamiltonian, thus reformulating the original problem as an unconstrained optimization problem. This strategy can be seamlessly integrated into the current algorithm, ensuring that both state and control constraints are respected during the optimization process, while maintaining numerical stability and preventing constraint violations.*

3.5.4 Application of the Algorithm to a Qutrit System

We now apply the developed algorithm to the specific case of a qutrit, a three-level quantum system, subjected to Markovian decoherence. The qutrit consists of three quantum states, $|0\rangle$, $|1\rangle$, and $|2\rangle$, and is described by a density matrix $\rho \in \mathbb{C}^{3\times 3}$: $\rho = \begin{pmatrix} \rho_{00} & \rho_{01} & \rho_{02} \\ \rho_{10} & \rho_{11} & \rho_{12} \\ \rho_{20} & \rho_{21} & \rho_{22} \end{pmatrix}$.

Algorithm 3.2 Solving the State-Constrained Quantum Optimal Control Problem with Coherence Preservation.

Step 1 - Initialization
Set number of time steps N and initialize the iteration counter $j = 0$.
for $m = 0, \ldots, N-1$ **do**
    Initialize control u_m^j.
    Initialize multiplier μ_m^j.
end for
Set initial state ρ_0 at time t_0.
Set the adjoint variable π_f at final time t_f according to the transversality condition.
Set convergence tolerance ε, and learning rates η_i, η_d.
Step 2 - Computation of the state trajectory
for $m = 0, \ldots, N-1$ **do**
    Update the state ρ_m^j by solving the Lindblad master equation numerically using a time-stepping method

$$\dot{\rho}_m^j = -\frac{i}{\hbar}[H_m^j, \rho_m^j] + \mathcal{L}(\rho_m^j)$$

end for
Step 3 - Computation of the adjoint trajectory
for $m = N-1$ **to** 0 **do**
    Update the adjoint variable π_m^j by solving the adjoint equation numerically using the chosen time-stepping method

$$\pi_m^j = \chi(\pi_m^\dagger) + \mu_m \sum_{j<k} \left(\delta_{jk}^{Re} \langle \chi(\delta_{jk}^{Re}) \rangle_{\rho_m^j} + \delta_{jk}^{Im} \langle \chi(\delta_{jk}^{Im}) \rangle_{\rho_m^j} \right)$$

end for
Step 4 - Update of Lagrange multipliers for state constraint
for $m = 0, \ldots, N-1$ **do**
    Compute the coherence function $C^2(\rho_m^j)$
    if $C^2(\rho_m^j) < \beta$ **then**
        Set $\mu_{1,m}^j = \mu_{1,m-1}^j$
    else if $C^2(\rho_m^j) > \alpha$ **then**
        Set $\mu_{2,m}^j = \mu_{2,m-1}^j$
    else if $C^2(\rho_m^j) = \beta$ **then**
        Update $\mu_{1,m}^j = \mu_{1,m-1}^j + \eta_i (C^2(\rho_m^j) - C^2(\rho_{m-1}^j))$
    else if $C^2(\rho_m^j) = \alpha$ **then**
        Update $\mu_{2,m}^j = \mu_{2,m-1}^j - \eta_d (C^2(\rho_m^j) - C^2(\rho_{m-1}^j))$
    end if
    Update the combined Lagrange multiplier:

$$\mu_m^j = 2\left(\mu_{1,m}^j - \mu_{2,m}^j\right)$$

end for
Step 5 - Computation of the Pontryagin Hamilton function
for $m = 0, \ldots, N-1$ **do**
    Compute the Pontryagin Hamiltonian function $\mathcal{H}_m^j$ as:

$$\mathcal{H}_m^j = \mathrm{Tr}\left(\left(\pi_m^j + \mu_m^j \sum_{j<k} \left(\langle \delta_{jk}^{\mathrm{Re}}, \rho_m^j \rangle \delta_{jk}^{\mathrm{Re}} + \langle \delta_{jk}^{\mathrm{Im}}, \rho_m^j \rangle \delta_{jk}^{\mathrm{Im}} \right) \right)^\dagger \left(-\frac{i}{\hbar}[H_m^j, \rho_m^j] + \mathcal{L}(\rho_m^j) \right) \right) + {u_m^j}^2$$

end for

Step 6 - Update the control function
for $m = 0, \ldots, N-1$ **do**
    Update the control values u_m^{j+1} using convex combination, where $\zeta_1 + \zeta_2 = 1$

$$u_m^{j+1} = \zeta_1 \frac{i}{2\hbar} \mathrm{Tr}\Big(\big(\pi_m^j - \mu_m^j \sum_{j<k} \big(\langle \delta_{jk}^{\mathrm{Re}} \rangle_{\rho_m^j} \delta_{jk}^{\mathrm{Re}} + \langle \delta_{jk}^{\mathrm{Im}} \rangle_{\rho_m^j} \delta_{jk}^{\mathrm{Im}} \big) \big)^\dagger \Big[H_{C_m}^j, \rho_m^j \Big] \Big) + \zeta_2 u_m^j$$

end for
Step 7 - Stopping Test
Define tolerance values: ε_u and ε_μ (small positive numbers).
for $m = 0, \ldots, N-1$ **do**
    Check the convergence criteria for the state trajectory:

$$|\rho_m^{j+1} - \rho_m^j| < \varepsilon_\rho$$

    Check the convergence criteria for the adjoint variable:

$$|\pi_m^{j+1} - \pi_m^j| < \varepsilon_\pi$$

    Check the convergence criteria for the control:

$$|u_m^{j+1} - u_m^j| < \varepsilon_u$$

    Check the convergence criteria for the Lagrange multipliers:

$$|\mu_m^{j+1} - \mu_m^j| < \varepsilon_\mu$$

end for
if $\max\{|\rho_m^{j+1} - \rho_m^j|, |\pi_m^{j+1} - \pi_m^j|, |u_m^{j+1} - u_m^j|, |\mu_m^{j+1} - \mu_m^j|\} < \epsilon$
Stop
else if increment $j = j + 1$ and go to **Step 2**.

The basis states for the qutrit system are represented as follows:

$$|0\rangle = \begin{pmatrix} 1 \\ 0 \\ 0 \end{pmatrix}, \quad |1\rangle = \begin{pmatrix} 0 \\ 1 \\ 0 \end{pmatrix}, \quad |2\rangle = \begin{pmatrix} 0 \\ 0 \\ 1 \end{pmatrix}.$$

The off-diagonal elements ρ_{01}, ρ_{02}, and ρ_{12} represent the coherence between the different pairs of states. In this qutrit system, the coherence between states $|0\rangle$ and $|1\rangle$ can be captured by the following operators:

$$\begin{aligned} \delta_{01}^{\mathrm{Re}} &= |0\rangle\langle 1| + |1\rangle\langle 0|, \\ \delta_{01}^{\mathrm{Im}} &= -i\left(|0\rangle\langle 1| - |1\rangle\langle 0|\right). \end{aligned}$$

Similarly, the coherence between states $|0\rangle$ and $|2\rangle$, and between $|1\rangle$ and $|2\rangle$, is described by their respective real and imaginary coherence operators $\delta_{02}^{\mathrm{Re}}$, $\delta_{02}^{\mathrm{Im}}$, and $\delta_{12}^{\mathrm{Re}}$, $\delta_{12}^{\mathrm{Im}}$. The total coherence between states $|0\rangle$ and $|1\rangle$ is then computed using the coherence function

$$C(\rho) = \sqrt{\left(\langle \delta_{01}^{\mathrm{Re}} \rangle_\rho\right)^2 + \left(\langle \delta_{01}^{\mathrm{Im}} \rangle_\rho\right)^2}.$$

The loss of coherence between the two states can be due to decoherence, often caused by interaction with the environment. However, by applying a control field, it is possible to drive the transitions between these states and counteract this decay process.

In the context of this qutrit, we assume the system has energy levels associated with the states $|0\rangle$, $|1\rangle$, and $|2\rangle$, with corresponding energies E_0, E_1, and E_2. The drift Hamiltonian describes the free evolution of the system without external control fields and can be written as follows:

$$H_0 = \frac{E_2 - E_0}{3}(|2\rangle\langle 2| - |0\rangle\langle 0|) + \frac{E_2 - E_1}{3}(|2\rangle\langle 2| - |1\rangle\langle 1|) + \frac{E_0 - E_1}{3}(|0\rangle\langle 0| - |1\rangle\langle 1|),$$

where each term represent the population differences between the corresponding energy levels in the system. Thus, the drift Hamiltonian H_0 captures the natural dynamics of the system, reflecting the energy differences between the three states. We assume that the transition dipole moments for the linearly polarized field are real. Hence, the control field, in the dipole approximation, can be described by a time-dependent envelope of the field $u(t)$, driving frequency ω_d, and initial phase ϕ_d, hence, the corresponding control Hamiltonian is given by

$$H_C = u(t)\left(e^{i\phi_d}|0\rangle\langle 1| + e^{-i\phi_d}|1\rangle\langle 0|\right)\cos(\omega_d t)$$

This control $u(t)$ is designed to influence the system's coherence and dynamics, allowing precise control over the quantum states.

In the context of our qutrit system, the Lindblad operators describe the decay processes from the excited state $|2\rangle$ to the two lower states $|0\rangle$ and $|1\rangle$, with respective decay rates γ_0 and γ_1. These transitions are modeled by the Lindblad operator, which introduces the dissipative effects into the system's dynamics.

The Lindblad operators L_k for the qutrit system are defined as

$$L_0 = |0\rangle\langle 2|, \quad L_1 = |1\rangle\langle 2|, \quad L_3 = |0\rangle\langle 0| - |1\rangle\langle 1|.$$

The operator L_0 represents the transition from the excited state $|2\rangle$ to the ground state $|0\rangle$, while L_1 represents the transition from $|2\rangle$ to $|1\rangle$. Additionally, dephasing between the states $|0\rangle$ and $|1\rangle$ is introduced via a dephasing operator L_3. Thus, the full Lindblad term that governs the system's evolution under decoherence is given by

$$\begin{aligned}\mathcal{L}(\rho) =& \frac{1}{2}\gamma_0 \left(2|0\rangle\langle 2|\rho|2\rangle\langle 0| - |2\rangle\langle 2|\rho - \rho|2\rangle\langle 2|\right) + \frac{1}{2}\gamma_1 \\ & \left(2|1\rangle\langle 2|\rho|2\rangle\langle 1| - |2\rangle\langle 2|\rho - \rho|2\rangle\langle 2|\right) + \frac{1}{2}\gamma_d \left(2\left(|0\rangle\langle 0| - |1\rangle\langle 1|\right)\right. \\ & \left.\rho\left(|0\rangle\langle 0| - |1\rangle\langle 1|\right) - \left(|0\rangle\langle 0| - |1\rangle\langle 1|\right)^2\rho - \rho\left(|0\rangle\langle 0| - |1\rangle\langle 1|\right)^2\right)\end{aligned} \tag{3.43}$$

This formulation reflects the combined effects of energy dissipation and coherence loss due to interactions with the environment.

Proposition 3.5 *The indicated Lindbladian $\mathcal{L}(\rho)$ in (3.43) is non-unital.*

Proof: To confirm that the Lindbladian $\mathcal{L}$ is non-unital, we must show that $\mathcal{L}(I)$, when acting on the identity matrix I for a qutrit system, yields a non-zero result . By applying the Lindblad operators to I and evaluating this expression, one obtains $\mathcal{L}(I) = \text{diag}(\gamma_0, \gamma_0 + \gamma_1, -2\gamma_0 - \gamma_1)$. Since $\mathcal{L}(I) \neq 0$, this confirms that the Lindbladian is non-unital, reflecting that the system's evolution includes irreversible processes. □

3.5.4.1 Numerical Simulation

In this section, we describe the numerical simulation of a qutrit subjected to Markovian decoherence and dephasing. The decay rates γ_0 and γ_1 are set to 0.1 and 0.001 for the transitions from state $|2\rangle$ to states $|0\rangle$ and $|1\rangle$, respectively. The dephasing rate between states $|0\rangle$ and $|1\rangle$, γ_d, is set to 0.005. The energy levels are set to $E_0 = 1$, $E_1 = 1.5$, and $E_2 = 2$. The system's evolution is computed over a time span of 20 a.u. (arbitrary units), and the density matrix is updated at 1000 time points to numerically solve the Lindblad equation. In our numerical simulation, we consider initial state $\rho_0 = \begin{pmatrix} 0.21 & 0.195-0.195i & 0 \\ 0.195+0.195i & 0.78 & 0 \\ 0 & 0 & 0.01 \end{pmatrix}$. First, we consider the system evolution without application of any external control field. This allows analyzing the effects of decay and dephasing captured by the Lindblad operators under the natural dynamics of the system. The coherence between states $|0\rangle$ and $|1\rangle$ is computed. The simulation results, as shown in

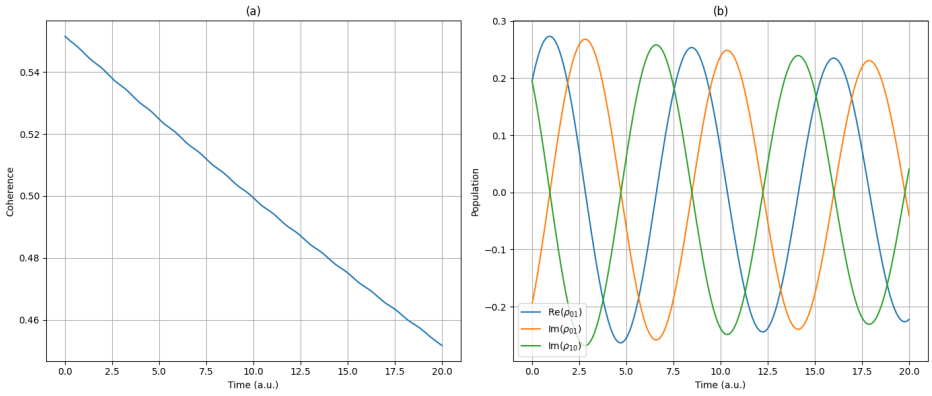


Figure 3.3: (a) Coherence between states $|0\rangle$ and $|1\rangle$; (b) Evolution of off-diagonal density matrix elements over time (with no action of control).

Fig. 3.3(a), indicate that the coherence decays over time. This behavior aligns with theoretical expectations for a system subject to Markovian decoherence, where coherence is gradually lost due to interactions with the environment. The evolution of the key density matrix elements, the real and imaginary parts of the off-diagonals, ρ_{01} and ρ_{10}, is plotted in Fig. 3.3(b). The real and imaginary components of the coherence between states $|0\rangle$ and $|1\rangle$, represented by Re(ρ_{01}) and Im(ρ_{01}), show oscillations that gradually dampen, reflecting the loss of coherence due to dephasing. We now consider including the control Hamiltonian with parameters set to control amplitude $u = 0.1$, the phase $\phi_d = \pi/2$, and the driving frequency $\omega_d = 0.1$. As illustrated in Fig. 3.4, the coherence between states shows an oscillatory decay over time, indicating that while the control field momentarily preserves coherence, it cannot completely counteract the effects of decoherence and dephasing. The density matrix elements also exhibit oscillations, reflecting the influence of the control field on the population redistribution among the qutrit states. The behavior highlights the transient effect of the control field in partially mitigating the loss of coherence.

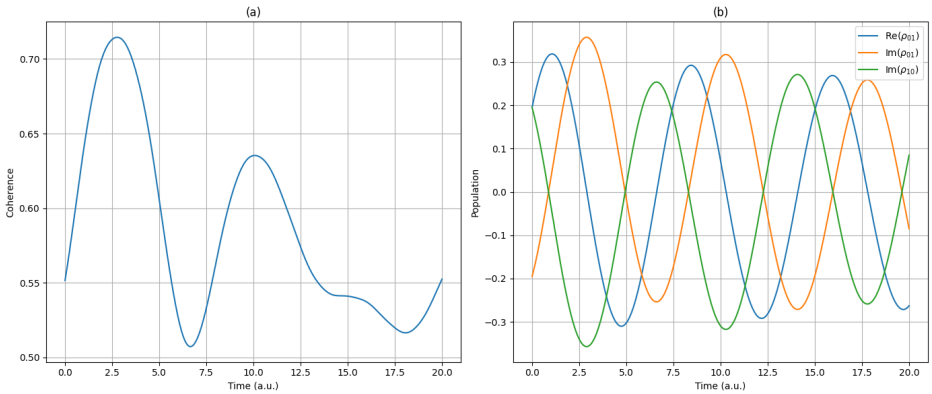


Figure 3.4: (a) Coherence between states $|0\rangle$ and $|1\rangle$ (b) Evolution of density matrix elements over time (with constant control parameters, with dephasing).

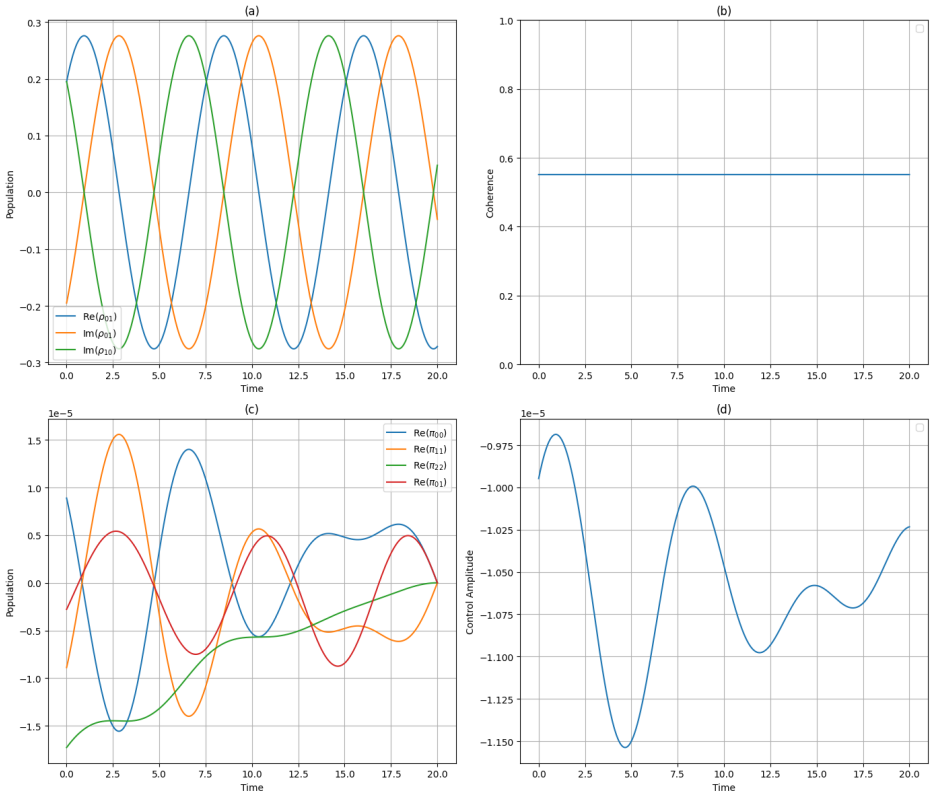


Figure 3.5: (a) Evolution of the real and imaginary components of the density matrix element ρ_{01} under the optimized control strategy. (b) Coherence measured between states $|0\rangle$ and $|1\rangle$ over time. (c) Population dynamics for the adjoint variables π_{00}, π_{01}, π_{12}, and π_{10} during the control process. (d) Control amplitude evolution over time illustrating the modulation applied to influence the system's state.

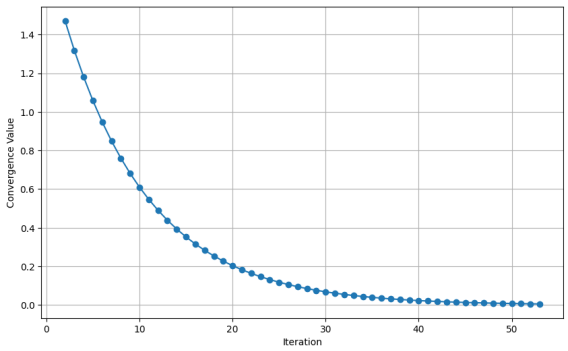


Figure 3.6: Convergence plot showing the evolution of the convergence value as a function of iterations. The plot illustrates how the convergence value decreases progressively.

Finally, we demonstrate the results obtained from solving the state constrained optimal control problem for preserving quantum coherence. The initial coherence is $C(\rho_0) = 0.551$, and the lower and upper bounds were set to $\alpha = 0.550$ and $\beta = 0.553$, respectively. To provide a comprehensive view of the quantum system's behavior under optimal control, Fig. 3.5 includes four subplots. Subplot (a) displays the temporal evolution of the

real and imaginary parts of the off-diagonal density matrix element ρ_{01}. The controlled oscillations indicate active modulation aimed at preserving coherence despite environmental interactions. Subplot (b) shows the coherence between the states $|0\rangle$ and $|1\rangle$ over time. The flat behavior of the coherence in this subplot suggests that the applied control manages to maintain a consistent coherence level across the time span. In subplot (c), the dynamics of the adjoint variables π_{00}, π_{01}, π_{12}, and π_{10} are presented. These represent the real components associated with the system's costate evolution. The behavior of these variables provides insight into how the optimization process adjusts the state trajectory to meet the control objectives. Lastly, subplot (d) captures the control amplitude's time-dependent modulation, which directly impacts the system's evolution. The variations in control illustrate the adaptive strategy employed to counteract the dissipative and dephasing effects, thereby aiding in the coherence preservation. This analysis demonstrates the effectiveness of the control strategy in mitigating coherence loss and guiding the system's dynamics toward desired outcomes. Fig. 3.6 presents the convergence plot, which depicts the progression of the convergence value over multiple iterations. The decreasing trend observed in the plot demonstrates the effectiveness of the control or optimization strategy being applied, as the convergence value approaches zero or stabilizes, indicating that the system is nearing an optimal or steady state. This behavior is consistent with expectations in optimization scenarios where iterative adjustments progressively refine the solution.

3.6 Concluding Remarks and Discussions

In this chapter, we delved into various aspects of quantum optimal control, focusing on the application of Pontryagin's Minimum Principle to formulate and solve control problems for quantum systems. We explored the utility of PMP in deriving optimality conditions for both two-level and three-level quantum systems, considering real-world constraints like energy consumption and decoherence effects. By leveraging this framework, we demonstrated the feasibility of achieving high-fidelity quantum state transfers while simultaneously managing energy efficiency, especially in scenarios such as spin-½ particle control and decoherence-constrained systems.

The work presented underscores the flexibility and power of PMP-based methods in quantum control, showing how these techniques can effectively address different control problems, ranging from simple, unconstrained systems to more complex, constrained environments. This breadth of applicability highlights the relevance of PMP in advancing the field of quantum control, where precision, efficiency, and adaptability are crucial.

The work presented here opens multiple avenues for future research in quantum optimal control. One promising direction is extending the PMP framework to address non-Markovian dynamics, which are more representative of practical quantum systems

interacting with complex environments. Another valuable extension could be the incorporation of machine learning techniques to enhance the computational efficiency of solving optimal control problems, particularly in high-dimensional quantum systems.

Chapter 4

Quantum Pontryagin Neural Networks

In this chapter, we investigate a minimum time-energy optimal control problem (OCP) for dissipative quantum systems interacting with the environment, whose dynamics is governed by the Lindblad equation, and is subjected to preserve the state purity in a quantum state transition process. We consider the purity of quantum channels as state constraints, such that the purity is preserved within some bounds. The technique to deal with this problem leans upon the revisited method of Gamkrelidze's version of Pontryagin's Minimum Principle (PMP) (Arutyunov et al., 2011). We address the constrained control restriction through the technique of saturation functions and system extensions by extending (Graichen et al., 2010) to the quantum context, and show its compatibility with the Gamkrelidze version of PMP. We derive the necessary optimality PMP conditions, and show that they are also sufficient conditions for (local) optimality. We then solve the resulted Boundary Value Problem (BVP) via a recently developed neural network approach known as Pontryagin Neural Networks (PoNNs) derived from the Theory of Functional Connection (TFC) (Johnston, 2021). In particular, we exploit the PoNNs method for the Gamkrelidze version of PMP by introducing an additional multiplier and extra optimality conditions. We also apply the technique of saturation functions presented in (D'ambrosio et al., 2021)-(Johnston et al., 2020) to PoNNs, by showing its compatibility with Gamkrelidze version of PMP. The main results of this chapter were published in (Dehaghani and Aguiar, 2023a; Dehaghani et al., 2023b).

4.1 The Lindbladian Dynamics Equation

The general mathematical tool to describe our knowledge of the state of an n-level quantum system is through the density operator ρ, which is a Hermitian positive semi-definite

operator of trace one acting on the Hilbert space $\mathbb{H}$ of the system. In quantum mechanics, the evolution of density operator through the Lindblad (or Gorini-Kossakowski-Sudarshan-Lindblad) master equation represents the most extensive generator of Markovian dynamics which takes the form,

$$\dot{\rho} = -i\,[H,\rho] + \sum_k \gamma_k \left[L_k \rho L_k^\dagger - \frac{1}{2}\left\{ L_k^\dagger L_k, \rho \right\} \right] \tag{4.1}$$

in which the first term represents the unitary evolution of the quantum system, where H is a Hermitian operator called the quantum-mechanical Hamiltonian defined as

$$H = diag(E_1, E_2, \cdots, E_n) + \sum_{l=1}^{m} u_l(t) H_l$$

where the diagonal term implies that the basis corresponds to the eigenvectors, and E_i represents a real number concerning the energy level. The control $u_l(t) \in \mathbb{R}$ demonstrates a set of external functions coupled to the quantum system via time independent interaction Hamiltonians H_l. The second term of (4.1) represents the dissipative part of the state evolution, where L_k indicates the sequence of arbitrary Lindblad operators, and $\gamma_k \geq 0$ is the damping rate. Master equations can be bothersome due to the commutation term and the Poisson bracket. Since convex combination gives the preservation of the trace and positive definiteness, it is possible to create a Hilbert space of density operators via defining a scalar product. The next result provides a linear space of density operators, called Fock-Liouville space, by which we present a solution of the master equation via vectorization such that the resulting Liouvillian superoperator is governed by a linear system.

Proposition 4.1 *Consider the Lindbladian dynamical system* (4.1)*. There exists a linear isomorphism, coordinate transformation, such that the transformed system is linear in the states and real.*

Proof: We show the results by providing a coordinate transformation given by the following composition of 3 linear isomorphisms (whose notation is defined in the sequel):
i) $\mathcal{L} :\ \rho \mapsto \mathcal{L}\rho$,
ii) $|\cdot\rangle\rangle :\ \rho \mapsto |\rho\rangle\rangle$,
iii) $\tilde{\cdot} :\ v \mapsto \tilde{v} := \begin{bmatrix} \mathrm{Re}(v) & \mathrm{Im}(v) \end{bmatrix}^T$
and finally $\tilde{\mathcal{L}} = (\tilde{\cdot}) \circ |\cdot\rangle\rangle \circ \mathcal{L} \circ |\cdot\rangle\rangle^{-1} \circ (\tilde{\cdot})^{-1}$. To obtain i, we apply the Choi-Jamiolkowski isomorphism for vectorization, through the mapping $|\cdot\rangle\rangle :\ |i\rangle\langle j| \mapsto |j\rangle \otimes |i\rangle$, to (4.1) obtaining the Liouville superoperator acting on the Hilbert space of density operator as

$$|\dot{\rho}\rangle\rangle = \mathcal{L}\,|\rho\rangle\rangle\,,$$

where

$$\mathcal{L} = -i\left(I \otimes H - H^T \otimes I\right) + \sum_k \gamma_k \left[L_k^* \otimes L_k - \frac{1}{2} I \otimes L_k^\dagger L_k - \frac{1}{2}\left(L_k^\dagger L_k\right)^T \otimes I\right]$$

in which I is the identity matrix. To show ii, note that, for an arbitrary density operator $\rho = \sum_{i,j} \rho_{i,j} |i\rangle \langle j|$, its vectorized form is given by $|\rho\,\rangle\rangle = \sum_{i,j} \rho_{i,j} |j\rangle \otimes |i\rangle$. Finally to get iii, we implement the system state and superoperator as

$$|\tilde{\rho}\rangle\rangle = \begin{bmatrix} \mathrm{Re}\left(|\rho\rangle\rangle\right) \\ \mathrm{Im}\left(|\rho\rangle\rangle\right) \end{bmatrix}, \quad \tilde{\mathcal{L}} := \begin{pmatrix} \mathrm{Re}\left(\mathcal{L}\right) & -\mathrm{Im}\left(\mathcal{L}\right) \\ \mathrm{Im}\left(\mathcal{L}\right) & \mathrm{Re}\left(\mathcal{L}\right) \end{pmatrix}$$

so that we obtain

$$|\dot{\tilde{\rho}}\,\rangle\rangle = \tilde{\mathcal{L}}\,|\tilde{\rho}\,\rangle\rangle \tag{4.2}$$

□

We consider (4.2) as the system dynamics in the rest of this chapter.

4.2 Optimal Control Formulation

This section describes the problem formulation. To this end, we have first to describe the state constraint that arises from the concept of quantum purity.

4.2.1 Quantum purity

Quantum purity is a fundamental property of a quantum state. For pure states, the purity $P = 1$, while $P < 1$ shows that the quantum state is mixed. In dissipative quantum systems, a state may be initialized as pure, i.e., $\rho = |\psi\rangle \langle\psi|$, and then due to the interaction with the environment and through a channel χ is decohered and mapped to a mixed state. A quantum channel χ over the space $\mathbb{H}$ represents a completely positive trace-preserving quantum map, i.e., $\chi \in CPTP(\mathbb{H})$. Hence, the purity of the channel χ is considered as just the purity of the state ρ. Therefore, one can write

$$P(\rho) = tr\left(\chi(\rho)^2\right) = tr\left(\rho^2\right) = \left(vec\left(\rho^\dagger\right)\right)^\dagger vec\left(\rho\right)$$

which leads to $\tilde{P}(\rho) = \left\langle\left\langle \tilde{\rho}^\dagger \,|\tilde{\rho}\,\right\rangle\right\rangle$. Preservation or maximization of the purity of a state transmitted through a quantum channel, i.e., a dissipative quantum system, is an important objective in quantum information processing. To do so, several decoherence-reduction techniques, such as quantum error correcting codes, and decoherence-free subspaces have been developed. In this work, following the study in (Cong, 2014, Chapter 12) that imposes an equality state constraint, we use a less restricted form by keeping the

quantum purity above some predefined level, i.e., $\bar{\alpha} P_0 \leq \tilde{P}(\rho) \leq P_0$ with $0 < \bar{\alpha} < 1$, where $P_0 = P(\rho_0)$ is the purity of the initial state.

4.2.2 Problem Formulation

Quantum operations such as quantum state transition need to be done in the shortest possible time. However, due to the inverse relation between control time and amplitude, a fast operation may cause a very large control amplitude, which is practically impossible. The methods to design the quantum optimal controller vary according to the choice of the cost functional, the construction of the Pontryagin-Hamiltonian function, and the computation scheme to solve the PMP optimality conditions. We deal with a time-energy minimization state constrained OCP (P) with bounded control aiming to transfer the initial state $|\tilde{\rho}(t_0)\rangle\rangle = \rho_0$ to a desired target state $\left|\tilde{\rho}(t_f)\right\rangle\rangle = \rho_f$. The problem casts as the following:

$$
(P)\begin{cases}
\min\limits_{u,t_f}\left\{J = \Gamma\, t_f + \eta \int_{t_0}^{t_f} u^2(t)\, dt\right\} \\
\text{subject to} \\
|\dot{\tilde{\rho}}(t)\rangle\rangle = \tilde{\mathcal{L}}\,|\tilde{\rho}\,\rangle\rangle \text{ a.e. } t \in [t_0, t_f] \\
|\tilde{\rho}(t_0)\rangle\rangle = \rho_0 \in \mathbb{R}^{4n} \\
u(t) \in \mathcal{U} := \{u \in L_\infty : u(t) \in \Omega \subset \mathbb{R}\} \\
\Omega = [u_{\min}, u_{\max}] \text{ a.e. } t \in [t_0, t_f] \\
h\left(|\tilde{\rho}(t)\rangle\rangle\right) \leq 0 \text{ for all } t \in [t_0, t_f]
\end{cases}
$$

where Γ and η in the performance index J are positive coefficients, and t_f shows the free final time to be optimized. The second term of J is a common choice for the cost functional in molecular control, which measures the energy of the control field in the interval $[t_0, t_f]$. The control is represented as a measurable bounded function. The inequality $h\left(|\tilde{\rho}(t)\rangle\rangle\right) \leq 0$ defines the state constraints for the density operator - see the specific example in (4.5). In this setup, we assume that all the sets are Lebesque measurable and the functions are Lebesgue measurable and Lebesgue integrable. The goal is to obtain a pair $(\rho^\star, u^\star)$ which is optimal in the sense that the value of cost functional is the minimum over the set of all feasible solutions.

Remark 4.1 *It is important to assert the existence of a solution to problem (P) in the class of measurable controls. Following the Filippov's theorem, (Filippov, 1959), since the right-hand side of the dynamical system is linear with respect to the control, and the set of control values is convex and compact, then one can conclude that there exists a feasible control process to this problem.*

4.3 Pontryagin's Minimum Principle in Gamkrelidze Form with Saturation Functions

To deal with the indicated problem, one can identify two Lagrangian multipliers: μ, and λ, where

- μ is bounded variation, non-increasing $\mu : [t_0, t_f] \to \mathbb{R}^2$, such that $\mu(t)$ is constant on the time interval in which the state constraint is inactive.
- $|\lambda\rangle\rangle : [t_0, t_f] \to \mathbb{R}^{4n}$ is the time-varying Lagrange multiplier vector, whose elements are called the costates of the system.

We handle control constraints with saturation functions, (Graichen et al., 2010), such that the indicated inequality-constraint for control is transformed into a new equality-constraint. To do so, we define a new unconstrained control variable $\nu(t)$, and substitute the control constraint with a smooth and monotonically increasing saturation function $\phi : \mathbb{R} \to (u_{\min}, u_{\max})$ such that

$$\phi(\nu) = u_{max} - \frac{u_{max} - u_{min}}{1 + \exp(s\nu)} \quad \text{with} \quad s = \frac{c}{u_{\max} - u_{\min}}$$

in which $c > 0$ is a constant parameter, useful for modifying the slope of $\phi(\nu)$ at $\nu = 0$. The advantage of using a saturation function is that it is defined within the range of Ω, and asymptotically approaches the saturation limits for $\nu \to \pm\infty$. The next steps are the following:

- We add a regularization term to the cost functional J via a regularization parameter α, and define the new cost functional as $\tilde{J} = J + \alpha \int_{t_0}^{t_f} \nu^2(t)dt$, and solve the OCP successively by decreasing α_k. We use the result that if u_{k+1} and u_k are the optimal control inputs for $\alpha_{k+1} < \alpha_k$, then with $\lim_{k\to\infty} \alpha_k = 0$, $\tilde{J}(u_k, \alpha_k)$ converges to a non-increasing optimal cost, (Graichen et al., 2010), i.e., by bringing α closer to 0, we approach to the original problem.
- We consider an additional optimality condition for the new control variable by minimizing the Pontryagin-Hamilton function with respect to ν. Moreover, we need to consider the constraint equation

  $$u(t) - \phi(\nu) = 0 \tag{4.3}$$

  for the boundary value problem.
- We introduce a multiplier $\beta : [t_0, t_f] \to \mathbb{R}$ to take the equality constraint into account.

In this new setup, we will now obtain the optimality conditions. To this end, we first construct the Pontryagin Hamiltonian $\mathcal{H}$ defined for all $t \in [t_0, t_f]$ by (see detail derivation

in the proof of Proposition below).

$$\begin{aligned}\mathcal{H}(\rho,\lambda,u,\nu,\delta,\alpha,\beta,t) = (|\lambda(t)\rangle\rangle + 2\delta(t)\,|\tilde{\rho}(t)\rangle\rangle)^T \tilde{\mathcal{L}}\,|\tilde{\rho}(t)\rangle\rangle \\ + \eta u^2(t) + \alpha\nu^2(t) + \beta(t)\,(u(t) - \phi(\nu))\end{aligned} \tag{4.4}$$

where $\delta(t) = [1\ -1]\,\mu(t)$.

Proposition 4.2 *Consider the OCP (P1) that is given by (P), but with cost function $\tilde{J}$, and the additional constraint (4.3). Let $u^\star(t)$ be an optimal control and $\tilde{\rho}^\star(t)$ the corresponding state trajectory response. Then, there exist the multiplier $\lambda^\star(t)$ that together with $\delta, \beta : [t_0, t_f] \to \mathbb{R}$ satisfy the PMP necessary conditions. More precisely,*

$$\mathcal{H}(\rho^\star,\lambda^\star,u^\star,\nu,\mu,\alpha,\beta,t) \leq \mathcal{H}(\rho,\lambda,u,\nu,\mu,\alpha,\beta,t)$$

for all $t \in [t_0, t_f]$, and all feasible controls $u \in \Omega$. Moreover,

$$\begin{aligned}\frac{\partial\mathcal{H}}{\partial u} &= (|\lambda^\star\rangle\rangle + 2\delta\,|\tilde{\rho}^\star\rangle\rangle)^T \tilde{\mathcal{L}}_u\,|\tilde{\rho}^\star\rangle\rangle + 2\eta u^\star + \beta = 0 \\ \frac{\partial\mathcal{H}}{\partial\nu} &= 2\alpha\nu - \beta\frac{\partial\phi(\nu)}{\partial\nu} = 0\end{aligned}$$

The remaining first-order necessary conditions for the state and costate variables are given as

$$\begin{aligned}|\dot{\tilde{\rho}}^\star\rangle\rangle &= \frac{\partial\mathcal{H}}{\partial\,|\lambda\rangle\rangle} = \tilde{\mathcal{L}}\,|\tilde{\rho}^\star\,\rangle\rangle, \quad |\tilde{\rho}^\star(t_0)\rangle\rangle = \rho_0 \\ \left|\dot{\lambda}^\star\right\rangle\!\right\rangle^T &= \frac{-\partial\mathcal{H}}{\partial|\tilde{\rho}\rangle\rangle} = \tilde{\mathcal{L}}^T\,|\lambda^\star\rangle\rangle + 4\delta\tilde{\mathcal{L}}\,|\rho^\star\rangle\rangle, |\lambda^\star(t_f)\rangle\rangle = \lambda_f = \mathbf{0}\end{aligned}$$

In addition, the transversality condition imposes that

$$\mathcal{H}(t_f) + \Gamma = 0$$

Proof: Following similar arguments as in (Arutyunov et al., 2011) for the indicated set of conditions, the extended Hamilton-Pontryagin function is

$$\begin{aligned}\mathcal{H}(\rho,\lambda,u,\nu,\mu,\alpha,\beta,t) = (|\lambda(t)\rangle\rangle + \mu^T(t)\nabla_{\tilde{\rho}}h(|\tilde{\rho}(t)\rangle\rangle)^T \\ \tilde{\mathcal{L}}\,|\tilde{\rho}(t)\,\rangle\rangle + \eta u^2(t) + \alpha\nu(t)^2 + \beta(t)\,(u(t) - \phi(\nu))\end{aligned}$$

where the state constraint $h(|\tilde{\rho}(t)\rangle\rangle)$ and multiplier $\mu(t)$ are

$$h(|\tilde{\rho}(t)\rangle\rangle) = \begin{pmatrix}\tilde{P}[\chi(\rho)] - P_0 \\ \tilde{\alpha}P_0 - \tilde{P}[\chi(\rho)]\end{pmatrix} \leq 0, \quad \mu(t) = \begin{pmatrix}\mu_1(t) \\ \mu_2(t)\end{pmatrix} \tag{4.5}$$

Therefore, the gradient is given by

$$\nabla_{\tilde{\rho}}h(|\tilde{\rho}(t)\rangle\rangle) = \begin{pmatrix}\nabla_{\tilde{\rho}}\tilde{P}[\chi(\rho)] & -\nabla_{\tilde{\rho}}\tilde{P}[\chi(\rho)]\end{pmatrix}^T$$

where $\nabla_{\tilde{\rho}}\tilde{P}[\chi(\rho)] = 2|\tilde{\rho}(t)\rangle\rangle$. Then, the Pontryagin Hamiltonian forms as written in (4.4) from which the necessary conditions according to the PMP have been indicated. □

Proposition 4.3 *Let $\rho^\star(t)$, $u^\star(t)$, $\lambda^\star(t)$ be an optimal trajectory of (P1). Then, $\rho^\star(t)$, $u^\star(t)$, $\lambda^\star(t)$ is a local minimizer of the Pontryagin Hamiltonian (4.4) as long as α satisfies the condition*

$$\alpha > \frac{\beta}{2}\epsilon \tag{4.6}$$

where $\epsilon = \max_{v\in\mathbb{R}} |\frac{\partial^2\phi(v)}{\partial v^2}|$ is a finite bound.

Proof: A similar case of obtaining the second-order sufficient condition for local optimality is indicated in (Aronna, 2011), however, in our case since we have two control variables $\bar{u} = (u, v)$, the second derivative of our Pontryagin Hamiltonian is a 2×2 matrix rather than a scalar. Accordingly, if the Pontryagin Hamiltonian has a positive definite Hessian with respect to $\bar{u}$, then it is guaranteed that $u^\star(t)$ is the local minimizer of the Hessian, i.e., the generalized Legendre-Clebsch condition guarantees that over a singular arc, the Pontryagin Hamiltonian is minimized. In this case, the Hessian is given by $\mathcal{H}_{\bar{u}\bar{u}} = \begin{pmatrix} 2\eta & 0 \\ 0 & 2\alpha - \beta\frac{\partial^2\phi}{\partial v^2} \end{pmatrix} > 0$. Clearly, it is positive definite since η is positive, $\frac{\partial^2\phi}{\partial v^2}$ is bounded and α satisfies (4.6). □

4.4 Physics-Informed Neural Networks Based on the Theory of Functional Connections

In this section, we exploit the newly developed Pontryagin PINN method derived from the theory of functional connection, (Johnston, 2021; D'ambrosio et al., 2021). We give a short overview on how physics-informed neural networks derived from TFC can be used to solve BVPs. Consider a generic differential equation

$$F(t, y(t), \dot{y}(t)) = \mathbf{0}, \quad y(t_k) = y_{t_k}, \quad k \in \emptyset \cup \{1, 2, \ldots\} \tag{4.7}$$

where $F : \mathbb{R} \times \mathbb{R}^n \times \mathbb{R}^n \to \mathbb{R}^n$ is a given map, and $y(t) \in \mathbb{R}^n$ is the state variable that has known values at instant of time t_k. Note that here we utilize a unified process to resolve problems involving initial, boundary, or multiple values, so $k \in \emptyset$ refers to the boundary-free functions. The goal is to obtain the (approximated) solution $\hat{y}(\cdot)$ of (4.7) along time. Algorithm 4.1 describes the main steps of the application of TFC method. The first step is to apply a morph transformation (change of time) so that the problem can be written in the domain of the activation functions to be used in the next steps. Next, we impose the solution to be on the form of (4.8), where $g(\cdot) : \mathbb{R} \to \mathbb{R}^n$ indicates a user-specified function, and Ω is the so-called switching function. The free function $g(\cdot)$, as developed in (Huang et al., 2006) based on the theory of extreme learning machine (ELM), is modeled by a single hidden layer feedforward neural network (4.10), where the summation is over all L hidden neurons, and $\sigma(\cdot)$ is the activation function. In (4.10),

Algorithm 4.1 Modelling and training the PoNN (main steps)

1: Morphing transformation

$$\tau = \tau_0 + c\,(t - t_0) \leftrightarrow t = t_0 + \frac{1}{c}\,(\tau - \tau_0)\,, \quad c > 0$$

2: Derive the approximated formulations for $y(t)$

$$\hat{y}(\tau) = g\,(\tau) + \sum_{n=1}^{k} \Omega_k\,(\tau)\,(y(\tau_k) - g(\tau_k)) \tag{4.8}$$

3: Obtain a new equation as a function of the independent variable τ, $g\,(\tau)$, and its derivative

$$F(\tau, \hat{y}(\tau), \dot{\hat{y}}(\tau)) = \tilde{F}(\tau, g(\tau), \dot{g}(\tau)) = 0 \tag{4.9}$$

4: Formulate $g\,(\tau)$ through a single layer neural network

$$g\,(\tau) = \sum_{l=1}^{L} \xi_l \sigma\,(\omega_l \tau + b_l) = \boldsymbol{\sigma}^T\,(\tau)\boldsymbol{\xi} \tag{4.10}$$

in which $\boldsymbol{\sigma}^T\,(\tau) = \sigma^T(\tau) \otimes I_{n\times n}$, where $\sigma^T(\tau) = [\sigma\,(\omega_1\tau + b_1), \ldots, \sigma\,(\omega_L\tau + b_L)]$, and $\boldsymbol{\xi} = vec([\xi_1, \ldots, \xi_L])$.

5: Compute the derivatives of $g\,(\tau)$ as $\dot{g}(\tau) = c\boldsymbol{\sigma}'^T(\tau)\boldsymbol{\xi}$ where $\boldsymbol{\sigma}' = \frac{d\boldsymbol{\sigma}(\tau)}{d\tau}$ and obtain (4.9) in terms of unknowns, so $\tilde{F}(\tau, \boldsymbol{\xi}) = 0$.

6: Discretize τ into N points, and express the obtained set of differential equations as loss functions at each point as $\mathbb{L}^T\,(\boldsymbol{\xi}) = \left[\tilde{F}\,(\tau_0, \boldsymbol{\xi}), \ldots, \tilde{F}\,(\tau_N, \boldsymbol{\xi})\right]$ and obtain the unknown $\boldsymbol{\xi}$, by computing the solution of $\mathbb{L} = \mathbf{0}$.

ξ_l, ω_l and b_l denote the output weight, input weight, and bias of the lth hidden node,, respectively. These parameters correspond to the learning factors to be updated in the training phase. We then obtain a new set of equations $\tilde{F}(\tau, \boldsymbol{\xi})$, solved via the augmented loss function $\mathbb{L}$. Now, let proceed with the solution of optimality conditions obtained for (P_1). We approximate the state and costate as

$$\begin{aligned} |\tilde{\rho}\rangle\rangle\,(\tau, \boldsymbol{\xi}_\rho) &= \left(\boldsymbol{\sigma}_{\tilde{\rho}}\,(\tau) - \Omega_1\,(\tau)\boldsymbol{\sigma}_{\tilde{\rho}}\,(\tau_0) - \Omega_2\,(\tau)\boldsymbol{\sigma}_{\tilde{\rho}}\,(\tau_f)\right)^T \boldsymbol{\xi}_{\tilde{\rho}} \\ &\quad + \Omega_1\,(\tau)\,\rho_0 + \Omega_2\,(\tau)\,\rho_f \\ |\lambda\rangle\rangle\,(\tau, \boldsymbol{\xi}_\lambda) &= \left(\boldsymbol{\sigma}_\lambda\,(\tau) - \Omega_2\,(\tau)\boldsymbol{\sigma}_\lambda\,(\tau_f)\right)^T \boldsymbol{\xi}_\lambda + \Omega_2\,(\tau)\,\lambda_f \end{aligned}$$

where the switching functions are described by $\Omega_1\,(\tau) = 1 + \frac{2\Delta\tau^3}{\Delta\tau_f{}^3} - \frac{3\Delta\tau^2}{\Delta\tau_f{}^2}$ and $\Omega_2\,(\tau) = -\frac{2\Delta\tau^3}{\Delta\tau_f{}^3} + \frac{3\Delta\tau^2}{\Delta\tau_f{}^2}$ with $\Delta\tau = \tau - \tau_0$ and $\Delta\tau_f = \tau_f - \tau_0$, (Johnston et al., 2020). By taking the derivatives of the above expressions, we obtain

$$\begin{aligned} |\dot{\tilde{\rho}}\rangle\rangle\,(\tau, \boldsymbol{\xi}_\rho) &= c\Big(\boldsymbol{\sigma}'_{\tilde{\rho}}\,(\tau) - \Omega'_1\,(\tau)\boldsymbol{\sigma}_{\tilde{\rho}}\,(\tau_0) - \Omega'_2\,(\tau)\boldsymbol{\sigma}_{\tilde{\rho}}\,(\tau_f)\Big)^T \boldsymbol{\xi}_{\tilde{\rho}} \\ &\quad + \Omega'_1\,(\tau)\,\rho_0 + \Omega'_2\,(\tau)\,\rho_f \\ |\dot{\lambda}\rangle\rangle\,(\tau, \boldsymbol{\xi}_\lambda) &= c\left(\boldsymbol{\sigma}'_\lambda\,(\tau) - \Omega'_2\,(\tau)\boldsymbol{\sigma}_\lambda\,(\tau_f)\right)^T \boldsymbol{\xi}_\lambda + \Omega'_2\,(\tau)\,\lambda_f \end{aligned}$$

Regarding the control variables, the following functional approximation are introduced

$$u(\tau,\boldsymbol{\xi}) = \boldsymbol{\sigma}_u^T(\tau)\boldsymbol{\xi}_u, \quad \nu(\tau,\boldsymbol{\xi}) = \boldsymbol{\sigma}_\nu^T(\tau)\boldsymbol{\xi}_\nu$$

We also expand the equality constraint multiplier $\beta(\tau,\boldsymbol{\xi}) = \boldsymbol{\sigma}_\beta^T(\tau)\boldsymbol{\xi}_\beta$. In addition, the state constraint multipliers are

$$\mu_1(\tau,\boldsymbol{\xi}) = \boldsymbol{\sigma}_{\mu_1}^T(\tau)\boldsymbol{\xi}_{\mu_1}, \quad \mu_2(\tau,\boldsymbol{\xi}) = \boldsymbol{\sigma}_{\mu_2}^T(\tau)\boldsymbol{\xi}_{\mu_2}$$

In line with the ELM algorithm, (Huang et al., 2006), for the free final time problems, the vector of PoNNs' parameters to be learned is constructed as $\boldsymbol{\zeta} = \left[\boldsymbol{\xi}_{\tilde{\rho}}\ \boldsymbol{\xi}_\lambda\ \boldsymbol{\xi}_u\ \boldsymbol{\xi}_\nu\ \boldsymbol{\xi}_\beta\ \boldsymbol{\xi}_{\mu_1}\ \boldsymbol{\xi}_{\mu_2}\ c\right]^T$. Now, we express the set of loss functions to be minimized as

$$\begin{aligned}
&\mathbb{L}_{\tilde{\rho}} = |\dot{\tilde{\rho}}\rangle\rangle - \tilde{\mathcal{L}}\,|\tilde{\rho}\,\rangle\rangle \\
&\mathbb{L}_\lambda = |\dot{\lambda}\rangle\rangle^T - (\tilde{\mathcal{L}}^T|\,\lambda\rangle\rangle + 4\delta\tilde{\mathcal{L}}\,|\tilde{\rho}\rangle\rangle) \\
&\mathbb{L}_u = (|\,\lambda\rangle\rangle + 2\delta\,|\tilde{\rho}\rangle\rangle)^T\tilde{\mathcal{L}}_u\,|\tilde{\rho}\rangle\rangle + 2\eta u + \beta \\
&\mathbb{L}_\nu = 2\alpha\nu - \beta\phi'(\nu), \quad \mathbb{L}_\phi = u - \phi(\nu) \\
&\mathbb{L}_{\mathcal{H}} = \mathcal{H}\left(t_f\right) + \Gamma \\
&\mathbb{L}_{\mu_1} = \tilde{P}[\chi(\rho)] - P_0, \quad \mathbb{L}_{\mu_2} = \bar{\alpha}P_0 - \tilde{P}[\chi(\rho)]
\end{aligned}$$

leading to an augmented form of the loss function as

$$\mathbb{L} = \begin{bmatrix}\mathbb{L}_{\tilde{\rho}} & \mathbb{L}_\lambda & \mathbb{L}_u & \mathbb{L}_\nu & \mathbb{L}_\phi & \mathbb{L}_{\mathcal{H}} & \mathbb{L}_{\mu_1} & \mathbb{L}_{\mu_2}\end{bmatrix}^T \tag{4.11}$$

Equation (4.11) can be solved by a numerical minimization scheme, and the PoNN's parameter will be learnt during the procedure. The iterative least-square method has proved to be an efficient scheme for such problem, (D'ambrosio et al., 2021). Through this method, the estimation of $\boldsymbol{\zeta}$ is adjusted and refined to improve accuracy and convergence towards the desired outcome at $k+1$th iteration, such that $\boldsymbol{\zeta}_{k+1} = \boldsymbol{\zeta}_k + \Delta\boldsymbol{\zeta}_k$, where $\Delta\boldsymbol{\zeta}_k = -\left(\mathbb{J}(\boldsymbol{\zeta}_k)^T\mathbb{J}(\boldsymbol{\zeta}_k)\right)^{-1}\mathbb{J}(\boldsymbol{\zeta}_k)^T\mathbb{L}(\boldsymbol{\zeta}_k)$, in which $\mathbb{J}$ is the Jacobian matrix, compiling the partial derivatives of the loss function with respect to each unknown parameter, and, therefore provides a complete representation of the sensitivity of the losses to changes in the unknowns. The iterative procedure continues to be repeated until the convergence criteria is satisfied, meaning that for a predefined tolerance $\bar{\varepsilon} > 0$, we reach to $L_2\left[\mathbb{L}\left(\boldsymbol{\zeta}_k\right)\right] < \bar{\varepsilon}$.

4.5 Simulation Results

In the following, we show the feasibility of our results in a numerical study. Let consider a quantum system consisting of a two-level atom and a vacuum environment. The dissi-

pation is captured via the decay of the atom through a photon emission, which is a result of the atom - environment interaction. The environment in this case is the surrounding vacuum state. Therefore, the system dynamics must be expressed through the master equation (4.1), in which the term $H(u(t))$ describes the total atom-vacuum quantum-mechanical Hamiltonian as

$$H\left(u\left(t\right)\right) = E\left|1\right\rangle\left\langle 1\right| + u\left(t\right)\left(\left|0\right\rangle\left\langle 1\right| + \left|1\right\rangle\left\langle 0\right|\right) \tag{4.12}$$

where $u(t)$ is the driving control coherently switching between the two states. We work with the implemented dynamics in (4.2). For this problem, the damping rate γ is the atom-vacuum coupling, and the Liouvillian superoperator in the Fock-Liouvillian space is

$$\mathcal{L} = \begin{pmatrix} 0 & iu & -iu & \gamma \\ iu & -iE-\frac{\gamma}{2} & 0 & -iu \\ -iu & 0 & -iE-\frac{\gamma}{2} & iu \\ 0 & -iu & iu & -\gamma \end{pmatrix},$$

which is mapped to the extended superoperator $\tilde{\mathcal{L}}$. The parameters are considered as the following: $N = 40$, $L = 30$, $\eta = 0.1$, $\Gamma = 0.01$, $\gamma = 0.9$, $\bar{\alpha} = 0.99$, $\alpha = 10^{-5}$, $E = 1$. Moreover, we use the Chebyshev orthogonal polynomials as the basis for TFC implementation. Regarding the constraints for the components of the control $u(t)$, they have been set as $u_{min} = -1$ and $u_{max} = +1$. The results are obtained after 48 iterations. For all results, the state is initiated as $\rho_{11} = 1$, with no coherence between different states. First, we neglect the dissipation part, so the solution reduces to the resolution of the Liouville-von Neumann equation, see Fig. 4.1(a). As the next case, we consider the dissipation while there is no coherent driving. The population of the excited state experiences an exponential decay, see Fig. 4.1(b). Afterward, it becomes feasible to compute the behavior of a dissipative quantum system that undergoes both coherent driving and decay. In such cases, oscillations and decay co-occur as both behaviors exist simultaneously, see Fig. 4.1(c). In the following, we plot the state evolution under the action of optimal control. We initiate by the pure state $\rho_{11} = 1$ and target to $\rho_{00} = 1$, while following the constraints on purity preservation. The population evolution is shown in Fig. 4.1(d). According to the data depicted in the graph, there is a clear trend of exponential decay in the population of the initial state, while there is a corresponding upward trend in the population of the target as time passes. In order to check the security level of reaching the target, we have to calculate the transition probability known as the quantum fidelity, referring to the degree of similarity between two quantum states, typically the system state $\rho(t)$ and target φ. We study fidelity in terms of state purity computed by $\mathcal{F}\left(\rho,\varphi\right) = \frac{\left(tr(\rho\varphi)\right)^2}{P(\rho)P(\varphi)}$, (Indrajith et al., 2022). Since our target φ is a pure state, i.e., $\varphi = \left|\psi\right\rangle\left\langle\psi\right|$, fidelity can simply be assessed as $\mathcal{F}\left(\rho,\varphi\right) = \frac{\left\langle\psi\right|\rho\left|\psi\right\rangle}{P(\rho)}$. Fig. 4.2 shows the effects of purity preservation on fidelity.

Remark 4.2 *Recently, the theory of functional connections has been extended to n-dimensions, as described in (Mortari and Leake, 2019). Therefore, a natural question is whether the proposed*

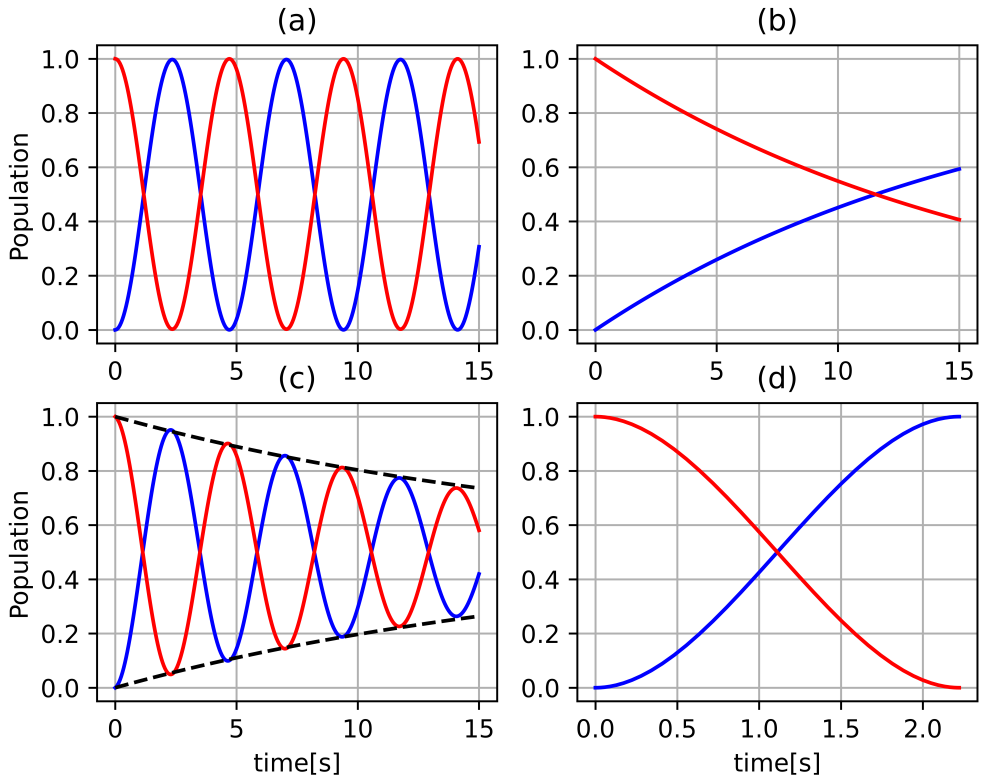


Figure 4.1: Population evolution under quantum dynamics. The blue and red lines represent the evolution of ρ_{00} and ρ_{11}, respectively. (a) Coherent driving with no decay. (b) Decay with no coherent driving. (c) Coherent driving and decay. (d) Optimal coherent driving and decay.

method using PoNNs is scalable enough to be applied to systems with any number of levels. From this work, we can observe that for an n-level system, the dimension of the Liouville superoperator $\tilde{\mathcal{L}}$ *in* (4.2) *is* $2n^2 \times 2n^2$*, which also leads to an increase in the dimension of the augmented loss vector* $\mathbb{L}$ *in* (4.11)*, and therefore an overall increase in computational complexity. On the other hand, as pointed out in (Mortari and Furfaro, 2021), TFC approach presents a low condition number, and typically is numerically robust, as indeed we could attest from our numerical computations, that revealed good robustness to poor initialization and insensitivity to small changes in the input data. Therefore, the proposed strategy can perform well in practical applications, where there may be noise or other sources of uncertainty in the system.*

4.6 Concluding Remarks and Discussions

In this chapter, we proposed a framework for preserving quantum purity during a quantum state transition problem. Specifically, we aim to minimize both the time and energy

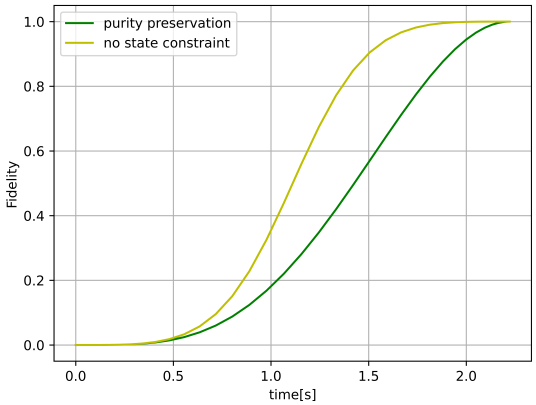


Figure 4.2: State transition probability quantified by purity.

required for the transition, while adhering to the Lindblad master equation, which governs the system dynamics. To achieve this goal, we employed a combination of two techniques, namely the Gamkrelidze revisited method and the concept of saturation functions and system extensions. The resulting boundary value problem is then solved using Pontryagin neural networks, which are well-suited for this type of problem formulation. Our approach allows us to preserve the purity of the quantum state during the transition while minimizing the resources required. Furthermore, we analyze the effects of state constraints on the evolution of quantum fidelity, providing a numerical example for a two-level system. As future work, we intend to extend our approach to higher-order dimensional systems, which could yield valuable insights and applications in various fields, including quantum computing and quantum communication. Our results have important implications for the practical implementation of quantum state transitions.

Chapter 5

State Estimation and Control for Stochastic Quantum Dynamics with Homodyne Measurement: Stabilizing Qubits under Uncertainty

This chapter introduces a Lyapunov-based control strategy alongside two filtering methods for controlling and estimating the evolution of coherence vector elements from sequential homodyne measurements. The methods include traditional quantum filtering and a novel extended Kalman filter, which explicitly addresses the dynamics of a stochastic master equation with correlated noise, thereby ensuring the quantum properties of the estimated state variable by design. We also explore scenarios where the system's Hamiltonian is unknown, demonstrating that both filters exhibit reduced performance with increased estimation errors. To address this, we propose a multiple model estimation scheme applicable to either filter. The estimated density operator is then controlled using the proposed switching-based Lyapunov scheme, which guarantees noise-to-state practical stability in probability. We demonstrate the effectiveness of our approach in stabilizing a qubit coupled to a leaky cavity under homodyne detection, even with uncertainty in the resonance frequency. This work was published in (Dehaghani et al., 2024e).

5.1 Stochastic Quantum Control and Estimation

Stochastic quantum dynamics encompass the complex interactions between quantum systems and classical control mechanisms. This section delves into the mathematical frameworks and problem statements essential for controlling and estimating the states of such quantum systems.

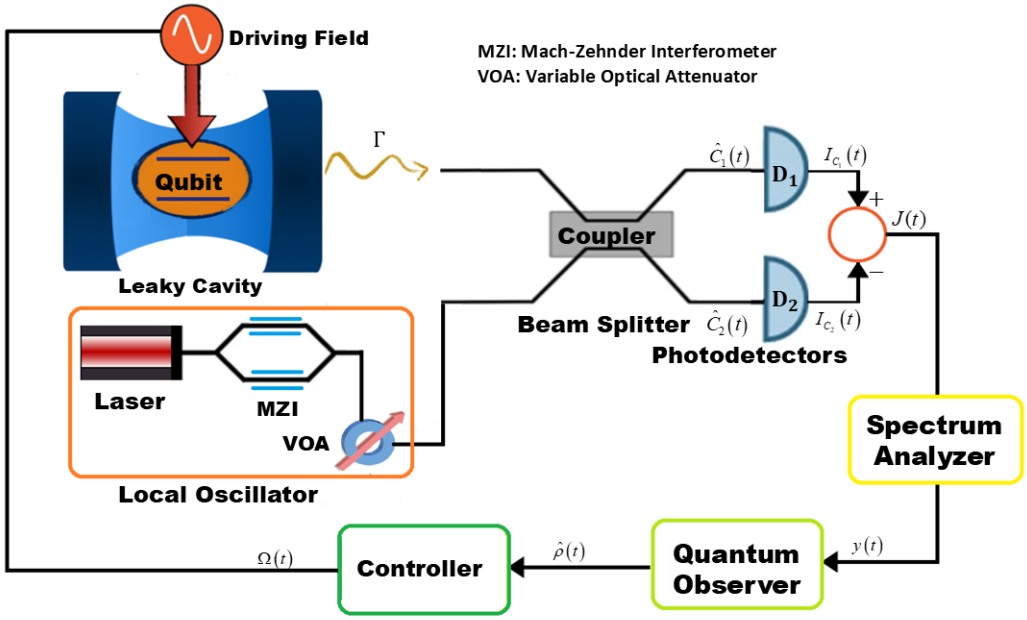


Figure 5.1: Illustration of the proposed configuration: A qubit coupled to a leaky cavity is continuously monitored via homodyne detection. The emitted radiation from the qubit is combined with a local oscillator laser at a beam splitter. The transformations of the field operators through the beam splitter are denoted by $C_1(t)$ and $C_2(t)$, which are then detected by photodetectors D_1 and D_2, respectively. The difference of the two produced signals I_{c1} and I_{c2} generates the resulting signal $J(t)$. This signal is sent to a quantum observer, which estimates the quantum state $\hat{\rho}(t)$. The estimated state is then transmitted to a controller. The controller adjusts the driving field $\Omega(t)$ through the control Hamiltonian to the qubit, aiming to generate and stabilize the qubit into a desired target set.

5.1.1 Quantum Stochastic Evolution

The stochastic quantum dynamics can be accurately described by well-structured stochastic differential equations known as Stochastic Master Equations (SME). These equations define the relationships between the classical control input $\Omega(t)$, tuned by the controller, and the classical output $J(t)$ corresponding to instantaneous value of the observed measurements. For such a setup, as indicated in Fig. 5.1, the diffusive quantum stochastic master equation, interpreted in the context of Itô calculus, is expressed as (Rouchon, 2022)

$$\begin{aligned} d\rho(t) = &-i[H_d + \Omega(t)H_c, \rho(t)]\,dt + \Gamma\mathcal{D}[c_d]\rho(t)\,dt \\ &+ M\mathcal{D}[c_m]\rho(t)\,dt + \sqrt{\eta M}\mathcal{H}[c_m]\rho(t)\,dW(t), \end{aligned} \tag{5.1}$$

where the quantum density operator $\rho \in \mathbb{H}_\rho$. The unitary aspects of the dynamics (5.1) is characterized by the quantum mechanical system Hamiltonian composed of drift H_d and control H_c terms. The dissipative part of the dynamics is described through arbitrary Lindblad operators c_d and c_m, corresponding to decoherence and measurement chan-

nels. The superoperators $\mathcal{D}[c]\rho$ corresponding to dissipation, and $\mathcal{H}[c]\rho$ corresponding to measurement for a generic operator c are defined as follows

$$\mathcal{D}[c]\rho = c\rho c^\dagger - \frac{1}{2}(c^\dagger c\rho + \rho c^\dagger c),$$
$$\mathcal{H}[c]\rho = c\rho + \rho c^\dagger - \left\langle c + c^\dagger \right\rangle \rho.$$

The coefficient $\Gamma > 0$ indicates the decay rate, $M > 0$ is the interaction strength corresponding to the measurement process, and $\eta \in [0,1]$ indicates the detector efficiency with $\eta = 1$ implying perfect detection and $\eta = 0$ lack of information about the quantum state. The differential $dW(t)$ denotes an infinitesimal Wiener increment satisfying Itô's lemma with $\mathbb{E}[dW(t)] = 0$, $\mathbb{E}[dW^2(t)] = dt$. The same Wiener process is shared by the outcome of classical measurement homodyne current

$$J(t) = \sqrt{\eta M}\left\langle c_m + c_m^\dagger \right\rangle + \xi(t), \tag{5.2}$$

where $\xi(t) = dW(t)/dt$, follows Gaussian white noise properties with $\mathbb{E}[\xi(t)\xi(t')] = \delta(t - t')$.

5.1.2 Problem Statement

This subsection outlines the primary two research objectives pursued in this chapter.

Problem 5.1 *Given the quantum system presented in* (5.1)-(5.2)*, develop a set of estimators to directly estimate the evolution of the density operator $\rho(t)$ from the continuous sequence of homodyne current measurements. In addition, consider that the drift Hamiltonian H_d contains* unknown *constant parameters.*

Prior to expressing the second problem, we introduce the following stability definition pertinent to the stochastic quantum system problem at hand, drawing upon the frameworks in (Ito and Nishimura, 2015; Deng et al., 2001).

Definition 5.1 *(Noise-to-State Practically Stable in Probability): Let χ be a closed and invariant set under the dynamics governed by the stochastic differential equation in Itô form*

$$d\rho(t) = f(\rho)dt + g(\rho)\sigma(t)dW(t),$$

where $\rho \in \mathbb{H}_\rho$, $\sigma(t)$ is the intensity of noise at time t, and $W(t)$ denotes a 1-dimensional standard Wiener process. The set χ is noise-to-state practically stable (NSpS) in probability if, for every $\varepsilon > 0$, there exists a function $\beta \in \mathcal{KL}$, a function $\gamma \in \mathcal{K}$, and a non-negative real number $b \geq 0$, ensuring that for every initial density operator $\rho(0) \in \mathbb{H}_\rho$, the following holds with probability at least $1 - \varepsilon$, for every $t \geq 0$

$$\mathbb{P}\left\{ d(\rho(t),\chi) < \beta\left(d(\rho(0),\chi),t\right) + \gamma(\sup_{\tau\in[0,t]} \sigma^2(\tau)) + b \right\} \geq 1 - \varepsilon \tag{5.3}$$

If $b = 0$, χ is noise-to-state stable (NSS) in probability.

Remark 5.1 *Note that NSpS implies that the set χ is asymptotically practically stable in probability, that is, condition (5.3) holds without the term $\gamma(\sup_{\tau\in[0,t]}\sigma^2(\tau))$, (but maybe with a different b) since $\sigma(t)$ is bounded. Moreover, in that case, if $\beta(r,t) = cre^{-\lambda t}$ for some $c > 0$ and $\lambda > 0$, the set χ is said to be practically exponentially stable in probability.*

Definition 5.1 is introduced to measure the resilience of a quantum system's stability in the face of noise. It ensures that, probabilistically, the system's state stays within a practical vicinity of the invariant set χ, notwithstanding the influence of quantum noise. The extent of this vicinity is contingent upon the intensity of the noise, as characterized by the variance of the Wiener process $W(t)$.

We can now proceed with the second problem. To this end, let χ_f be a desired target state characterized by all the elements $\rho_f \in \mathbb{H}_\rho$ that commutes with the drift Hamiltonian H_d, that is, $[\rho_f, H_d] = 0$. This commutation condition ensures that the target states ρ_f remain invariant under the evolution governed by H_d. Then, the goal is the following.

Problem 5.2 *Using the solutions to Problem 5.1 to estimate the system's state $\rho(t)$, design a controller that commands the signal $\Omega(t)$ with the aim of steering $\rho(t)$ from an arbitrary initial state $\rho_0 \in \mathbb{H}_\rho$, towards a stationary point within the predetermined target set χ_f. Moreover, the controller should guarantee that χ_f is NSpS with respect to the estimation error variance.*

5.2 Estimation Techniques in Stochastic Quantum Dynamics

This section introduces and elaborates on three estimation techniques: Quantum Filter Estimator, Quantum Extended Kalman Filter Estimator, and finally a Multiple-Model Adaptive Estimator to address the uncertainty on the drift Hamiltonian H_d. In the following, we leverage the fact that a general mixed state of a qubit can be expressed as a linear combination of the Pauli matrices, which, along with the identity matrix, form a basis for the 2×2 self-adjoint matrices, i.e.,

$$\rho(t) = \frac{1}{2}I + \frac{1}{2}\sum_{k=1}^{3} x_k(t)\sigma_k, \tag{5.4}$$

where the real-valued functions $x_k(t) = \langle\sigma_k\rangle$ are the coordinates of a point within the unit ball and are taken to be components of the so-called coherence vector $\mathbf{x}(t) = [x_1, x_2, x_3]^T \in \mathbb{R}^3$. By rewriting (5.1) one attains the following stochastic system dynamics for $\mathbf{x}(t)$ in Itô form

$$d\mathbf{x}(t) = \mathbf{f}(\mathbf{x}, \Omega(t))\,dt + \mathbf{g}(\mathbf{x})\,dW(t), \tag{5.5}$$

where $\mathbf{f}(\mathbf{x},\Omega) = [f_1(\mathbf{x},\Omega), f_2(\mathbf{x},\Omega), f_3(\mathbf{x},\Omega)]^T$ and $\mathbf{g}(\mathbf{x}) = [g_1(\mathbf{x}), g_2(\mathbf{x}), g_3(\mathbf{x})]^T$, whose elements for $k = 1,2,3$ are

$$\begin{aligned}\mathbf{f}_k(\mathbf{x},\Omega) &= -i\,\mathrm{Tr}\{[H_d + \Omega(t)H_c, \rho(t)]\sigma_k\} + \mathrm{Tr}\{(\Gamma\mathcal{D}[c_d] + M\mathcal{D}[c_m])\,\rho(t)\sigma_k\},\\ \mathbf{g}_k(\mathbf{x}) &= \sqrt{\eta M}\,\mathrm{Tr}\{\mathcal{H}[c_m]\rho(t)\sigma_k\},\end{aligned}$$

with $\rho(t)$ substituted by (5.4). Accordingly, by rewriting the output equation (5.2), one attains

$$dy(t) = h(\mathbf{x}(t))dt + dV(t), \tag{5.6}$$

where the term $dV(t) = dW(t) + dZ(t)$ includes an additional infinitesimal Wiener increment with $\mathbb{E}[dZ(t)] = 0$, $\mathbb{E}[dZ^2(t)] = \sigma_z^2 dt$ corresponding to the measurement noise associated with the spectrum analyzer, and the term $h(\mathbf{x}(t))$ is given as

$$h(\mathbf{x}) = \frac{\sqrt{\eta M}}{2}\left(\mathrm{Tr}\Big\{c_m + c_m^\dagger\Big\} + \sum_{k=1}^{3} x_k(t)\,\mathrm{Tr}\Big\{(c_m + c_m^\dagger)\sigma_k\Big\}\right).$$

5.2.1 Quantum Filter Estimator

The Quantum Filter Estimator is a fundamental tool in the estimation of quantum states. It provides a systematic approach to updating the state of a quantum system based on continuous measurement results. This estimator relies on the principles of quantum measurement theory and stochastic calculus to produce an estimate of the quantum state in real-time. In particular, since the quantum stochastic dynamics (5.1) is inherently a filtering equation, one can use it to predict the estimated state $\hat{\mathbf{x}}_{QF}(t)$ following the approach in (Bouten et al., 2007), but in our case adapted for the coherence vector dynamics in (5.5), which results in

$$d\hat{\mathbf{x}}_{QF}(t) = \mathbf{f}(\hat{\mathbf{x}}_{QF}(t), \Omega(t))\,dt + \mathbf{g}(\hat{\mathbf{x}}_{QF}(t))\,(dy(t) - h(\hat{\mathbf{x}}_{QF})dt). \tag{5.7}$$

Here, $\hat{\mathbf{x}}_{QF}(t)$ represents the estimated state vector of quantum filtering equation at time t, $\mathbf{f}(t, \hat{\mathbf{x}}_{QF}(t))$ is the drift term, and $\mathbf{g}(\hat{\mathbf{x}}_{QF}(t))$ is the diffusion term influenced by the Wiener increment $dW(t)$, that in (5.7) is replaced by the innovation term $dy(t) - h(\hat{\mathbf{x}}_{QF})dt$.

5.2.2 Quantum Kalman Filter estimator

The Quantum Kalman Filter Estimator extends the classical Kalman filter to the quantum domain. It is particularly useful for systems where the noise and disturbances can be modeled as Gaussian processes. By leveraging the properties of the Kalman filter, this estimator offers a robust and efficient means of tracking the evolution of quantum states under noisy conditions, yielding high-quality estimates in the presence of measurement and process noise while also providing the associated confidence or uncertainty levels. It is however important to stress that in this setup one have first to deal with the following

points: (i) the stochastic system dynamics for the coherence vector in (5.5) is nonlinear; (ii) the noise in the output equation (5.6) is correlated with process noise in (5.5) by noting that dV includes dW; and (iii) the coherence vector space for a qubit is a ball with radius 1, known as the Bloch ball, thereby satisfying $\|\mathbf{x}\|^2 \leq 1$. To address (i), we apply an Extended Kalman Filter (EKF) based approach by linearizing the non-linear functions around the current estimate using a first-order Taylor expansion. For (ii), we make use of a de-correlating approach, see (Simon, 2006), but tailored for our case, such that the new transformed equivalent system satisfies the property of uncorrelated process and measurement noises, and therefore one can then make use of the standard EKF equations. To address (iii), we integrate the structural properties of a valid quantum state into the observer equations by constraining the state estimate $\hat{\mathbf{x}}_{KF}(t)$ at the update equation to always belong to the Bloch ball. To this end, we define the following operator acting on the coherence vector $\mathbf{x}$ and a real vector $\mathbf{a} \in \mathbb{R}^3$ as

$$\mathbf{x} \oplus \mathbf{a} = \text{Proj}\,(\mathbf{x} + \mathbf{a}), \tag{5.8}$$

where the operator $\text{Proj}(\mathbf{x}) = 1/\max\{1, \|\mathbf{x}\|\}\mathbf{x}$ projects $\mathbf{x}$ onto the closed ball. The operator (5.8) is pivotal within our proposed filtering algorithm, ensuring that the state and consequently the estimate of the density matrix adheres to the necessary properties of a density operator, and maintains the physical relevance of our estimated states.

With the established setup, we proceed to construct a quantum Kalman filter estimator. In this framework, we treat the measurement noise $dW(t)$ and the noise of spectrum analyzer $dZ(t)$ uncorrelated, that is $\mathbb{E}[dW(t)\,dZ(t)] = 0$. Then, its correlation with process noise is given by $\mathbb{E}[dW(t)\,dV(t)] = dt$ since we have been considered $\mathbb{E}[dW^2(t)] = dt$. Note also that the variance $\mathbb{E}[dV^2(t)]$ is defined as $\mathbb{E}[dV^2(t)] = \sigma_v^2 dt$, with $\sigma_v^2 = (1 + \sigma_z^2)$. Now, we establish the following result.

Proposition 5.1 *Consider the stochastic differential equation (SDE)*

$$d\bar{\mathbf{x}} = \bar{\mathbf{f}}(\bar{\mathbf{x}}, \Omega, dy)dt + \mathbf{g}(\bar{\mathbf{x}})d\bar{W}(t), \tag{5.9}$$

where

$$\bar{\mathbf{f}}(\bar{\mathbf{x}}, \Omega, dy)dt = \mathbf{f}(\bar{\mathbf{x}}, \Omega)dt - \bar{\sigma}\mathbf{g}(\bar{\mathbf{x}})h(\bar{\mathbf{x}})dt + \bar{\sigma}\mathbf{g}(\bar{\mathbf{x}})dy,$$

$\bar{\sigma} = 1/(1 + \sigma_z^2)$, *and* $d\bar{W} = dW - \bar{\sigma}dV$. *Then, the process and measurement noises associated with the system formed by* (5.9) *and* (5.6) *are uncorrelated, that is,* $\mathbb{E}[d\bar{W}dV] = 0$. *Moreover,* (5.9) *is equivalent to* (5.5) *in the sense that if both SDEs start with the same initial condition and all the exogenous signals have the same trajectory, then* $\mathbf{x}(t) = \bar{\mathbf{x}}(t)$, *for every* $t \geq t_0$.

Proof: To show uncorrelated noises, we compute

$$\mathbb{E}[d\bar{W}(t)dV(t)] = \mathbb{E}[dW(t)dV(t)] - \bar{\sigma}\mathbb{E}[dV^2(t)] = 0.$$

To show the equivalence of both SDEs, we first start to note using (5.6) that the term $\bar{\sigma}\mathbf{g}(\mathbf{x})\Big(dy - h(\mathbf{x})dt - dV\Big)$ is zero. If we now add this null term to the right-hand-side of (5.5), and replace the variable $\mathbf{x}$ by $\bar{\mathbf{x}}$, we obtain precisely (5.9). □

We can now propose our state estimator that continuously updates its state estimate $\hat{\mathbf{x}}_{KF}(t)$ as new measurements are acquired through the propagation and update steps for the state and covariance matrix. In the propagation step, the current estimate of the state is propagated through the deterministic system dynamics

$$d\hat{\mathbf{x}}_{KF}^{-}(t) = \bar{\mathbf{f}}(\hat{\mathbf{x}}_{KF}(t), \Omega(t), y(t))\, dt, \tag{5.10}$$

producing an a priori state estimate $\hat{\mathbf{x}}_{KF}^{-}(t)$. Similarly, an a priori estimation of the prediction error covariance matrix $P_{3\times 3}$ is computed as

$$dP^{-}(t) = (A(t)P(t) + P(t)A^{\dagger}(t) + G(t)\sigma_{\bar{w}}^{2}(t)G^{\dagger}(t))dt \tag{5.11}$$

for which the initial guess $P(0) = P_0$ encodes the confidence in the estimate of the initial condition $\hat{\mathbf{x}}_{KF}(0)$, and $\sigma_{\bar{w}}^{2} = 1 + \bar{\sigma}$.

Note that in (5.11), to evaluate the propagation of P, we need to compute the matrices $A(t) = \frac{\partial \bar{\mathbf{f}}(\mathbf{x},\Omega)}{\partial \mathbf{x}}$ and $G(t) = \frac{\partial \mathbf{g}(\mathbf{x})}{\partial \mathbf{x}}$. It turns out that only the term $\mathbf{g}(\mathbf{x})$ introduces a nonlinear term (in fact quadratic) in $\mathbf{x}$. All the other ones are linear with $\mathbf{x}$, and therefore the linearizations for these terms are not approximations. This is not surprising since the Lindblad equation can be transformed into an inhomogeneous linear vector equation using the coherence vector formulation (Alicki and Lendi, 2007).

Next, the update step integrates the most recent measurement by updating the prediction equations (5.10) and (5.11) to obtain the a posteriori estimates

$$\begin{aligned}\hat{\mathbf{x}}_{KF}(t) &= \hat{\mathbf{x}}_{KF}^{-}(t) \oplus K(t)\left(dy(t) - h(\mathbf{x}(t))dt\right),\\ P(t) &= P^{-}(t) - P^{-}(t)C^{\dagger}\sigma_{v}^{-2}CP^{-}(t).\end{aligned}$$

Here, the Kalman gain is computed as $K(t) = P(t)C^{\dagger}\sigma_{v}^{-2}$, where $C = \Big[c_1, c_2, c_3\Big]$, with $c_k = \frac{\sqrt{\eta M}}{2}\mathrm{Tr}\{(c_m + c_m^{\dagger})\sigma_k\}$, $k = 1,2,3$. By estimating the components of the Bloch vector, we can then reconstruct an estimate for the density matrix as follows:

$$\hat{\rho}(t) = \frac{1}{2}I + \frac{1}{2}\sum_{k=1}^{3}\hat{x}_{kKF}(t)\sigma_k. \tag{5.12}$$

We can now state the following result.

Proposition 5.2 *Consider the proposed extended Kalman-based filter with initial condition $\hat{\rho}_0 \in \mathbb{H}_\rho$, which implies an adequate initial condition $\hat{\mathbf{x}}_{KF}(0)$. Then, the state estimate $\hat{\rho}(t)$ leaves in $\mathbb{H}_\rho$ for every $t \geq 0$.*

Proof: In the propagation step, the coherence vector $\hat{\mathbf{x}}_{KF}(t)$ is the solution of the differential equation (5.10), which from Proposition 5.1 is equivalent to the deterministic part of (5.5). In the measurement step, we make use of the operator (5.8), which guarantees that $\|\hat{\mathbf{x}}_{KF}(t)\|^2 \leq 1$, which in turn implies positive semi-definiteness of $\hat{\rho}(t)$, and norm preservation since $\mathrm{Tr}\{\frac{I}{2} + \sum_k \hat{\mathbf{x}}_{kKF}(t)\sigma_k\} = 1$ using the fact that $\mathrm{Tr}(\sigma_k) = 0$. □

5.2.3 Multiple-model adaptive estimator

This section presents a class of Multiple Model Adaptive Estimators (MMAEs) designed to address the challenges of quantum systems with parametric model varying dynamics or uncertainties, more precisely, in the quantum-mechanical Hamiltonian. The MMAE operates with a finite number N of selected models from the original (potentially infinite) set of system models and consists of two main components: i) a dynamic generator for N weighting signals $p_\ell(t)$, $\ell = 1,\ldots,N$, and ii) a bank of N estimators, each designed based on one of the selected models. In our case, the estimators are precisely either the Quantum estimator or the Extended Kalman filter presented in previous subsections designed to a specific value of H_d. The state estimate is produced by a weighted sum of the local state estimates $\hat{\mathbf{x}}_\ell(t)$, i.e.,

$$\hat{\mathbf{x}}(t) = \sum_{\ell=1}^{N} p_\ell(t)\hat{\mathbf{x}}_\ell(t).$$

By employing a set of parallel filters, each corresponding to a different model of the system's dynamics, the MMAE adapts to the most likely model based on measurement data. This provides a flexible and accurate estimation method capable of handling sudden changes in the system's behavior or parameters.

The evolution of each dynamic weight $p_\ell(t)$ is set to be piecewise constant, updating its value at instants of time $t = t_k$, according to following equation, (Hassani et al., 2009):

$$p_\ell(t_{i+1}) = \frac{\beta_\ell e^{-w_\ell(t_k)}}{\sum_{j=1}^{N} p_j(t_k)\beta_j e^{-w_j(t_k)}} p_\ell(t_k), \tag{5.13}$$

In (5.13), β_ℓ is a positive weighting constant value and $w_\ell(t_k)$ is a scalar continuous function called an error measuring function that maps the measurable signals of the quantum system and the states of the ℓ^{th} local estimator to a nonnegative real value. This error measuring function evaluates the discrepancy between the observed measurements and the predicted state from the ℓ^{th} model. An example is $w_\ell(t_k) = \|y_\ell(t_k) - h(\mathbf{x}_\ell(t_k)\|^2$. It can be proved (using similar arguments as in (Hassani et al., 2009)) that due to the particular structure of equation (5.13), the weights $p_\ell(t)$ are positive, bounded, and the overall sum $\sum_{\ell=1}^{N} p_\ell(t)$ is always one for all $t \geq 0$, independently of the error measuring function $w_\ell(t)$. In this chapter, we implemented the MMAE method for both Quantum Filter (QF)

and Quantum Extended Kalman Filter (KF). The obtained results are presented in Section 5.4.

5.3 Lyapunov-based state feedback control

This section addresses Problem 2. Drawing inspiration from the concepts presented in (d'Alessandro, 2021), we begin by considering a state $\rho_f \in \chi_f$, and select a matrix $\Pi = I - \rho_f$. This selection leads us to define the Lyapunov function as

$$V(\rho) = \mathrm{Tr}\{\Pi\rho\}. \tag{5.14}$$

It is important to note that Π is Hermitian, ensuring that it possesses real eigenvalues. Furthermore, Π is positive semi-definite, which guarantees that the Lyapunov function $V(\rho)$ is non-negative for all states ρ, i.e., $V(\rho(t)) \geq 0$. Additionally, a significant characteristic of Π is its commutativity with the final state ρ_f, that is, $[\rho_f, \Pi] = 0$.

Remark 5.2 *Stationary points of the Lyapunov function $V(\rho)$ are identified as states $\bar{\rho}$ that commute with ρ_f, see (d'Alessandro, 2021), i.e., $[\bar{\rho}, \rho_f] = 0$. Given the definition of $\Pi = I - \rho_f$, this commutation property implies $[\bar{\rho}, \Pi] = 0$.*

We initially derive a controller to minimize $V(\rho)$, assuming access to the actual state $\rho(t)$.

Theorem 5.1 *Consider the quantum system (5.1) and let $\chi_f = \{\rho \in \mathbb{H} : [\rho, \Pi] = 0\}$ be the desired stationary set. Consider the feedback control law*

$$\Omega(t) = \begin{cases} -i\frac{\mathrm{Y}_0}{\mathrm{Y}_1}, & \text{for } t \in [t_{k-1}, t_k),\ k = 1,3,5,\ldots \\ 0, & \text{otherwise} \end{cases} \tag{5.15}$$

where $\mathrm{Y}_0 = \Gamma\,\mathrm{Tr}\{\Pi\mathcal{D}[c_d]\rho\} + M\,\mathrm{Tr}\{\Pi\mathcal{D}[c_m]\rho\} + \alpha\,\mathrm{Tr}\{\Pi\rho\}$, with $\alpha \in \mathbb{R}^+$, and $\mathrm{Y}_1 = \mathrm{Tr}\{\Pi[H_c, \rho]\}$. In the above, we set the control value to switch at event times $\{t_0, t_1, \ldots\}$ when Y_1 crosses an $\varepsilon > 0$ value and the period of time between the last switching and current is larger than some dwell time, that is, t_k is defined as

$$\begin{cases} t_k = \min\limits_t\{t \geq t_{k-1} + \Delta_1 : \mathrm{Y}_1 \leq \varepsilon\} & \text{for } k \text{ odd}, \\ t_k = \min\limits_t\{t \geq t_{k-1} + \Delta_2 : \mathrm{Y}_1 \geq \varepsilon\} & \text{for } k \text{ even}, \end{cases}$$

for some appropriate dwell times $\Delta_1, \Delta_2 \in \mathbb{R}^+$. Then, the resulting closed-loop system exhibits the property that the set χ_f is practically exponentially stable in probability.

Proof: Given that ρ_f is selected to commute with Π, it follows that ρ_f becomes a stationary point of the Lyapunov function $V(\rho)$, as discussed in (d'Alessandro, 2021). Furthermore, according to Remark 5.2, the set χ_f is identified as a stationary set. To investigate

its stability, we consider the infinitesimal generator of $\rho(t)$ applied to $V(\rho)$. This analysis involves the diffusion process described in (5.1) and leverages the Itô formula, resulting in

$$\begin{aligned} L(V(\rho)) = \operatorname{Tr}\Big\{\Pi^T\Big(&-i[H_d,\rho(t)] + \Gamma\mathcal{D}[c_d]\rho(t) \\ &+ M\mathcal{D}[c_m]\rho(t) - i[H_c,\rho(t)]\Omega(t)\Big)\Big\} \\ &+ \frac{1}{2}\operatorname{Tr}\Big\{Z(\rho)H_V Z^T(\rho)\Big\} \end{aligned}$$

where $L(V(\rho))$ is the quantum Markov generator for the Lyapunov function V, and $Z(\rho) = \sqrt{\eta M}\mathcal{H}[c_m]\rho(t)$. Note that the last term is zero because the Hessian matrix H_V of $V(\rho)$ is null. Considering the commutation relation $[\rho_f, H_d] = 0$ and the definition $\Pi = I - \rho_f$, we deduce $[\Pi, H_d] = 0$ since $[I - \rho_f, H_d] = -[\rho_f, H_d] = 0$. By employing the trace property $\operatorname{Tr}\{A[B,C]\} = \operatorname{Tr}\{C[A,B]\}$, it follows that $\operatorname{Tr}\{\Pi[H_d,\rho]\} = \operatorname{Tr}\{\rho[\Pi,H_d]\} = 0$. Thus, we obtain

$$\begin{aligned} L(V(\rho)) = &-i\Omega(t)\operatorname{Tr}(\Pi[H_c,\rho(t)]) + \Gamma\operatorname{Tr}(\Pi\mathcal{D}[c_d]\rho(t)) \\ &+ M\operatorname{Tr}(\Pi\mathcal{D}[c_m]\rho(t)). \end{aligned} \tag{5.16}$$

At this point, our objective is to identify a control function $\Omega(t)$ that satisfies $L(V(\rho)) \leq -\alpha V(\rho)$, ensuring that $V(t) = V(\rho(t))$ is a supermartingale and decreases exponentially with a rate $\alpha > 0$. Among the potential solutions, we opt for the one that minimizes the control effort $\Omega^2(t)$ pointwise in time. Hence, we seek $\Omega(t)$ that solves the optimization problem:

$$\begin{aligned} \underset{\Omega(t)}{\text{minimize}} \quad & \Omega^2(t) \\ \text{subject to} \quad & -i\Omega(t)\mathrm{Y}_1 + \mathrm{Y}_0 \leq 0. \end{aligned}$$

The solution to this optimization problem is precisely the control law presented in (5.15). Caution is advised when Y_1 approaches zero to prevent computational inaccuracies and excessive control signal magnitudes. As a preventive measure, the control strategy switches $\Omega(t)$ to zero once $\mathrm{Y}_1 \leq \varepsilon$. To avoid Zeno behavior, characterized by an infinite number of switches within a finite time, we enforce a minimum dwell time between switching, $t_k - t_{k-1} > \Delta$.

Taking now into account the results and reasoning presented in (Aguiar et al., 2007) for switching systems with stable and unstable modes, and acknowledging that $L(V)$ remains bounded when $\Omega = 0$, the practical stability in probability of the set χ is conclusively established by noticing that $L(V) \leq -\eta(V) + \eta_0$, for some class $\mathcal{K}$ function η and constant $\eta_0 \geq 0$. □

We now adapt the proposed controller for the case that we do not have direct access to the state $\rho(t)$. By applying the methodology from the previous section, we compute an estimated state $\hat{\rho}(t)$ and use it in place of $\rho(t)$. The next result shows that we still recover

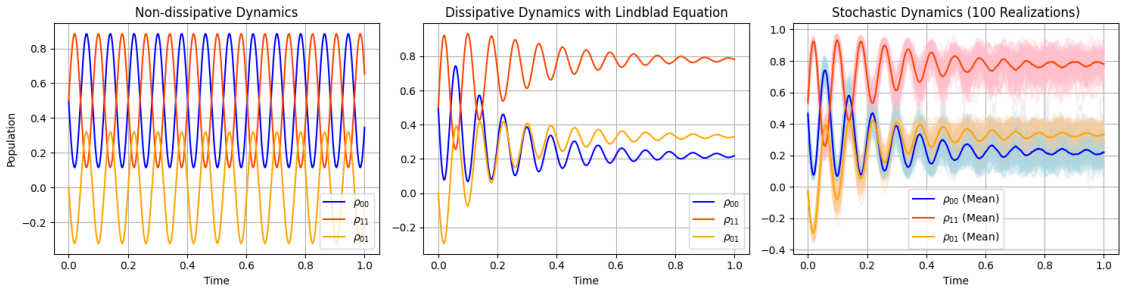


Figure 5.2: Comparative evolution of quantum state populations. This figure illustrates the population dynamics of a quantum system under three different scenarios: (a) Non-dissipative dynamics; (b) Dissipative dynamics with the Lindblad equation; and (c) Stochastic dynamics over 100 realizations. In each subplot, the populations $\rho_{00}(t)$, $\rho_{11}(t)$, and the real part of the off-diagonal $\rho_{01}(t)$ (or $\rho_{10}(t)$) are plotted in time. The non-dissipative dynamics exhibit periodic oscillations, the dissipative dynamics show damped oscillations leading to steady-state populations, and the stochastic dynamics reveal ensemble-averaged behaviors with individual realizations contributing to the shaded regions.

practically stability in probability and moreover that the set χ_f is NSpS with respect to the estimation error.

Theorem 5.2 *Consider the same conditions of Theorem 1, but now replacing* (5.15) *by*

$$\Omega(t) = \begin{cases} -i\frac{\hat{\Upsilon}_0}{\hat{\Upsilon}_1}, & \text{for } t \in [t_{k-1}, t_k),\ k = 1,3,5,\ldots \\ 0, & \text{otherwise} \end{cases} \tag{5.17}$$

where $\hat{\Upsilon}_0 = \Gamma \operatorname{Tr}\{\Pi\mathcal{D}[c_d]\hat{\rho}\} + M\operatorname{Tr}\{\Pi\mathcal{D}[c_m]\hat{\rho}\} + \alpha\operatorname{Tr}\{\Pi\hat{\rho}\}$, *with* $\alpha \in \mathbb{R}^+$, *and* $\hat{\Upsilon}_1 = \operatorname{Tr}\{\Pi[H_c, \hat{\rho}]\}$ *with* $\hat{\rho}$ *denoting the output estimate of the quantum observer. Let* $\tilde{\sigma}^2(t)$ *be the incremental variance associated to the noisy estimation error* $\operatorname{Tr}\{\tilde{\rho}\} = \operatorname{Tr}\{\rho - \hat{\rho}\}$, *which is considered to be bounded. Then, the set* χ_f *is NSpS with respect to* $\tilde{\sigma}^2(t)$.

Proof: From (5.16), it follows that $L(V(\rho))$ satisfies

$$L(V(\rho)) = -i\hat{\Upsilon}_1\Omega(t) + \hat{\Upsilon}_0 - i\tilde{\Upsilon}_1\Omega(t) + \tilde{\Upsilon}_0, \tag{5.18}$$

where $\tilde{\Upsilon}_0 = \Upsilon_0 - \hat{\Upsilon}_0$ and $\tilde{\Upsilon}_1 = \Upsilon_1 - \hat{\Upsilon}_1$. Using Proposition 5.2, we deduce that $\hat{\rho}$ is bounded. Consequently, $\hat{\Upsilon}_0$ is also bounded. Additionally, since $\hat{\Upsilon}_1 > \epsilon$ for $k = 1,3,5,\ldots$, the control signal Ω is bounded as well. This implies that $\tilde{\Upsilon}_0$ and $\tilde{\Upsilon}_1$ can be bounded by class $\mathcal{K}$ functions of $\tilde{\sigma}^2$.

Applying now the same reasoning as in the previous proof, we can conclude from (5.18) that the generator $L(V)$ for $V(\rho) \geq \eta_1(\tilde{\sigma}^2)$ satisfies

$$L(V) \leq -\eta(V) + \eta_0,$$

for some class $\mathcal{K}$ function η, a positive definite function η_1, and a constant $\eta_0 \geq 0$. Therefore, by invoking the results from (Deng et al., 2001), the desired conclusions follow. □

5.4 Application to Qubits in Leaky Cavities

The methodology presented here for the illustrated example is applicable to any two-level atom experiencing classical influences such as driving, damping, and detuning. Our examination specifically focuses on a qubit interacting with a leaky cavity in a rotating frame. The drift Hamiltonian, $H_d = \frac{\omega_R}{2}\sigma_3$, incorporates the effective detuning, $\omega_\Delta = \omega_R + \Delta\omega_R - \omega_0$, which represents the adjusted frequency discrepancy of the qubit. Here, ω_R denotes the frequency gap between the excited $|e\rangle$ and ground $|g\rangle$ states, ω_0 signifies the oscillation frequency of the driving field, and $\Delta\omega_R$ refers to the frequency shift. The Pauli operator $\sigma_3 = |g\rangle\langle g| - |e\rangle\langle e|$ serves as the inversion operator for the qubit. The control Hamiltonian, $H_C = -\Omega(t)\sigma_1$, where $\Omega(t)$ is the Rabi frequency, is directly proportional to the transition dipole moment and the amplitude of the driving electromagnetic field. For the annihilation and creation field operators, we utilize the Pauli lowering and raising operators, $a = \sigma_-$ and $a^\dagger = \sigma_+$, respectively. The initial density operator is chosen as $\rho_0 = \left[\begin{smallmatrix} 0.5 & -0.5i \\ 0.5i & 0.5 \end{smallmatrix}\right]$ corresponding to the Bloch vector $\mathbf{x}_0 = [0,1,0]^T$. The parameters used in simulations are defined as follows: The decay rate (Γ) is set to 10 s^{-1}, representing the rate at which the system loses energy to its environment. The Rabi frequency (ω_R) is 5Γ rad/s, characterizing the frequency of oscillation for a two-level system driven by a resonant electromagnetic field. The interaction strength (M) used in the Lindblad term is set to $1s^{-1}$, representing the strength of certain dissipative processes. The detection efficiency (η) is set to 0.8, indicating that 80% of the signals are correctly detected. The time step for numerical integration (dt) is set to 0.001 seconds to improve accuracy, and the total simulation time (T) is set to 1.0 second, defining the duration over which the simulation is run. For now, we consider the amplitude of the driving field (Ω), which represents the strength of the external field, as 3Γ rad/s. We later change this value with the one obtained from control method.

Figure 5.2 shows our analysis of three distinct scenarios. The first scenario depicts the evolution without dissipation or noise, highlighting the ideal oscillatory behavior resulting from the coherent superposition of quantum states. The second scenario illustrates the dissipative dynamics governed by the Lindblad Equation, modeling how environmental impacts cause the decay of these oscillations. The third scenario introduces stochastic dynamics, where random environmental disturbances are represented by stochastic noise. In this scenario, the stochastic evolution is shown across 100 realizations, with the mean values highlighted to provide a clear understanding of the system's overall behavior.

Figure 5.3 illustrates a comparative analysis of the quantum filter estimator and the quantum extended Kalman filter estimator for the elements of the coherence vectors. Both filters are initialized with $\hat{\mathbf{x}}_0 = [1,0,0]^T$, corresponding to the density matrix $\hat{\rho}_0 = \left[\begin{smallmatrix} 0.5 & 0.5 \\ 0.5 & 0.5 \end{smallmatrix}\right]$. The analysis reveals that both filters closely track the true state across all three variables, with minor deviations primarily during the initial transient phase. The Kalman

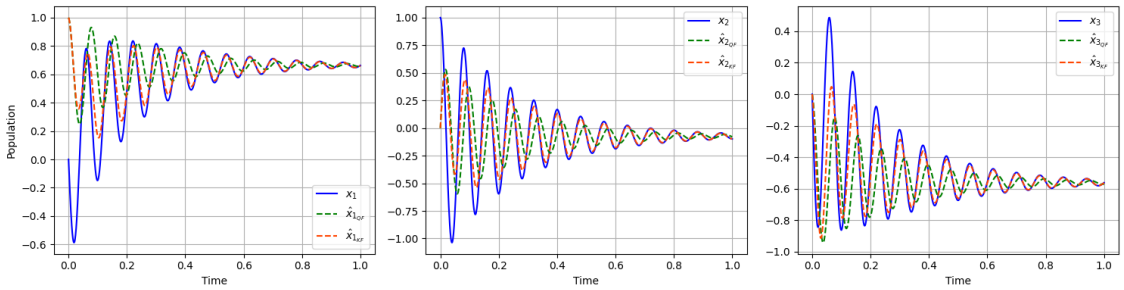


Figure 5.3: Comparative analysis of true state, quantum filter, and quantum extended Kalman filter in the **x**-representation. The plots show the population dynamics over time for three different state variables in the coherence vector representation: (a) x_1; (b) x_2; and (c) x_3. The blue solid lines represent the true state (x_1, x_2, x_3), the green dashed lines represent the estimates obtained from the quantum filter $(\hat{x}_{1QF}, \hat{x}_{2QF}, \hat{x}_{3QF})$, and the red dashed lines represent the estimates from the Kalman filter $(\hat{x}_{1KF}, \hat{x}_{2KF}, \hat{x}_{3KF})$.

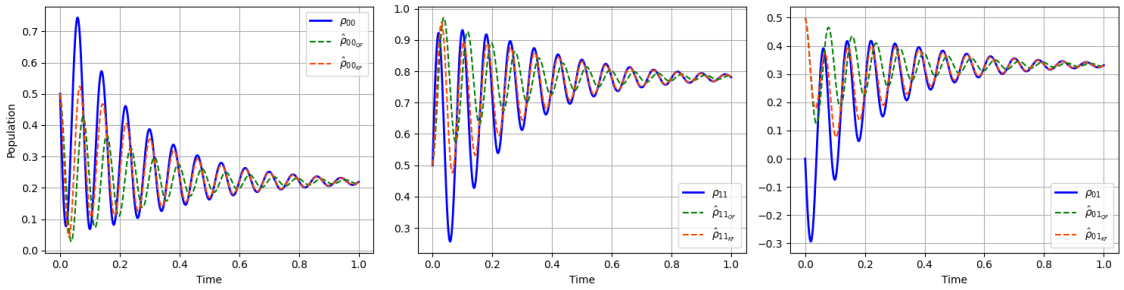


Figure 5.4: Comparison of true density matrix elements with quantum and quantum extended Kalman filter estimates. The plots display the evolution of the real parts of the density matrix elements over time, comparing the true values (solid blue lines) with the estimates obtained from the quantum filter (dashed green lines) and the Kalman filter (dashed red lines).

filter estimates (red dashed lines) demonstrate faster convergence to the true state compared to the quantum filter estimates (green dashed lines), particularly noticeable in the initial peaks. Despite these differences in the transient phase, both filters achieve nearly identical accuracy in steady-state estimation. The slight deviations observed in the quantum filter during the early phase indicate a higher sensitivity to initial conditions and noise, which gradually corrects over time. Overall, both filters effectively estimate the quantum state's dynamics, offering valuable insights into the system's behavior.

Figure 5.4 shows the reconstruction of the density matrix $\hat{\rho}(t)$ from the elements of the coherence vector $\hat{\mathbf{x}}$. This process involves transforming the state space representation back into the density matrix form, ensuring that the estimates are consistent with the physical properties of the quantum state. The figure demonstrates that both the quantum filter and the quantum extended Kalman filter estimates converge to the true values for all elements. Notably, the Kalman filter exhibits faster convergence. In the steady-state region, both filters provide estimates that closely match the true values, indicating their robustness for long-term state estimation. Although minor discrepancies are observed during the transient phase, these are corrected over time, with both filters showing high

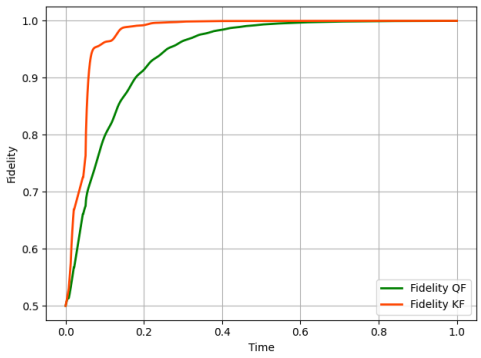


Figure 5.5: Fidelity comparison over time between true and estimated density matrices. The plot shows the fidelity values between the true density matrix and the estimates obtained from the Kalman filter and the quantum filter over time.

fidelity in tracking the true state of the system. This analysis highlights the robustness and accuracy of both the quantum and Kalman filters in estimating the state of a quantum system.

Figure 5.5 shows the fidelity between the true density operator and the estimated state, computed using $F(\rho,\hat{\rho}) = \left(\mathrm{Tr}\left(\sqrt{\sqrt{\rho}\hat{\rho}\sqrt{\rho}}\right)\right)^2$ for both the quantum filter and Kalman filter. This measure quantifies the proximity of the estimated density matrix to the true density matrix, with values ranging from 0 (completely different) to 1 (identical). The figure illustrates that both filters achieve high fidelity with the true state, particularly in the steady state, indicating accurate tracking of the quantum state. While there are slight discrepancies initially, both filters converge to high fidelity values, demonstrating their effectiveness in quantum state estimation. The transient region displays fluctuations, reflecting the filters' adaptation to the initial state dynamics. The Kalman filter exhibits slightly faster convergence compared to the quantum filter, which is particularly important for real-time applications. It is important to emphasize that the Kalman filter offers the significant advantage of allowing the tuning of its gains (specifically, the covariances Q and R) to enhance performance. In contrast, the Quantum filter lacks this flexibility.

Figure 5.6 delves deeper into the analysis of the proposed Kalman filtering by showing the trace of the error covariance matrix P. The trace of P can be seen (in an ideal scenario) as an indicator of the Kalman filter's performance, as it quantifies the evolution of uncertainty in the state estimates, demonstrating the filter's effectiveness in reducing this uncertainty over time. As depicted in the figure, the trace of P is initially high, reflecting significant uncertainty in the initial state estimates, which is typical at the start of the filtering process when the initial state is often based on a rough estimate. As the Kalman filter processes measurements, the trace of P decreases, indicating that the filter effectively reduces uncertainty in the state estimates by incorporating new measurement information. This reduction is evident from the rapid decline in the trace of P during the initial phase of filtering. Eventually, the trace of P reaches a steady-state value, signifying

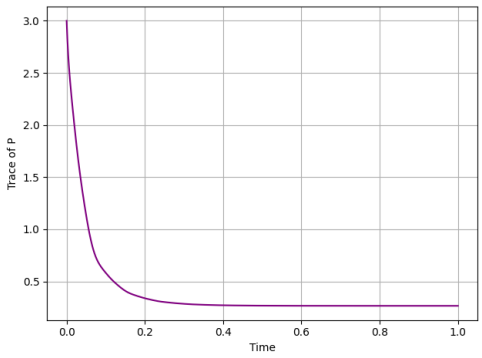


Figure 5.6: Evolution of the trace of the error covariance matrix P over time. The plot shows the trace of the error covariance matrix P as a function of time in the Kalman filtering process. The trace of P is a scalar measure of the total estimation error variance across all state variables.

that the filter has minimized the uncertainty in the state estimates. The steady-state value of the trace of P is influenced by process noise and measurement noise.

Figure 5.7 shows the time evolution of the quantum state populations x_1, x_2, and x_3 under multiple model implementations for both quantum and Kalman filtering approaches. Each row corresponds to a specific ω_R multiplier (0.8, 0.9, 1.0, 1.1, 1.2), and each column represents a state variable. When ω_R is set to the nominal value (1.0), both QF and KF estimates converge to the true states, demonstrating accuracy and robustness. However, for other ω_R values, discrepancies between the true states and filter estimates become noticeable, highlighting the system's sensitivity to variations in ω_R. These results underscore the robustness of the MMAE approach, where dynamic weights adjust the contributions of each model based on the observed data. The adaptive nature of the MMAE ensures that the most probable model predominantly influences the state estimation, effectively handling uncertainties in ω_R. This adaptability is crucial for maintaining accurate state estimates in quantum systems with variable dynamics, providing a reliable framework for practical quantum state monitoring and control applications.

Figure 5.8 demonstrates the dynamic adaptation of model weights in the MMAE framework. Each weight p_i corresponds to a model with a different ω_R multiplier. Initially, all weights are set equally, reflecting no prior knowledge about which model is most accurate. As the estimation process progresses, the weights dynamically adjust based on the error measures between the observed measurements and the predicted states from each model. This adjustment is governed by a dynamic recursion equation, enabling the MMAE to identify and emphasize the most likely model over time. The results show that the weight p_3, corresponding to the nominal ω_R, gradually becomes dominant as the most probable model. This is evidenced by its increase and stabilization at a higher value compared to the other weights, which decrease as the system identifies them as less probable. The convergence of p_3 demonstrates the effectiveness of the MMAE in correctly identifying the model that best represents the true system dynamics.

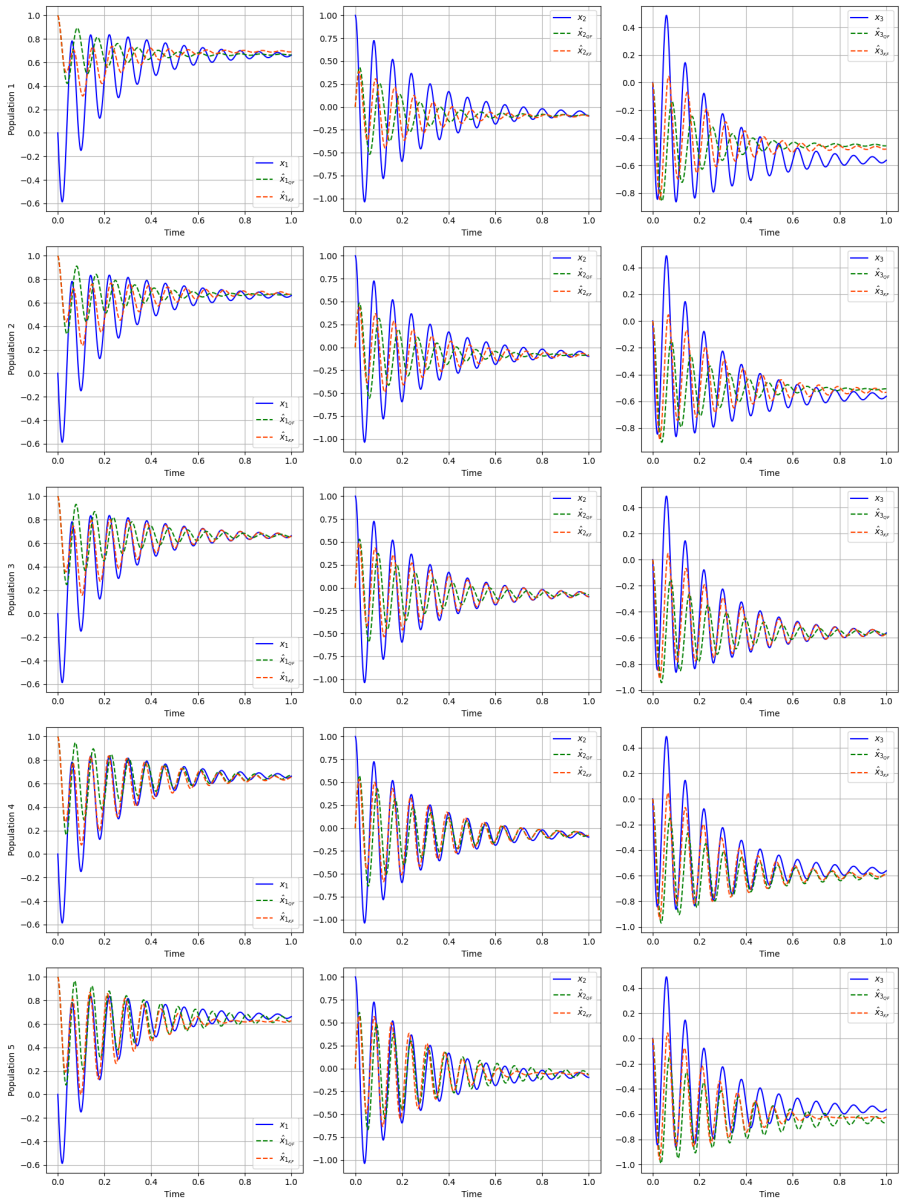


Figure 5.7: Time evolution of quantum state populations with multiple models of ω_R. This figure illustrates the dynamic behavior of the quantum state populations x_1, x_2, and x_3 under varying ω_R values, with true states shown in blue, quantum filter estimates in green, and Kalman filter estimates in orange. Each row corresponds to a different ω_R multiplier: 0.8 (Population 1), 0.9 (Population 2), 1 (Population 3), 1.1 (Population 4), and 1.2 (Population 5). Columns represent the state variables x_1, x_2, and x_3 respectively. The plots highlight the performance of the QF and KF in tracking the true quantum state across different ω_R scenarios.

The variations and eventual stabilization of the weights illustrate the MMAE's capability to adapt to the true system parameters, ensuring robust state estimation even under model uncertainties. This dynamic adaptation is crucial for accurately tracking the quantum state in systems where parameters may not be precisely known or may vary over time.

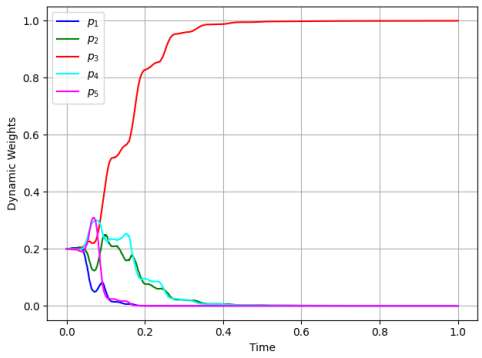


Figure 5.8: Dynamic evolution of model weights p_i in the MMAE framework. This figure illustrates the time evolution of the dynamic weights p_1, p_2, p_3, p_4, and p_5 associated with different models in the MMAE. The weights are represented to show their adaptation over time as the MMAE converges to the most probable model.

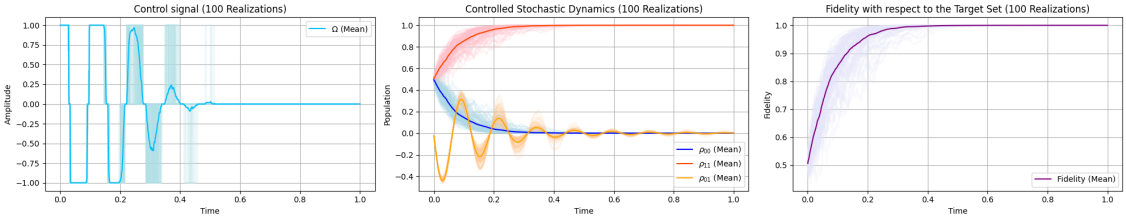


Figure 5.9: Control signal, controlled state evolution, and fidelity over 100 stochastic realizations. The first subplot displays the control signal $\Omega(t)$ applied over time for 100 realizations (light blue lines) with the mean control signal. The second subplot illustrates the controlled time evolution of the elements of the density operator, depicting how the state evolves towards the target set. The third subplot presents the fidelity with respect to the target state, demonstrating that the target state is achieved with high accuracy.

Figure 5.9 presents our results regarding the dynamic control of the studied quantum system under stochastic influences, with the goal of steering the system towards a specified target set. All simulations are conducted over 100 realizations to account for the effects of noise and randomness. The first subplot displays the control signal $\Omega(t)$ over time for each of the 100 realizations, shown in light blue, with the mean control signal highlighted. This control signal is dynamically adjusted using feedback from the system's state to steer the system towards the desired target state, employing our Lyapunov switching approach. The variability in the control signals across realizations reflects the system's adaptive response to stochastic disturbances. The second subplot shows the evolution of the density matrix elements over time, with the control signal $\Omega(t)$ used to achieve controlled evolution. This plot illustrates the convergence of the state populations' trajectory towards the desired target under the applied control signal. The third subplot focuses on the fidelity of the system's state relative to the target, computed as $F(\rho,\rho_f) = \left(\mathrm{Tr}\left(\sqrt{\sqrt{\rho_f}\rho\sqrt{\rho_f}}\right)\right)^2$ for $\rho_f \in \chi_f$. This plot confirms that the control strategy effectively drives the system towards the target state, as evidenced by the high fidelity values over time.

5.5 Concluding Remarks and Discussions

This chapter has presented a comprehensive approach to state estimation and control for stochastic quantum dynamics, with a particular focus on qubits subjected to homodyne measurements. The proposed methodology integrated Lyapunov-based control strategies with two advanced filtering techniques: the traditional quantum filtering method and a novel extended Kalman filter (EKF). These methods have been designed to estimate the coherence vector's evolution in a quantum system under continuous homodyne measurements, addressing the challenges posed by correlated noise and uncertainties in the system's Hamiltonian.

A contribution of this work is the introduction of a multiple model estimation scheme, which enhances the robustness of the state estimation process, especially in the face of unknown or variable system parameters, such as the drift Hamiltonian. This multiple model framework allows the system to adapt dynamically, switching between models based on observed data, which is critical for systems with uncertainties in key parameters. The effectiveness of this estimation scheme was demonstrated through simulations, where it maintained accurate state estimation even when the system's resonance frequency was uncertain.

In terms of control, the chapter explored a switching-based Lyapunov approach that ensures noise-to-state practical stability (NSpS) in probability. This method successfully controlled the qubit's evolution, driving it towards a desired target state while compensating for uncertainties and stochastic disturbances. The results illustrated the practical viability of this control strategy in stabilizing qubits in a leaky cavity under homodyne detection.

The comparative analysis of the quantum filter and the EKF revealed that while both methods are effective, the Kalman filter offers superior performance due to its ability to handle correlated noise and its flexibility in tuning gains. The Kalman filter's advantage in convergence speed and steady-state accuracy makes it particularly suitable for real-time quantum control applications.

Looking forward, several directions for future research emerge from this work. First, while this study has focused on qubits, the proposed methodologies can be extended to more complex quantum systems, such as multi-qubit systems or higher-dimensional quantum systems. As the system's dimensionality increases, more sophisticated estimation and control techniques will be required to manage the larger state spaces and more intricate dynamics. Real-time implementation is another important area for future development. Quantum control requires prompt decision-making, and future efforts should focus on developing efficient computational algorithms and leveraging hardware acceleration techniques to ensure these methods can be used in real-time quantum information processing systems.

Additionally, while the current methods address stochastic disturbances, further research could explore enhancing these techniques to handle adversarial disturbances in quantum systems. Developing robust control methods such as H_∞-filtering could improve the resilience of quantum systems against external perturbations, leading to more reliable control outcomes. There is also potential for hybrid classical-quantum control systems, where quantum systems interact with classical controllers. Extending the current framework to account for such interactions could yield more robust control designs, especially in noisy intermediate-scale quantum (NISQ) technologies.

Lastly, these techniques hold promise for applications in quantum metrology and quantum computing, where precise control over quantum states is crucial. Future research could focus on tailoring these methods for specific applications in quantum error correction, quantum sensors, and quantum communication protocols.

In conclusion, integrating Lyapunov-based control with advanced filtering methods provides a promising framework for stabilizing and controlling quantum systems under uncertainty. The methods developed here provide a strong foundation for future advancements in quantum control, particularly in real-time applications and more complex quantum systems.

Chapter 6

Quantum Entanglement Synthesis and Optimization

This chapter studies an optimal control strategy to generate maximally entangled states in bipartite quantum systems. Leveraging the Pontryagin Principle, we derive time-dependent control fields that maximize the entanglement measure, specifically concurrence, within minimal time while adhering to input constraints. Our formulation addresses the Liouville-von Neumann dynamics of the reduced density matrix under unitary evolution. The strategy is numerically validated through simulations, demonstrating its ability to drive the system from an initial perturbed separable state to a maximally entangled target state. The results showcase the effectiveness of switching control fields in optimizing entanglement, with potential applications in quantum technologies, including communication, computation, and sensing. We also study entanglement synthesis using the Chopped Random Basis (CRAB) algorithm. The CRAB algorithm is utilized to drive the evolution of quantum states, transitioning them from approximately separable states to maximally entangled states. This is achieved by optimizing control pulses, which are designed using a tailored Hamiltonian. Together, these techniques showcase quantum control methods that address challenges in quantum computing, communication, and metrology. The main results of this chapter were published in (Dehaghani et al., 2024a,b).

6.1 Entanglement Monotones and Measures

In this subsection, we introduce fundamental concepts from entanglement theory, focusing on entanglement monotones and measures.

Entanglement measures must satisfy specific criteria to accurately reflect the entanglement properties of quantum states. For a bipartite entanglement measure $E(\rho)$, the following postulates are generally accepted as defining characteristics Donald et al. (2002); Vedral and Plenio (1998); Vidal (2000); Horodecki (2001):

1. Quantification of Entanglement: A measure $E(\rho)$ quantifies the intensity of entanglement of a state ρ by mapping system density matrices to positive real numbers, i.e., $\rho \mapsto E(\rho) \in \mathbb{R}^+$.

2. Zero for Separable States: The measure $E(\rho) = 0$ if and only if ρ is separable, indicating the absence of quantum entanglement.

3. Monotonicity under LOCC: The measure $E(\rho)$ does not increase on average under Local Operations and Classical Communication (LOCC) operations. For any LOCC operation Λ, it holds that $E(\Lambda\rho) \leq E(\rho)$, reflecting the principle that entanglement cannot be increased through local actions and classical communication alone.

4. Agreement with Entropy of Entanglement for Pure States: For pure states $\rho = |\psi\rangle\langle\psi|$, the measure converges to the entropy of entanglement, aligning the entanglement measure with the von Neumann entropy for pure bipartite systems.

Any function $E(\rho)$ satisfying the first three conditions is considered an entanglement monotone, while functions that meet conditions 1, 2, and 4 are recognized as entanglement measures. Some authors further define entanglement measures by imposing additional criteria, such as convexity, additivity, and continuity, as detailed in Donald et al. (2002); Vedral and Plenio (1998).

Key entanglement measures include the entropy of entanglement, Renyi entropy, entanglement of formation, Negativity, and Concurrence. Given the importance and widespread use of concurrence as an entanglement monotone, our work will primarily focus on analyzing quantum entanglement through the lens of concurrence, as it provides a practical and insightful tool for quantifying entanglement.

6.1.1 Analysis of Quantum Entanglement Using Concurrence

For a bipartite quantum system described by a pure state $|\psi\rangle$ in the Hilbert space $\mathbb{H}_A \otimes \mathbb{H}_B$, the state can be expressed in the computational basis $\{|ij\rangle\}$ as Zhao et al. (2011),

$$|\psi\rangle = \sum_{i=1}^{d_A}\sum_{j=1}^{d_B} \alpha_{ij}|i\rangle_A|j\rangle_B, \tag{6.1}$$

where $\alpha_{ij} \in \mathbb{C}$ are complex coefficients and satisfy the normalization condition

$$\sum_{i=1}^{d_A}\sum_{j=1}^{d_B} |\alpha_{ij}|^2 = 1. \tag{6.2}$$

The concurrence $C(\rho)$ provides a compact way to quantify the entanglement of the state $|\psi\rangle$. For separable states, the concurrence is zero. Conversely, for maximally entangled states, the maximum concurrence value achieves its maximum value of 1. This corresponds to maximally entangled states such as the Bell states. The degree of entanglement

is quantified as

$$C(\rho) = \sqrt{2\left(1 - \mathrm{Tr}(\rho_A^2)\right)}, \tag{6.3}$$

where ρ_A is the reduced density matrix of subsystem A, obtained by tracing out the degrees of freedom of subsystem B, that is,

$$\rho_A = \mathrm{Tr}_B(|\psi\rangle\langle\psi|). \tag{6.4}$$

To analyze the structure of $|\psi\rangle$, we use the Schmidt decomposition, which expresses the pure state as Lee et al. (2022); Nielsen (1999)

$$|\psi\rangle = \sum_{k=1}^{r} \sqrt{\lambda_k}\,|u_k\rangle_A \otimes |v_k\rangle_B, \tag{6.5}$$

where $\sqrt{\lambda_k}$ are the Schmidt coefficients, with $\lambda_k \geq 0$ and $\sum_{k=1}^{r} \lambda_k = 1$, $|u_k\rangle_A$ and $|v_k\rangle_B$ are orthonormal basis sets for $\mathbb{H}_A$ and $\mathbb{H}_B$, respectively, and r is the Schmidt rank. The Schmidt decomposition highlights the shared entanglement structure between the two subsystems. Using the Schmidt decomposition, the reduced density matrices of subsystems A and B can be written in their spectral decompositions

$$\rho_A \triangleq \mathrm{Tr}_B(\rho_{AB}) = \sum_{k=1}^{r} \left(\mathbb{I}_A \otimes \langle v_k^B|\right) \rho_{AB} \left(\mathbb{I}_A \otimes |v_k^B\rangle\right) \tag{6.6}$$

where $\mathbb{I}_A$ is the identity matrix in $\mathbb{H}_A$. These reduced density matrices encapsulate the bipartite system's entanglement, with their eigenvalues and eigenvectors derived directly from the Schmidt decomposition.

6.2 Optimal Control Based on Quantum Entanglement Measures

This section explores the application of optimal control strategies to maximize the utility of entangled states.

6.2.1 Optimal Control Problem Statement

Consider a bipartite quantum system composed of two interacting particles. The objective is to manipulate the system's state to achieve a high degree of entanglement. To achieve this, we apply Pontryagin's Minimum Principle (PMP) to compute time-dependent external control fields that guide the system's time evolution toward desired states exhibiting maximum entanglement.

We propose a cost function designed to facilitate the generation of entangled states using the concurrence measure, aiming to achieve this within the minimum possible time.

The optimal control problem is formulated as follows:

$$\min_{\rho_A, t_f} J = -C(\rho(t_f)) + \Gamma t_f$$

subject to:

$$\begin{aligned}
&\dot{\rho}_A(t) = F(\rho(t), u(t)), && \text{(dynamics)}\\
&\rho(t_0) = \rho_0 \in \mathbb{H}_\rho, && \text{(initial condition)}\\
&u(t) \in \mathcal{U} := \{u \in L_\infty^m : \|u\|_\infty \leq u_{\max}\} && \text{(control constraint)}\\
&t_f \in (t_0, \infty) && \text{(final time constraint)}
\end{aligned}$$

where Γ is a positive coefficient that balances the minimization of the time required and the concurrence. The final time t_f is treated as free and optimized. The control fields $u(t)$ are modeled as time-dependent bounded measurable functions.

The time evolution of the density operator $\rho(t)$ is modeled using the Liouville-von Neumann equation

$$\dot{\rho}(t) = -i[H_0 + H_c(t), \rho(t)], \quad H_c(t) = \sum_{k=1}^{m} u_k(t) H_k \tag{6.7}$$

where H_0 represents the system's intrinsic Hamiltonian, H_k is the fixed control Hamiltonian, and $u_k(t)$ is the time-dependent scalar control input. Note that the dynamics in the optimal control formulation is considered for the reduced density matrix ρ_A with the action of the partial trace:

$$F(\rho(t), u(t)) = \mathrm{Tr}_B \dot{\rho},$$

where the partial trace operation $\mathrm{Tr}_B(\cdot)$ is performed over subsystem B, leaving the reduced density matrix $\rho_A(t)$ of subsystem A. In this framework, the control field $u(t)$ is optimized to guide $\rho_A(t)$ toward a state that maximizes the quantum property of interest, concurrence, while adhering to the system constraints and dynamics.

The existence of an optimal solution to this control problem is guaranteed by the application of PMP, under the regularity conditions (smoothness of dynamics, controllability, compactness of the control space and the continuity of the cost functional). The objective is to determine the pair (ρ^*, u^*) that is optimal in the sense that the value of the cost functional is minimized over the set of all feasible solutions, achieving the desired entanglement in minimum time.

6.2.2 Necessary Optimality Conditions in the Form of Pontryagin's Minimum Principle

In this subsection, we explore the solution to the proposed optimal control problem, which focuses on minimizing the time required to achieve high degrees of entanglement in a bipartite quantum system. This problem is subject to bounded control inputs

and aims to maximize the concurrence. The solution involves determining the optimal state trajectory ρ^*, the optimal control u^*, and the corresponding Lagrange multiplier π^*. These components are derived using PMP, which provides the necessary optimality conditions.

Proposition 6.2.1 *According to Pontryagin's Minimum Principle, the optimal control law u^*, corresponding to the proposed optimal control problem, exhibits a bang-bang nature, where the control $u^*(t)$ alternates between its extreme values.*

Proof: To determine ρ^*, u^*, and π^*, the Pontryagin Hamiltonian function $\mathcal{H}$ is defined as

$$\mathcal{H}(\rho(t),u(t),\pi(t)) = \mathrm{Tr}\left(\pi^\dagger(t)\dot{\rho}_A\right), \quad t \in [t_0,t_f] \tag{6.8}$$

According to Pontryagin's Minimum Principle, the optimal control $u^*(t)$ must minimize the Hamiltonian $\mathcal{H}$ at every time t. To obtain the optimal control law, we further analyze the Pontryagin Hamiltonian as

$$\mathcal{H}(\rho(t),u(t),\pi(t)) = \mathrm{Tr}\left(\pi^\dagger(t)\dot{\rho}_A\right) = -i\,\mathrm{Tr}\left(\pi^\dagger(t)\,\mathrm{Tr}_B([H,\rho])\right)$$

where $H = H_0 + H_C$. Since the quantum mechanical Hamiltonian H and the density matrix ρ are both Hermitian, one concludes that $([H,\rho])^\dagger = -[H,\rho]$. This means that the commutator $[H,\rho]$ results is a skew-Hermitian matrix, so, its diagonal elements are purely imaginary. Hence, its diagonal and offdiagonals elements satisfy $([H,\rho])_{jj} = -([H,\rho])^*_{jj}$ and $([H,\rho])_{jk} = -([H,\rho])^*_{jk}$, respectively. In addition, according to trace properties, $\mathrm{Tr}([H,\rho]) = \mathrm{Tr}(H\rho) - \mathrm{Tr}(\rho H) = 0$, which means that the trace of $\mathrm{Tr}_B([H,\rho])$ is also zero. Hence, we obtain the following form for $\beta \in \mathbb{C}$ and $\alpha \in \mathbb{IM}$,

$$\mathrm{Tr}_B([H,\rho]) = \begin{pmatrix} \alpha & \beta \\ -\beta^* & -\alpha \end{pmatrix}$$

so the Pontryagin Hamiltonian can be written as

$$\begin{aligned}
\mathcal{H}(\rho(t),u(t),\pi(t)) &= -i\,\mathrm{Tr}\Big(\begin{pmatrix} \pi_{11} & \pi_{12} \\ \pi_{12}^* & \pi_{22} \end{pmatrix}\begin{pmatrix} \alpha & \beta \\ -\beta^* & -\alpha \end{pmatrix}\Big) \\
&= -i(\pi_{11}\alpha - \pi_{12}\beta^* + \pi_{12}^*\beta - \pi_{22}\alpha) \\
&= -i((\pi_{11} - \pi_{22})\alpha + (\pi_{12}^*\beta - (\pi_{12}^*\beta)^*))
\end{aligned}$$

since $\pi_{11}, \pi_{11} \in \mathbb{R}$ and $(\pi_{12}^*\beta - (\pi_{12}^*\beta)^*)$ also gives a pure imaginary number, the Pontryagin Hamiltonian results in a real number. Now, we need to consider minimizing the Pontryagin Hamiltonian since the optimal control is determined by

$$u^*(t) = \underset{u(t)\in\mathcal{U}}{\arg\min}\,\mathcal{H}(\rho(t),u(t),\pi(t)),$$

for all $t \in [t_0, t_f]$, subject to $u(t) \in \mathcal{U}$, the admissible set of controls. The minimization depends on the control-dependent term in $\mathcal{H}$, i.e., $\mathrm{Tr}\left(\pi^\dagger(t)\,\mathrm{Tr}_B([H_c, \rho(t)])\right)$. Thus, the optimal control law $u^*(t)$ is determined by the sign of $\mathrm{Tr}\sum_k(\pi^\dagger(t)\,\mathrm{Tr}_B([H_k, \rho(t)]))$, and is given as

$$u_k^*(t) = \begin{cases} u_{k,\max}, & \text{if } -i\,\mathrm{Tr}(\pi^\dagger(t)\,\mathrm{Tr}_B([H_k, \rho(t)])) < 0, \\ -u_{k,\max}, & \text{otherwise.} \end{cases} \tag{6.9}$$

This control law explicitly incorporates the partial trace Tr_B, which accounts for the dynamics of the reduced subsystem A by tracing out the influence of subsystem B. The linear dependence of $\mathcal{H}$ on $u(t)$, specifically through the term $-iu_k(t)\,\mathrm{Tr}\left(\pi^\dagger(t)\,\mathrm{Tr}_B([H_k, \rho(t)])\right)$, ensures that the optimal solution lies on the boundaries of the admissible control set, leading to a bang-bang nature of $u^*(t)$. This bang-bang control strategy, as described in (6.9), drives the system efficiently toward the desired entangled state while satisfying the constraints of the control problem. □

Proposition 6.2.2 *Under PMP, the evolution of the adjoint variable $\pi(t)$ is governed by the adjoint equation*

$$\dot{\pi}(t) = -\pi^\dagger \dot{\rho}'_A,$$

where $\dot{\rho}'_A = \frac{\partial \dot{\rho}_A}{\partial \rho_A}$ represents the functional derivative of the time evolution operator $\dot{\rho}_A$ with respect to the state ρ_A. At the final time t_f, the adjoint variable satisfies the terminal condition

$$\pi(t_f) = \frac{\sqrt{2}\rho_A(t_f)}{\sqrt{1 - \mathrm{Tr}(\rho_A(t_f)^2)}}. \tag{6.10}$$

Proof: Under PMP, the adjoint variable $\pi(t)$ evolves according to the adjoint equation

$$\dot{\pi}(t) = -\frac{\partial \mathcal{H}}{\partial \rho_A(t)} = -\frac{\partial}{\partial \rho_A}\mathrm{Tr}(\pi^\dagger(t)\dot{\rho}_A(t)) = -\pi^\dagger \frac{\partial \dot{\rho}_A(t)}{\partial \rho_A},$$

where the Hamiltonian depends on $\rho_A(t)$ implicitly through $\dot{\rho}_A(t)$.

The terminal condition for $\pi(t)$ follows from PMP and the specific structure of the problem. At the final time t_f, the adjoint variable must satisfy

$$\pi(t_f) = \frac{\partial J}{\partial \rho_A} = -\frac{\partial C(\rho)}{\partial \rho_A} = -\sqrt{2}\frac{1}{2\sqrt{1 - \mathrm{Tr}(\rho_A^2)}}(-2\rho_A),$$

which leads to (6.10) for the final time. □

Remark 6.1 *The explicit expression for the functional derivative of $\dot{\rho}_A$ with respect to ρ_A depends on the form of ρ and the correlation term between the two systems A and B. To analyze this, we*

first implement the time derivative of ρ using the Schmidt decomposition as

$$\begin{aligned}\dot{\rho}_A &= \mathrm{Tr}_B(-i[H_0 + H_c, \rho]) = -i\,\mathrm{Tr}_B([H_0 + H_c, \rho]) \\ &= -i\sum_{k=1}^{r}\left(\mathbb{I}_A \otimes \langle v_k^B|\right)[H_0 + H_c, \rho]\left(\mathbb{I}_A \otimes |v_k^B\rangle\right)\end{aligned} \tag{6.11}$$

We now consider the derivative of $\dot{\rho}_A$ with respect to ρ_A, referred to as $\dot{\rho}'_A$, so

$$\dot{\rho}'_A = -i\sum_{k=1}^{r}\left(\mathbb{I}_A \otimes \langle v_k^B|\right)\frac{\partial[H_0 + H_c, \rho]}{\partial \rho_A}\left(\mathbb{I}_A \otimes |v_k^B\rangle\right) \tag{6.12}$$

Given the total density matrix $\rho = \rho_A \otimes \rho_B + \rho_{cor}$, where ρ_{cor} represents the correlation term. We analyze two cases:

- *Case 1: $\rho_{\mathrm{cor}} = 0$ (No Correlations Between A and B)*

  If there are no correlations, the total density matrix ρ is separable:

  $$\rho = \rho_A \otimes \rho_B.$$

  In this case, the derivative of ρ with respect to ρ_A is straightforward. Since ρ_B is independent of ρ_A, we have

  $$\frac{\partial \rho}{\partial \rho_A} = \mathbb{I}_B \otimes \rho_B.$$

  Substituting this into the functional derivative of $\dot{\rho}_A$, we obtain

  $$\dot{\rho}'_A = -i\sum_{k=1}^{r}\left(\mathbb{I}_A \otimes \langle v_k^B|\right)[H_0 + H_c, \mathbb{I}_B \otimes \rho_B]\left(\mathbb{I}_A \otimes |v_k^B\rangle\right).$$

  Here, the commutator simplifies because of the separability of ρ.

- *Case 2: $\rho_{\mathrm{cor}} \neq 0$ (Presence of Correlations)*

  When correlations exist, the total density matrix ρ includes the correlation term ρ_{cor}, and the derivative becomes more complicated. Specifically, the functional derivative of ρ with respect to ρ_A is given by

  $$\frac{\partial \rho}{\partial \rho_A} = \mathbb{I}_B \otimes \rho_B + \frac{\partial \rho_{\mathrm{cor}}}{\partial \rho_A}.$$

  The second term $\frac{\partial \rho_{\mathrm{cor}}}{\partial \rho_A}$ accounts for the interdependence between subsystems A and B through their correlations. Substituting this into the expression for $\dot{\rho}'_A$, we have

  $$\begin{aligned}\dot{\rho}'_A = -i\sum_{k=1}^{r}&\left(\mathbb{I}_A \otimes \langle v_k^B|\right)\left[H_0 + H_c, \mathbb{I}_B \otimes \rho_B + \frac{\partial \rho_{\mathrm{cor}}}{\partial \rho_A}\right] \\ &\left(\mathbb{I}_A \otimes |v_k^B\rangle\right)\end{aligned}$$

Here, the correlation term ρ_{cor} introduces additional complexity, and its specific form determines the nature of the functional derivative.

Proposition 6.2.3 *Given the cost functional J and the Pontryagin Hamiltonian $\mathcal{H}(t)$, for the Pontryagin Hamiltonian associated with the optimization problem, at the final time t_f, the following transversality condition holds:*

$$\mathcal{H}(t_f) = \frac{\sqrt{2}\rho_A}{2\sqrt{1 - Tr(\rho_A^2)}}\dot{\rho}_A - \Gamma \tag{6.13}$$

Proof: From the transversality condition of the final time one has

$$\mathcal{H}(t_f) = -\frac{\partial J}{\partial t_f} = -\frac{\partial(-C(\rho(t_f)) + \Gamma t_f)}{\partial t_f}.$$

We need to compute

$$\frac{\partial C(\rho(t_f))}{\partial t_f} = \frac{\partial C(\rho)}{\partial \rho_A(t_f)}\frac{\partial \rho_A(t_f)}{\partial t_f} = \frac{\sqrt{2}\rho_A}{2\sqrt{1 - \text{Tr}(\rho_A^2)}}\dot{\rho}_A$$

In addition $-\frac{\partial \Gamma t_f}{\partial t_f} = -\Gamma$, so by summing the two terms one obtains (6.13). □

6.3 Numerical Validation of Optimal Entanglement Control

In this section, we numerically validate the entanglement control strategy developed in the preceding section. We begin by introducing the system Hamiltonian. In the proposed example, we consider that the internal Hamiltonian H_0 (in the absence of external fields) is given as

$$H_0 = \sigma_z \otimes \sigma_z.$$

The control Hamiltonian $H_c(t)$, driven by time-dependent control fields $u_k(t)$, consists of a linear combination of coupling Hamiltonians H_k, where $k = 1,2,3$, constructed from Pauli matrices as

$$H_1 = \sigma_x \otimes \sigma_y + \sigma_z \otimes \sigma_z,$$
$$H_2 = \sigma_x \otimes \sigma_z + \sigma_z \otimes \sigma_x,$$
$$H_3 = \sigma_y \otimes \sigma_z + \sigma_z \otimes \sigma_y.$$

Here, the Pauli matrices are defined as

$$\sigma_x = \begin{pmatrix} 0 & 1 \\ 1 & 0 \end{pmatrix}, \quad \sigma_y = \begin{pmatrix} 0 & -i \\ i & 0 \end{pmatrix}, \quad \sigma_z = \begin{pmatrix} 1 & 0 \\ 0 & -1 \end{pmatrix}.$$

We consider a general two-qubit superposition state expressed as

$$|\psi(t)\rangle = \alpha_{00}|00\rangle + \alpha_{01}|01\rangle + \alpha_{10}|10\rangle + \alpha_{11}|11\rangle,$$

where α_{ij} are complex coefficients. The corresponding density matrix is given by

$$\rho = \begin{bmatrix} |\alpha_{00}|^2 & \alpha_{00}\alpha_{01}^* & \alpha_{00}\alpha_{10}^* & \alpha_{00}\alpha_{11}^* \\ \alpha_{01}\alpha_{00}^* & |\alpha_{01}|^2 & \alpha_{01}\alpha_{10}^* & \alpha_{01}\alpha_{11}^* \\ \alpha_{10}\alpha_{00}^* & \alpha_{10}\alpha_{01}^* & |\alpha_{10}|^2 & \alpha_{10}\alpha_{11}^* \\ \alpha_{11}\alpha_{00}^* & \alpha_{11}\alpha_{01}^* & \alpha_{11}\alpha_{10}^* & |\alpha_{11}|^2 \end{bmatrix}.$$

To quantify entanglement, we compute the partial trace over subsystem B, resulting in the reduced density matrix:

$$\mathrm{Tr}_B(\rho) = \begin{bmatrix} |\alpha_{00}|^2 + |\alpha_{01}|^2 & \alpha_{00}\alpha_{10}^* + \alpha_{01}\alpha_{11}^* \\ \alpha_{10}\alpha_{00}^* + \alpha_{11}\alpha_{01}^* & |\alpha_{10}|^2 + |\alpha_{11}|^2 \end{bmatrix}.$$

We focus on driving the system toward Bell states, which represent maximally entangled two-qubit states. The Bell states are defined as

$$\begin{aligned} |\Phi^+\rangle &= \frac{1}{\sqrt{2}}(|00\rangle + |11\rangle), \\ |\Phi^-\rangle &= \frac{1}{\sqrt{2}}(|00\rangle - |11\rangle), \\ |\Psi^+\rangle &= \frac{1}{\sqrt{2}}(|01\rangle + |10\rangle), \\ |\Psi^-\rangle &= \frac{1}{\sqrt{2}}(|01\rangle - |10\rangle). \end{aligned}$$

These states exhibit specific entanglement patterns and serve as benchmarks for evaluating the effectiveness of our control strategy. To investigate the dynamics of entanglement generation, we initialize the system in a perturbed separable state to avoid critical points where the entanglement gradient vanishes. The initial state takes the form

$$\rho_0 = (1 - \epsilon)\rho_{\text{sep}} + \epsilon\delta\rho,$$

where ρ_{sep} represents a separable state, $\delta\rho$ introduces a small entangled component, and $0 < \epsilon \ll 1$ controls the perturbation magnitude. This setup ensures the system starts close to separable while still enabling smooth optimization dynamics. By applying the control fields $u_k(t)$, we numerically optimize the state evolution to achieve a maximally entangled target state. For instance, we considered a perturbed separable state by expressing $\rho_{\text{sep}} = |00\rangle\langle 00|$ and $\delta\rho = |\Phi^+\rangle\langle\Phi^+|$.

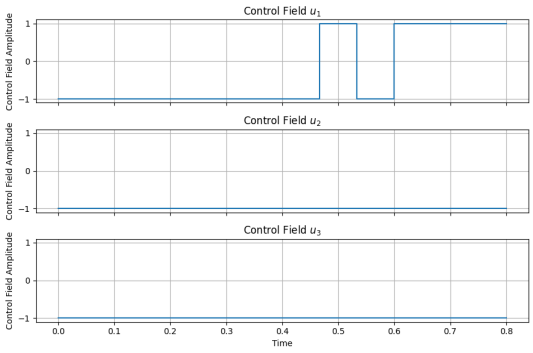


Figure 6.1: Control field amplitudes u_1, u_2, and u_3 as a function of time.

Figure 6.1 illustrates the evolution of the control fields u_1, u_2, and u_3 over time. Notably, the control field u_1 exhibits switching behavior, transitioning between -1 and 1 at specific times. This behavior is interpreted as a bang-bang control strategy. The observed switching aligns with the principles of the PMP, where the control input is driven to its extremal values to maximize system performance. The abrupt transitions (e.g., around $t = 0.5$) correspond to changes in the system's switching function, which determines the optimal control direction. The fields u_2 and u_3 remain constant at the lower bound.

Figure 6.2 illustrates the evolution of concurrence over time under the influence of optimal switching control fields: The figure demonstrates the effectiveness of optimal control in generating entanglement in a quantum system. Key observations include: At the beginning ($t < 0.3$), the concurrence increases steadily as the control fields drive the system from a separable state toward an entangled state. After $t = 0.6$, the concurrence approaches its maximum value of 1, representing a maximally entangled state. The rapid transitions in the control fields, as seen in the previous figure, optimize the state evolution to maximize entanglement efficiently. Such behavior is essential for quantum technologies, including quantum communication and quantum computing, where high levels of entanglement are crucial.

6.4 Application of CRAB Algorithm for Enhanced Entanglement Synthesis

This section explores the application of the Chopped Random Basis (CRAB) algorithm, integrated within the Quantum Toolbox in Python (QuTiP), to control and manipulate entanglement dynamics in a two-qubit quantum system. The primary focus is on enabling the transition from a perturbed separable state to a maximally entangled state via the strategic design of control pulses. By employing a tailored Hamiltonian, we optimize the pulses to meet a predefined fidelity error target, thus assessing the algorithm's efficacy in achieving precise quantum state transformations.

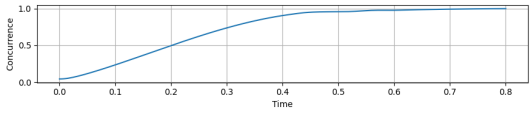


Figure 6.2: Evolution of concurrence as a function of time using optimal switching control fields. The switching behavior in the control fields ensures a rapid increase in concurrence, reaching its maximum value of 1, indicative of maximal entanglement.

With the ability to model the trajectory of a quantum state under the influence of an external field, it naturally prompts us to explore the converse scenario: Given known initial and target states, can we determine the precise light pulse necessary for this transition? A light pulse is a brief, controlled burst of light energy characterized by its short duration and specific spectral properties, serving as a critical tool in quantum manipulations (Paschotta, 2008). These pulses can be finely tuned to interact with quantum states in a manner that drives the system from its current state to a desired configuration with minimal collateral effects. The capacity to utilize light pulses enables precise control over quantum transitions, crucial for applications ranging from quantum computing to high-resolution spectroscopy.

In QOC context, consider a quantum mechanical Hamiltonian $H(u(t))$, dependent on one or multiple time-dependent driving fields $u(t)$, acting on a Hilbert space $\mathcal{H} = \mathbb{C}^N$. The Hamiltonian is composed of two components: the drift Hamiltonian H_d and the time-dependent control Hamiltonian $H_c(u(t))$. The control Hamiltonian is given by $H_c(u(t)) = \sum_{l=1}^{m} H_l u_l(t)$, where each H_l denotes an interaction Hamiltonian linked to the control field $u_l(t)$. These interaction Hamiltonians H_l specify the manner in which the system interacts with the external control fields $u_l(t)$. Given a fixed final time T, an initial state $|\psi(t=0)\rangle = |\psi_0\rangle$, and a Hermitian operator $\hat{O}$, the objective is to find the function $u(t)$ that optimizes the expectation value $\langle\psi_f|\hat{O}|\psi_f\rangle$ in the final state $|\psi(t=T)\rangle = |\psi_f\rangle$. Typically, the operator $\hat{O}$ is chosen as the projection operator onto a designated target state $|\psi_d\rangle$, i.e., $\hat{O} = |\psi_d\rangle\langle\psi_d|$. Consequently, the optimal control objective centers around maximizing the fidelity, $F(|\psi_f\rangle) = |\langle\psi_f|\psi_d\rangle|^2$ or equivalently minimizing the infidelity $\bar{F}(|\psi_f\rangle) = 1 - |\langle\psi_f|\psi_d\rangle|^2$.

However, the choice of the control objective is not unique, and can be defined in a variety of ways. For all choices, the control objective can be implicitly expressed as a function of the control pulse, since the state of the system itself depends on $u(t)$. In this chapter, we consider $J(u) = \bar{F}(|\psi_f\rangle)$. This mapping of the control objective as a function of the control pulse is referred to as the control landscape (Wu et al., 2012). The challenge in control theory is to find the control pulse $u(t)$ that minimizes $J(u)$. Furthermore, $J(u)$ might include a term dependent only on $u(t)$, such as the power of the driving field $\frac{1}{T}\int_0^T u(t)^2\,dt$, quantifying the energy used by the pulse over time T. For now, we only consider the case where achieving the minimum infidelity is the figure of merit.

In the illustrative scenario for the case that the system's evolution is governed by the

time-dependent Schrödinger equation, the optimization problem can be formulated as follows:

$$(P)\begin{cases}\min\limits_{u}\left\{J(u)=1-\left|\langle\psi_f|\psi_d\rangle\right|^2\right\}\\ \text{subject to}\\ i\hbar\dfrac{d}{dt}|\Psi(t)\rangle=H(u(t))|\Psi(t)\rangle \text{ a.e. } t\in[0,T]\\ |\psi(t=0)\rangle=|\psi_0\rangle\in\mathcal{H}\end{cases}$$

In the remainder of this chapter, we set $\hbar = 1$ for simplicity. Problem (P) focuses on identifying the optimal control field $u(t)$ via an optimization algorithm, with the aim of minimizing the cost function $J(u)$. Without specific constraints, $u(t)$ is typically selected from function spaces such as L_2 — the space of square-integrable functions, or L_∞ — the space of measurable essentially bounded functions. Consequently, this may involve searching through an infinite-dimensional space (see (Boscain et al., 2020)).

6.4.1 CRAB Algorithm in Quantum Optimal Control

The chopped random basis quantum optimization (Caneva et al., 2011) has represented an advancement in the field of QOC. The CRAB algorithm has demonstrated its effectiveness in various applications, such as qubit manipulation (Scheuer et al., 2014), due to its efficiency and versatility. This section explores the mathematical underpinnings of CRAB and discusses its application in optimizing pulse parameters. In order to delve into the mathematical formulation of CRAB, let consider a quantum system subjected to a control field $u(t)$ over a fixed time period T. The fundamental principle of CRAB algorithm for minimizing $J(u(t))$ is to approximate the control function, $u(t)$, essential for steering the dynamics of a quantum system, using a truncated and randomized basis. The functional form of a control pulse $u(t)$ is expressed as a sum over a finite number, N_c, of basis functions $\phi_i(t)$:

$$u(t)=\sum_{i=1}^{N_c} c_i\phi_i(t),$$

where each $\phi_i(t)$ is a basis function and c_i are the coefficients to be optimized. This formulation reduces the problem to a lower-dimensional subspace, where the task is to find the optimal set of coefficients c_i. Optimization is conducted within this subspace using various direct search algorithms like the Nelder-Mead simplex (Nelder and Mead, 1965), Powell's method (Powell, 1964), particle swarm optimization (Fan et al., 2004), Monte Carlo techniques (Metropolis et al., 1953), or evolutionary strategies like covariance matrix adaptation evolution strategy (Hansen et al., 2003). Alternatively, the optimization may involve gradient calculations that adapt the coefficients based on the derivative of the parametrization, which leads to the so called GOAT (Machnes et al., 2018) or GROUP (Sørensen et al., 2018) algorithms. In this discussion, we concentrate on the Nelder-Mead simplex method, a well-established direct search optimization technique. This method

uniquely relies on repeated evaluations of the cost function at various points within the search space, without the need for additional derivative information.

If starting from an approximate initial guess $u^{guess}(t)$ that does not fit the basis well, the control function can be adjusted as

$$u(t) = u^{guess}(t)\left(1 + \sum_{i=1}^{N_c} c_i \phi_i(t)\right). \tag{6.14}$$

Limiting the optimization to just N_c dimensions may introduce constraints that potentially trap the algorithm in suboptimal local minima, known as "false traps". As a first step to weaken this constraint, the basis functions can be randomized. This can further be mitigated by iteratively introducing new random basis functions, utilizing the optimal solution from the previous optimization as the initial guess for the subsequent iteration. The basis are often chosen as trigonometric functions modified by a shaping function to fix the pulse values at the start and end times:

$$u(t) = u^{guess}(t)\left(1 + \Lambda(t)\sum_{i=1}^{N_c}\left(\alpha_i \sin(\omega_i t) + \beta_i \cos(\omega_i t)\right)\right) \tag{6.15}$$

in which $\Lambda(t)$ is a time dependent function with the boundary conditions $\Lambda(0) = \Lambda(T) = 0$, assuring the pulse shape being smooth. The frequencies ω_i are selected randomly around the principal harmonics within some specified range $[0, \omega_{max}]$. Different choices of basis functions are possible, including possibly generalized Chebyshev polynomials with randomly chosen orders, All admissible basis functions together span a subspace $\Omega \subset L_2$, the space of admissible controls. Each selection of random basis functions thus defines a unique N_c-dimensional subspace of Ω, enabling the exploration of different sections of the potentially infinite dimensional space of admissible controls. This approach underlies the algorithm's robustness, allowing it to explore and optimize within a potentially infinite-dimensional control space.

For the control expression defined in (6.15), the algorithm aims to optimize the coefficients $\boldsymbol{\alpha}$ and $\boldsymbol{\beta}$ until a minimum of J is achieved. In other words, the control function $u^{CRAB}(t)$ is fixed by choosing the optimization parameters $\boldsymbol{\alpha}$, $\boldsymbol{\beta}$, and $\boldsymbol{\omega}$, where the dimension of each vector is N_c, therefore, the cost function can be expressed solely as a function of control parameters, i.e., $J := J^{CRAB}(\boldsymbol{\alpha}, \boldsymbol{\beta}, \boldsymbol{\omega})$. In order to find optimal control parameters, the system dynamics is integrated multiple times with various control parameters during every iteration of Nelder–Mead optimization. Pseudo-code of CRAB-based optimal control is given in Algorithm 1.

6.4.2 Application of CRAB Algorithm in Entanglement Synthesis

We consider a theoretical model, depicted in Fig.6.3, which comprises two qubits, each located within a separate cavity. These cavities are interconnected through a closed-loop

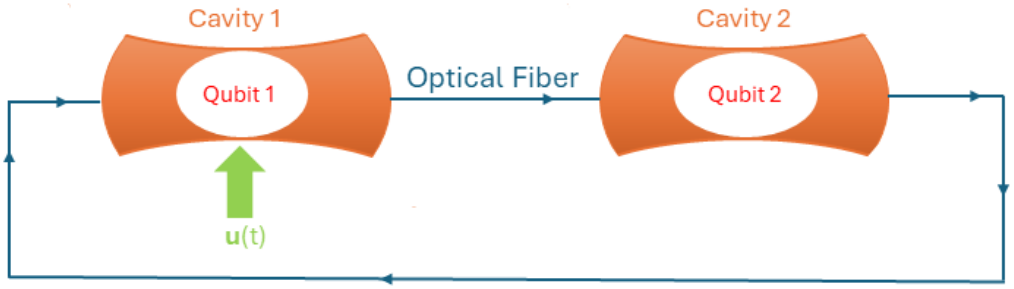


Figure 6.3: The system consists of two qubits, each positioned in an individual cavity. These cavities are linked by a closed-loop optical fiber network. A coherent input field $u(t)$ is applied to Qubit 1, with the outputs from each cavity being routed back into the other.

Table 6.1: Entanglement synthesis studied under CRAB optimization.

No.	Initial State and Deviation	Target State	Number of iterations	Final fidelity error
1	$(1+\epsilon)\|\beta_{00}\rangle + \|\beta_{01}\rangle \approx \|00\rangle$	$\|\beta_{00}\rangle$	587	9.69×10^{-8}
2	$\|\beta_{00}\rangle + (1+\epsilon)\|\beta_{01}\rangle \approx \|00\rangle$	$\|\beta_{01}\rangle$	480	9.85×10^{-8}
3	$(1+\epsilon)\|\beta_{10}\rangle + \|\beta_{11}\rangle \approx \|01\rangle$	$\|\beta_{10}\rangle$	508	9.47×10^{-8}
4	$\|\beta_{10}\rangle - (1+\epsilon)\|\beta_{11}\rangle \approx \|10\rangle$	$\|\beta_{11}\rangle$	562	8.61×10^{-8}

optical fiber network. One of the qubits receives a coherent input field $u(t)$, and the outputs from each cavity are directed into the other. By neglecting the radiation field, we select the internal Hamiltonian as

$$H_d = 2J\sigma_z \otimes \sigma_z, \tag{6.16}$$

where J, the spin-spin coupling constant, varies with the frequency of the applied radiation field, and is set to $J = 0.5$ in our calculations. In this model, the radiation field is mathematically eliminated to simplify the dynamics, focusing solely on the internal spin-spin interactions between the qubits. This elimination reduces computational complexity and isolates the effects of controlled entanglement mechanisms, allowing for a direct analysis of how the spin coupling constant J, adjusted by the frequency of the previously applied radiation field, influences the system. The control Hamiltonian $H_c = \sum_{k=1}^{3} H_k u_k(t)$ is generated by a local laser, with each coupling Hamiltonian H_k being a combination of the Pauli matrices σ_x, σ_y, and σ_z and modulated by control functions $u_k(t)$. Specifically, we define:

$$\begin{aligned} H_1 &= \sigma_x \otimes \sigma_y + \sigma_z \otimes \sigma_z, \\ H_2 &= \sigma_x \otimes \sigma_z + \sigma_z \otimes \sigma_x, \\ H_3 &= \sigma_y \otimes \sigma_z + \sigma_z \otimes \sigma_y. \end{aligned} \tag{6.17}$$

We now address the challenge of solving problem (P) using Algorithm 6.1, where the objective is to transition an initial state, specifically a perturbed separable state, into a maximally entangled state. This process is explored within the framework of two-qubit

Algorithm 6.1 Chopped Random Basis Optimization with Nelder–Mead

Require: $\bar{F}_{\text{err}}$: minimum desired infidelity, j: iteration count, $j_{\max}$: maximum iteration count, d: dimension of simplex

Ensure: Optimised control amplitudes for minimum infidelity

Initialize Fourier base frequencies and amplitudes to form an initial simplex in R^d with vertices $u_1, u_2, \ldots, u_{d+1}$.
Set the iteration count $j = 0$.
while $j \leq j_{\max}$ **do**
    Sort vertices such that $J(u_1) \leq J(u_2) \leq \ldots \leq J(u_{d+1})$.
    if $J(u_1) \leq \bar{F}_{err}$ **then**
        break
    end if
    Compute centroid u_0 of first d ordered points via $u_0 = \frac{1}{d}\sum_{i=1}^{d} u_i$.
    Reflect: $u_r = u_0 + \alpha(u_0 - u_{d+1})$ where $\alpha > 0$.
    if $J(u_1) \leq J(u_r) < J(u_d)$ **then**
        Replace u_{d+1} with u_r.
    else if $J(u_r) < J(u_0)$ **then**
        Expand: $u_e = u_0 + \gamma(u_r - u_0)$ where $\gamma > 1$.
        if $J(u_e) < J(u_r)$ **then**
            Replace u_{d+1} with u_e.
        else
            Replace u_{d+1} with u_r.
        end if
    else
        Contract: $u_c = u_0 + \beta(u_0 - u_{d+1})$ where $0 < \beta < 1$.
        if $J(u_c) < J(u_{d+1})$ **then**
            Replace u_{d+1} with u_c.
        else
            Shrink the simplex: For $i = 2$ to $d + 1$, set $u_i = u_1 + \delta(u_i - u_1)$ where $0 < \delta < 1$.
        end if
    end if
    $j \leftarrow j + 1$
end while

quantum states. For the basic two-qubit inputs—$|00\rangle$, $|01\rangle$, $|10\rangle$, and $|11\rangle$—the quantum state $|\psi(t)\rangle$ at any time t is expressed in the computational basis as follows:

$$|\psi(t)\rangle = c_{00}|00\rangle + c_{01}|01\rangle + c_{10}|10\rangle + c_{11}|11\rangle, \tag{6.18}$$

where the coefficients c_{ij} indicate the probability amplitude of each basis in the quantum state. The targets of our transformation are the four Bell states, i.e., from a known initial state we target a predefined maximally entangled state. The Bell states represent the simplest and most profound forms of quantum entanglement, expressed as

$$|\beta_{00}\rangle = \frac{1}{\sqrt{2}}(|00\rangle + |11\rangle), \qquad |\beta_{01}\rangle = \frac{1}{\sqrt{2}}(|00\rangle - |11\rangle),$$
$$|\beta_{10}\rangle = \frac{1}{\sqrt{2}}(|01\rangle + |10\rangle), \qquad |\beta_{11}\rangle = \frac{1}{\sqrt{2}}(|01\rangle - |10\rangle).$$

Each of these Bell states encapsulates a key aspect of entanglement and serves as an ideal target state for demonstrating the efficacy of quantum state manipulation through Algorithm 6.1. We consider four different cases declared in Table 6.1, where $\epsilon = 0.1$ in our computations. In all cases, to compute the system's evolution, the control amplitudes are assumed to be constant within designated piecewise time-slots. Consequently, the evolution within each time-slot is determined using the unitary evolution $U(t_k) = \exp(-iH(t_k)\Delta t)$. By aggregating these calculations across all time-slots, we approximate the system's evolution from the initial state ψ_0 at $t = 0$ to $U(T)$ at the final evolution time, $t = T$. The number of time-slots (t_s) and the total evolution time must be selected to ensure that the duration of each time-slot (Δt) is sufficiently small relative to the system's dynamics. To this end, we considered the number of time slots $n_{t_s} = 200$ and $T = 20$ in our simulations. In addition the maximum elapsed time is set to 120 seconds and the maximum iteration is consider 1000, and the fidelity error target is 10^{-7}. All the results shown in Table 6.1 are obtained through the termination of the algorithm due to goal being achieved. To show an illustration of the optimization process, we present a comparison between the initial control amplitudes, which have been generated randomly, and optimized control amplitudes for the three distinct control fields over a time period of 20 seconds in Fig. 6.4. Each subplot corresponds to one of the control fields used in the CRAB optimization process, aiming to transfer the perturbed separable state to the desired maximally entangled Bell state. During all our optimization procedures, the control pulses are optimized through the CRAB algorithm, employing the Nelder-Mead simplex method, aiming to minimize the fidelity error. This is done by adjusting the control amplitudes $u(t)$, whose effectiveness is assessed quantitatively by the cost function $J(u)$, which indeed indicates the infidelity. The infidelity criterion yields a value between 1 and 0, where 1 denotes no overlap, and 0 indicates perfect alignment (the system is precisely in the target state). In Fig. 6.5, we present two scenarios: Fig. 6.4 illustrates the cost evolution without optimal control amplitudes, which exhibits considerable

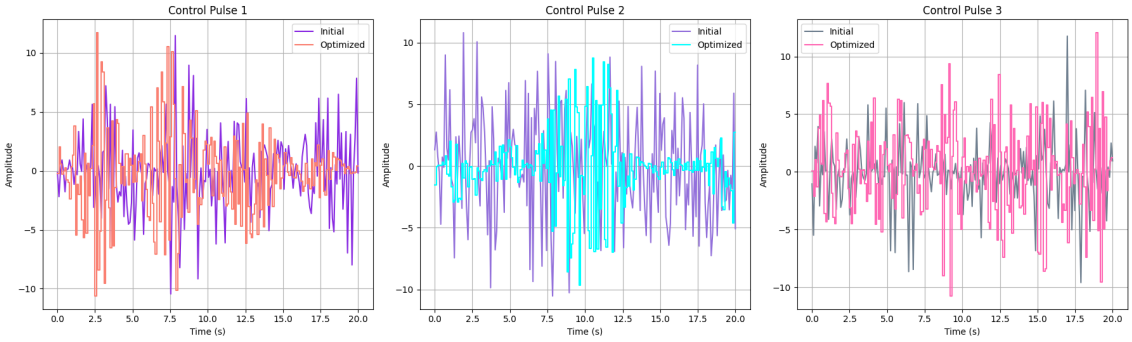


Figure 6.4: Initial and optimized control fields for quantum state transfer from a perturbed separable state $|\psi_0\rangle \approx |00\rangle$ to the target Bell state $|\beta_{00}\rangle$.

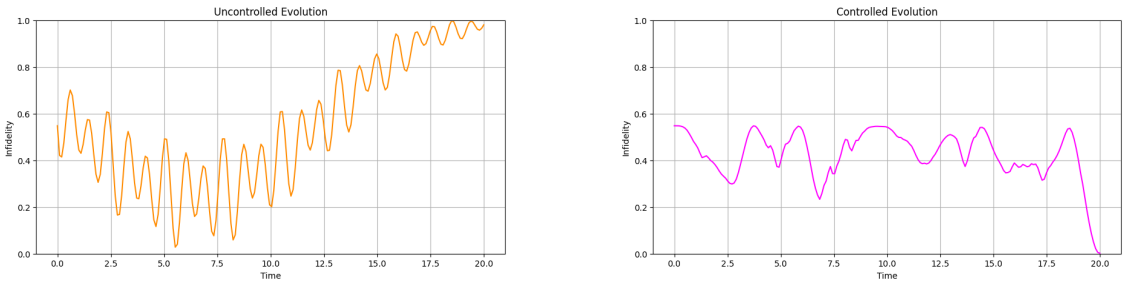


Figure 6.5: The graphs compare the infidelity of quantum states over time between controlled and uncontrolled evolutions. The controlled evolution shows a more stable and lower infidelity, indicating effective management of quantum state deviations, while the uncontrolled evolution demonstrates higher and increasing infidelity, reflecting the system's vulnerability.

infidelity, and Fig. 6.4 depicts a decline in infidelity, indicating that the target state is successfully achieved In our computational study, we solve the time-dependent Schrödinger equation considering our time-dependent control amplitudes derived from the optimization process. This plot illustrates how the infidelity between the evolving state $|\psi(t)\rangle$ and the desired target state $|\psi_d\rangle$ varies over time, providing a visual and quantitative assessment of the control strategy's performance. An infidelity curve reaching 0 indicates a successful control strategy that effectively steers the state towards the target configuration, thereby validating the efficacy of the optimized control pulses. The infidelity evolution plot serves as a crucial diagnostic tool in quantum control experiments, helping to confirm the theoretical and computational approaches to steering quantum states and guiding further experimental and theoretical investigations in quantum dynamics and control.

6.5 Concluding Remarks and Discussions

In this chapter, we investigated entanglement generation and optimization. By using the Pontryagin Minimum Principle, we formulated an optimal control problem focused on maximizing the entanglement measure within the shortest possible timeframe under

input constraints. We derived optimality conditions for a matrix-valued dynamic control system of a closed quantum system governed by the Liouville-von Neumann equation.

Additionally, we explored the Chopped Random Basis (CRAB) algorithm in the context of quantum entanglement synthesis, particularly for two-qubit systems. The algorithm effectively optimized control pulses to transition quantum systems from separable to maximally entangled states. This demonstrated its potential for advanced quantum computing and information processing tasks. By leveraging the CRAB algorithm, we minimized infidelity across different entanglement generation scenarios, showcasing the flexibility and robustness of this approach.

The combination of the Pontryagin Minimum Principle and the CRAB algorithm provides complementary perspectives for addressing quantum optimal control problems. While PMP offers a rigorous analytical framework to derive necessary optimality conditions and guide control strategies systematically, the CRAB algorithm leverages numerical optimization to explore a broader control landscape, particularly when analytical solutions are infeasible.

To conclude, this chapter presented control methods for quantum state manipulation, emphasizing their role in driving future progress in quantum technologies. The work lays a foundation for further research while offering practical insights into the development of optimized quantum control protocols essential for realizing the full potential of quantum systems.

Chapter 7

A Hybrid Quantum-Classical Physics-Informed Neural Network Architecture for Solving Quantum Optimal Control Problems

This chapter proposes an integrated quantum-classical approach that merges quantum computational dynamics with classical computing methodologies tailored to address control problems based on Pontryagin's minimum principle within a Physics-Informed Neural Network (PINN) framework. By leveraging a dynamic quantum circuit that combines Gaussian and non-Gaussian gates, the study showcases an innovative approach to optimizing quantum state manipulations. The proposed hybrid model effectively applies machine learning techniques to solve optimal control problems. This is illustrated through the design and implementation of a hybrid PINN structure to solve a quantum state transition problem in a two and three-level system, highlighting its potential across various quantum computing applications. The main contents of this chapter were published in (Dehaghani et al., 2024c).

7.1 Hybrid Quantum-Classical Optimization

The indicated QPINN architecture is built upon a hybrid quantum-classical model, where a surrogate neural network developed in the continuous variable quantum framework approximates the solutions to the differential equations governing the system dynamics. Our QPINN model, depicted in Fig. 7.1 merges QNN, implemented in a continuous variable quantum framework, with the theory of functional connections. The core of our implementation involves defining the quantum circuits and the optimization algorithm necessary for training the QPINNs. In this section, we first delve into the implementation of the exploited quantum circuit and continuous variable model. In the second

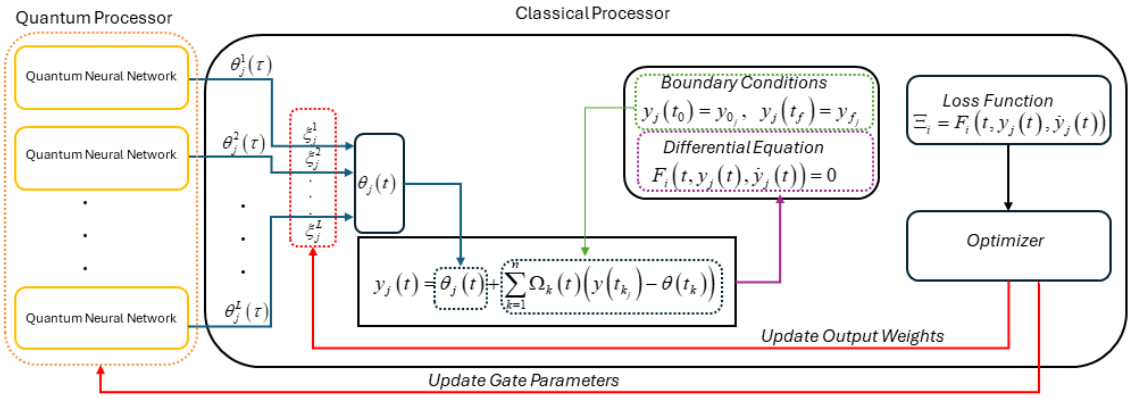


Figure 7.1: An integrated quantum-classical approach to solve differential equations. Here, the subscript i indicates a particular differential equation from a finite set forming the system of differential equations, j is the index of unknown functions of time which are the solutions to the system, and L indicates the number of quantum neural network in the quantum processor. The circuit output, symbolized as $\theta_j(t)$, informs the formulation of solution $y_j(t)$, subject to initial and terminal conditions, ensuring boundary conditions adherence and enabling the substitution of the solution into the differential equation framework. This is followed by the computation of a loss function that quantifies the error in satisfying the differential equation, which an optimizer then minimizes to derive the approximated solution. The optimizer updates both the output weights ζ_j^l and the gate parameters. The optimizer effectively links the quantum computation outputs with the classical optimization objectives.

subsection, we explain the implementation of our hybrid approach based on the theory of functional connections.

7.1.1 Quantum Circuit implementation

The continuous variable quantum computing framework is centered around the concept of the qumode, which serves as the fundamental unit of information. In this framework, the qumode $|\psi\rangle$ is represented through the basis expansion of quantum states, as $|\psi\rangle = \int \psi(x)|x\rangle dx$ where the states represent the eigenstates of the $\hat{x}-$quadrature, $\hat{x}|x\rangle = x|x\rangle$, with $x \in \mathbb{R}$ is the eigenvalue. The continuous variable quantum computing model presents an alternative to the widely recognized qubit-based approach. In the qubit framework, quantum information is represented using discrete states, as exemplified by a qubit $|\phi\rangle$ which can be expressed as a linear combination of the basis states $|0\rangle$ and $|1\rangle$: $|\phi\rangle = \phi_0|0\rangle + \phi_1|1\rangle$. Conversely, continuous variable quantum computing utilizes the concept of qumodes, where states are defined across a continuum of possible values, rather than discrete coefficients. This approach employs a continuous spectrum of coefficients, reflecting a continuous eigenvalue spectrum. This framework is particularly suited to scenarios involving continuous quantum operators, aligning seamlessly with the principles of continuous variable quantum computing. Here, we consider each

qumode i associated with a pair of non-commuting position $\hat{x}_i$ and momentum $\hat{p}_i$ operators. These operators constitute the phase space and are good instances of continuous quantum variables, defined as $\hat{x} = \int_{-\infty}^{\infty} x \left|x\right\rangle \left\langle x\right| dx$ and $\hat{p} = \int_{-\infty}^{\infty} p \left|p\right\rangle \left\langle p\right| dp$ with $\left|x\right\rangle$ and $\left|p\right\rangle$ being orthogonal vectors. The non commuting nature of these operators leads to the Heisenberg uncertainty principle for the simultaneous measurements of $\hat{x}$ and $\hat{p}$.

Similar to the established qubit-based approach, continuous variable quantum computing can be described through the use of basic gates, which may be implemented as optical devices. A continuous variable quantum program typically involves a sequence of gates affecting one or several qumodes. Essential to the development of continuous variable quantum neural networks are the following four basic Gaussian gates (Killoran et al., 2019)

- **Displacement Gate** This gate translates the state within the phase space by a complex number α, effectively modifying both the position and momentum coordinates by α's real and imaginary components, respectively. Symbolically, the transformation is represented as a shift in the phase space variables.

$$\begin{bmatrix} x \\ p \end{bmatrix} \rightarrow \boxed{\begin{array}{c}\text{D-gate:} \\ D(\alpha)\end{array}} \rightarrow \begin{bmatrix} x + \alpha_{\text{Re}} \\ p + \alpha_{\text{Im}} \end{bmatrix}$$

- **Rotation Gate** $R(\varphi)$: This gate rotates the state in phase space around the origin by an angle φ, where φ spans the interval $[0, 2\pi]$. The action of this gate can be represented by a rotation matrix that multiplies the phase space vector, leading to a new configuration defined by the rotated coordinates.

$$\begin{bmatrix} x \\ p \end{bmatrix} \rightarrow \boxed{\begin{array}{c}\text{R-gate:} \\ R(\varphi)\end{array}} \rightarrow \begin{bmatrix} \cos(\varphi) & \sin(\varphi) \\ -\sin(\varphi) & \cos(\varphi) \end{bmatrix} \begin{bmatrix} x \\ p \end{bmatrix}$$

- **Squeezing Gate** $S(r)$: By applying the squeezing gate, the quantum state experiences a scaling transformation that alters the variances of the position and momentum. The scaling factor r, a real number, either compresses or expands the state in the phase space, resulting in a 'squeezed' state that has reduced uncertainty in one variable while increasing it in the conjugate variable, in accordance with Heisenberg's uncertainty principle.

$$\begin{bmatrix} x \\ p \end{bmatrix} \rightarrow \boxed{\begin{array}{c}\text{S-gate:} \\ S(r)\end{array}} \rightarrow \begin{bmatrix} e^{-r} & 0 \\ 0 & e^{r} \end{bmatrix} \begin{bmatrix} x \\ p \end{bmatrix}$$

- **Beam-Splitter Gate** $BS(\theta)$: Acting on two qumodes, the beam-splitter gate mixes their states, analogous to the interference effects observed in classical optics. It is mathematically described by a transformation that combines rotation-like effects on the two qumodes' phase space coordinates, parameterized by an angle θ in the

range $[0, 2\pi]$. The output state is a hybridization of the input states, with the mixing determined by θ.

$$\begin{bmatrix} x_1 \\ x_2 \\ p_1 \\ p_2 \end{bmatrix} \rightarrow \boxed{BS(\theta)} \rightarrow \begin{bmatrix} \cos(\theta) & -\sin(\theta) & 0 & 0 \\ \sin(\theta) & \cos(\theta) & 0 & 0 \\ 0 & 0 & \cos(\theta) & -\sin(\theta) \\ 0 & 0 & \sin(\theta) & \cos(\theta) \end{bmatrix} \begin{bmatrix} x_1 \\ x_2 \\ p_1 \\ p_2 \end{bmatrix}$$

A crucial composite gate, the interferometer, can be constructed using a sequence of beam-splitter and rotation gates. When only one qumode is involved, the function of the interferometer simplifies to that of a rotation gate. These Gaussian gates together facilitate the creation of an affine transformation as implemented in (Killoran et al., 2019; Markidis, 2022), which plays a pivotal role in enabling the computational processes of neural networks.

Beyond the four primary Gaussian gates outlined earlier, we use a non-Gaussian gate, Kerr gate, introducing a type of non-linearity akin to that of activation functions in classical neural networks. Notably, the integration of non-Gaussian gates with Gaussian gates in a sequence significantly enhances the capabilities of continuous variable quantum circuits. This combination achieves universality, ensuring that any continuous variable state can be generated with at most polynomial computational overhead.

- **Kerr Gate** $K(\kappa)$: This gate applies a nonlinear phase shift proportional to the square of the photon number, introducing significant nonlinearity into quantum circuits. The transformation enacted by the Kerr gate $K(\kappa)$ on a photon number state $|n\rangle$ can be expressed as $|n\rangle \rightarrow \exp(i\kappa n^2)|n\rangle$, where $\kappa \in \mathbb{R}$ serves as the gate parameter, and is the strength of the nonlinearity. This transformation is crucial for tasks that Gaussian gates alone cannot perform, such as specific types of quantum state entanglement and enhanced quantum computation processes.

$$\left[|n\rangle\right] \rightarrow \boxed{\begin{matrix}\text{K-gate:} \\ K(\kappa)\end{matrix}} \rightarrow \left[\exp(i\kappa n^2)|n\rangle\right]$$

Having defined the basic five continuous variable quantum gates, we now delve into the circuit structure of a quantum neural network unit as depicted in Fig. 7.2. The quantum neural network unit comprise a sequence consisting of a first interferometer, local squeeze gates, a second interferometer, local displacements, and non-Gaussian Kerr gates. The interferometers are general N-port linear optical elements containing beamsplitter $BS(\theta)$ and rotation $R(\varphi)$ gates. The outcome obtained from the combination of the first interferometer $U(\theta_1, \varphi_1)$, local squeeze gates $\otimes_{i=1}^{N} S(r_i)$ and $\otimes_{i=1}^{N} S(r_i)$, a second interferometer $U(\theta_2, \varphi_2)$ effectively multiplies the phase space vector by the neural network weights w, which are determined by the parameters of the interferometers and squeezing gates. Similar to classical neural networks, the displacement gate

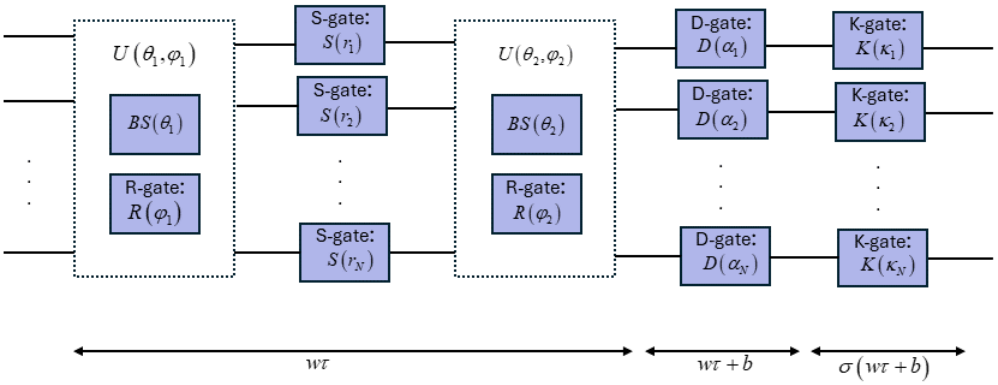


Figure 7.2: Schematic depiction of a quantum neural network unit utilizing continuous variable quantum gates. The architecture integrates unitary transformations $U(\theta_i,\phi_i)$, consisting of beam-splitter $BS(\theta)$ and rotation $R(\phi)$ gates, along with squeezing operations $S(r_i)$ and followed by displacement $D(\alpha_i)$ gates to implement affine transformations, analogous to the neural network's weights and biases. This setup portrays the flow from input through quantum processing stages, resulting in a non-linearly transformed output introduced by the Kerr gates $K(\kappa_i)$, thereby drawing a parallel with classical neural network operations.

$\otimes_{i=1}^{N} D(\alpha_i)$ serves to add a bias term b. The sequence of these Gaussian transformations, i.e., $\otimes_{i=1}^{N} D(\alpha_i) \circ U(\theta_2,\varphi_2) \circ \otimes_{i=1}^{N} S(r_i) \circ U(\theta_1,\varphi_1)$ is enough for parametrization of all possible unitary affine transformation on N qumodes. Ultimately, a Kerr gate introduces non-linearity, analogous to the activation function σ used in classical neural networks, therefore, for an input τ one attains $|\tau\rangle \rightarrow |\sigma(w\tau+b)\rangle$.

By arranging multiple quantum neural units in sequence, a quantum neural network can be constructed, as illustrated in Fig. 7.3. For a single qumode, control of each gate involves seven gate parameters (α, φ, r, θ, and κ), where φ, θ, and κ are real values, and α and r can be either real or complex numbers. Quantum circuit parameters are categorized into passive and active types. Parameters such as the beam-splitter angles and all gate phases fall into the passive category, whereas parameters for displacement, squeezing, and the magnitude of the Kerr effect are considered active. The objective of training quantum neural networks is to optimize these parameters (α, φ, r, θ, and κ) across various qumodes and units to minimize the hybrid physics-informed neural network loss function.

7.1.2 Implementation of a Hybrid Approach Based on the Theory of Functional Connections

In this section, we combine the illustrated QNN (see Fig. 7.3) with the theory of functional connection, (Johnston, 2021; D'ambrosio et al., 2021; Johnston et al., 2020; Dehaghani et al., 2023b; Dehaghani and Aguiar, 2023a) to obtain a hybrid physics-informed neural networks. This theory can be used to solve boundary value problems. Consider a

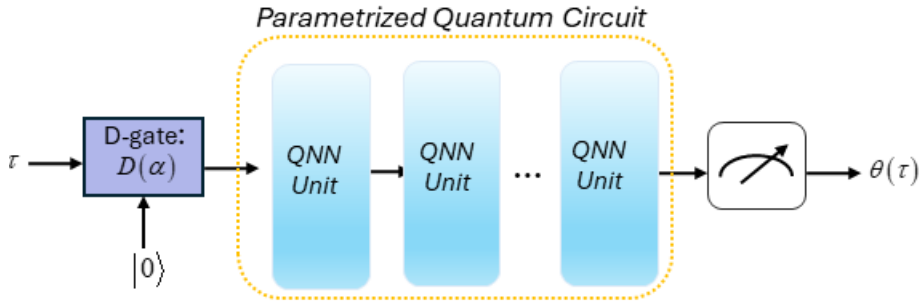


Figure 7.3: The input τ is encoded by means of a displacement gate on the vacuum. Then, the approximator network, illustrated by a parametrized quantum circuit consisting of several connected quantum neural network units, whose output $\theta(t)$ is obtained by applying measurement.

generic system composed by n differential equations

$$F_i(t, y(t), \dot{y}(t)) = \mathbf{0}, \quad y_j(t_k) = y_{t_k,j}, \quad k \in \emptyset \cup \{1,2,\ldots\} \tag{7.1}$$

where $y(t) = vec(y_1(t),\ldots,y_n(t))$, with $y_j(t) \in \mathbb{R}^{n_j}$, $j = 1,\ldots n$ is the state variable that has known values at instant of time t_k, and $F_i : \mathbb{R} \times \mathbb{R}^N \times \mathbb{R}^N \to \mathbb{R}^N$ is a given map that characterizes the $i \in \{1,\ldots,n\}$ ODE, with $N = n_1 + \ldots + n_n$. Note that here we utilize a unified process to resolve problems involving initial, boundary, or multiple values, so $k \in \emptyset$ refers to the boundary-free functions. As an example, suppose that we would like to solve a BVP with two ($n = 2$) ODEs, where the first one ($j = 1$) starts at $t = t_0$ with some initial condition $y_{0,1}$, and the second one ($j = 2$) at $t = t_f$ with a final condition $y_{f,2}$. Then, $y(t) = vec(y_1(t), y_2(t))$, and $y_1(t_0) = y_{0,1}$, and $y_2(t_f) = y_{f,2}$.

The goal is to obtain the (approximated) solution $\hat{y}(\cdot)$ of (7.1) along time. For simplicity of presentation and in order to avoid cumbersome notation, at this point, we will consider only one ODE. The first step is to apply a morph transformation (change of time) so that the problem can be written in the domain of the activation functions to be used in the next steps. More precisely, we make the time transformation $\tau = \tau_0 + c(t - t_0)$, with $c > 0$. Next, we impose the solution to be of the form

$$\hat{y}(\tau) = \theta(\tau) + \sum_{n=1}^{k} \Omega_k(\tau)\,(y(\tau_k) - \theta(\tau_k)), \tag{7.2}$$

where $\theta(\cdot) : \mathbb{R} \to \mathbb{R}^N$ indicates a free function, and the scalar function $\Omega_k(\tau)$ is the so-called switching function. These switching functions are described in (Johnston et al., 2020) and for $k = 1,2$ take the form $\Omega_1(\tau) = 1 + \frac{2\Delta\tau^3}{\Delta\tau_f{}^3} - \frac{3\Delta\tau^2}{\Delta\tau_f{}^2}$ and $\Omega_2(\tau) = -\frac{2\Delta\tau^3}{\Delta\tau_f{}^3} + \frac{3\Delta\tau^2}{\Delta\tau_f{}^2}$ with $\Delta\tau = \tau - \tau_0$ and $\Delta\tau_f = \tau_f - \tau_0$.

In this chapter, we propose to model the free function $\theta(\tau)$ as a combination of the QNN depicted in Fig. 7.3, where the architecture of each QNN unit is designed by a

quantum circuit as illustrated in Fig. 7.2. By considering L qumodes, the outputs of the QNNs are linearly weighted in accordance with (See Fig. 7.1)

$$\theta(\tau) = \sum_{l=1}^{L} \xi_l \sigma(\tau) = \boldsymbol{\sigma}^T(\tau)\boldsymbol{\xi}, \tag{7.3}$$

where $\boldsymbol{\sigma}^T(\tau) = \sigma^T(\tau) \otimes I_{n\times n}$, and the weight $\boldsymbol{\xi} = vec(\xi_1,\ldots,\xi_L)$ is a given parameter. Now, substituting (7.3) and (7.2) into (7.1), we then obtain a new set of equations

$$F_i(\tau,\hat{y}(\tau),\dot{\hat{y}}(\tau)) = \tilde{F}_i(\tau,\theta(\tau),\dot{\theta}(\tau)) = 0,$$

where $\dot{\theta}(\tau) = c\boldsymbol{\sigma}'^T(\tau)\boldsymbol{\xi}$ with $\boldsymbol{\sigma}'(\tau) = \frac{d\boldsymbol{\sigma}(\tau)}{d\tau}$. Thus, $\tilde{F}_i(\cdot)$ can be expressed in terms of parameters $\Theta = (\theta,\phi,r,\alpha,\lambda)$ and $\boldsymbol{\xi}$, that is,

$$\tilde{F}_i(\tau;\Theta,\boldsymbol{\xi}) = 0. \tag{7.4}$$

The next step consists in defining a loss function to be minimized by updating the parameters in (7.4). At this point, we can identify three options to solve (7.4):

1. Only $\boldsymbol{\xi}$ is updated.
2. Only Θ is updated.
3. Both parameters $\boldsymbol{\xi}$ and Θ are updated.

Option 1) has the advantage of not needing to change the default parameters of the QNN circuit and making the training fast. In this case, a simple approach is to discretize τ into N points, and express the obtained set of differential equations as loss functions at each point as $\Xi_i^T(\boldsymbol{\xi}) = \left[\tilde{F}_i(\tau_0,\boldsymbol{\xi}),\ldots,\tilde{F}_i(\tau_N,\boldsymbol{\xi})\right]$ and obtain the unknown $\boldsymbol{\xi}$, by computing the solution of the augmented loss function $\Xi = \left[\Xi_1^T,\ldots,\Xi_n^T\right]$ associated to the overall system composed by n differential equations. This can be solved by a numerical minimization scheme, such as for example the iterative least-square method. Through this method, we obtain the iterative procedure $\boldsymbol{\zeta}_{k+1} = \boldsymbol{\zeta}_k + \Delta\boldsymbol{\zeta}_k$, where $\Delta\boldsymbol{\zeta}_k = -\left(\mathbb{J}(\boldsymbol{\zeta}_k)^T\mathbb{J}(\boldsymbol{\zeta}_k)\right)^{-1}\mathbb{J}(\boldsymbol{\zeta}_k)^T\mathbb{L}(\boldsymbol{\zeta}_k)$, in which $\mathbb{J}$ is the Jacobian matrix, compiling the partial derivatives of the loss function with respect to each unknown parameter (which here is just ξ and therefore simple to obtain). The iterative procedure continues to be repeated until the convergence criteria is satisfied, meaning that for a predefined tolerance $\bar{\varepsilon} > 0$, we reach to $L_2\left[\Xi(\boldsymbol{\zeta}_k)\right] < \bar{\varepsilon}$.

Option 2) addresses the case of only updating the QNN parameters Θ. Let $|\psi_\tau\rangle$ be the output state of the circuit given input $D(\tau)|0\rangle$. Then, in this case, the goal is to train the QNN to produce output states whose expectation value for the quadrature operator $\hat{\tau}$, that is, $\langle\psi_\tau|\hat{\tau}|\psi_\tau\rangle$ is such that $\tilde{F}_i(\tau_\ell;\Theta)$ is zero for each sample time τ_ℓ. A simple approach is to use as loss function the mean square error of the obtained values $\tilde{F}_i(\tau_\ell;\Theta)$ and employ a minimizer (usually based on stochastic gradient descent) to update Θ.

Option 3) makes use of the complete set of parameters. To update them, one needs to minimize the loss function, using a backpropagation algorithm which may need the computation of the gradients with respect to the parameters that could be analytical derived or numerically estimated through finite differences. Another approach is to implement an alternating gradient descent scheme by updating Θ and ξ in an alternating manner.

In summary, the implementation in Fig. 7.1 illustrates the proposed integrated quantum-classical approach to solve differential equations. In the next section, we use the described approach to solve optimal control problems using the indirect method that results in solving the related boundary value problem, which consists of a set of differential equations derived from the necessary optimality conditions of the Pontryagin Minimum Principle.

7.2 Quantum Optimal Control

The design of optimal controllers using the indirect approach is influenced by several factors, including the selection of the cost functional, the formulation of the Pontryagin-Hamiltonian function, and the computational methods used to solve the Pontryagin Minimum Principle (PMP) optimality conditions. In this section, we provide an example for a quantum optimal control problem. We model the system as an open quantum system, meaning it interacts with its environment. This interaction results in dynamics that are non-unitary yet retain trace-preserving and completely positive properties across all initial conditions. We proceed to outline the optimal control problem by considering a control constrained time-energy minimization problem. To this end, we consider a quantum state transition from the initial state ρ_i to a desired target state ρ_f, governed by the Lindblad master equation.

7.2.1 System Description

Our study takes into account an open quantum system controlled by a time dependent modulation to illustrate the use of physics-informed quantum neural networks for a quantum optimal control problem. We describe open quantum systems by the most general form of Markovian master equations, i.e., the Lindblad form. The Lindblad master equation for system's density operator ρ can be written as (Dehaghani et al., 2022a)

$$\dot{\rho} = -\frac{i}{\hbar}[H(u(t)), \rho] + \sum_i \gamma_i \left(L_i \rho L_i^\dagger - \frac{1}{2} \left\{ L_i^\dagger L_i, \rho \right\} \right), \tag{7.5}$$

where $[a,b] = ab - ba$ is the commutator, and $\{a,b\} = ab + ba$ is the anticommutator of a and b. $H(u(t))$ indicates the system Hamiltonian comprising the drift H_d and control interaction H_C Hamiltonians, i.e., $H(u(t)) = H_d + H_c u(t)$, where $u(t)$ is the control input.

The L_i symbols denote a group of jump operators that outline the dissipative component of the dynamic processes. The configuration of these jump operators elucidates the environmental impact on the system, which requires accurate determination from the microscopic models that describe the dynamics between the system and its surrounding environment. Moreover, the $\gamma_i \geq 0$ represent a series of non-negative values referred to as damping rates. Corresponding to the dynamics (7.5), we now represent it in terms of the superoperator $\mathcal{L}(\alpha, u(t))$ as following

$$\dot{\tilde{\rho}} = \mathcal{L}(\alpha, u(t))\tilde{\rho}(t),$$

where $\tilde{\rho}$ is the state vector, expressed in terms of the elements of density operator $\rho_{ee} = \langle e|\rho(t)|e\rangle$, $\rho_{gg} = \langle g|\rho(t)|g\rangle$, and $\rho_{ge} = \langle g|\rho(t)|e\rangle$ as $\tilde{\rho}(t)^T = \begin{pmatrix}\rho_{gg} & \rho_{ee} & \mathrm{Re}(\rho_{ge}) & \mathrm{Im}(\rho_{ge})\end{pmatrix}$, and α encapsulates the system parameters, i.e., coupling strengths and decay rates.

7.2.2 Optimal Control Problems (Indirect Method)

We deal with a constrained optimal control problem, where the control $u(t)$ belongs to an interval $[\mu^-, \mu^+]$. To this end, we first define a new unconstrained control variable $v(t)$. The approach entails replacing the constraint μ with a smooth and monotonically increasing saturation function defined within the range $u \in [\mu^-, \mu^+]$, such that $u = \phi(v)$, where

$$\phi(v) = \mu^+ - \frac{\Delta\mu}{1 + \exp\left(\frac{cv}{\Delta\mu}\right)}, \qquad \Delta\mu = \mu^+ - \mu^-$$

for some constant $c > 0$ (Graichen et al., 2010). Optimal control problems typically revolve around a cost function J , which in its most general form can be expressed as the sum of a terminal cost and the integral over time from t_0 to t_f of the running cost. Since we introduced a new control variable, we need to also consider an additional term in the cost function. Hence, for our problem, we define the cost function as the following

$$J = \Gamma t_f + \eta \int_{t_0}^{t_f} u^2(t)\, dt + \varepsilon \int_{t_0}^{t_f} v^2(t)\, dt,$$

where Γ and η are positive coefficients, with t_f representing the free final time to be optimized. The second term of J, frequently used in molecular control cost functions, quantifies the energy of the control signal over the interval $[t_0, t_f]$, and the last term is a regularization term defined through a regularization parameter $\varepsilon > 0$.

Remark 7.1 *A low ε value suggests the new unconstrained control problem approximates the original constrained one. However, as ε approaches zero, the control variable v may rise to infinity, presenting numerical challenges. Therefore, caution is advised in selecting ε to ensure stability and accuracy in the control outcomes. For more on ε's impact on control parameters, see (Antony, 2018).*

The goal is to minimize the cost function J subject to the dynamics $\dot{\tilde{\rho}} = \mathcal{L}(\alpha, u(t))\tilde{\rho}(t)$. When using the Pontryagin Minimum Principle (PMP) within the indirect method (Ross, 2009), the Pontryagin Hamiltonian $\mathcal{H}$ for the new unconstrained optimal control problem for all $t \in [t_0, t_f]$ is formulated by indicating the adjoint variables (costates) $\lambda(t)$ of the system. Hence,

$$\begin{aligned}\mathcal{H}(\rho,\lambda,u,\nu,\varepsilon,\xi,t) = \eta u^2(t) + \varepsilon\nu^2(t) + \lambda^T(t)\mathcal{L}(\alpha,u(t))\tilde{\rho}(t) \\ + \beta(t)\left(u(t) - \phi(\nu)\right)\end{aligned} \tag{7.6}$$

where $\beta(t)$ is an additional multiplier defined for consideration of equality constraint raised from control constraints. Having defined (7.6), the optimal control law can be derived from the first-order optimality conditions of the PMP, where one obtains

$$\frac{\partial \mathcal{H}}{\partial u} = \lambda^T(t)\frac{\partial \mathcal{L}}{\partial u}(\alpha, u(t))\tilde{\rho}(t) + 2\eta u(t) + \beta(t) = 0 \tag{7.7}$$

Note that (7.7) may result in a transcendental equation, which typically does not yield a closed-form solution for the control. Since a new unconstrained control has been introduced, an additional equation must be incorporated into the optimality condition for the control, which is

$$\frac{\partial \mathcal{H}}{\partial \nu} = 2\varepsilon\nu - \beta(t)\frac{\partial \phi(\nu)}{\partial \nu} = 0 \tag{7.8}$$

Subsequently, the first-order necessary conditions for the state and costate variables are derived as follows

$$\begin{aligned}\dot{\tilde{\rho}} &= \frac{\partial \mathcal{H}}{\partial \lambda} = \mathcal{L}(\alpha, u(t))\tilde{\rho}(t), \quad \tilde{\rho}(t_0) = \tilde{\rho}_i \\ \dot{\lambda} &= -\frac{\partial \mathcal{H}}{\partial \tilde{\rho}} = -\mathcal{L}^T(\alpha, u(t))\lambda(t)\end{aligned} \tag{7.9}$$

In addition the following transversality conditions are also applicable for our problem:

$$\lambda(t_f) = \lambda_f = \frac{\partial J}{\partial \tilde{\rho}_f} = \mathbf{0}, \qquad \mathcal{H}(t_f) = -\frac{\partial J}{\partial t_f} = -\Gamma. \tag{7.10}$$

Equations in (7.9), together with the transversality conditions (7.10) applied to the Pontryagin Hamiltonian, and the equality constraint

$$u(t) - \phi(\nu) = 0 \tag{7.11}$$

constitute a boundary value problem, which we will solve by the techniques explained in the preceding sections.

7.2.3 Application of the integrated quantum-classical approach

In accordance with the theory of functional connections in (7.2), see also Fig. 7.1, we approximate the state $\tilde{\rho}$ and costate λ variables as

$$\begin{aligned}\tilde{\rho}(\tau) &= \theta_{\tilde{\rho}}(\tau) - \Omega_1(\tau)\theta_{\tilde{\rho}}(\tau_0) - \Omega_2(\tau)\theta_{\tilde{\rho}}(\tau_f) + \Omega_1(\tau)\tilde{\rho}_i \\ &\quad + \Omega_2(\tau)\tilde{\rho}_f \\ \lambda(\tau) &= \theta_\lambda(\tau) - \Omega_2(\tau)\theta_\lambda(\tau_f) + \Omega_2(\tau)\lambda_f\end{aligned}$$

By taking the derivatives of the above equation, one obtains

$$\begin{aligned}\dot{\tilde{\rho}}(\tau) &= \dot{\theta}_{\tilde{\rho}}(\tau) - \Omega_1'(\tau)\theta_{\tilde{\rho}}(\tau_0) - \Omega_2'(\tau)\theta_{\tilde{\rho}}(\tau_f) + \Omega_1'(\tau)\tilde{\rho}_i \\ &\quad + \Omega_2'(\tau)\tilde{\rho}_f \\ \dot{\lambda}(\tau) &= \dot{\theta}_\lambda(\tau) - \Omega_2'(\tau)\theta_\lambda(\tau_f) + \Omega_2'(\tau)\lambda_f\end{aligned}$$

In addition, for the control variables and also for the equality constraint multiplier, we consider the functional approximation as a free function only, i.e.,

$$u(\tau) = \theta_u(\tau), \quad \nu(\tau) = \theta_\nu(\tau), \quad \beta(\tau) = \theta_\beta(\tau)$$

Now, we are in the position to define an augmented loss function to be minimized. Note that the setup indicated in Fig. 7.1 is for minimization of only one loss function. To solve the problem for an augmented loss function, we consider an augmented network that minimizes all elements of the augmented loss simultaneously which are indicated as

$$\begin{aligned}\Xi_{\tilde{\rho}} &= \dot{\tilde{\rho}} - \mathcal{L}(\alpha, u(\tau))\tilde{\rho}(\tau) \\ \Xi_\lambda &= \dot{\lambda} + \mathcal{L}^T(\alpha, u(\tau))\lambda(\tau) \\ \Xi_u &= \lambda^T(\tau)\frac{\partial \mathcal{L}}{\partial u}(\alpha, u(\tau))\tilde{\rho}(\tau) + 2\eta u(\tau) + \beta(\tau) \\ \Xi_\nu &= 2\varepsilon\nu - \beta(\tau)\frac{\partial \phi(\nu)}{\partial \nu} \\ \Xi_\phi &= u(\tau) - \phi(\nu) \\ \Xi_{\mathcal{H}} &= \mathcal{H}(\tau_f) + \Gamma\end{aligned}$$

leading to an augmented form of the loss function as

$$\mathbb{L} = \begin{bmatrix}\Xi_{\tilde{\rho}} & \Xi_\lambda & \Xi_u & \Xi_\nu & \Xi_\phi & \Xi_{\mathcal{H}}\end{bmatrix}^T$$

which will be minimized during the procedure.

7.3 Simulations and Results

We consider an open two-level quantum system (a qubit) controlled by a time dependent modulation as a principle example to illustrate the use of physics-informed quantum neural networks for a quantum optimal control problem. In this regard, quantum transitions can be written in terms of the operators $\sigma_{ab} = |a\rangle\langle b|$ where $|a\rangle, |b\rangle = |e\rangle, |g\rangle$ being $|e\rangle$ and $|g\rangle$ the excited and ground state, respectively. Consider the quantum system Hamiltonian with a phase damping control $u(t)$ where the drift term is defined through the system parameters ω_x and ω_z as

$$H_d = \omega_x \left(\sigma_{eg} + \sigma_{ge}\right) + \omega_z \left(\sigma_{ee} - \sigma_{gg}\right)$$

and the interaction control Hamiltonian is $H_c = \sigma_{ee}$. We consider two jump operators, i.e., for absorption $L_1 = \sigma_{eg}$ with decay rate γ_{eg} and emission $L_2 = \sigma_{ge}$ with decay rate γ_{ge}. Hence, the dynamics in terms of the superoperator $\mathcal{L}(\alpha, u(t))$ is given by (Norambuena et al., 2024)

$$\dot{x} = \begin{pmatrix} -\gamma_{eg} & \gamma_{ge} & 0 & -2\omega_x \\ \gamma_{eg} & -\gamma_{ge} & 0 & 2\omega_x \\ 0 & 0 & \frac{-(\gamma_{ge}+\gamma_{eg})}{2} & -(2\omega_z + u(t)) \\ \omega_x & -\omega_x & 2\omega_z + u(t) & \frac{-(\gamma_{ge}+\gamma_{eg})}{2} \end{pmatrix} x(t)$$

We consider the parameters as follows: $\gamma_{eg} = 0.1$, $\gamma_{ge} = 0.3$, $\omega_x = 1$, $\omega_z = 2$. In Fig. 7.4, we have shown different state transitions processes. The time-dependent behavior of the ground state population and the excited state population is depicted for three different initial state configurations transitioning towards their respective target states. The plots succinctly capture the essence of quantum state transitions, ranging from complete population transfer to the achievement of a balanced superposition, showcasing the intricate nature of quantum dynamics.

To show the scalability of our method, we also demonstrate quantum state transition for a three-level system. Three-level quantum systems, also known as qutrits in the context of quantum computing, are deemed to be significant in various areas of quantum research due to their potential to represent more complex states than two-level systems and their applications in quantum information processing, quantum simulations, and precise control in quantum optics and spectroscopy (Petiziol et al., 2020; Dehaghani et al., 2022a; Sugny and Kontz, 2008; D'Alessandro and Işik, 2024). The Hamiltonian for the three-level system under study is given by

$$H = \delta\sigma_{22} + \Delta_1\sigma_{33} + \left(\frac{u_p(t)}{2}\sigma_{13} + \frac{u_s(t)}{2}\sigma_{23} + h.c.\right),$$

where the parameters are defined as follows: δ=0.1 is the two-photon detuning, Δ_1 is

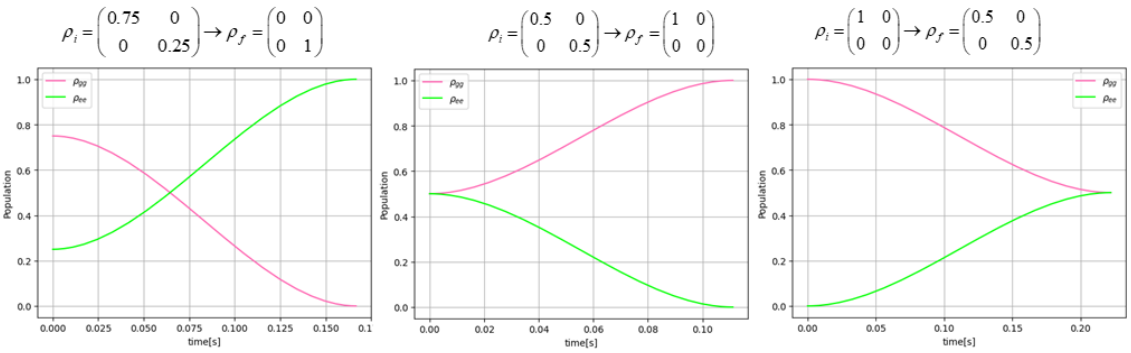


Figure 7.4: The plots illustrate the time evolution of populations in a two-level quantum system from different initial states to specific target states, highlighting the dynamics of the ground and excited state probabilities over time. Each plot shows a distinct trajectory of population transfer, reflecting various quantum processes such as relaxation and population inversion.

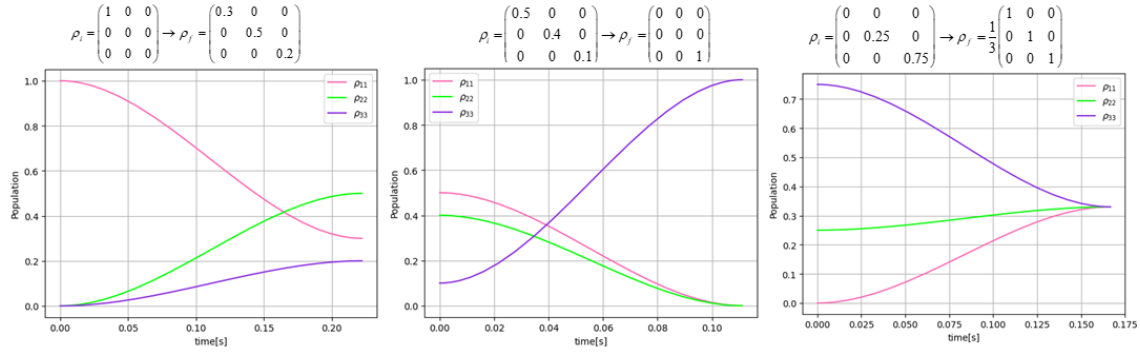


Figure 7.5: The figure displays the evolution of state populations in a three-level quantum system across three distinct scenarios. Each plot tracks the probabilities of the system over time, beginning from different initial mixed states and converging towards predetermined target states. The dynamics reveal transitions such as population inversion, decay to the ground state, and equilibration to a specific superposition, demonstrating the versatile control achievable in quantum state engineering.

the one-photon detuning, calculated as $\Delta_1 = \omega_0 - \omega_p - \omega_s$, where ω_0 is the transition frequency between the ground state and the first excited state, $u_p(t)$ and $u_s(t)$ are the Rabi frequencies for the pump and Stokes fields, respectively. and σ_{ij} are the transition operators between the states i and j. calculated as before. The dynamics of the system are influenced by the interaction terms σ_{13} and σ_{23}, which couple the ground state to the two excited states via the external fields characterized by their respective Rabi frequencies. These interactions are crucial for the control schemes aimed at achieving state transitions or implementing quantum gates within this three-level system. The results can be seen in Fig. 7.5. The depicted figure provides a compelling visualization of the temporal dynamics of state populations within a three-level quantum system under controlled transitions. For each subplot, we initiate the system in a distinct mixed state, observing

its evolution towards a designated target state. These evolutions underscore the nuanced manipulation of quantum states, which is vital for applications in quantum computing, communication, and sensing.

7.4 Concluding Remarks and Discussions

The hybrid quantum-classical approach proposed in this chapter represents an advancement in the application of quantum computing to solve quantum optimal control problems. By integrating continuous-variable quantum circuits with classical machine learning techniques, we offer a novel framework that leverages both quantum computational power and classical optimization tools. This approach enables us to address complex control challenges, particularly those grounded in Pontryagin's Minimum Principle, within a Physics-Informed Neural Network (PINN) architecture.

The use of hybrid Physics-Informed Quantum Neural Networks (QPINNs) demonstrates the potential for improving the efficiency and scalability of quantum control systems. Our work highlights the versatility of this approach across various applications, from simple two-level quantum systems to more complex three-level systems. The results obtained from the simulations validate the effectiveness of the QPINN model and illustrate its applicability to open quantum systems, which are relevant in fields such as quantum computing, quantum optics, and quantum information processing.

Looking forward, several areas can be explored to extend and refine the presented work. One direction is the extension of this framework to higher-dimensional quantum systems. While the current framework successfully handles two- and three-level systems, applying it to more complex quantum systems with higher-dimensional Hilbert spaces would be crucial for practical quantum computing and quantum communication protocols. Another area for future work is the improvement of quantum circuit efficiency. Designing more refined quantum gate arrangements or incorporating advanced quantum algorithms could enhance the model's performance, especially in real-time applications.

Additionally, there is significant potential in exploring alternative quantum control strategies. While this work focused on Pontryagin's Minimum Principle, integrating other methods, such as reinforcement learning and stochastic control, could expand the framework's robustness in dealing with uncertainties in quantum systems. Another important direction is scalability and hardware implementation. Transitioning from theoretical models to practical, hardware-based implementations on quantum processors, such as those provided by IBM Quantum, will be essential to validate the model's practical viability.

Finally, managing noise and decoherence in quantum systems remains a critical challenge for real-world applications. As quantum systems are inherently sensitive to environmental noise, incorporating noise models into the simulations or designing noise-

resilient quantum circuits could enhance the robustness and reliability of the hybrid approach.

In conclusion, this chapter outlines an approach to addressing quantum optimal control problems through a hybrid quantum-classical framework. By integrating quantum computing with classical optimization techniques, we propose a model that may help meet some of the demands of emerging quantum technologies. This approach offers a potential pathway for improving the efficiency of solving certain control problems and provides a basis for future exploration. As quantum technologies continue to develop, this methodology could contribute to further advancements in quantum control solutions.

Chapter 8

Conclusions

This chapter summarizes the contributions and findings of this thesis, which aimed to contribute to the field of quantum control. By applying classical control principles alongside quantum-classical hybrid approaches, this work has explored challenges in controlling quantum systems. The results indicate the potential effectiveness of these techniques in supporting quantum technologies, particularly in quantum computation, communication, and sensing.

8.1 Summary of Contributions

This thesis has explored quantum control strategies, focusing on both theoretical foundations and practical applications. The main contributions include developments in quantum control through the use of classical control theory methods, such as the Pontryagin Minimum Principle (PMP), and hybrid quantum-classical approaches. Each chapter has contributed to a broader understanding of the complexities of quantum systems and the control strategies needed for their manipulation.

The thesis began by examining classical control methods, such as open-loop and feedback control, and their limitations when applied to quantum systems. As quantum systems operate under fundamentally different physical laws, these classical methods were modified and enhanced to address the unique challenges posed by quantum dynamics. By combining quantum filtering techniques, optimal control strategies, and state estimation methods, this research has demonstrated novel approaches to the control of quantum systems, even in the presence of noise and uncertainties.

A significant portion of this work focused on applying the PMP to quantum control problems, particularly in two-level and three-level quantum systems. This methodology was shown to be effective in managing quantum state transformations, maximizing fidelity, and minimizing energy consumption. Furthermore, this thesis introduced Lyapunov-based control strategies combined with extended Kalman filtering techniques,

addressing the issue of stabilizing quantum systems subjected to stochastic dynamics and measurement noise.

Another contribution of this work is the integration of machine learning techniques, particularly Physics-Informed Neural Networks (PINNs), within quantum control. By combining classical and quantum computation, this hybrid approach shows potential for solving complex control problems more efficiently, especially in systems where traditional control strategies may be limited. The application of PINNs to quantum systems represents a novel contribution to quantum computing and control theory.

Lastly, the exploration of entanglement synthesis using the Chopped Random Basis (CRAB) algorithm presented practical applications in enhancing quantum information processes. This algorithm's ability to efficiently manage transitions between separable and maximally entangled states demonstrates its potential utility in the development of quantum computing technologies and quantum communication networks.

8.2 Impact on the Field of Quantum Control

The contributions presented in this thesis address important aspects of quantum control. By developing robust and optimal control methods for quantum systems, this work tackles a key challenge in the field: the fragility and instability of quantum states in real-world environments. Quantum systems, while offering vast potential for computation and information processing, are highly sensitive to external influences, and effective control is essential to ensuring their reliability and scalability.

The application of classical control methods, such as PMP, to quantum systems opens new pathways for further exploration of optimal control strategies in quantum mechanics. These methods, when adapted for quantum dynamics, provide powerful tools for managing quantum state transitions, fidelity maximization, and resource optimization. As quantum technologies continue to evolve, these control strategies will play a crucial role in bridging the gap between theoretical quantum models and practical implementations.

Moreover, the introduction of hybrid quantum-classical methods, particularly the use of PINNs, highlights the potential of integrating machine learning techniques into quantum control. This approach not only enhances the accuracy and efficiency of control strategies but also opens up new avenues for solving complex quantum control problems that may be infeasible using purely classical or quantum techniques alone.

In addition to the theoretical advancements, the numerical demonstrations in this research, including various algorithms, highlight the practical impact of quantum control systems. Efficient control and manipulation of quantum states are essential for advancing quantum communication protocols, computing, and the development of quantum networks.

8.3 Limitations of the Work

Despite the advancements made in this thesis, several limitations should be acknowledged. First, while the control strategies presented have been tested in simulation and through theoretical analysis, real-world quantum systems are often subject to additional complexities that may not be fully captured in the models used. Factors such as hardware limitations, unforeseen environmental interactions, and measurement inaccuracies may affect the applicability and performance of the proposed control methods.

Furthermore, while the hybrid quantum-classical approaches introduced in this work have demonstrated promising results, they remain computationally intensive. Current quantum hardware, especially noisy intermediate-scale quantum (NISQ) devices, may not yet be capable of fully realizing the potential of these methods. As quantum computing hardware continues to advance, the practical implementation of these strategies will require further refinement and adaptation.

Another limitation lies in the scalability of the proposed control methods. While effective for small-scale quantum systems, such as two-level or three-level systems, the extension of these control techniques to larger quantum systems, particularly those with a higher number of qubits, presents a significant challenge. Future research will need to focus on developing control strategies that can scale efficiently with system size while maintaining robustness and reliability.

8.4 Future Directions

Building on the contributions of this thesis, several future research directions emerge:

- Real-World Implementation: To fully validate the effectiveness of the control strategies presented in this thesis, future research should focus on applying these methods to real-world quantum systems. Collaborations with experimental quantum laboratories would provide valuable insights into the practical challenges and opportunities associated with implementing these control methods on physical quantum devices.

- Scaling to Larger Quantum Systems: One of the most pressing challenges in quantum control is the scalability of control methods. As quantum systems grow in size, so do the complexity and the difficulty of maintaining control over them. Future work should explore how the methods developed here can be extended to larger systems, particularly in the context of quantum computing platforms with many qubits.

- Improving Quantum-Classical Hybrid Methods: The hybrid quantum-classical methods presented in this thesis, particularly the use of PINNs, have shown significant potential. However, further research is needed to refine these methods, improve

their computational efficiency, and adapt them to more complex quantum systems. As quantum hardware improves, so too will the opportunities for leveraging hybrid methods for real-time quantum control.

- Robust Control under Uncertainty: While this thesis addresses control under certain types of noise and uncertainty, future research could delve deeper into developing control methods that are highly resilient to a broader range of uncertainties. This is particularly important for quantum systems operating in uncontrolled environments, such as those encountered in quantum communication and sensing applications.

- Quantum Machine Learning for Control: The integration of machine learning techniques, such as PINNs, within quantum control is still in its early stages. Future research could explore the potential of other machine learning models, such as reinforcement learning and deep learning, to further enhance quantum control strategies, especially in dynamic environments where real-time adaptation is critical.

- Control in High-Energy Physics: The control of quantum phenomena in high-energy physics, particularly in systems like neutral kaons, represents a promising direction for future research. Developing methods to manipulate entanglement and mitigate decoherence in these systems could enable precise tests of fundamental physics, and offer insights into new physics beyond the Standard Model. The integration of control strategies with experimental advancements could also pave the way for leveraging high-energy particle systems in quantum information science, bridging the gap between foundational physics and emerging quantum technologies. For a detailed explanation refer to Appendix A.

8.5 Final Remarks

This thesis has explored the rapidly evolving field of quantum control, contributing to its theoretical and practical dimensions. By blending classical control theory with innovative quantum-classical hybrid approaches, it has advanced the state of the art in controlling quantum systems under various constraints and challenges.

The findings underscore the transformative potential of robust and optimal control strategies in mitigating the fragility and instability inherent in quantum systems. From theoretical advancements, such as the application of Pontryagin's Maximum Principle to quantum dynamics, to practical contributions like the development of hybrid methods, this work has laid a foundation for future exploration.

While acknowledging the limitations of the proposed methods, such as their computational intensity and scalability challenges, this thesis provides a roadmap for future

research. The proposed directions—ranging from real-world implementation and scalability to the enhancement of hybrid quantum-classical methods and exploration of novel machine learning techniques—highlight the immense scope for further innovation.

Ultimately, the contributions of this research enhance our understanding of quantum control and provide practical tools for advancing quantum technologies. As the field continues to evolve, the insights and methodologies developed here will serve as a foundation for the realization of reliable, scalable, and efficient quantum systems, supporting progress in computation, communication, and sensing. This work is a basement to the interdependence between theoretical innovation and practical application in driving the progress of quantum science and technology.

Appendix A

Exploring Strange Entanglement: Experimental and Theoretical Perspectives on Neutral Kaon Systems

This chapter provides an in-depth analysis of the properties and phenomena associated with neutral K-mesons. Kaons are quantum systems illustrating strange behaviours. We begin by examining the significance of strangeness and charge parity violation in understanding these particles. The concept of strangeness oscillations is then introduced, explaining oscillations between K^0 and $\bar{K}^0$ states. The regeneration of K_S is investigated, uncovering the underlying mechanisms involved. The discussion moves on to quasi-spin space, exploring its bases and their implications. The entangled states of kaon pairs $(K^0, \bar{K}^0)$ are considered, with a focus on maximally entangled neutral kaons and non-maximally entangled states. Decoherence effects on entangled kaons are examined, utilizing the density matrix description to capture the dynamics. A dedicated decoherence parameter is introduced to quantify the impact of decoherence. Furthermore, the chapter investigates the loss of entanglement through measures such as Von Neumann entanglement entropy, entanglement of formation, and concurrence. These measures provide insights into quantifying and characterizing entanglement in the context of neutral kaons. Through this comprehensive exploration of properties, phenomena, and entanglement dynamics, this chapter aims to pointing out recent works on neutral kaons, contributing to advancements in particle physics. This chapter has been published as a chapter of the book "Quantum Entanglement in High Energy Physics", see (Dehaghani et al., 2023a).

A.1 Introduction

Quantum entanglement, being among the most counterintuitive and subtle foundational elements of quantum mechanics, pertains to the correlations observed between distant components of certain composite systems. This intriguing phenomenon was brought to light by the pioneering work of Einstein, Podolsky and Rosen (EPR) in (Einstein et al., 1935) and Schrödinger in (Schrödinger, 1935), who uncovered a "spooky" characteristic of quantum machinery, better featured as nonlocality in the correlations of an EPR pair. Well-known and valuable tools for exploring this nonlocality are obtained by means of subsequent development of initial Bell inequalities, (Bell, 1987), and their subsequently reformulated variations, (Clauser and Horne, 1974; Wigner, 1997). Experimental tests have consistently demonstrated the violation of Bell inequalities (Aspect et al., 1982; Tittel et al., 1998), indicating the failure of local realistic theories and affirming the nonlocal nature of the universe.

Consequently, there is considerable interest in exploring the EPR-Bell correlations of measurements in various branches of physics, including particle physics. As a result, several pioneering researchers in particle physics have proposed investigating EPR-entangled massive particles, such as neutral kaons, (Feynman, 1999; Lee, 1981; Okun, 2013). They referred to the unique characteristics of individual neutral kaon states, which exhibit various rare phenomena such as strangeness oscillation, small mass splitting, different lifetimes between the physical states, violations of two primary symmetries: charge parity (CP) and time reversal (T), regeneration when traversing a slab of material, and most notably, strange entanglement. Neutral kaons exhibit a unique form of entanglement known as strange entanglement, referring to the specific entanglement between two neutral kaons, (Bernabeu and Di Domenico, 2022).

Numerous studies have been conducted to test quantum mechanics in the neutral kaon systems and search for CPT violation through neutral-meson oscillations. Notably, a significant focus on CP, T, and CPT violation in the neutral kaon system was first conducted at CERN in the CPLEAR experiment, (Apostolakis et al., 1998). Additional contributions came from experiments such as NA48 and NA62, (Bizzeti, 2023), which played key roles in discovering direct CP violation, yielding crucial experimental results. Moreover, experiments like KLOE, (Aloisio et al., 2002), conducted at the DAΦNE collider, and its successor KLOE-2, (Gauzzi P, 2019), at the Frascati National Laboratory, achieved enhanced precision in investigating CPT violations and conducting quantum decoherence tests. The LHCb experiment, located at CERN's Large Hadron Collider (LHC), (Collaboration, 2015), and KOTO, performed at the Japan Proton Accelerator Research Complex (J-PARC), (Yamanaka and Collaboration, 2012), were amongst the other experiments which significantly contributed to our understanding of strange entanglement in neutral kaon system, providing valuable insights into the properties and behavior of entangled kaon states.

The investigation of the evolution of an entangled kaon system subjected to decoherence is a crucial aspect. This analysis is carried out by studying the system's behavior over time using the so-called master equation. As time progresses, the level of decoherence in the initially entangled kaon system increases, leading to a loss in the system's entanglement. This reduction in entanglement can be accurately assessed as in the field of quantum information, where the degree of entanglement in a state is quantified using specific measures, such as entropy of entanglement, concurrence, and entanglement of formation. These measures are widely employed for quantifying quantum entanglement. The unique characteristics of strange entanglement exhibited by neutral kaons, distinct from any other system, enable the exploration of novel phenomena. Considering the high importance of strange entanglement, a significant portion of the chapter is dedicated to exploring the stability of the entangled quantum system and examining the potential occurrence of decoherence due to interactions with its surrounding environment. We aim to understand the extent of these effects and their impact on entanglement by focusing on the correlation between decoherence and the loss of entanglement.

The structure of the chapter is as follows: In Section II, we review the strange behaviour of neutral kaons through several phenomena, i.e., strangeness and CP violation, strangeness oscillation, and regeneration. Section III introduces the bases in quasi–spin formalism, including the strangeness basis, free-space basis, and inside-matter basis. In Section IV, entangled states of kaon pairs are studied in two main subsections, i.e., maximally and non-maximally entangled states. In the next section, the effects of decoherence on entangled kaons are studied. Density matrix description of entangled kaon system is introduced and its evolution is studied through the Gorini-Kossakowski-Sudarshan-Lindblad equation. In section VI, the decline in entanglement is quantitatively measured, and explicit evidence of the loss of entanglement is provided. The chapter ends with conclusion and an overview on prospective research challenges.

A.1.1 Notation

The ket symbol is used to denote a column vector in a Hilbert space, indicating the quantum state of the particle, i.e., $\left|K^0\right\rangle$ represents the state vector of a neutral kaon particle. The bra vector is used to describe the dual space or the bra state in quantum mechanics. In the case of a neutral kaon, $\langle K^0|$ represents the bra vector corresponding to the quantum state of the neutral kaon particle. We use the superscript † to show the conjugate transpose of a matrix (or vector). The symbol $\otimes$ indicates the tensor product, and $\oplus$ the direct sum. For A and B being operators, we use the notation $[A,B] = AB - BA$, and $\{A,B\} = AB + BA$. The expression $A(t = t_i; t_r)$ represents the state (or probability) A at a specific time, where the time t is equal to t_i, and t_r represents a specific reference time. For a generic function $f(t)$, its derivative with respect to time is denoted by $\dot{f}(t)$. For

a composite system consisting of subsystem A and subsystem B, the partial trace over subsystem B is denoted as tr_B. The imaginary unit is shown by $i = \sqrt{-1}$.

A.2 Properties of the Neutral Kaons

Kaons are the lightest strange mesons whose quark content is understood as $u\bar{s}$, $s\bar{u}$, $d\bar{s}$ for the charged kaons $K^+(494MeV/c^2)$ and $K^-(494MeV/c^2)$, and the neutral kaon $K^0(498MeV/c^2)$, respectively, (Martin and Shaw, 2016). Neutral K-mesons exhibit fascinating quantum phenomena that showcase their peculiar and intriguing behavior. In the following, we study notable instances that exemplify this strangeness.

A.2.1 Strangness and Charge Parity Violation

The neutral kaon and its antiparticle $\bar{K}^0(498MeV/c^2) = s\bar{d}$ are distinguished by a quantum number $\mathcal{S}$, known as strangeness, such that $\mathcal{S}\left|K^0\right\rangle = +\left|K^0\right\rangle$, and $\mathcal{S}\left|\bar{K}^0\right\rangle = -\left|\bar{K}^0\right\rangle$. Kaons are pseudoscalar particles with a total spin of 0 and parity $P = -1$ ($J^P = 0^-$). They exhibit charge conjugation symmetry (C), which corresponds to the transformation $K^0 \rightleftarrows \bar{K}^0$. Hence, for the joint transformation, one can write

$$CP\left|K^0\right\rangle = -\left|\bar{K}^0\right\rangle, \qquad CP\left|\bar{K}^0\right\rangle = -\left|K^0\right\rangle$$

From a theoretical point of view, in order to obtain the CP eigenstates, one can implement the superposition of $\bar{K}^0$ and K^0 as

$$\left|K_1^0\right\rangle = \frac{1}{\sqrt{2}}\left(\left|K^0\right\rangle - \left|\bar{K}^0\right\rangle\right), \qquad \left|K_2^0\right\rangle = \frac{1}{\sqrt{2}}\left(\left|K^0\right\rangle + \left|\bar{K}^0\right\rangle\right).$$

where $CP\left|K_1^0\right\rangle = +\left|K_1^0\right\rangle, CP\left|K_2^0\right\rangle = -\left|K_2^0\right\rangle$. The state K_1 principally decays to two pions while K_2 primarily decays to three pions, which occurs around 600 times slower in comparison to the decay of K_1 into two pions. The reason why this decay occurs so slowly is due to the fact that the mass of K_2 is a bit greater than the total masses of the three pions. Strangness is not conserved in weak interactions, moreover, such interactions are CP violating. The observation of these two modes of decay led to the establishment of the existence of two weak eigenstates of the neutral kaons, called K_L (K-long, T) and K_S (K-short, θ). The weak eigenstates are slightly different in mass, $\Delta m = m(K_L) - m(K_S) = 3.49 \times 10^{-12} MeV$, however, they differ considerably in their lifetimes and decay modes. The state K_L (K_S) is a combination of K_2 (K_1) with a small portion of K_1 (K_2), expressed as

$$|K_S\rangle = \frac{1}{\sqrt{|p|^2 + |q|^2}}\left(p\left|K^0\right\rangle - q\left|\bar{K}^0\right\rangle\right) \qquad |K_L\rangle = \frac{1}{\sqrt{|p|^2 + |q|^2}}\left(p\left|K^0\right\rangle + q\left|\bar{K}^0\right\rangle\right)$$

where $p = 1 + \epsilon$ and $q = 1 - \epsilon$, with ϵ being the complex CP violating parameter that is the same for K_L and K_S, i.e., $\epsilon_L = \epsilon_S = \epsilon$. According to the CPT Theorem, (Gross, 2012), since CP symmetry is violated, time reversal (T) symmetry must also be violated to maintain the overall CPT symmetry. The decay of K_L (long-lived neutral kaon) is dominantly governed by CP violation, similar to the decay of K_2. The primary decay mode of K_L is the three-pion decay, represented as $K_L \to 3\pi$, with a lifetime of approximately $\tau_L = 5.17 \times 10^{-8}$ seconds. Similarly, K_S (short-lived neutral kaon) predominantly decays via the strong interaction, similar to the decay of K_1. The main decay mode of K_S is the two-pion decay, denoted as $K_S \to 2\pi$, with a lifetime of approximately $\tau_S = 8.954 \times 10^{-11}$ seconds. It is important to note that while the dominant decay mode of K_L is $K_L \to 3\pi$, there is also a small amount of CP-violating decay observed, specifically $K_L \to 2\pi$, (Griffiths, 2020).

A.2.2 Strangeness oscillation

The two kaons K^0 and $\bar{K}^0$ transfer to common states, and subsequently they mix, meaning that they oscillate between K^0 and $\bar{K}^0$ before they decay. Consider the time dependent Schrödinger equation for the state vector $|\psi(t)\rangle$ as

$$i\hbar\,|\dot{\psi}(t)\rangle = H\,|\psi(t)\rangle$$

where $\hbar$ is the plank constant, and H is the non-Hermitian effective mass Hamiltonian describing the decay characteristics and strangeness oscillations of kaons, defined as

$$H = M - \frac{i}{2}\mathbf{\Gamma} \tag{A.1}$$

whose eigenstates are K_S and K_L. The matrices M, related to mass, and $\mathbf{\Gamma}$, a decay-matrix, are 2×2 Hermitian expressed as

$$M = \begin{pmatrix} M_{11} & M_{12} \\ M_{12}^* & M_{11} \end{pmatrix}, \qquad \mathbf{\Gamma} = \begin{pmatrix} \Gamma_{11} & \Gamma_{12} \\ \Gamma_{12}^* & \Gamma_{11} \end{pmatrix},$$

in which $\begin{cases} M_{11} = \frac{1}{2}(m_L + m_S) \\ M_{12} = \frac{1}{2}(m_L - m_S) \end{cases}$ and $\begin{cases} \Gamma_{11} = \frac{\hbar}{2}(\Gamma_L + \Gamma_S) \\ \Gamma_{12} = \frac{\hbar}{2}(\Gamma_L - \Gamma_S) \end{cases}$, with $\Gamma_j = \tau_j^{-1}$, $j = S, L$. The eigenvalues of H satisfy $\begin{cases} H\,|K_S(t)\rangle = \left(m_S - \frac{i\hbar}{2}\Gamma_S\right)|K_S(t)\rangle \\ H\,|K_L(t)\rangle = \left(m_L - \frac{i\hbar}{2}\Gamma_L\right)|K_L(t)\rangle \end{cases}$. The system evolves exponentially; i.e., the solutions to the Hamiltonian are obtained as

$$|K_S(t)\rangle = e^{-(\frac{i}{\hbar}m_S + \frac{\Gamma_S}{2})t}\,|K_S(t=0)\rangle\,, \qquad |K_L(t)\rangle = e^{-(\frac{i}{\hbar}m_L + \frac{\Gamma_L}{2})t}\,|K_L(t=0)\rangle \tag{A.2}$$

Subsequently, one can find the solution for K^0 and $\bar{K}^0$ as

$$\left|K^0(t)\right\rangle = \frac{1}{2}\left(e^{-\left(\frac{i}{\hbar}m_S+\frac{\Gamma_S}{2}\right)t} + e^{-\left(\frac{i}{\hbar}m_L+\frac{\Gamma_L}{2}\right)t}\right)\left|K^0\right\rangle + \frac{q}{2p}\left(-e^{-\left(\frac{i}{\hbar}m_S+\frac{\Gamma_S}{2}\right)t} + e^{-\left(\frac{i}{\hbar}m_L+\frac{\Gamma_L}{2}\right)t}\right)\left|\bar{K}^0\right\rangle$$

$$\left|\bar{K}^0(t)\right\rangle = \frac{p}{2q}\left(-e^{-\left(\frac{i}{\hbar}m_S+\frac{\Gamma_S}{2}\right)t} + e^{-\left(\frac{i}{\hbar}m_L+\frac{\Gamma_L}{2}\right)t}\right)\left|K^0\right\rangle + \frac{1}{2}\left(e^{-\left(\frac{i}{\hbar}m_S+\frac{\Gamma_S}{2}\right)t} + e^{-\left(\frac{i}{\hbar}m_L+\frac{\Gamma_L}{2}\right)t}\right)\left|\bar{K}^0\right\rangle$$

Suppose an experiment in which a beam of pure K^0 is produced at $t = t_i$, where t_i is the initial time, via strong interaction. The probability of observing a K^0 in the beam at a subsequent time t is determined by

$$\begin{aligned}\left|\left\langle K^0\left|K^0(t)\right.\right\rangle\right|^2 &= \frac{1}{4}\left(e^{\left(\frac{i}{\hbar}m_S-\frac{\Gamma_S}{2}\right)t} + e^{\left(\frac{i}{\hbar}m_L-\frac{\Gamma_L}{2}\right)t}\right)\left(e^{-\left(\frac{i}{\hbar}m_S+\frac{\Gamma_S}{2}\right)t} + e^{-\left(\frac{i}{\hbar}m_L+\frac{\Gamma_L}{2}\right)t}\right)\\ &= \frac{1}{4}\left(e^{-\Gamma_S t} + e^{-\Gamma_L t} + 2e^{-\frac{t}{2}(\Gamma_S+\Gamma_L)}\cos\left(\frac{t(m_L-m_S)}{\hbar}\right)\right)\end{aligned}$$

where the third term shows interference, which is the reason for an oscillation in the K^0 beam, (Martin and Shaw, 2016). By following the same procedure, one can compute the probability of observing $\bar{K}^0$ particles in a beam at a later time, given that the beam initially consists of K^0 particles. Therefore,

$$\left|\left\langle \bar{K}^0\left|K^0(t)\right.\right\rangle\right|^2 = \frac{1}{4}\frac{|q|^2}{|p|^2}\left(e^{-\Gamma_S t} + e^{-\Gamma_L t} - 2e^{-\frac{t}{2}(\Gamma_S+\Gamma_L)}\cos\left(\frac{t(m_L-m_S)}{\hbar}\right)\right)$$

The K^0 beam oscillates with frequency $f = \frac{(m_L-m_S)}{2\pi}$, with $(m_L - m_S)\tau_S = 0.47$. The probability of finding a K^0 or $\bar{K}^0$ from an initially pure K^0 beam is shown in **Figure A.1**. The plank constant $\hbar$ is considered as a unit for convenience. The oscillation becomes apparent when considering times on the order of a few τ_S, before all K_S mesons have decayed and only K_L mesons remain in the beam. Therefore, in a beam initially consisting of only K^0 mesons at $t = 0$, the presence of the $\bar{K}^0$ is observed at a distance from the production source through its equal probability of being found in the K_L meson. A similar phenomenon occurs when starting with a $\bar{K}^0$ beam, (Bertlmann, 2006).

Over time, the composition of the beam undergoes variations in strangeness due to the different nature of K^0 and $\bar{K}^0$ particles. This intriguing phenomenon is commonly referred to as strangeness oscillations, reflecting the oscillating strangeness content within the beam. In a broader context, this fascinating occurrence is known as flavor oscillations.

A.2.3 Regeneration of K_S

A beam of K-meson decays in flight after a few centimeters, so the short-lived kaon state K_S disappears, and only a pure beam of long-lived K_L is left. By shooting the K_L beam into a block of matter, which is usually regarded as a composition of protons and neutrons for all practical purposes, then the K^0 and $\bar{K}^0$ components of the beam interact dissimilarly

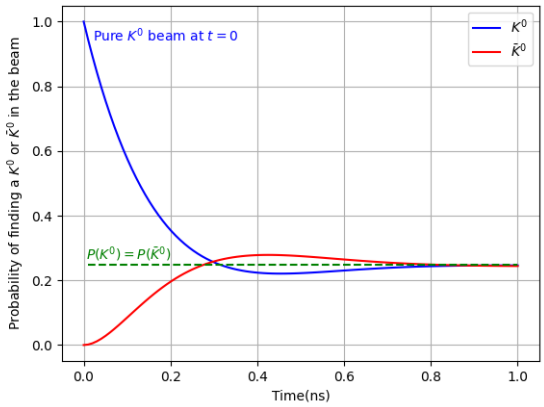


Figure A.1: Probability of finding a K^0 or $\bar{K}^0$ state in an initially produced K^0 beam over time

with matter, which also causes the loss of quantum coherence between them. The K^0 particle engages in quasi-elastic scattering interactions with nucleons, while $\bar{K}^0$ has the ability to produce hyperons. Since the emerging beam contains various different linear combinations of K^0 and $\bar{K}^0$, i.e., a mixture of K_L and K_S, the K_S would eventually be regenerated in the beam, (Pais and Piccioni, 1955).

A.3 Bases in quasi–spin space

The "quasi-spin" picture for kaons, initially proposed by Lee and Wu, (Lee and Wu, 1966), and later developed by Lipkin, (Lipkin, 1968), offers notable advantages when compared to spin-$\frac{1}{2}$ particles or photons with vertical (V)/horizontal (H) polarization. The strangeness eigenstates K^0 and $\bar{K}^0$ are regarded as members of a quasi–spin doublet, where $K^0 = \begin{pmatrix} 1 \\ 0 \end{pmatrix}$ (or V polarized photon) and $\bar{K}^0 = \begin{pmatrix} 0 \\ 1 \end{pmatrix}$ (or H polarized photon) are considered as the quasi-spin states up $|\Uparrow\rangle_z$ and down $|\Downarrow\rangle_z$, respectively. All operators acting in the quasi–spin space can be expressed by Pauli matrices, i.e., σ_x, σ_y, σ_z. The strangeness operator $\mathcal{S}$ is identified by σ_z, i.e.,

$$\sigma_z|K^0\rangle = +|K^0\rangle, \qquad \sigma_z|\bar{K}^0\rangle = -|\bar{K}^0\rangle,$$

the CP operator with $-\sigma_x$, and the CP violation is relative to σ_y. This formalism is suitable for all two–level quantum systems. In this regard, the Hamiltonian in Eq. (A.1) can be implemented as

$$H = \alpha I + \beta\left(\sin\theta\sigma_x + \cos\theta\sigma_y\right)$$

where $\alpha = \frac{1}{2}\left(m_L + m_S - \frac{i}{2}\left(\Gamma_L + \Gamma_S\right)\right)$, $\beta = \frac{1}{2}\left(m_L - m_S - \frac{i}{2}\left(\Gamma_L - \Gamma_S\right)\right)$, and the phase θ corresponds to the CP parameter ϵ such that $e^{i\theta} = \frac{1-\epsilon}{1+\epsilon}$.

Overall, in the quasi–spin formalism, we may work with one of the following bases, (Bramon et al., 2007):

- Strangeness basis $\{K^0, \bar{K}^0\}$: This basis is well-suited for examining electromagnetic and strong interaction processes that conserve strangeness, including the formation of $K^0\bar{K}^0$ systems from non-strange initial states, for instance $e^+e^- \to \phi(1020) \to K^0\bar{K}^0$ or $p\bar{p} \to K^0\bar{K}^0$, and the detection of neutral kaons through strong kaon-nucleon interactions. This is an orthonormal basis, i.e., $\langle K^0|\bar{K}^0\rangle = 0$.

- Free–space basis: $\{K_S, K_L\}$: In the quasi–spin space, the weak interaction eigenstates are similar to the CP eigenstates $|K_1\rangle$ and $|K_2\rangle$. However, the K_S, K_L basis provides a useful framework for analyzing the propagation of particles in free space while the CP basis is particularly suited for studying weak kaon decays. This basis is quasi–orthonormal with $\langle K_S|K_S\rangle = \langle K_L|K_L\rangle = 1$, and $\langle K_S|K_L\rangle = \langle K_L|K_S\rangle = \frac{\epsilon+\epsilon^*}{1+|\epsilon|^2} \simeq 0$.

- Inside–matter basis: $\{K'_S, K'_L\}$: The behavior of neutral kaons as they travel through a homogeneous medium of nucleonic matter, serving as both a regenerator and an absorber is determined by the medium Hamiltonian, which includes an extra strong interaction term as

$$H_{medium} = H - \frac{2\pi\nu}{m_K}\begin{pmatrix} f_0 & 0 \\ 0 & \bar{f}_0 \end{pmatrix}$$

where ν indicates the nucleonic density of the homogeneous medium, m_K is the mean value of $K_{S,L}$ mass, f_0 and $\bar{f}_0$ show the forward scattering amplitudes for K^0 and $\bar{K}^0$, respectively. The $|K'_L\rangle$ and $|K'_S\rangle$ are the eigenstates of H_{medium} expressed as

$$\left|K'_L\right\rangle = \frac{1}{\sqrt{1+|r\bar{\rho}|^2}}\left(|K^0\rangle + r\bar{\rho}\,|\bar{K}^0\rangle\right), \quad \left|K'_S\right\rangle = \frac{1}{\sqrt{1+\left|r(\bar{\rho})^{-1}\right|^2}}\left(|K^0\rangle - r(\bar{\rho})^{-1}\,|\bar{K}^0\rangle\right)$$

where the dimensionless regenerator parameter ρ, the auxiliary parameter $\bar{\rho}$ and its inverse $(\bar{\rho})^{-1}$ are introduced as

$$\rho \equiv \frac{\pi\nu}{m_K}\frac{f_0 - \bar{f}_0}{m_L - m_S - \frac{i}{2}(\Gamma_L - \Gamma_S)}$$
$$\bar{\rho} \equiv \sqrt{1+4\rho^2} + 2\rho, \quad (\bar{\rho})^{-1} = \sqrt{1+4\rho^2} - 2\rho$$

and $r = \frac{1-\epsilon}{1+\epsilon}$. This basis is also quasi–orthonormal.

$$\langle K'_S|K'_L\rangle = \langle K'_L|K'_S\rangle^* = \frac{1-|r|^2(\bar{\rho}^*/\bar{\rho})}{\sqrt{1+|r\bar{\rho}|^2}\sqrt{1+|r/\bar{\rho}|^2}}$$

Two limiting cases exist:

1. For a very low density medium: $|K'_S\rangle \to |K_S\rangle$ and $|K'_L\rangle \to |K_L\rangle$
2. For extremely high density media: $|K'_L\rangle \to |\bar{K}^0\rangle$ and $|K'_S\rangle \to |K^0\rangle$

A.4 Entangled states of kaon pairs

In general terms, we classify a state as entangled when it cannot be expressed as a convex combination of product states, otherwise it is separable, (Bruß, 2002). Quantum entanglement, as a central feature of quantum mechanic, is a phenomenon where two or more particles can become correlated in such a way that the properties of one particle are immediately affected by the properties of the other particle, regardless of the distance between them. In quantum information, entanglement is regarded as a resource. Hence, one is interested in maximally entangled quantum states. To this end, we investigate the entangled states of kaon pairs in two main class, i.e., maximally and non-maximally entangled states.

A.4.1 Maximally entangled neutral kaons

The spin-singlet states, initially proposed by Bohm, are the most commonly studied and simplest form of bipartite states. These states involve a pair of spin-1/2 particles. In analogy to the standard Bohm state, we consider entangled states of $K^0\bar{K}^0$, (Bramon et al., 2004; Bertlmann, 2006). In both cases of $\Phi-$resonance decays and s–wave proton–antiproton annihilation, the process begins at time $t = 0$ with an initial state denoted as $|\phi(0)\rangle$ with global spin, charge conjugation and parity $J^{PC} = 1^{--}$ expressed as $|\phi(t=0)\rangle = \frac{1}{\sqrt{2}}\left(|K^0\rangle_l \otimes |\bar{K}^0\rangle_r - |\bar{K}^0\rangle_l \otimes |K^0\rangle_r\right)$, which can further be written in free–space basis as

$$|\phi(t=0)\rangle = \frac{1+|\varepsilon|^2}{\sqrt{2}|1-\varepsilon^2|}\left[|K_S\rangle_l \otimes |K_L\rangle_r - |K_L\rangle_l \otimes |K_S\rangle_r\right] \tag{A.3}$$

The neutral kaons separate and can be observed both to the left (l) and right (r) of the source. The weak interactions, which violate CP symmetry, come into play only in Eq. (A.3). It is worth noting that this state is both antisymmetric and maximally entangled in the two observable bases. Consequently, any measurements performed will consistently yield left–right anticorrelated outcomes. After production, the left-moving and right-moving kaons undergo evolution as described by Eq. (A.2) for respective proper times t_l and t_r. This formal evolution results in the formation of the "two-times" state. Therefore,

$$|\phi(t_l,t_r)\rangle = \frac{1}{\sqrt{2}}e^{-(\Gamma_S t_l+\Gamma_L t_r)/2}\left(|K_S\rangle_l \otimes |K_L\rangle_r - e^{(i\Delta m+\Delta\Gamma/2)\Delta t}|K_L\rangle_l \otimes |K_S\rangle_r\right) \tag{A.4}$$

where $\Delta t = t_l - t_r$, $\Delta m = m_L - m_S$, $\Delta\Gamma = \Gamma_L - \Gamma_S$, and $\epsilon \to 0$. Equivalently, Eq. (A.4) can be written in strangeness basis

$$\begin{aligned}|\phi(t_l,t_r)\rangle = \frac{1}{2\sqrt{2}} e^{-(\Gamma_S t_l + \Gamma_L t_r)/2} \Big(\Big(1 - e^{(i\Delta m + \Delta\Gamma/2)\Delta t}\Big) \left(|K^0\rangle_l \otimes |K^0\rangle_r - |\bar{K}^0\rangle_l \otimes |\bar{K}^0\rangle_r\right) \\ + \Big(1 - e^{(i\Delta m + \Delta\Gamma/2)\Delta t}\Big) \left(|K^0\rangle_l \otimes |\bar{K}^0\rangle_r - |\bar{K}^0\rangle_l \otimes |K^0\rangle_r\right)\end{aligned}$$

Typically, it is common to examine two-kaon states at a unique time, i.e., $t \equiv t_r = t_l$. In this scenario, we have the following equation

$$\begin{aligned}|\phi(t,t)\rangle &= \frac{1}{\sqrt{2}} e^{-(\Gamma_S + \Gamma_L)t/2} \left(|K^0\rangle_l \otimes |\bar{K}^0\rangle_r - |\bar{K}^0\rangle_l \otimes |K^0\rangle_r\right) \\ &= \frac{1}{\sqrt{2}} e^{-(\Gamma_S + \Gamma_L)t/2} \left(|K_S\rangle_l \otimes |K_L\rangle_r - |K_L\rangle_l \otimes |K_S\rangle_r\right)\end{aligned} \tag{A.5}$$

exhibiting similar maximal entanglement and anti-correlations over time.

A.4.2 Non–maximally entangled states

In addition to the previously discussed maximally entangled state of kaons, there is interest in exploring other non-maximally entangled states for testing the local realism versus Quantum Mechanics theories. To prepare these states, we begin with the initial state described in Eq. (A.3). A thin and homogeneous regenerator is positioned along the right beam, as close as possible to the source of the two-kaon state. If the regenerator is placed in close proximity to this origin and the proper time (Δt) required for the right-moving neutral kaon to pass through the regenerator is sufficiently short, i.e. much smaller than τ_S, weak decays can be neglected, and the resulting state after traversing the thin regenerator is obtained as

$$|\phi(\Delta t)\rangle = \frac{1}{\sqrt{2}} \left(|K_S\rangle \otimes |K_L\rangle - |K_L\rangle \otimes |K_S\rangle + \eta \left(|K_S\rangle \otimes |K_S\rangle - |K_L\rangle \otimes |K_L\rangle\right)\right) \tag{A.6}$$

The regeneration effects is designated by $\eta = i\rho\left(\Delta m - \frac{i}{2}\Delta\Gamma\right)\Delta t$. One may note the difference of Eqs. (A.5) and (A.6) at $t = 0$ made by the terms linear in η. To intensify that difference, let the state Eq. (A.6) propagate in free space up to a proper time $\tau_S \leq T \leq \tau_L$, so

$$\begin{aligned}|\phi(T)\rangle = &\frac{e^{-(\Gamma_L \tau_l + \Gamma_S \tau_r)/2}}{\sqrt{2}} \left(|K_S\rangle \otimes |K_L\rangle - |K_L\rangle \otimes |K_S\rangle\right. \\ &\left. -\eta \left(e^{-(i\Delta m + \Delta\Gamma/2)T} |K_L\rangle \otimes |K_L\rangle - e^{(i\Delta m + \Delta\Gamma/2)T} |K_S\rangle \otimes |K_S\rangle\right)\right)\end{aligned} \tag{A.7}$$

Equation (A.7) shows that the $|K_L\rangle \otimes |K_L\rangle$ component has exhibited remarkable resilience against weak decays compared to the accompanying terms $|K_S\rangle \otimes |K_L\rangle$ and $|K_L\rangle \otimes |K_S\rangle$, resulting in its significant enhancement. Conversely, the $|K_S\rangle \otimes |K_S\rangle$ component has experienced substantial suppression and can therefore be disregarded provided that $T >>$

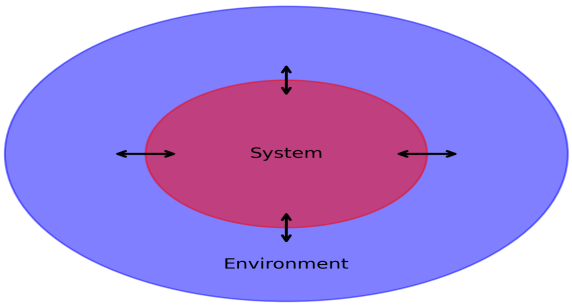


Figure A.2: The overall system can be divided into two components: the system of interest, referred to as the “system", and the surrounding “environment".

τ_S. By normalizing Eq. (A.7) to the surviving pairs, one obtains

$$|\Phi\rangle = \frac{1}{\sqrt{2+|R_L|^2+|R_S|^2}}\left(|K_S\rangle \otimes |K_L\rangle - |K_L\rangle \otimes |K_S\rangle + R_L\,|K_L\rangle \otimes |K_L\rangle + R_S\,|K_S\rangle \otimes |K_S\rangle\right)$$

in which $R_L = -re^{-(i\Delta m+\Delta\Gamma/2)T}$, $R_S = re^{(i\Delta m+\Delta\Gamma/2)T}$. The state Φ, which is non-maximally entangled, encompasses all pairs of kaons wherein both the left and right partners persist until the common proper time T. Due to the specific normalization of Φ, kaon pairs exhibiting decay of one or both members prior to time T need to be identified and excluded. This exclusion occurs before any measurement utilized in a Bell-type test, rendering this approach a “pre-selection" procedure rather than a “post-selection” one, thereby avoiding any conflicts between local realism and quantum mechanics. Upon the establishment of the state $|\Phi\rangle$, it becomes essential to examine alternative joint measurements on each corresponding pair of kaons when conducting a Bell-type test.

A.5 Decoherence effects on entangled kaons

Exploring the factors that could potentially lead to decoherence of entangled kaons is of high importance, (Syahbana et al., 2022; Bertlmann et al., 2003; Bertlmann, 2006; Di Domenico et al., 2009, 2022). Besides, the decoherence allows us to gather insights into the quality of the entangled state. In the subsequent analysis, we explore potential decoherence effects that may arise from interactions between the quantum “system" and its surrounding “environment" as shown in **Figure** A.2. Decoherence effects are mainly divided into two groups: standard and nonstandard, (Bertlmann, 2006). Examples of “standard" decoherence effects can be found in various sources, including:

- Strong interaction scatterings of kaons with nucleons

- Weak interaction decays
- Noise from the experimental setup

Nonstandard decoherence effects are due to the fundamental modifications of quantum mechanics, such as:

- Influence of quantum gravity (C, 2004; Kiefer, 2007; Gambini et al., 2007)
- Quantum fluctuations in the space-time structure at Planck mass scale (Sivaram, 2007)
- Dynamical state-reduction theories (Pearle, 1989)

A.5.1 Density matrix description of entangled kaon system

We will now delve into the decoherence model within the Hilbert space $\mathcal{H} = \mathbb{C}^2$, which represents a two-dimensional complex vector space. Our analysis will specifically focus on the usual effective mass Hamiltonian, as denoted by Eq. (A.1). Here, it is supposed that CP invariance is not violated as in the case of CPLEAR experiment, (Apostolakis et al., 1998), whose data are not sensitive to the impacts of CP violation. Therefore, $p = q = 1$ meaning that

$$\left|K_1^0\right\rangle \equiv \left|K_S\right\rangle, \quad \left|K_2^0\right\rangle \equiv \left|K_L\right\rangle, \quad \left\langle K_S|K_L\right\rangle = 0$$

We can effectively track the evolution of the density operator ρ by employing the so-called Gorini-Kossakowski-Sudarshan-Lindblad equation representing the dynamics of a subsystem within a Markovian system as the entire system expressed as, (Dehaghani et al., 2022a),

$$\dot{\rho}(t) = \mathcal{L}\rho(t) = -i\left(H\rho(t) - \rho(t)H^{\dagger}\right) + \underbrace{\sum_j \left(L_j\rho(t)L_j^{\dagger} - \frac{1}{2}\left\{L_j^{\dagger}L_j, \rho(t)\right\}\right)}_{\mathcal{D}(\rho)} \tag{A.8}$$

in which $\mathcal{L}$ is the Liouville superoperator, and L_j is the Lindblad (or jump) operator. The effect of decoherence is added by the dissipation term $\mathcal{D}(\rho)$, for which we consider the following ansatz, (Bertlmann et al., 2003),

$$\mathcal{D}(\rho) = \frac{\lambda}{2}\sum_j \left[P_j, \left[P_j, \rho\right]\right] \quad \text{with} \quad P_j = \left|K_j\right\rangle\left\langle K_j\right|, \quad j = S, L \tag{A.9}$$

where $\lambda \geq 0$ is the decoherence parameter. Equation (A.9) shows an especial case of dissipation where $L_j = \sqrt{\lambda}P_j$. Therefore, for the elements of density operator $\rho(t) =$

$\sum_{i,j=S,L} \rho_{ij}(t) |K_i\rangle \langle K_j|$, we attain

$$\begin{aligned}
\rho_{SS}(t) &= \rho_{SS}(0) e^{-\Gamma_S t} \\
\rho_{LL}(t) &= \rho_{LL}(0) e^{-\Gamma_L t} \\
\rho_{LS}(t) &= \rho_{LS}(0) e^{-(i(m_L - m_S) - \Gamma - \lambda)t}
\end{aligned}$$

where $\Gamma = \frac{1}{2}(\Gamma_S + \Gamma_L)$.

Consider the maximally entangled state Eq. (A.5) at initial time $t = 0$ as

$$|\psi^-\rangle = \frac{1}{\sqrt{2}} (|e_1\rangle - |e_2\rangle) \tag{A.10}$$

where $|e_1\rangle = |K_S\rangle_l \otimes |K_L\rangle_r$ and $|e_2\rangle = |K_L\rangle_l \otimes |K_S\rangle_r$. The total system Hamiltonian is then described by a tensor product of the one-particle Hilbert spaces as $H = H_l \otimes I_r + I_l \otimes H_r$ with l and r denoting the direction of the moving particles. The state in Eq. (A.10) is a Bell state, (Nielsen and Chuang, 2010; Kurgalin and Borzunov, 2021; Zaman et al., 2018), and is equivalently expressed by the density operator

$$\rho(0) = \frac{1}{2} (|e_1\rangle \langle e_1| + |e_2\rangle \langle e_2| - |e_1\rangle \langle e_2| - |e_2\rangle \langle e_1|) \tag{A.11}$$

In this case, the projectors are $P_1 = |e_1\rangle \langle e_1|$ and $P_2 = |e_2\rangle \langle e_2|$, which project to the eigenstates of two-particle Hamiltonian. Therefore, the element wise time evolution obtained from Eq. (A.8) with the ansatz Eq. (A.9) is expressed as

$$\begin{aligned}
\dot{\rho}_{ij}(t) &= -2\Gamma \rho_{ij}(t) && \text{for } i = j : \rho_{ij}(t) = \rho_{ij}(0) e^{-2\Gamma t} \\
\dot{\rho}_{ij}(t) &= -(2\Gamma + \lambda) \rho_{ij}(t) && \text{for } i \neq j : \rho_{ij}(t) = \rho_{ij}(0) e^{-(2\Gamma + \lambda)t}
\end{aligned}$$

From Eq. (A.11), we already know $\rho_{11}(0) = \rho_{22}(0) = \frac{1}{2}$ and $\rho_{12}(0) = \rho_{21}(0) = -\frac{1}{2}$. As a result, we acquire the time-varying density operator as the following:

$$\rho(t) = \frac{1}{2} e^{-2\Gamma t} \left(|e_1\rangle \langle e_1| + |e_2\rangle \langle e_2| - e^{-\lambda t} (|e_1\rangle \langle e_2| + |e_2\rangle \langle e_1|) \right) \tag{A.12}$$

From Eq. (A.8), it follows that $\rho(t) = e^{\mathcal{L}t} \rho(0)$. This means that the initial state $\rho(0)$ is transformed to $\rho(t)$ by the completely positive and trace preserving (CPTP) map $\mathcal{V}(t) = e^{\mathcal{L}t}$ generated by the superoperator $\mathcal{L}$, (Breuer and Petruccione, 2002; Manzano, 2020). Note that while $\mathcal{V}(t)$ should satisfy trace-preserving characteristics, the non-Hermitian nature of the system Hamiltonian results in a deviation from the property of trace preservation. Specifically, we observe that $tr(\rho(0)) = 1$ but $tr(\rho(t)) = e^{-2\Gamma t}$, in other words, $tr(\dot{\rho}(t)) \neq 0$. The issue arising from the non-Hermitian Hamiltonian in this particular system has been addressed in previous studies, (Caban et al., 2005; Bertlmann et al., 2006). By introducing certain modifications to the Hilbert space and the dynamical equation, one can effectively

work with this Hamiltonian. Therefore, the Hilbert space $\mathcal{H}$ of the system is extended by adding the Hilbert space $\mathcal{H}_0$ which corresponds to the decay states resulting from the dissipation, so $\mathcal{H}_{tot} = \mathcal{H} \oplus \mathcal{H}_0$. By using the effective mass Hamiltonian defined in Eq. (A.1), the dynamical equation is then expressed as

$$\dot{\rho}(t) = -i[M, \rho(t)] - \left\{\frac{1}{2}\mathbf{\Gamma}, \rho(t)\right\} \tag{A.13}$$

Let define $B : \mathcal{H} \to \mathcal{H}_0$, and $\mathbf{\Gamma} = B^\dagger B$, then we obtain $tr(\dot{\rho}) = -tr(B^\dagger B\rho(t)) \neq 0$. By adding $B\rho(t)B$ to Eq. (A.13), such that $\dot{\rho}(t) = -i[M, \rho(t)] - \left\{\frac{1}{2}\mathbf{\Gamma}, \rho(t)\right\} + B\rho(t)B$, then $tr(\dot{\rho}(t)) = 0$, meaning that the trace of $\rho(t)$ is preserved.

A.5.1.1 Purity

Decoherence arises exclusively from the influence of the factor $e^{-\lambda t}$ on the off-diagonal elements. Hence, for $t = 0$, the density operator corresponds to a pure state, however, for $t > 0$ and $\lambda \neq 0$, the state $\rho(t)$ does not exihibit a pure state anymore. As time elapses and environmental factors come into play, the quantum effects, characterized by coherences, gradually fade away, giving rise to the phenomenon of decoherence.

In quantum mechanics and particularly in the field of quantum information theory, the purity of a quantum state described by the density operator is defined as $\mathcal{P}(t) = tr(\rho^2(t))$. The purity expresses a measure on quantum states, and provides information regarding the degree of mixture in a given state. Here, the purity of $\rho(t)$ is, (Syahbana et al., 2022),

$$\mathcal{P}(t) = \frac{1}{2}e^{-4\Gamma t}\left(1 + e^{-2\lambda t}\right)$$

that is, for $t = 0$, $\mathcal{P}(t) = 1$, and for $t > 0$, $\mathcal{P}(t) < 1$. We can conclude that the evolution of $\rho(t)$ transfers a pure state to a mixed state, which is due to the occurrence of decoherence phenomenon. In addition, the purity of a normalized quantum state satisfies $\frac{1}{2} \leq \mathcal{P}(t) \leq 1$ for a state defined upon a 2 dimensional Hilbert space. However, in this case the value of $\mathcal{P}(t)$ can be less than $\frac{1}{2}$. It happens when one of the conditions of density operator is not satisfied for $t > 0$, i.e., $tr(\rho(t)) \neq 1$.

A.5.2 Decoherence parameter associated to entangled kaon system

In the CPLEAR experiment, as described in (Apostolakis et al., 1998), entangled kaons are generated. Subsequently, the strangeness content (S) of the right-moving and left-moving particles is measured at time $t = t_r$ and $t = t_l$, respectively. Consider a specific scenario where the detection reveals that a $\bar{K}^0$ is observed at the right side at time $t = t_r$, while a K^0 is detected at the left side at time $t = t_l$, where $t_r \leq t_l$. We indicate two operators S_r^+ and S_l^- to represent the measurement of strangeness at the right and left side, respectively (see **Figure A.3**). After the measurement is occurred at the right side, the density operator of

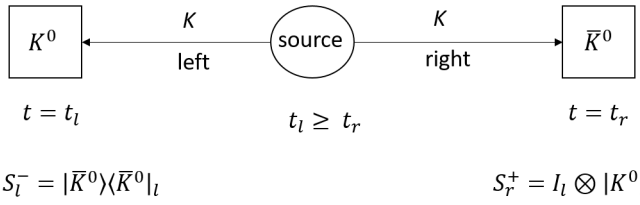


Figure A.3: We consider a case that $\bar{K}^0$ and K^0 are detected at the right side at $t = t_r$ and left side at $t = t_l$, respectively, where $t_l \geq t_r$. The operators S_r^+ and S_l^- correspond to strangeness measurement at right and left sides.

the left moving particle turns out to be

$$\rho_l\left(t = t_r; t_r\right) = tr_r\left(S_r^+ \rho\left(t_r\right)\right) \tag{A.14}$$

From here, the probability of this case becomes, (Syahbana et al., 2022),

$$P\left(\bar{K}^0, t_l; K^0, t_r\right) = tr\left(S_l^- \rho_l\left(t_l; t_r\right)\right) = tr\left(tr_r\left(S_r^+ \rho_l\left(t_r\right)\right)\right) \tag{A.15}$$

In the following, we obtain $P\left(\bar{K}^0, t_l; K^0, t_r\right)$. For the other cases, the same procedure can be employed. In order to determine Eq. (A.15), one can use $|K_S\rangle$ and $|K_L\rangle$ as the basis, and write Eq. (A.14) as

$$\rho_l\left(t = t_r; t_r\right) = \frac{1}{4} e^{-2\Gamma t_r}\left(|K_S\rangle\langle K_S|_l + |K_L\rangle\langle K_L|_l - e^{-\lambda t_r}\left(|K_S\rangle\langle K_L|_l + |K_L\rangle\langle K_S|_l\right)\right) \tag{A.16}$$

Suppose the density operator related to a left moving particle is expressed as

$$\begin{aligned}\rho_l\left(t; t_r\right) =& \rho_{SS}\left(t; t_r\right)|K_S\rangle\langle K_S|_l + \rho_{SL}\left(t; t_r\right)|K_S\rangle\langle K_L|_l \\ &+ \rho_{LS}\left(t; t_r\right)|K_L\rangle\langle K_S|_l + \rho_{LL}\left(t; t_r\right)|K_L\rangle\langle K_S|_l\end{aligned} \tag{A.17}$$

which is supposed to evade decoherence for the time interval $t > t_r$. Therefore, it evolves according to $\dot{\rho}_l\left(t; t_r\right) = -i\left(H\rho_l\left(t; t_r\right) - \rho_l\left(t; t_r\right)H^\dagger\right)$. Hence, the following equation is obtained

$$\begin{aligned}\dot{\rho}_l\left(t; t_r\right) =& -\Gamma_S \rho_{SS}\left(t; t_r\right)|K_S\rangle\langle K_S|_l + \left(i\Delta m - \Gamma\right)\rho_{SL}\left(t; t_r\right)|K_S\rangle\langle K_L|_l \\ &- \left(i\Delta m + \Gamma\right)\rho_{LS}\left(t; t_r\right)|K_L\rangle\langle K_S|_l - \Gamma_L \rho_{LL}\left(t; t_r\right)|K_L\rangle\langle K_L|_l\end{aligned}$$

Let assume that C_{ij} with $i, j = S, L$ is constant, so

$$\begin{aligned}\rho_{SS}\left(t; t_r\right) &= C_{SS} e^{-\Gamma_S t}, \qquad \rho_{LL}\left(t; t_r\right) = C_{LL} e^{-\Gamma_L t}, \\ \rho_{SL}\left(t; t_r\right) &= C_{SL} e^{(i\Delta m - \Gamma)t}, \qquad \rho_{LS}\left(t; t_r\right) = C_{LS} e^{-(i\Delta m + \Gamma)t}\end{aligned}$$

From our knowledge of Eqs. (A.16) and (A.17), the values of C_{ij} and subsequently $\rho_{ij}(t; t_r)$ can be obtained. Finally, by replacing $t = t_l$, we attain $P\left(\bar{K}^0, t_l; K^0, t_r\right)$.

Explicitly, by assuming that $\Delta t = t_l - t_r$, we have the following results

$$\begin{aligned} P\left(K^0,t_l;\bar{K}^0,t_r\right) &= P\left(\bar{K}^0,t_l;K^0,t_r\right) \\ &= \frac{1}{8}e^{-2\Gamma t_r}\left(e^{-\Gamma_S\Delta t}+e^{-\Gamma_L\Delta t}+2e^{-\lambda t_r}\cos\left(\Delta m\Delta t\right)e^{-\Gamma\Delta t}\right) \end{aligned} \tag{A.18}$$

$$\begin{aligned} P\left(K^0,t_l;K^0,t_r\right) &= P\left(\bar{K}^0,t_l;\bar{K}^0,t_r\right) \\ &= \frac{1}{8}e^{-2\Gamma t_r}\left(e^{-\Gamma_S\Delta t}+e^{-\Gamma_L\Delta t}-2e^{-\lambda t_r}\cos\left(\Delta m\Delta t\right)e^{-\Gamma\Delta t}\right) \end{aligned} \tag{A.19}$$

Let consider $\Delta t = 0$, i.e., $t_l = t_r = t$, then from Eq. (A.18), one obtains

$$P\left(K^0,t_l;\bar{K}^0,t_r\right) = P\left(\bar{K}^0,t_l;K^0,t_r\right) = \frac{1}{4}e^{-2\Gamma t}(1-e^{-\lambda t})$$

which is in contradiction to the pure quantum mechanical EPR-correlations. The asymmetry of probabilities is the captivating factor of interest, as it directly responds to the interference term and can be quantified by means of experimental measurements. In the realm of pure quantum mechanics, where a system does not experience decoherence, we encounter this phenomenon by A^{QM} expressed as

$$\begin{aligned} A^{QM}\left(t_l,t_r\right) &= \frac{P\left(K^0,t_l;\bar{K}^0,t_r\right)+P\left(\bar{K}^0,t_l;K^0,t_r\right)-P\left(K^0,t_l;K^0,t_r\right)-P\left(\bar{K}^0,t_l;\bar{K}^0,t_r\right)}{P\left(K^0,t_l;\bar{K}^0,t_r\right)+P\left(\bar{K}^0,t_l;K^0,t_r\right)+P\left(K^0,t_l;K^0,t_r\right)+P\left(\bar{K}^0,t_l;\bar{K}^0,t_r\right)} \\ &= \frac{\cos\left(\Delta m\Delta t\right)}{\cosh\left(\frac{1}{2}\Delta\Gamma\Delta t\right)} \end{aligned} \tag{A.20}$$

in which $\Delta\Gamma = \Gamma_L - \Gamma_S$. In the decoherence model of entangled kaon system, since it is not known which particle will first be detected, t_r in Eqs. (A.18) and (A.19) needs to be replaced by $\tau = min(t_r,t_l)$. By inserting Eqs. (A.18) and (A.19), we obtain

$$A^{\lambda}\left(t_l,t_r\right) = A^{QM}\left(t_l,t_r\right)e^{-\lambda\tau} \tag{A.21}$$

which indicates that the decoherence effect represented by $e^{-\lambda\tau}$ is dependent on the time of the first detected kaon.

The decoherence model in Eq. (A.21) can be introduced in a phenomenological way, where the decoherence parameter λ corresponds to an effective decoherence parameter ζ as $\zeta(t_l,t_r) = 1 - e^{-\lambda\tau}$. Apparently, the value of $\zeta = 0$ represents pure quantum mechanics, and $\zeta = 1$ corresponds to complete decoherence or spontaneous factorization of the wave function (Schrödinger-Furry hypothesis). By means of standard least squares method, (Barlow, 1993; Bevan, 2013), $\zeta = 0.13 \pm 0.865$ is obtained in (Syahbana et al., 2022), which is in agreement with the results obtained from the effective variance method, where $\zeta = 0.13^{+0.16}_{-0.15}$, (Bertlmann et al., 1999; Wiseman and Cavalcanti, 2017), correspondent to $\lambda = (1.84^{-2.17}_{+2.50}) \times 10^{-12} MeV$. The value of both parameters are compatible with quantum mechanics, i.e., $\zeta = 0$ and $\lambda = 0$ and far away from the total decoherence, i.e., $\zeta = 1$

or $\lambda = \infty$. It indicates that the interaction between the system and its environment has negligible influence on the system. As a result, the quantum properties related to the entanglement of the strangeness are preserved without significant alteration.

A.6 Loss of entanglement

As time progresses, the degree of decoherence in the initially fully entangled $K^0\bar{K}^0$ system increases, leading to a decrease in the system's entanglement. This loss of entanglement, defined as the disparity between an entanglement value and its maximum unity, can be precisely measured, (Bertlmann, 2006; Hiesmayr, 2002). In the realm of quantum information, the quantification of entanglement in a state is assessed by employing specific measures designed for quantifying entanglement. In this context, entropy plays a pivotal role. The entropy serves as a measure of the level of uncertainty or lack of knowledge associated with a quantum state. If the quantum state is pure, maximum information about the system is provided, however, mixed states only offer partial information. The entropy quantifies the extent to which maximal information is absent. In the following, we focus on the three most important and wildly-used entanglement measures: Von Neumann entanglement entropy, Entanglement of formation, and concurrence. When the interest is focused on the effect of decoherence, one needs to compensate for the decay up to time t to attain a proper density operator for the kaon system. Therefore, we divide the state Eq. (A.12) with its trace, i.e., $\rho_N(t) = \frac{\rho(t)}{tr(\rho(t))}$.

A.6.1 Von Neumann entanglement entropy

Von Neumann's entropy of the quantum state $\rho_N(t)$ is expressed as

$$S(\rho_N(t)) = -tr(\rho_N(t) log_d \rho_N(t))$$

where d is the dimension of the Hilbert space, i.e., for the Hilbert space of a qubit $d = 2$, hence $0 < S(\rho_N(t)) < 1$. For $t = 0$, the entropy is zero, meaning that the state is pure and also maximally entangled. However, as $t \to \infty$, the entropy approaches to one, i.e., the system become mixed. The Von Neumann entropy is a good criteria of entanglement, specifically for pure quantum states, (Varizi, 2017; Bertlmann et al., 2003; Bertlmann, 2006).

The bipartite von Neumann entanglement entropy can be defined as the von Neumann entropy of any of its reduced states. This definition holds true because both reduced states have the same value, as can be demonstrated through the Schmidt decomposition of the state with respect to the bipartition. Consequently, the outcome remains unchanged regardless of the specific reduced state chosen. Generally, two subsystems are maximally entangled when their reduced density operators are maximally mixed. In our case, the left- (subsystem l) and right- (subsystem r) propagating kaons are our

subsystems. Therefore, the reduced density operators are defined as

$$\rho_N^l(t) = tr_r(\rho_N(t)), \qquad \rho_N^r(t) = tr_l(\rho_N(t))$$

The von Neumann entropy of $\rho_N^l(t)$ (or $\rho_N^r(t)$) provides the uncertainty in the subsystem l (or r) before measuring the subsystem r (or l). In the case of kaon system, we have

$$S(\rho_N^l(t)) = S(\rho_N^r(t)) = 1 \quad \forall t \geq 0$$

which are independent of decoherence parameter λ, meaning that the correlation stored in the entire system is lost to the environment and not to the subsystems.

A.6.2 Entanglement of formation

Entanglement entropy is also known as the entanglement of formation for pure states. It is possible to express any density matrix as a collection of pure states forming an ensemble $\rho_i = |\psi_i\rangle\langle\psi_i|$, with each pure state having a corresponding probability p_i, that is $\rho = \sum_i p_i \rho_i$. For mixed states, entanglement of formation can be generalized by defining a quantity minimized over all the ensemble realizations of the mixed state. For the kaon system, we have

$$E_f(\rho) = \min \sum_i p_i S\left(\rho_i^l\right)$$

The entanglement of formation can be simplified to $E_f(\rho) \geq \mathcal{E}(f(\rho))$ by introducing the lower bound of $E_f((\rho))$, given by

$$\mathcal{E}(f(\rho)) = H\left(\frac{1}{2} + \sqrt{f(\rho)(1-f(\rho))}\right) \quad \text{for} \quad f(\rho) \geq \frac{1}{2}$$
$$\mathcal{E}(f(\rho)) = 0 \quad \text{for} \quad f(\rho) < \frac{1}{2}$$

where $f(\rho) = \max\langle e|\rho|e\rangle$, known as the fully entangled fraction of ρ, is the maximum over all completely entangled states $|e\rangle$, and

$$H(x) = -x log_2 x - (1-x) log_2 (1-x).$$

For our model, the lower bound expressed for $E_f(\rho)$ is saturated, i.e., $E_f(\rho) = \mathcal{E}(f(\rho))$. Therefore, one can calculate the entanglement of formation simply by computing $\mathcal{E}(f(\rho))$, (Bertlmann, 2006).

The fully entangled fraction of $\rho_N(t)$ is $f(\rho_N(t)) = \frac{1}{2}(1 + e^{-\lambda t}) \geq 0$. Therefore, the entanglement of formation for the $K^0\bar{K}^0$ is assessed in terms of $E_f(\lambda)$ as

$$E_f(\lambda) = -\frac{1+\sqrt{1-e^{-2\lambda t}}}{2} \log_2 \frac{1+\sqrt{1-e^{-2\lambda t}}}{2} - \frac{1-\sqrt{1-e^{-2\lambda t}}}{2} \log_2 \frac{1-\sqrt{1-e^{-2\lambda t}}}{2}$$

From which one can obtain the entanglement loss $L_E(t)$ as

$$\begin{aligned} L_E(t) &= 1 - E\left(\rho_N(t)\right) \\ &\simeq \frac{\lambda}{\ln 2} t = \frac{1}{\ln 2}\xi(t) = 1.44\xi(t) \end{aligned} \tag{A.22}$$

approximated for small values of λ. Equation (A.22) shows that the entanglement loss equals the weighted amount of decoherence.

A.6.3 Concurrence

Wootters and Hill, in their research publications (Wootters, 1998; Hill and Wootters, 1997; Wootters, 2001), discovered a relation between entanglement of formation and a measure known as concurrence. This connection allows the expression of entanglement of formation for a general mixed state ρ of two qubits in terms of the concurrence as

$$E_f(\rho) = \mathcal{E}\left(C(\rho)\right) = H\left(\frac{1}{2} + \frac{1}{2}\sqrt{1 - C^2(\rho)}\right)$$

with $0 \leq C(\rho) \leq 1$. As The function $\mathcal{E}\left(C(\rho)\right)$ is monotonically increasing from 0 to 1 as $C(\rho)$ goes from 0 to 1.

The concurrence $C(\rho)$ in defined as $C(\rho) \equiv max\{0, \lambda_1 - \lambda_2 - \lambda_3 - \lambda_4\}$ with λ_i's representing the square roots of the eigenvalues, in decreasing order, of $R = \rho\tilde{\rho}$ matrix where $\tilde{\rho}$ is the spin-flipped state of ρ defined as

$$\tilde{\rho} = (\sigma_y \otimes \sigma_y)\rho^*(\sigma_y \otimes \sigma_y)$$

The complex conjugate of ρ, i.e., ρ^* is taken in the basis $\{|\Uparrow\Uparrow\rangle, |\Downarrow\Downarrow\rangle, |\Uparrow\Downarrow\rangle, |\Downarrow\Uparrow\rangle\}$. In our model, since $\rho_N(t)$ is not variant under spin flip, hence $R = \rho_N^2$, and the concurrence is

$$C(\rho_N(t)) \equiv max\{0, e^{-\lambda t}\} = e^{-\lambda t}$$

Hence, $L_C(t)$ is computed as

$$L_C(t) = 1 - C\left(\rho_N(t)\right) = 1 - e^{-\lambda t} = \xi(t) \tag{A.23}$$

The value of $L_C(t)$ is precisely equivalent to decoherence $\xi(t)$, describing the factorization of the initial spin singlet state to the state $|K_S\rangle_l \otimes |K_L\rangle_r$ or $|K_S\rangle_l \otimes |K_L\rangle_r$. In both cases, Eqs. (A.22) and (A.23), show that the loss of entanglement is equivalent to decoherence, and increases linearly with time, (Bertlmann et al., 2003). In **Figure A.4**, we show the loss of information by the von Neumann entropy $S(\lambda)$ in comparison with the loss of entanglement of formation $L_E(t)$ depending on the normalized time τ of the propagating $K^0\bar{K}^0$ system for the experimental mean value $\lambda = 1.84 \times 10^{-12} MeV$, and the upper bound $\lambda = 4.34 \times 10^{-12} MeV$ of the decoherence parameter. The rate of increase in the

loss of entanglement of formation is slower as time progresses, indicating the amount of resources required to create a specific entangled state. In the overall state, the level of entanglement decreases until separability is achieved, which occurs exponentially fast as time approaches infinity. In the CPLEAR experiment, where the propagation of one kaon for 2 cm corresponds to the propagation time $\tau = 0.55$, until an absorber measures it, the loss of entanglement is approximately 0.18 and 0.38 for the mean value and upper bound of λ, respectively.

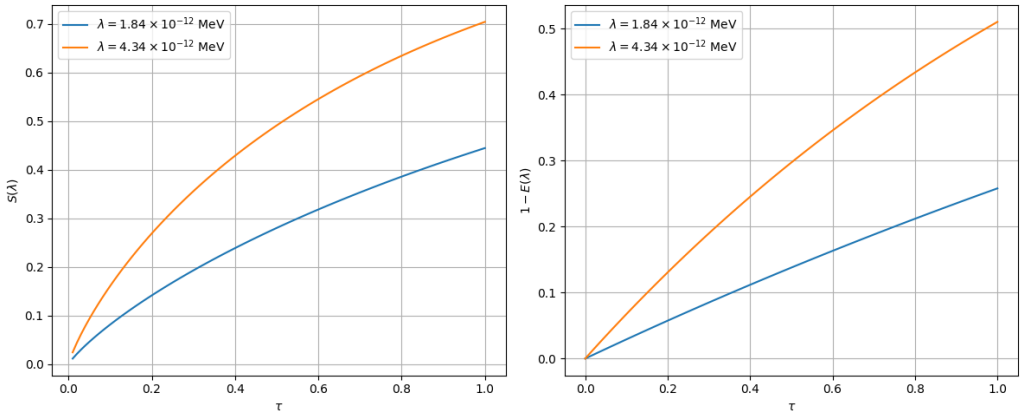


Figure A.4: The time dependence of von Neumann entropy and the loss of entanglement of formation for two values of λ. The time t is normalized versus τ_S, i.e. $\tau = \frac{t}{\tau_S}$.

A.7 Concluding Remarks and Discussions

This chapter has provided a comprehensive analysis of the properties and phenomena associated with neutral K-mesons, highlighting their intriguing and often puzzling behaviors. We began by emphasizing the significance of strangeness and charge parity violation in the understanding of these particles. Next, the concept of strangeness oscillations, exemplified by the oscillations between K^0 and $\bar{K}^0$ states, was introduced and thoroughly explored. We delved into the regeneration of K_S and unraveled the underlying mechanisms that govern these oscillations, shedding light on the intricate dynamics involved. Next, we examined the quasi-spin space and its bases, unraveling their implications and providing insights into the entangled states of kaon pairs, particularly focusing on both maximally and non-maximally entangled neutral kaons. This exploration has broadened our understanding of the entanglement properties exhibited by these particles. Furthermore, we dedicated significant attention to the study of decoherence effects on entangled kaons. Through the use of density matrix formalism, we captured the dynamic nature of decoherence and introduced a dedicated parameter to quantify its impact. Measures such as Von Neumann entanglement entropy, entanglement of formation, and concurrence were employed to explore the loss of entanglement, providing valuable tools for

characterizing and quantifying entanglement in the context of neutral kaons. However, several intriguing questions for future research remain open.

The study of kaon entanglement and decoherence raises a host of intriguing open questions that drive ongoing research and exploration. How do environmental interactions, such as scattering or absorption, impact the entanglement and coherence properties of neutral kaons? Can we develop methods to quantify and control these effects? Additionally, investigating entanglement dynamics in multipartite kaon systems, involving more than two neutral kaons, presents an exciting avenue of research. How does multipartite entanglement and its degradation relate to the underlying interactions and dynamics? Developing novel experimental techniques and theoretical models to explore these phenomena could shed light on the intricate nature of entanglement in kaon systems.

Furthermore, the generation and manipulation of entangled kaon states offer intriguing possibilities. Can we create specific entanglement patterns or preserve entanglement over extended timescales? Understanding and enhancing entanglement in kaon systems could have implications for quantum information processing and communication. The role of entanglement in comprehending and quantifying CP violation in kaon systems is another crucial aspect. How does entanglement contribute to our understanding of the underlying mechanisms driving CP violation? Exploring connections between the entanglement properties of neutral kaons and other areas of physics, such as quantum information theory, quantum field theory, or quantum gravity, holds promise for uncovering fundamental principles and phenomena.

Additionally, the presence of decoherence poses significant challenges. How does decoherence affect the entanglement properties of neutral kaons? Can we develop techniques to mitigate or minimize its detrimental effects and preserve entanglement over longer durations? Exploring the entanglement and coherence properties of neutral kaons within non-standard models beyond the Standard Model of particle physics could provide insights into new physics and phenomena. Moreover, extending the study of entanglement and decoherence to other meson systems or particles with similar characteristics is a compelling direction. How do the entanglement properties differ or align between different types of particles? Finally, experimental methodologies and theoretical frameworks for directly observing or measuring entanglement in kaon systems, as well as exploring the implications of entanglement for quantum computing and communication, open up exciting possibilities for practical applications in quantum technologies.

These open questions highlight the ongoing exploration and research endeavors, presenting intriguing avenues for further investigation and potential breakthroughs.

References

A Pedro Aguiar, Joao P Hespanha, and Antonio M Pascoal. Switched seesaw control for the stabilization of underactuated vehicles. *Automatica*, 43(12):1997–2008, 2007.

Charlene Ahn, Andrew C Doherty, and Andrew J Landahl. Continuous quantum error correction via quantum feedback control. *Physical Review A*, 65(4):042301, 2002.

Francesca Albertini and Domenico D'Alessandro. Notions of controllability for quantum mechanical systems. In *Proceedings of the 40th IEEE Conference on Decision and Control (Cat. No. 01CH37228)*, volume 2, pages 1589–1594. IEEE, 2001.

Robert Alicki and Karl Lendi. N-level systems and applications to spectroscopy, lect. notes phys. *Quantum Dynamical Semigroups and Applications*, 717:47–107, 2007.

A Aloisio, F Ambrosino, A Antonelli, M Antonelli, C Bacci, G Bencivenni, S Bertolucci, Cesare Bini, C Bloise, V Bocci, et al. Recent results from KLOE at DAΦNE. *Nuclear Physics B-Proceedings Supplements*, 111(1-3):213–218, 2002.

Joseba Alonso, Florian M Leupold, Ben C Keitch, and JP Home. Quantum control of the motional states of trapped ions through fast switching of trapping potentials. *New Journal of Physics*, 15(2):023001, 2013.

Claudio Altafini and Francesco Ticozzi. Modeling and control of quantum systems: an introduction. *IEEE Transactions on Automatic Control*, 57(8):1898–1917, 2012.

Sirine Amri, Robin Corgier, Dominique Sugny, Ernst M Rasel, Naceur Gaaloul, and Eric Charron. Optimal control of the transport of Bose-Einstein condensates with atom chips. *Scientific reports*, 9(1):1–11, 2019.

Thomas Antony. *Large scale constrained trajectory optimization using indirect methods*. PhD thesis, Purdue University, 2018.

A Apostolakis, E Aslanides, G Backenstoss, P Bargassa, O Behnke, A Benelli, V Bertin, F Blanc, P Bloch, P Carlson, et al. An EPR experiment testing the non-separability of the K0K0 wave function. *Physics Letters B*, 422(1-4):339–348, 1998.

Maria Soledad Aronna. *Second order analysis of optimal control problems with singular arcs. Optimality conditions and shooting algorithm.* PhD thesis, Ecole Polytechnique X, 2011.

Aram V Arutyunov, D Yu Karamzin, and F Lobo Pereira. The maximum principle for optimal control problems with state constraints by RV Gamkrelidze: revisited. *Journal of Optimization Theory and Applications*, 149(3):474–493, 2011.

Alain Aspect, Jean Dalibard, and Gérard Roger. Experimental test of Bell's inequalities using time-varying analyzers. *Physical review letters*, 49(25):1804, 1982.

Stéphane Attal. Quantum noises. In *Open Quantum Systems II*, pages 79–147. Springer, 2006.

Roger J Barlow. *Statistics: a guide to the use of statistical methods in the physical sciences*, volume 29. John Wiley & Sons, 1993.

Erik Bauch, Connor A Hart, Jennifer M Schloss, Matthew J Turner, John F Barry, Pauli Kehayias, Swati Singh, and Ronald L Walsworth. Ultralong dephasing times in solid-state spin ensembles via quantum control. *Physical Review X*, 8(3):031025, 2018.

John Stewart Bell. *Speakable and unspeakable in quantum mechanics: Collected papers on quantum philosophy*. Cambridge university press, 1987.

Michael Berman and Ronnie Kosloff. Time-dependent solution of the Liouville-von Neumann equation: Non-dissipative evolution. *Computer physics communications*, 63(1-3): 1–20, 1991.

Jose Bernabeu and Antonio Di Domenico. Can future observation of the living partner post-tag the past decayed state in entangled neutral K mesons? *Physical Review D*, 105 (11):116004, 2022.

RA Bertlmann, W Grimus, and BC Hiesmayr. Quantum mechanics, Furry's hypothesis, and a measure of decoherence in the K 0 K 0 system. *Physical Review D*, 60(11):114032, 1999.

Reinhold A Bertlmann. Entanglement, Bell inequalities and decoherence in particle physics. *Quantum Coherence: From Quarks to Solids*, pages 1–45, 2006.

Reinhold A Bertlmann, Katharina Durstberger, and Beatrix C Hiesmayr. Decoherence of entangled kaons and its connection to entanglement measures. *Physical Review A*, 68 (1):012111, 2003.

Reinhold A Bertlmann, Walter Grimus, and Beatrix C Hiesmayr. Open-quantum-system formulation of particle decay. *Physical Review A—Atomic, Molecular, and Optical Physics*, 73(5):054101, 2006.

Adrian Bevan. *Statistical data analysis for the physical sciences*. Cambridge University Press, 2013.

Andrea Bizzeti. Recent results from the NA62 and NA48/2 experiments at CERN. *Nuclear and Particle Physics Proceedings*, 324:113–118, 2023.

William M Boothby and Edward N Wilson. Determination of the transitivity of bilinear systems. *SIAM journal on control and optimization*, 17(2):212–221, 1979.

U Boscain, M Sigalotti, and D Sugny. Introduction to the foundations of quantum optimal control. *arXiv e-prints*, pages arXiv–2010, 2020.

Ugo Boscain and Grégoire Charlot. Resonance of minimizers for n-level quantum systems with an arbitrary cost. *ESAIM: Control, Optimisation and Calculus of Variations*, 10 (4):593–614, 2004.

Ugo Boscain and Benedetto Piccoli. *Optimal syntheses for control systems on 2-D manifolds*, volume 43. Springer Science & Business Media, 2003.

Luc Bouten, Ramon Van Handel, and Matthew R James. An introduction to quantum filtering. *SIAM Journal on Control and Optimization*, 46(6):2199–2241, 2007.

A Bramon, G Garbarino, and BC Hiesmayr. Quantum marking and quantum erasure for neutral kaons. *Physical review letters*, 92(2):020405, 2004.

A Bramon, R Escribano, and G Garbarino. A review of Bell inequality tests with neutral kaons, 2007.

Agata M Brańczyk, Paulo EMF Mendonça, Alexei Gilchrist, Andrew C Doherty, and Stephen D Bartlett. Quantum control of a single qubit. *Physical Review A*, 75(1):012329, 2007.

Heinz-Peter Breuer and Francesco Petruccione. *The theory of open quantum systems*. Oxford University Press, USA, 2002.

Constantin Brif, Raj Chakrabarti, and Herschel Rabitz. Control of quantum phenomena: past, present and future. *New Journal of Physics*, 12(7):075008, 2010.

Dagmar Bruß. Characterizing entanglement. *Journal of Mathematical Physics*, 43(9):4237–4251, 2002.

Rovelli C. *Quantum gravity*. Cambridge university press, 2004.

Paweł Caban, Jakub Rembieliński, Kordian A Smoliński, and Zbigniew Walczak. Unstable particles as open quantum systems. *Physical Review A—Atomic, Molecular, and Optical Physics*, 72(3):032106, 2005.

Tommaso Caneva, Tommaso Calarco, and Simone Montangero. Chopped random-basis quantum optimization. *Physical Review A*, 84(2):022326, 2011.

Fuyang Chen, Rui Hou, Bin Jiang, and Gang Tao. Study on fast terminal sliding mode control for a helicopter via quantum information technique and nonlinear fault observer. *International Journal of Innovative Computing, Information and Control*, 9(8):3437–3447, 2013.

John F Clauser and Michael A Horne. Experimental consequences of objective local theories. *Physical review D*, 10(2):526, 1974.

LHCb Collaboration. LHCb detector performance. *International Journal of Modern Physics A*, 30(07):1530022, 2015.

Shuang Cong. *Control of quantum systems: theory and methods*. John Wiley & Sons, 2014.

Shuang Cong and Fangfang Meng. A survey of quantum Lyapunov control methods. *The Scientific World Journal*, 2013, 2013.

Domenico D'Alessandro. Topological properties of reachable sets and the control of quantum bits. *Systems & control letters*, 41(3):213–221, 2000.

Domenico D'alessandro and Mohammed Dahleh. Optimal control of two-level quantum systems. *IEEE Transactions on Automatic Control*, 46(6):866–876, 2001.

Nahid Binandeh Dehaghani and A Pedro Aguiar. An application of pontryagin neural networks to solve optimal quantum control problems. In *2023 9th International Conference on Control, Decision and Information Technologies (CoDIT)*, pages 202–207. IEEE, 2023a.

Nahid Binandeh Dehaghani and A Pedro Aguiar. Quantum state transfer optimization: Balancing fidelity and energy consumption using Pontryagin maximum principle. In *2023 IEEE 11th International Conference on Systems and Control (ICSC)*, pages 94–99. IEEE, 2023b.

Nahid Binandeh Dehaghani and Fernando Lobo Pereira. High fidelity quantum state transfer by Pontryagin maximum principle. *IFAC-PapersOnLine*, 55(16):214–219, 2022a.

Nahid Binandeh Dehaghani and Fernando Lobo Pereira. Optimal control of quantum systems by Pontryagin maximum principle. *U. Porto Journal of Engineering*, 8(2):194–201, 2022b.

Nahid Binandeh Dehaghani, Fernando Lobo Pereira, and António Pedro Aguiar. Quantum control modelling, methods, and applications. *Extensive Reviews*, 2(1):75–126, 2022a.

Nahid Binandeh Dehaghani, Fernando Lobo Pereira, and António Pedro Aguiar. A quantum optimal control problem with state constrained preserving coherence. In *2022 IEEE 61st Conference on Decision and Control (CDC)*, pages 5831–5836. IEEE, 2022b.

Nahid Binandeh Dehaghani, A Pedro Aguiar, and Rafal Wisniewski. Exploring strange entanglement: Experimental and theoretical perspectives on neutral kaon systems. *Quantum Entan- glement in High Energy Physics*, 2023a.

Nahid Binandeh Dehaghani, A Pedro Aguiar, and Rafal Wisniewski. Quantum Pontryagin neural networks in Gamkrelidze form subjected to the purity of quantum channels. *IEEE Control Systems Letters*, 2023b.

Nahid Binandeh Dehaghani, A Pedro Aguiar, and Rafal Wisniewski. Optimizing maximally entangled state generation via Pontryagin's principle. 2024a.

Nahid Binandeh Dehaghani, A Pedro Aguiar, and Rafal Wisniewski. Application of CRAB algorithm for enhanced entanglement synthesis. *16th APCA International Conference on Automatic Control and Soft Computing (CONTROLO 2024)*, 2024b.

Nahid Binandeh Dehaghani, A Pedro Aguiar, and Rafal Wisniewski. A hybrid quantum-classical physics-informed neural network architecture for solving quantum optimal control problems. *IEEE International Conference on Quantum Computing and Engineering (QCE24)*, 2024c.

Nahid Binandeh Dehaghani, A Pedro Aguiar, and Rafal Wisniewski. State-constrained optimal control for coherence preservation in multi-level open quantum systems. *arXiv preprint arXiv:2411.10840*, 2024d.

Nahid Binandeh Dehaghani, A Pedro Aguiar, and Rafal Wisniewski. State estimation and control for stochastic quantum dynamics with homodyne measurement: Stabilizing qubits under uncertainty. *IEEE Access*, 2024e.

Hua Deng, Miroslav Krstic, and Ruth J Williams. Stabilization of stochastic nonlinear systems driven by noise of unknown covariance. *IEEE Transactions on automatic control*, 46(8):1237–1253, 2001.

Antonio Di Domenico et al. Search for CPT violation and decoherence effects in the neutral kaon system. In *Journal of Physics: Conference Series*, volume 171, page 012008. IOP Publishing, 2009.

Antonio Di Domenico et al. Latest results on kaon physics at KLOE-2. In *65th ICFA Advanced Beam Dynamics Workshop on High Luminosity Circular e+ e-Colliders (eeFACT'22), Frascati, Italy, 12-16 September 2022*, pages 30–34. JACOW Publishing, Geneva, Switzerland, 2022.

Paul Adrien Maurice Dirac. *The principles of quantum mechanics*. Oxford university press, 1981.

Matthew J Donald, Michał Horodecki, and Oliver Rudolph. The uniqueness theorem for entanglement measures. *Journal of Mathematical Physics*, 43(9):4252–4272, 2002.

Daoyi Dong and Ian R Petersen. Sliding mode control of quantum systems. *New Journal of Physics*, 11(10):105033, 2009a.

Daoyi Dong and Ian R Petersen. Variable structure control of uncontrollable quantum systems. *IFAC Proceedings Volumes*, 42(6):237–242, 2009b. doi: 10.3182/20090616-3-IL-2002.00041.

Daoyi Dong and Ian R Petersen. Controllability of quantum systems with switching control. *International Journal of Control*, 84(1):37–46, 2011.

Daoyi Dong and Ian R Petersen. Sliding mode control of two-level quantum systems. *Automatica*, 48(5):725–735, 2012.

Daoyi Dong, Chunlin Chen, Hanxiong Li, and Tzyh-Jong Tarn. Quantum reinforcement learning. *IEEE Transactions on Systems, Man, and Cybernetics, Part B (Cybernetics)*, 38(5):1207–1220, 2008.

Daoyi Dong, Ian R Petersen, and Herschel Rabitz. Sampled-data design for robust control of a single qubit. *IEEE Transactions on Automatic Control*, 58(10):2654–2659, 2013.

Domenico d'Alessandro. *Introduction to quantum control and dynamics*. Chapman and hall/CRC, 2021.

Domenico D'Alessandro and Yasemin Işik. Optimal control of quantum lambda systems with an occupancy cost. *Automatica*, 163:111595, 2024.

Andrea D'ambrosio, Enrico Schiassi, Fabio Curti, and Roberto Furfaro. Pontryagin neural networks with functional interpolation for optimal intercept problems. *Mathematics*, 9 (9):996, 2021.

Albert Einstein, Boris Podolsky, and Nathan Rosen. Can quantum-mechanical description of physical reality be considered complete? *Physical review*, 47(10):777, 1935.

Shu-Kai S Fan, Yun-chia Liang, and Erwie Zahara. Hybrid simplex search and particle swarm optimization for the global optimization of multimodal functions. *Engineering optimization*, 36(4):401–418, 2004.

Richard Phillips Feynman. *Feynman Lectures on Physics: Electrical and Magnetic Behavior. Volume 4*. Perseus Books, 1999.

A. F. Filippov. On certain problems of optimal regulation. *Vestn. MGU, Mat. Mekh*, 2: 25–38, 1959.

Wendell H Fleming and Raymond W Rishel. *Deterministic and stochastic optimal control*, volume 1. Springer Science & Business Media, 2012.

Rodolfo Gambini, Rafael A Porto, and Jorge Pullin. Fundamental decoherence from quantum gravity: a pedagogical review. *General Relativity and Gravitation*, 39:1143–1156, 2007.

Sara Gamble. Quantum computing: What it is, why we want it, and how we're trying to get it. In *Frontiers of Engineering: Reports on Leading-Edge Engineering from the 2018 Symposium*. National Academies Press, 2019.

Perez del Rio E Gauzzi P. The KLOE-2 experiment at DAΦNE. *EPJ Web Conf.*, 1(212), 2019.

Robert J Gordon, Langchi Zhu, and Tamar Seideman. Coherent control of chemical reactions. *Accounts of Chemical Research*, 32(12):1007–1016, 1999.

Knut Graichen, Andreas Kugi, Nicolas Petit, and Francois Chaplais. Handling constraints in optimal control with saturation functions and system extension. *Systems & Control Letters*, 59(11):671–679, 2010.

David Griffiths. *Introduction to elementary particles*. John Wiley & Sons, 2020.

Ari Gross. Pictures and pedagogy: The role of diagrams in Feynman's early lectures. *Studies in History and Philosophy of Science Part B: Studies in History and Philosophy of Modern Physics*, 43(3):184–194, 2012.

Nikolaus Hansen, Sibylle D Müller, and Petros Koumoutsakos. Reducing the time complexity of the derandomized evolution strategy with covariance matrix adaptation (CMA-ES). *Evolutionary computation*, 11(1):1–18, 2003.

Vahid Hassani, A Pedro Aguiar, Michael Athans, and António M Pascoal. Multiple model adaptive estimation and model identification usign a minimum energy criterion. In *2009 American Control Conference*, pages 518–523. IEEE, 2009.

Beatrix C Hiesmayr. *The puzzling story of the neutral kaon system: or what we can learn from entanglement*. na, 2002.

Charles Hill and Jason Ralph. Weak measurement and control of entanglement generation. *Physical Review A*, 77(1):014305, 2008.

Sam A Hill and William K Wootters. Entanglement of a pair of quantum bits. *Physical review letters*, 78(26):5022, 1997.

Michal Horodecki. Entanglement measures. *Quantum Inf. Comput.*, 1(1):3–26, 2001.

Guang-Bin Huang, Qin-Yu Zhu, and Chee-Kheong Siew. Extreme learning machine: theory and applications. *Neurocomputing*, 70(1-3):489–501, 2006.

VS Indrajith, R Muthuganesan, and R Sankaranarayanan. Fidelity-based purity and coherence for quantum states. *International Journal of Quantum Information*, 20(06): 2250016, 2022.

Hiroshi Ito and Yuki Nishimura. Stability of stochastic nonlinear systems in cascade with not necessarily unbounded decay rates. *Automatica*, 62:51–64, 2015.

Matthew R James, Hendra I Nurdin, and Ian R Petersen. H^∞ control of linear quantum stochastic systems. *IEEE Transactions on Automatic Control*, 53(8):1787–1803, 2008.

Lars M Johansen. Quantum theory of successive projective measurements. *Physical Review A*, 76(1):012119, 2007. doi: 10.1103/PhysRevA.76.012119.

Hunter Johnston, Enrico Schiassi, Roberto Furfaro, and Daniele Mortari. Fuel-efficient powered descent guidance on large planetary bodies via theory of functional connections. *The journal of the astronautical sciences*, 67(4):1521–1552, 2020.

Hunter Reed Johnston. *The theory of functional connections: A journey from theory to application*. PhD thesis, Texas A&M University, 2021.

Richard S Judson and Herschel Rabitz. Teaching lasers to control molecules. *Physical review letters*, 68(10):1500, 1992.

Claus Kiefer. Why quantum gravity? In *Approaches to Fundamental Physics: An Assessment of Current Theoretical Ideas*, pages 123–130. Springer, 2007.

Nathan Killoran, Thomas R Bromley, Juan Miguel Arrazola, Maria Schuld, Nicolás Quesada, and Seth Lloyd. Continuous-variable quantum neural networks. *Physical Review Research*, 1(3):033063, 2019.

AN Korotkov and DV Averin. Continuous weak measurement of quantum coherent oscillations. *Physical Review B*, 64(16):165310, 2001.

Robert L Kosut, Matthew D Grace, and Constantin Brif. Robust control of quantum gates via sequential convex programming. *Physical Review A*, 88(5):052326, 2013.

Sergei Kurgalin and Sergei Borzunov. *Concise guide to quantum computing*. Springer, 2021.

AG Lee. *Particle physics*, volume 1. CRC Press, 1981.

TD Lee and CS Wu. Weak interactions (second section) chapter 9: decays of neutral k mesons. *Annual Review of Nuclear Science*, 16(1):511–590, 1966.

Yun-Yan Lee, Daoyi Dong, and Ciann Dong Yang. Generation of maximally entangled states by Lyapunov control based on entanglement measure. 2022. URL https://api.semanticscholar.org/CorpusID:247794229.

Jr-Shin Li and Navin Khaneja. Ensemble control of Bloch equations. *IEEE Transactions on Automatic Control*, 54(3):528–536, 2009.

Daniel Liberzon. *Calculus of variations and optimal control theory: a concise introduction*. Princeton university press, 2011.

Harry J Lipkin. CP violation and coherent decays of kaon pairs. *Physical Review*, 176(5): 1715, 1968.

Gang-Qin Liu, Xi Feng, Ning Wang, Quan Li, and Ren-Bao Liu. Coherent quantum control of nitrogen-vacancy center spins near 1000 kelvin. *Nature communications*, 10(1): 1–8, 2019.

Shai Machnes, Elie Assémat, David Tannor, and Frank K Wilhelm. Tunable, flexible, and efficient optimization of control pulses for practical qubits. *Physical review letters*, 120 (15):150401, 2018.

Javier Madronero, Alexey Ponomarev, André RR Carvalho, Sandro Wimberger, Carlos Viviescas, Andrey Kolovsky, Klaus Hornberger, Peter Schlagheck, Andreas Krug, and Andreas Buchleitner. Quantum chaos, transport, and control—in quantum optics. *Advances In Atomic, Molecular, and Optical Physics*, 53:33–73, 2006.

Daniel Manzano. A short introduction to the lindblad master equation. *Aip advances*, 10 (2), 2020.

Stefano Markidis. On physics-informed neural networks for quantum computers. *Frontiers in Applied Mathematics and Statistics*, 8:1036711, 2022.

Brian R Martin and Graham Shaw. *Particle physics*. John Wiley & Sons, 2016.

Nicholas Metropolis, Arianna W Rosenbluth, Marshall N Rosenbluth, Augusta H Teller, and Edward Teller. Equation of state calculations by fast computing machines. *The journal of chemical physics*, 21(6):1087–1092, 1953.

Javier Miguel-Sánchez, Andreas Reinhard, Emre Togan, Thomas Volz, Atac Imamoglu, Benjamin Besga, Jakob Reichel, and Jérôme Estève. Cavity quantum electrodynamics with charge-controlled quantum dots coupled to a fiber Fabry–Perot cavity. *New Journal of Physics*, 15(4):045002, 2013.

Daniele Mortari and Roberto Furfaro. Univariate theory of functional connections applied to component constraints. *Mathematical and Computational Applications*, 26(1):9, 2021.

Daniele Mortari and Carl Leake. The multivariate theory of connections. *Mathematics*, 7 (3):296, 2019.

John A Nelder and Roger Mead. A simplex method for function minimization. *The computer journal*, 7(4):308–313, 1965.

Michael A Nielsen. Conditions for a class of entanglement transformations. *Physical Review Letters*, 83(2):436, 1999.

Michael A Nielsen and Isaac Chuang. Quantum computation and quantum information, 2002.

Michael A Nielsen and Isaac L Chuang. *Quantum computation and quantum information*. Cambridge university press, 2010.

Ariel Norambuena, Marios Mattheakis, Francisco J González, and Raúl Coto. Physics-informed neural networks for quantum control. *Physical Review Letters*, 132(1):010801, 2024.

Hendra I Nurdin, Matthew R James, and Ian R Petersen. Coherent quantum LQG control. *Automatica*, 45(8):1837–1846, 2009.

Lev Borisovich Okun. *Leptons and quarks*. Elsevier, 2013.

Abraham Pais and Oreste Piccioni. Note on the decay and absorption of the θ 0. *Physical Review*, 100(5):1487, 1955.

José P Palao and Ronnie Kosloff. Optimal control theory for unitary transformations. *Physical Review A*, 68(6):062308, 2003.

Rüdiger Paschotta. *Field guide to laser pulse generation*, volume 14. SPIE press Bellingham, 2008.

SJ Pauka, K Das, R Kalra, A Moini, Y Yang, M Trainer, A Bousquet, C Cantaloube, N Dick, GC Gardner, et al. A cryogenic CMOS chip for generating control signals for multiple qubits. *Nature Electronics*, 4(1):64–70, 2021.

Philip Pearle. Combining stochastic dynamical state-vector reduction with spontaneous localization. *Physical Review A*, 39(5):2277, 1989.

Francesco Petiziol, Ennio Arimondo, Luigi Giannelli, Florian Mintert, and Sandro Wimberger. Optimized three-level quantum transfers based on frequency-modulated optical excitations. *Scientific reports*, 10(1):2185, 2020.

L S Pontryagin, V G Bol'tanskii, R S Gamkrelidze, and E F Mischenko. *The Mathematical theory of optimal processes*. Pergamon Press, New York, 1964.

Michael JD Powell. An efficient method for finding the minimum of a function of several variables without calculating derivatives. *The computer journal*, 7(2):155–162, 1964.

Herschel Rabitz, Regina de Vivie-Riedle, Marcus Motzkus, and Karl Kompa. Whither the future of controlling quantum phenomena? *Science*, 288(5467):824–828, 2000.

Viswanath Ramakrishna and Herschel Rabitz. Relation between quantum computing and quantum controllability. *Physical Review A*, 54(2):1715, 1996. doi: 10.1103/physreva.54.1715.

Darragh Patrick Rooney. *Control of finite-dimensional quantum systems under Lindblad dissipation*. University of Michigan, 2012.

I Michael Ross. A primer on Pontryagin's principle in optimal control. *Collegiate Publications: Wales, UK*, 2009.

Pierre Rouchon. A tutorial introduction to quantum stochastic master equations based on the qubit/photon system. *Annual Reviews in Control*, 54:252–261, 2022.

Rusko Ruskov and Alexander N Korotkov. Quantum feedback control of a solid-state qubit. *Physical Review B*, 66(4):041401, 2002.

Yu L Sachkov. Controllability of right-invariant systems on solvable Lie groups. *Journal of dynamical and control systems*, 3(4):531–564, 1997.

Jochen Scheuer, Xi Kong, Ressa S Said, Jeson Chen, Andrea Kurz, Luca Marseglia, Jiangfeng Du, Philip R Hemmer, Simone Montangero, Tommaso Calarco, et al. Precise qubit control beyond the rotating wave approximation. *New Journal of Physics*, 16 (9):093022, 2014.

Erwin Schrödinger. Die gegenwärtige situation in der quantenmechanik. *Naturwissenschaften*, 23(50):844–849, 1935.

AJ Shaiju, Ian R Petersen, and Matthew R James. Guaranteed cost LQG control of uncertain linear stochastic quantum systems. In *2007 American Control Conference*, pages 2118–2123. IEEE, 2007.

Dan Simon. *Optimal state estimation: Kalman, H infinity, and nonlinear approaches*. John Wiley & Sons, 2006.

C Sivaram. What is special about the planck mass? *arXiv preprint arXiv:0707.0058*, 2007.

JJWH Sørensen, MO Aranburu, Till Heinzel, and JF Sherson. Quantum optimal control in a chopped basis: Applications in control of Bose-Einstein condensates. *Physical Review A*, 98(2):022119, 2018.

Rainer Storn and Kenneth Price. Differential evolution–a simple and efficient heuristic for global optimization over continuous spaces. *Journal of global optimization*, 11(4): 341–359, 1997. doi: 10.1023/a:1008202821328.

Dominique Sugny and Cyrill Kontz. Optimal control of a three-level quantum system by laser fields plus von Neumann measurements. *Physical Review A*, 77(6):063420, 2008.

Yingying Sun, Chengzhi Wu, Zhangqing Zhu, and Chunlin Chen. Comparison of learning methods for landscape control of open quantum systems. In *Proceeding of the 11th World Congress on Intelligent Control and Automation*, pages 1241–1246. IEEE, 2014.

Richard S Sutton and Andrew G Barto. *Reinforcement learning: An introduction*. MIT press, 2018.

Abas Syahbana, Freddy Permana Zen, and Donny Dwiputra. Study of entangled K-meson and its decoherence. *Indonesian Journal of Physics*, 33(1):39–44, 2022.

Katharine W Moore Tibbetts, Constantin Brif, Matthew D Grace, Ashley Donovan, David L Hocker, Tak-San Ho, Re-Bing Wu, and Herschel Rabitz. Exploring the tradeoff between fidelity and time optimal control of quantum unitary transformations. *Physical Review A*, 86(6):062309, 2012.

Wolfgang Tittel, Jürgen Brendel, Hugo Zbinden, and Nicolas Gisin. Violation of Bell inequalities by photons more than 10 km apart. *Physical review letters*, 81(17):3563, 1998.

Masaaki Tsubouchi and Takamasa Momose. Rovibrational wave-packet manipulation using shaped midinfrared femtosecond pulses toward quantum computation: Optimization of pulse shape by a genetic algorithm. *Physical Review A*, 77(5):052326, 2008.

T Untidt, B SCHULTE-HERBRÜGGEN, B Luy, SJ Glaser, C Griesinger, OW Sørensen, and NC Nielsen. Design of NMR pulse experiments with optimum sensitivity: coherence-order-selective transfer in I2S and I3S spin systems. *Molecular Physics*, 95(5):787–796, 1998.

Ramon Van Handel, John K Stockton, and Hideo Mabuchi. Feedback control of quantum state reduction. *IEEE Transactions on Automatic Control*, 50(6):768–780, 2005.

Adalberto Deybe Varizi. *Open quantum system approach to neutral Kaon interferometry*. Universidade Federal de Minas Gerais, 2017.

Vlatko Vedral and Martin B Plenio. Entanglement measures and purification procedures. *Physical Review A*, 57(3):1619, 1998.

Guifré Vidal. Entanglement monotones. *Journal of Modern Optics*, 47(2-3):355–376, 2000.

Xiaoting Wang and Sophie G Schirmer. Analysis of Lyapunov method for control of quantum states. *IEEE Transactions on Automatic control*, 55(10):2259–2270, 2010.

Warren S Warren, Herschel Rabitz, and Mohammed Dahleh. Coherent control of quantum dynamics: the dream is alive. *Science*, 259(5101):1581–1589, 1993.

Jacob R West, Daniel A Lidar, Bryan H Fong, and Mark F Gyure. High fidelity quantum gates via dynamical decoupling. *Physical review letters*, 105(23):230503, 2010.

Eugene P Wigner. On hidden variables and quantum mechanical probabilities. *Part I: Particles and Fields. Part II: Foundations of Quantum Mechanics*, pages 515–523, 1997.

Howard M Wiseman. Quantum theory of continuous feedback. *Physical Review A*, 49(3): 2133, 1994.

Howard M Wiseman and Eric G Cavalcanti. Quantum [un] speakables ii. the frontiers collection, 2017.

William K Wootters. Entanglement of formation of an arbitrary state of two qubits. *Physical Review Letters*, 80(10):2245, 1998.

William K Wootters. Entanglement of formation and concurrence. *Quantum Inf. Comput.*, 1(1):27–44, 2001.

Jian-Wu Wu, Chun-Wen Li, Tzyh-Jong Tarn, and Jing Zhang. Optimal bang-bang control for SU (1, 1) coherent states. *Physical Review A*, 76(5):053403, 2007.

Re-Bing Wu, Ruixing Long, Jason Dominy, Tak-San Ho, and Herschel Rabitz. Singularities of quantum control landscapes. *Physical Review A*, 86(1):013405, 2012.

Naoki Yamamoto and Luc Bouten. Quantum risk-sensitive estimation and robustness. *IEEE Transactions on Automatic Control*, 54(1):92–107, 2009.

Taku Yamanaka and KOTO Collaboration. The J-PARC KOTO experiment. *Progress of Theoretical and Experimental Physics*, 2012(1):02B006, 2012.

Shuyuan Yang, Min Wang, et al. A quantum particle swarm optimization. In *Proceedings of the 2004 congress on evolutionary computation (IEEE Cat. No. 04TH8753)*, volume 1, pages 320–324. IEEE, 2004.

Wen Yang, Zhen-Yu Wang, and Ren-Bao Liu. Preserving qubit coherence by dynamical decoupling. *Frontiers of Physics in China*, 6(1):2–14, 2011.

Fakhar Zaman, Youngmin Jeong, and Hyundong Shin. Counterfactual Bell-state analysis. *Scientific reports*, 8(1):14641, 2018.

Jing Zhang, Re-Bing Wu, Yu-xi Liu, Chun-Wen Li, and Tzyh-Jong Tarn. Quantum coherent nonlinear feedback with applications to quantum optics on chip. *IEEE transactions on automatic control*, 57(8):1997–2008, 2012.

Ming-Jing Zhao, Xue-Na Zhu, Shao-Ming Fei, and Xianqing Li-Jost. Lower bound on concurrence and distillation for arbitrary-dimensional bipartite quantum states. *Physical Review A*, 84(6):062322, 2011.

Konstantin Zhdanov. An improvement of D-MORPH method for finding quantum optimal control. *arXiv preprint arXiv:1709.05364*, 2017.

Lisa Zyga. Physicists find quantum coherence and quantum entanglement are two sides of the same coin. *Phys.org*, 2015.